

University of Nottingham
UK | CHINA | MALAYSIA

# Characterisation of knitted conductive textiles for wearable motion sensor applications

Cristina Isaia

MEng, University of Catania

Thesis submitted to The University of Nottingham

for the degree of Doctor of Philosophy

March 2018

# Abstract

Combining stainless steel with polyester fibres adds an attractive conductive behaviour to the yarn. Once knitted in such a manner, fabrics develop sensing properties that make them suitable for wearable applications as a consequence of the variation of their conductivity when subject to structural deformations. The use of such textiles as accurate strain/motion sensors can be considered the new frontier in wearable sensor applications, in opposition to their use as simple strain/motion detectors as mainly done until now.

This thesis aims to characterise the electrical properties of knitted conductive textiles made of 20% stainless steel and 80% polyester fibres in the context of their application as fabric strain sensors. However, the use of conductive textiles as sensors is challenging and requires the combined study of their electrical and mechanical behaviours.

In the first part of this thesis, the fabric resistance variation is analysed with a purposely built measurement system during a considerable number of stretch-recovery cycles performed by an Instron tensile machine. From the resulting electrical characterisation, it is possible to select the best knit pattern candidates for the second part of the study, which regards their integration into a supporting garment and further investigation of their electrical and mechanical properties in view of their application as wearable motion sensors.

Two acquisition systems capture both free and constrained motions of a participant's knee and the electrical resistance variation due to combined deformation of samples and supporting leggings. In both parts of this thesis, a detailed analysis in terms of linearity, stability, sensitivity and hysteresis confirms that the overall sensing performance progressively decreases during extended use as a consequence of the short-term irreversible fabric deformation and does not significantly recover after short rest periods.

For the development and use of high performance fabric-based strain sensors, it is therefore evident the importance of the long-term maintaining of a reversible stretch-recovery behaviour not only of the sensing fabrics but also of the supporting garments they are integrated in.

# Acknowledgements

I would like to thank my academic supervisors, Professor Donal McNally and Dr David Branson, for offering me the chance to study for a PhD. I am extremely grateful for their professional and human guidance which has helped me to grow as a student researcher.

Thanks are due to Simon McMaster and Footfalls & Heartbeats (UK) Limited for letting me investigate their knitted conductive textiles and for trusting the findings of my research. A special mention also goes to Nada Savic for her expert help during my tests at the Nottingham City Hospital. Her time and kindness were very much appreciated.

It was a great pleasure to be part of the Biomechanics Lab and share many good moments, laughs and cakes with Mark, Chris, Mohammed, Paco, Alan and Lorelei. They helped to make my days at the lab memorable and less stressful.

Thanks to all of my old friends for being loyal and caring over the years.

Finally, I wish to thank my family, Alberto, Claire, Alan, Linda and Auntie Pat for their love, support, patience and understanding.
To them, I dedicate this piece of work.

# Contents


**1 Introduction** **1**

1.1 Background . . . . . 1

1.2 Definition of wearable sensors . . . . . 2

1.3 Definition of fabrics . . . . . 2

1.4 Objectives . . . . . 4

1.5 Overview of thesis . . . . . 5

**2 Literature Review** **7**

2.1 Introduction . . . . . 7

2.2 Human motion . . . . . 8

2.3 Techniques for human motion analysis . . . . . 9

2.3.1 Static platform for human motion analysis . . . . . 9

2.3.2 Wearable platforms for human motion analysis . . . . 12

2.3.3 Comparison between static and wearable platforms and areas of application . . . . . 16

2.4 Smart fabric sensors . . . . . 19

2.5 Techniques to enable sensing functionality into fabrics . . . . 23

2.6 Fabric strain sensors . . . . . 26

2.7 Influencing factors of the fabric resistance . . . . . 31

2.7.1 Length-related resistance . . . . . 32

2.7.2 Contact resistance . . . . . 33

2.7.3 Fabric mechanical parameters . . . . . 34
2.7.4 Loop geometry . . . . . 35
2.7.5 Fibre-fibre slippage . . . . . 36
2.8 Conclusions . . . . . 39

**3 Characterisation of Knitted Conductive Fabrics 41**
3.1 Introduction . . . . . 41
3.2 Objectives . . . . . 42
3.3 Description of the knitted conductive samples . . . . . 42
3.3.1 Conductive yarn . . . . . 47
3.3.2 Non conductive yarn . . . . . 48
3.3.3 Sample preparation . . . . . 48
3.4 System for electrical characterisation of the conductive samples 49
3.4.1 Electronic system . . . . . 50
3.4.2 Mechanical system . . . . . 53
3.4.3 Acquisition system . . . . . 55
3.5 Testing of the knitted conductive fabrics . . . . . 57
3.5.1 Mechanical preconditioning . . . . . 58
3.5.2 Tests at different elongations . . . . . 60
3.6 Data Postprocessing . . . . . 61
3.6.1 Filtering of the raw data . . . . . 61
3.6.2 Peak analysis . . . . . 65
3.6.3 Interpolation . . . . . 67
3.6.4 Extraction of features of interest . . . . . 68
3.7 Conclusions . . . . . 73

**4 Analysis of the fabric electrical characterisation 74**
4.1 Introduction . . . . . 74
4.2 Objectives . . . . . 75

4.3 Analysis of the electrical behaviour of the conductive samples 75
4.3.1 Fabric critical loosening . . . . . 78
4.4 Results and discussion of the mechanical preconditioning . . 81
4.4.1 Stabilisation of the electrical resistance . . . . . 82
4.4.2 Decreasing number of cycles to settle during repeatability test . . . . . 84
4.4.3 Increasing stabilised average resistance from the preconditioning to repeatability tests . . . . . 86
4.5 Effects influencing the electrical features of the samples . . . 87
4.5.1 Analysis of the knitted fabric parameters . . . . . 88
4.5.2 Effect of the current on the electrical resistance of the fabrics . . . . . 91
4.5.3 Effect of the elongation rate on the electrical resistance of the fabrics . . . . . 93
4.6 Gauge factor of the stitch patterns . . . . . 94
4.7 Time dependent behaviour . . . . . 99
4.8 Elongation dependent behaviour . . . . . 101
4.8.1 Hysteresis at different elongations . . . . . 103
4.9 Time-frequency analysis . . . . . 107
4.9.1 Spectrogram . . . . . 107
4.9.2 Harmonics amplitude . . . . . 109
4.9.3 Signal-to-noise ratio . . . . . 110
4.10 Discussion . . . . . 112
4.11 Conclusions . . . . . 114

**5 Application of electrically conductive leggings for motion capture - Methodology 116**

5.1 Introduction . . . . . 116

5.2 Objectives . . . 117
5.3 Materials . . . 117
5.3.1 Description of the knitted conductive fabrics . . . 118
5.3.2 Description of the leggings . . . 118
5.3.3 How to embed the knitted conductive fabrics into leggings . . . 118
5.4 Method One- *Visual Motion Tracking System* . . . 120
5.4.1 Image acquisition and objects detection . . . 122
5.4.2 Issues with the markers detection and solutions . . . 125
5.5 Measurement system's objectives . . . 126
5.5.1 Task 1: Acquisition from the camera . . . 127
5.5.2 Task 2: Acquisition from the leggings . . . 127
5.5.3 Task 3: Synchronisation . . . 128
5.6 Calibration of the tracking system . . . 129
5.6.1 Calibration on a dummy . . . 129
5.6.2 Calibration on a participant . . . 133
5.7 Test procedure on a participant . . . 135
5.7.1 Flexion-extension trials . . . 137
5.8 Method Two- *HUMAC NORM System* . . . 138
5.9 Description of the measurement system . . . 139
5.9.1 Acquisition from the dynamometer . . . 140
5.9.2 Acquisition from the leggings . . . 141
5.9.3 Synchronisation . . . 141
5.10 HUMAC set-up and calibration . . . 142
5.11 Testing procedure on a participant . . . 143
5.12 Conclusions . . . 146

**6 Analysis of the use of wearable sensors on a participant 148**

6.1 Introduction . . . 148
6.2 Objectives . . . 148
6.3 *Visual Motion Tracking System*: Results and Discussion . . 149
6.3.1 Data post-processing for conductive samples embedded into leggings . . . 149
6.3.2 Analysis of the electrical behaviour of conductive samples embedded into leggings . . . 154
6.3.3 Linearity . . . 154
6.3.4 Stability . . . 156
6.3.5 Gauge factor and sensitivity . . . 162
6.3.6 Hysteresis . . . 169
6.3.7 Effect of the current on the fabric electrical resistance 170
6.4 *HUMAC NORM System*: Results and Discussion . . . 172
6.4.1 Data post-processing . . . 172
6.4.2 Analysis of the electrical behaviour . . . 175
6.4.3 Linearity . . . 175
6.4.4 Stability . . . 177
6.4.5 Sensitivity . . . 179
6.4.6 Hysteresis . . . 183
6.4.7 Effect of the supporting garment on the fabric parameters . . . 184
6.5 Comparison of the two methods . . . 185
6.6 Discussion . . . 188
6.7 Conclusions . . . 193

**7 Conclusions and future work** **195**
7.1 Introduction . . . 195
7.2 General summary and conclusions . . . 195

7.2.1 Characterisation of knitted conductive textiles . . . . 195
7.2.2 Use of knitted conductive textiles as wearable motion sensors . . . . . 199
7.2.3 Conclusions . . . . . 201
7.3 Recommendations for future work . . . . . 202
7.3.1 Improving the loose fabrics issue . . . . . 202
7.3.2 Modelling the knitted conductive sample under cyclic deformation . . . . . 203
7.3.3 Performing additional tests under new testing conditions and for different applications . . . . . 209
7.3.4 Making the applications of the sensing fabrics portable 210

**Bibliography** **212**

**Appendix I: Test sessions** **221**

**Appendix II: Matlab code for fabric analysis** **224**

**Appendix III: Test results** **234**

**Appendix IV: Fabric sensitivity** **239**

**Appendix V: Spectrograms and Harmonics Amplitude** **241**

**Appendix VI: Matlab code for the *Visual Motion Tracking System*** **243**

**Appendix VII: Matlab code for the *HUMAC NORM* System** **259**

**Appendix VIII: Data post processing results with the HUMAC NORM System** **263**

**Appendix IX: Statistical formula** **265**

**Appendix X: Participant Information Sheet** **267**

**Appendix XI: Participant Consent Form** **271**

**Appendix XII: Publications** **273**

# List of Figures


1.1 Fabric construction based on fabric structures: a) Woven, b) Knitted, c) Non-Woven, d) Nets, e) Braided and f) Tufted. Fabrics structures can be assembled in layers (e.g. three) to form composites (Castano and Flatau 2014) . . . . . 3

2.1 Scheme of the platforms used for human motion analysis . . 9

2.2 Example of motion camera system used in a movement analysis laboratory (Cappozzo et al. 2005) . . . . . 11

2.3 Angular displacements based on three pairs of accelerometers and gyroscopes attached on the foot, calf and thigh (Tao 2012) . . . . . 13

2.4 Example of (a) a biplanar electrogoniometer and (b) its application along the knee joint (Legnani et al. 2000) . . . . . 15

2.5 Scheme of techniques enabling conductivity in fabrics (Modified from Castano and Flatau 2014) . . . . . 24

2.6 Schematic of conductive fibre twisted with normal fibres (e.g. polyester) (Modified from Stoppa and Chiolerio 2014) . . . 24

2.7 Conductivity range of materials (Kaur et al. 2015) . . . . . 25

2.8 Example of flexion angle-resistance measurements proposed by Shyr et al. 2014 for (a) elbow and (b) knee movements. The strain-resistance sensor is an elastic conductive webbing made of polyamide fibre coated with carbon particles and polyester yarn. The flexion angle measured by the wearable gesture sensing device (red line) was compared with a variable resistor and a protractor (black line). The resistance of the elastic conductive webbing to the flexion angle showed a good linear relationship during the stretch-recovery cycles within 30% strain. . . . . 28

2.9 Example of wearable instrumented garment (named WEALTHY) based on knitted integrated sensors and conceived for electrocardiogram (ECG), respiration, activity and respiration monitoring (Paradiso et al. 2005). The fabric electrodes are realised with stainless-steel based yarns, whereas the piezoresistive fabric sensors are made of lycra fabric coated with carbon-loaded rubber and commercial electroconductive yarn (Scilingo et al. 2005). (a-b) Prototype model with: E-Einthoven, W-Wilson, R-reference, P-precordial leads for ECG measurement and B- breathing sensor (c) Part of the WEALTHY interface (d) Movement sensors . . . . . 29

2.10 Example of wearable biofeedback system (called the Intelligent Knee Sleeve) formed by polypyrrole-coated nylon-lycra sensor integrated into a base sleeve together with appropriate electronic circuitry (provided by CSIRO Textile and Fibre Technology). The system is conceived to alert the wearer that the desired knee flexion angle (i.e. a predetermined threshold resistance based on the stretching of the fabric sensor) is achieved according to a preventing injury program (Munro et al. 2008) . . . . . 30
2.11 (a) Single loop (represented in bold) -consisting of a head (H), two legs (L) and two sinker loops (S)- and contact points (red circles). (b) Corresponding resistive network model (modified from Isaia et al. 2018) . . . . . 36
2.12 Interaction between two fibres at a contact point (modified from Carnaby and Pan 1989) . . . . . 38

3.1 Knitted conductive samples used in the study: a) Single Jersey b) SP27 c) SP29 and d) SP31. . . . . 43
3.2 Type of stitches (Sarker 2016) . . . . . 44
3.3 Fabric scheme . . . . . 45
3.4 Loop geometrical parameters: loop height (red), loop width (green) and yarn diameter (yellow) . . . . . 46
3.5 Experimental set-up scheme . . . . . 49
3.6 The printed circuit board: a) top of the board, b) bottom of the board . . . . . 50
3.7 Schematic of the controlled current generator circuitry . . . 51
3.8 a) Instron 5969 testing machine b) Specimen in the customised clamps . . . . . 53
3.9 a)- b) Instron 8801 hydraulic machine c) Customised clamps 54

3.10 Signals captured with the Data Acquisition System . . . . . 56
3.11 Original fabric resistance and Savitzky-Golay filtered resistance for the SP29 sample sourced with 3 mA and tested at 9.6 mm/s. In the box: zoom of the first 25 elongations for the filtered signal . . . . . 63
3.12 Original fabric resistance, FIR low pass and Savitzky-Golay filtered resistances on the same graph for the SP29 sample sourced with 3 mA and tested at 9.6 mm/s . . . . . 64
3.13 a) Original fabric resistance, b) FIR low pass and c) Savitzky-Golay filtered resistances in ten cycles for the SP29 sample sourced with 3 mA and tested at 9.6 mm/s . . . . . 64
3.14 Detection of the maximum and minimum values of the filtered resistance for the SP29 sourced with 3 mA and tested at 9.6 mm/s. In the box: zoom of the detected peaks during the first 40 cycles . . . . . 66
3.15 Maximum and minimum values obtained with the peak analysis and filtered maximum and minimum points using the Savitsky-Golay filter for the SP29 sample sourced with 3 mA and tested at 9.6 mm/s . . . . . 66
3.16 Maximum and minimum filtered values and interpolation curves of the filtered maximum and minimum points for the SP29 sample sourced with 3 mA and tested at 9.6 mm/s. In the box: zoom of the first 100 seconds . . . . . 67
3.17 Peak-to-peak span for the SP29 sample sourced with 3mA and tested at 9.6 mm/s . . . . . 69
3.18 Change point analysis applied the peak-to-peak span for determining the settling time of the SP29 sample sourced with 3mA and tested at 9.6 mm/s . . . . . 70

3.19 Stabilised average resistance (red dash line) determined as the mean filtered resistance from the settling time onwards for the SP29 sample sourced with 3mA and tested at 9.6 mm/s 72

3.20 Stabilised span (red dash line) determined as the mean span value from the settling time onwards for the SP29 sample sourced with 3mA and tested at 9.6 mm/s . . . . . 72

4.1 Analysis of the electrical behaviour of the SP29 sample sourced with 3 mA and tested at 9.6 mm/s during preconditioning test: (a) Elongation versus time (b) Original resistance versus time (c) Original and Savitzy-Golay filtered resistance versus time (N=3 and f=151). The red arrows show the delay between the maximum resistance and minimum elongation. The red ellipses indicate the instant when the specimen starts its elongation and, correspondingly, the fabric electrical resistance begins to increase . . . . . 76

4.2 Loosening of the fabric during cyclic loading and its effect on the electrical resistance . . . . . 78

4.3 Analysis during the 50th-52nd cycles for the SP29 sample sourced with 3 mA and tested at 9.6 mm/s: (a) Area of investigation, (b) Extension, (c) Original resistance and (d) Savitzky-Golay filtered resistance . . . . . 79

4.4 Analysis during the 200th-202nd cycles for the SP29 sample sourced with 3 mA and tested at 9.6 mm/s: (a) Area of investigation, (b) Extension, (c) Original resistance and (d) Savitzky-Golay filtered resistance . . . . . 80

4.5 Effect of mechanical preconditioning on the peak-to-peak span for the SP29 sample sourced with 3 mA and tested at 9.6 mm/s during preconditioning (blue line) and repeatability tests (red line) . . . . . 83
4.6 Mean number of cycles to reach the electrical stabilisation for all samples at three different currents and two elongation rates . . . . . 84
4.7 $t$-test table obtained from the difference between means number of cycles for the electrical stabilisation during and after preconditioning . . . . . 85
4.8 Difference of means of number of cycles, standard error and $p$-values between the four pairs of samples during and after preconditioning . . . . . 86
4.9 Stabilised average resistance for all samples during preconditioning and repeatability tests as mean at three different currents and two elongation rates . . . . . 87
4.10 Analysis of the dimensions of the stitch for the SP29 before (a) and after preconditioning (b). Loop height, loop width and diameter are represented in red, green and yellow respectively. . . . . 88
4.11 Loop length for new and preconditioned samples . . . . . 90
4.12 Stabilised average resistance for all samples at three different currents during repeatability test, as mean at two elongation rates . . . . . 91
4.13 Variation of the stabilised average resistance at 1, 3 and 6 mA sourcing currents normalised with respect to the 1mA test . . . . . 92

4.14 Difference of mean number of cycles (N) to settle between preconditioning and the repeatability test at different elongation rates. The error bars correspond to the standard error. . . . . 93
4.15 Original and average resistance for the SP29 sample sourced at 3 mA and tested at 9.6 mm/s. Zoom of the reduced ripple following the original signal . . . . . 94
4.16 Gauge factor variation with number of cycles for Single Jersey, SP27, SP29 and SP31 under the same test conditions (3 mA and 9.6 mm/s) during (A) preconditioning and (B) repeatability tests . . . . . 96
4.17 Sensitivity variation with current for the SP29 sample tested at 9.6 mm/s during (A) preconditioning and (B) repeatability test . . . . . 98
4.18 Hysteresis during the first three cycles of preconditioning test for the SP29 sample sourced with 3mA and tested at 9.6 mm/s . . . . . 100
4.19 Hysteresis during the first three cycles of repeatability tests for the SP29 sample sourced with 3mA and tested at 9.6 mm/s 100
4.20 Contribution of contact and length-related resistances to the overall equivalent resistance for the SP29 sample sourced with 1 mA and elongated of 4 (black line), 8 (blue line), 12 (green line) and 16 mm (red line) . . . . . 101
4.21 (a) Elongation and (b) filtered resistance variation with time for the SP29 sample elongated of 4 mm . . . . . 102
4.22 Hysteresis during the first cycle for the SP29 sample sourced with 1 mA, tested at 9.6 mm/s and elongated of 8, 12 and 16 mm . . . . . 104

4.23 Characteristic curves for the stretching (a) and recovery (b) phases of the SP29 sourced with 1 mA, tested at 9.6 mm/s and elongated of 12 mm during the first cycle . . . . . 105
4.24 Characteristic curves for the stretching (a) and recovery (b) phases of the SP29 sourced with 1 mA, tested at 9.6 mm/s and elongated of 16 mm during the first cycle . . . . . 105
4.25 Hysteresis during the first and fiftieth cycles for the SP29 sample sourced with 1 mA, tested at 9.6 mm/s and elongated of 8, 12 and 16 mm . . . . . 106
4.26 Spectrogram of the SP29 sample sourced with 3 mA and tested at 9.6 mm/s during (a) preconditioning and (b) repeatability tests . . . . . 108
4.27 Amplitude variation of the most relevant components of the SP29 sample sourced with 3 mA and tested at 9.6 mm/s during (a) the preconditioning test and (b) the repeatability test . . . . . 109
4.28 Signal to noise ratio for the SP29 sample sourced with 1 mA and tested at 9.6 mmps during preconditioning and repeatability tests . . . . . 111

5.1 Copper tape sewn on top and bottom of the conductive area of the fabric to create conductive contacts . . . . . 119
5.2 Conductive thread used to sew the sample into the leggings . 119
5.3 The Visual Motion tracking system . . . . . 121
5.4 (a-c) Connections for the electrical acquisition from the fabric (4 wires measurement) . . . . . 121

5.5 Screenshot of the knee angle measurement as the angle between two lines connecting the coordinates of red, green and blue markers. Position of markers is shown as text on the computer monitor . . . . . 124
5.6 Issues with the markers detection: the blue marker is not detected for light condition (a) and the green for the initial (rectangular) shape of the marker (b) . . . . . 125
5.7 Flat and spherical markers attached to anatomical positions of the leggings . . . . . 126
5.8 Parameters calibration by using a dummy . . . . . 129
5.9 Parameters calibration on a dummy: (a) Camera-markers distance and height of the camera from the floor, (b) Distance between markers, (c) Matlab screenshot example of alignment of the markers in an upright position and (d) Matlab screenshot example of rotation of the blue marker determining the knee angle variation . . . . . 132
5.10 (a) Example of the distance between the markers and the focus of the camera, (b) Example of the distance between the markers on a participant, (c) Example of the alignment of the markers on a participant and (d) Example of the height of the camera from the floor and of the working area . . . . 134
5.11 Test on participant with the Visual Motion Tracking System 135
5.12 Screenshot of the knee angle measurement with the Visual Motion Tracking System . . . . . 136
5.13 Screenshot of the knee angle variation with the Visual Motion Tracking System following the knee bending . . . . . 136
5.14 The HUMAC NORM measurement system . . . . . 139

5.15 Knee full extension position before starting the tests and during the rest interval . . . . . 144
5.16 (a) Extension, (b) Flexion for the SP29 sample . . . . . 145
5.17 (a) Extension, (b) Flexion for the SP27 sample . . . . . 145

6.1 (a) Original and filtered resistance (N=3, f=151), (b) Original (red line), delay compensated (green line) and filtered delay compensated knee angle (blue line, N=1, f=151) for the SP29 embedded into leggings with 18% elastane and tested with the Visual Motion Tracking System . . . . . 150
6.2 Resistance signal post-processing for the SP29 embedded into a pair of leggings with 18% elastane and tested with the Visual Motion Tracking System: (a) Filtering, (b) Maximum and minimum detection, (c) Interpolation curves, (d) Peak-to-peak span . . . . . 152
6.3 Knee angle signal post-processing for the SP29 embedded into a pair of leggings with 18% elastane and tested with the Visual Motion Tracking System: (a) Filtering, (b) Maximum and minimum points detection, (c) Interpolation curves, (d) Peak-to-peak span . . . . . 153
6.4 Extension and flexion curves for the SP29 embedded into a pair of leggings with 18% elastane during the first cycle with the Visual Motion Tracking System . . . . . 155
6.5 Characteristic curves for the (a) flexion and (b) extension phases of the SP29 integrated into a pair of leggings with 18% elastane during the first cycle with the Visual Motion Tracking System . . . . . 156

6.6 (a) Filtered resistance (N=3, f=151) and (b) Filtered knee angle (N=1, f=351) for the SP29 embedded into a pair of leggings with 15% elastane and tested with the Visual Motion Tracking System as soon as the participant worn the leggings . . . . . 158

6.7 (a) Filtered resistance (N=3, f=151), (b) Filtered knee angle (N=1, f=351) for the SP29 embedded into a pair of leggings with 18% elastane and tested with the Visual Motion Tracking System after the participant worn the garment for one hour . . . . . 159

6.8 (a) Filtered resistance, (b) Filtered knee angle and (c) Peak-to-peak span for the SP29 embedded into a pair of leggings with 15% elastane and tested with the Visual Motion Tracking System for the fifth time after a 5 minute rest. The red ellipse shows when the non-linear effect of the contact resistance predominates on the length-related resistance (below a certain fabric elongation/knee angle) causing loss of accuracy in the electrical resistance and, correspondingly, the drop of span . . . . . 161

6.9 Relationship between the flexion angle $\theta$ and the length of arc $l$ (modified from Shyr et al. 2014) . . . . . 162

6.10 Original and average knee angle signals from the beginning of the movement for the SP29 integrated into 18% elastane leggings and tested with the Visual Motion Tracking System 164

6.11 Original and average resistance signals from the beginning of the movement for the SP29 integrated into 18% elastane leggings and tested with the Visual Motion Tracking System 164

6.12 Gauge factor variation with cycles for the SP29 embedded into a pair of leggings with 18% elastane and tested with the Visual Motion Tracking System . . . . . 165

6.13 (a) Span of the fabric resistance, (b) Span of the knee angle and (c) Sensitivity for the SP29 embedded into a pair of leggings with 18% elastane and tested with the Visual Motion Tracking System after one hour preconditioning in a seated position . . . . . 168

6.14 Sensitivity for the SP29 samples integrated into leggings with 15% and 18% elastane when studied with the Visual Motion Tracking System. The error bars represent the standard deviation . . . . . 169

6.15 Hysteresis during the first and last three cycles of flexion-extension for the SP29 integrated into 18% elastane and tested with the Visual Motion Tracking System . . . . . 170

6.16 (a) Fabric resistance and (b) knee angle for the SP29 embedded into a pair of leggings with 15% elastane when sourced with 1mA constant current and tested with the Visual Motion Tracking System . . . . . 171

6.17 (a) Fabric resistance and (b) knee angle for the SP29 embedded into a pair of leggings with 15% elastane when sourced with 3mA constant current and tested with the Visual Motion Tracking System . . . . . 171

6.18 (a) Original and filtered fabric resistance (N=3, f=651), (b) Knee angle and (c) Velocity during the first three cycles for the SP29 embedded into 15% elastane leggings and tested with the HUMAC NORM System . . . . . 173

6.19 (a) Original and filtered fabric resistance (N=3, f=651), (b) Knee angle and (c) Velocity during the first fifty cycles for the SP29 embedded into 15% elastane leggings and tested with the HUMAC NORM System . . . . . 173
6.20 (a) Filtered fabric resistance (N=3, f=651), (b) Peaks detection and interpolation curves and (c) Peak-to-peak span for the SP29 embedded into 15% elastane leggings and tested with the HUMAC NORM System . . . . . 174
6.21 Extension and flexion curves for the SP29 integrated into a pair of leggings with 18% elastane during the first cycle with the HUMAC NORM System . . . . . 176
6.22 Characteristic curves for the (a) extension and (b) flexion phases of the SP29 integrated into a pair of leggings with 18% elastane during the first cycle with the HUMAC NORM System . . . . . 177
6.23 Comparison between relative number of cycles to reach stability for the SP27 and SP29 tested for the first time in the Instron tensile machine and integrated into leggings with 15% and 18% elastane . . . . . 179
6.24 Sensitivity for: (a-b) the SP27 integrated into leggings with 15% and 18% elastane, (c-d) the SP29 embedded into 15% and 18% elastane leggings and tested with the HUMAC NORM System . . . . . 180
6.25 Sensitivity for the SP27 and SP29 embedded into leggings with 15% and 18% elastane when tested with the HUMAC NORM System. The error bars represent the standard deviation . . . . . 181

6.26 Hysteresis during the first and last three cycles of flexion-extension for the SP29 integrated into 18% elastane and tested with the HUMAC NORM System . . . . . 183
6.27 Loop lengths for the SP27 and SP29 embedded into leggings with 15% and 18% elastane in case of new specimens and samples tested with the HUMAC NORM System . . . . . 184

7.1 Loop geometry according to the Peirce's model (modified from Atalay O 2014) . . . . . 204
7.2 Simplified electrical diagram of one knitted conductive course (modified from Atalay O 2014) . . . . . 205
7.3 Equivalent resistive circuit network of one knitted conductive course . . . . . 205
7.4 Sensitivity variation with cycle at 1 mA for Single Jersey, SP27, SP29 and SP31 during (A) preconditioning and (B) repeatability tests . . . . . 239
7.5 Sensitivity variation with cycle at 6 mA for Single Jersey, SP27, SP29 and SP31 during (A) preconditioning and (B) repeatability tests . . . . . 240
7.6 Sensitivity variation with cycle at 1 mA, 3 mA and 6 mA for (a) Single Jersey, (b) SP27 and (c) SP31 during (A) preconditioning and (B) repeatability tests . . . . . 240
7.7 Spectrogram and amplitude variation of the most relevant components during preconditioning test ((a) and (b)) and during repeatability test ((c) and (d)) for the Single Jersey sample sourced with 3 mA and tested at 9.6 mm/s. . . . . 241

7.8 Spectrogram and amplitude variation of the most relevant components during preconditioning test ((a) and (b)) and during repeatability test ((c) and (d)) for the SP27 sample sourced with 3 mA and tested at 9.6 mm/s. . . . . 242

7.9 Spectrogram and amplitude variation of the most relevant components during preconditioning test ((a) and (b)) and during repeatability test ((c) and (d)) for the SP31 sample sourced with 3 mA and tested at 9.6 mm/s. . . . . 242

7.10 (a) Filtered fabric resistance (N=3, f=651), (b) Peaks detection and interpolation curves and (c) Peak-to-peak span for the SP29 embedded into a pair of leggings with 18% elastane 263

7.11 (a) Filtered fabric resistance (N=3, f=651), (b) Peaks detection and interpolation curves and (c) Peak-to-peak span for the SP27 embedded into a pair of leggings with 15% elastane 264

7.12 (a) Filtered fabric resistance (N=3, f=651), (b) Peaks detection and interpolation curves and (c) Peak-to-peak span for the SP27 embedded into a pair of leggings with 18% elastane 264

# List of Tables


2.1 Comparison between static and wearable platforms . . . . . 17

2.2 Area of investigation of static and wearable platforms and relative reference . . . . . 18

2.3 Fibre, yarn and fabric parameters influencing wrinkling (Leeder and Shishoo 1977) . . . . . 22

3.1 Fabric and stitch density counted in one inch (equivalent to 2.54 cm) of the four samples under investigation . . . . . 46

3.2 Mean values and standard deviations of the fabric parameters for the four samples under investigation considering 10 measurements . . . . . 47

4.1 Mean values and standard deviations of the fabric parameters for the four samples under investigation considering 10 measurements after preconditioning . . . . . 89

4.2 Comparison of loop lengths before and after preconditioning considering 10 measurements . . . . . 89

4.3 Regression curves for the SP29 sample sourced with 1 mA, tested at 9.6 mm/s and elongated at 12 and 16 mm during the first cycle . . . . . 104

6.1 Regression curves for the SP29 sample embedded into leggings with 18%elastane with the Visual Motion Tracking System . . . . . 156
6.2 Sensitivity for the SP29 integrated into 15% and 18% elastane leggings with the Visual Motion Tracking System . . . 167
6.3 Regression curves for the SP29 sample embedded into leggings with 18%elastane and tested with the HUMAC NORM System . . . . . 176
6.4 Sensitivity for the SP27 and SP29 integrated into 15% and 18% elastane leggings when studied with the HUMAC NORM System . . . . . 182
6.5 Comparison between method one and method two . . . . . 186

7.1 Preconditioning and repeatability tests in the Instron tensile machine . . . . . 221
7.2 Results of preconditioning and repeatability tests described in Table 7.1 of Appendix I (7.3.4) . . . . . 234
7.3 Signal-to-noise ratio for samples tested according to Table 7.1 of Appendix I (7.3.4) . . . . . 237

# Chapter 1

# Introduction

## 1.1 Background

Wearable sensing technology has developed rapidly over the last decades, becoming integrated into daily life. The high flexibility and comfort of wearable technology enable it to be used within various application areas (e.g. health, military, sport, domestic). Especially, over the past decades ***wearable sensors*** have gained the interest of researchers and clinicians thanks to their advantages. In fact, compared with standard measurement systems (e.g. electromagnetic tracking system, image-based techniques) they are lightweight, small, flexible and fitted closely to the human body. In particular, by embedding electronic components into a garment or integrating fibres and yarns with sensing properties (achieved by piezoresistive, piezoelectric or piezo capacitive materials), it is possible to transform a normal fabric into a ***sensing fabric***, which is able to detect physiological and mechanical parameters (e.g. posture, motion, respiration, heartbeat and joint angles).

The work presented in this thesis stems from the emerging need of applying textile-based wearable sensors (in particular electrically conductive fabrics)

as motion sensors. Measurements of the parameters of interest (e.g. joint angles) can be potentially achieved by tracking changes in the electrical resistance of the fabric positioned in the area of investigation.
The results of this research are applicable to other areas of investigation involving sensing fabrics to develop a wearable system based on the sensor information feedback (e.g. in rehabilitation, sport, etc).

## 1.2 Definition of wearable sensors

A sensor is a device that measures a physical quantity (pressure, temperature, light intensity etc) and converts it into a signal which can be stored and analysed. Sensors can be embedded into clothing and tailored to measure human motion and physiological parameters, including joint angles, heart rate and body posture. Sensors integrated in such a manner are *wearable* and make the fabric *smart*. Smart textiles represent a new and interesting area of investigation and a solution to the bulkiness of standard measurement systems, as largely described in Chapter 2.

## 1.3 Definition of fabrics

Fabrics are fibrous materials. The smallest unit is called **fibre** and their interlacement constitutes **thread**. Twisted threads form **yarn**. Thanks to different techniques such as knitting and weaving, yarn can be used to make a **fabric**. Figure 1.1 illustrates the fabric construction based on fabric structures:

- a) Woven: constructed by interlacing two or more threads at right angles to one another. The transverse threads are called *wefts*, the longitudinal threads *warps*;

- b) Knitted: formed by interlacing yarn or thread in a series of interconnections of loops of courses and wales. The *courses* are threads running horizontally across the fabric, whereas the *wales* run vertically;
- c) Non-Woven: made from filaments of fibre webs and strengthened by bonding techniques (e.g. mechanical interlocking by needling);
- d) Nets: produced from one thread and employing a single repeated movement to form loops.
- e) Braided: created by interweaving three or more yarns in a diagonally overlapping pattern;
- f) Tufted: consists of yarns inserted into fabric backing to form loops or cut loops (piles).

Starting from fibre, fabrics structures can be assembled in layers to form composites to be used in many industry areas (e.g. aerospace).

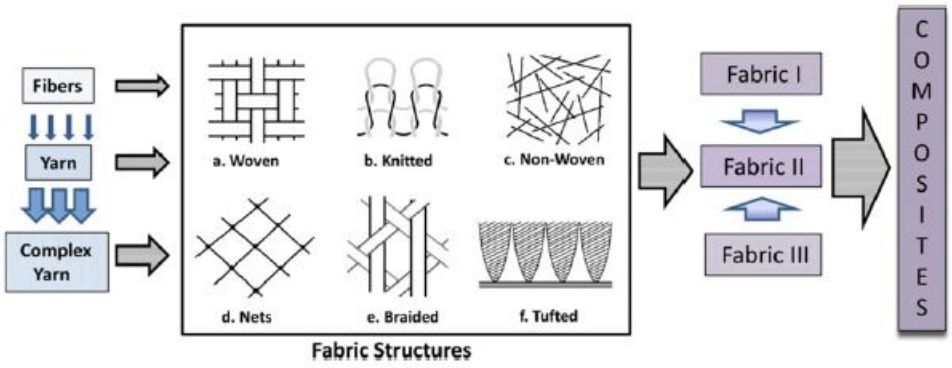


Figure 1.1: Fabric construction based on fabric structures: a) Woven, b) Knitted, c) Non-Woven, d) Nets, e) Braided and f) Tufted. Fabrics structures can be assembled in layers (e.g. three) to form composites (Castano and Flatau 2014)

Textiles are made from fibrous materials including fibres (e.g. natural or manufactured, short staples or continuous filaments), yarns (such as single strand or cabled) and fabrics (e.g. knitted, woven, braided or non-woven) (Chen 2009).

The fabric structure used in this thesis is the knit. Knits are easily deformable and compared to the other structures (e.g. woven, which are hard to deform) represent a better candidate to respond to deformation caused by an applied load or due to motion in a wearable application. In particular, fabrics made of conductive fibres described in this work have a sensing mechanism based on the changes of the electrical resistance responding to deformation.

## 1.4 Objectives

The aim of this thesis is to investigate both the characterisation and the use of knitted conductive textiles as wearable motion sensors. To improve the performance and the reliability of fabric-based sensors the electrical properties of conductive textiles require an attentive study during deformation. To fulfill this objective, this thesis first analyses the electrical behaviour of knitted conductive textiles during cyclic loading in a tensile machine. The reason is to determine the fabric electrical properties relative to extended structural deformations of the fibres (e.g. stretching) which change the conductivity of the sample.

Secondly, this research examines the integration of knitted conductive textiles into supporting garments as an example of the real life application of fabric transducer as motion sensors. Applied to the area of interest in the human body (e.g. across the knee joint), the samples undergo elongation-recovery phases similarly to the study in the tensile machine. In this case,

the aim is to analyse the effect of the garment on the variation of fabric electrical properties during human motion.

## 1.5 Overview of thesis

*Chapter 2* presents an overview of the methods used for human motion analysis and, in particular, of smart fabrics sensors belonging to the category of wearable platforms. Sensing features, parameters and properties influencing the fibre, the yarn and the fabric are presented to make the reader familiar with terms, phenomena and issues presented in the rest of the thesis.

*Chapter 3* describes the knitted conductive textiles studied in this thesis and the methods used for their electrical characterisation during cyclic unidirectional elongation in a tensile machine. The experimental set-up required for a proper investigation is introduced, consisting of an electronic circuitry directly connected to the fabric, clamps for reliable connection to the testing machine and an acquisition system and data processing algorithms based on the extraction of *ad-hoc* features of interest.

*Chapter 4* analyses the electrical response of knitted conductive samples to a considerable number of cycles of deformation. In particular, the effects of an extended cyclic mechanical loading (preconditioning) and repeatability test on the changes in the electrical properties are investigated. The factors influencing the electrical features of the samples, the time and elongation dependent behaviours are also analysed.

*Chapter 5* regards the integration of knitted conductive textiles into supporting garments for analysing their performances in view of their application as wearable motion sensors. The conductive samples, the leggings and the way the specimens are integrated into them are presented. In par-

ticular, two measurement systems (for free and constrained motions) are described to capture the fabric electrical resistance variation during the cyclic deformation of the garment they are integrated in.

*Chapter 6* discusses the results of the application of knitted conductive textiles into garments during cyclic deformation due to both free and constrained movements performed by/over a participant. The influence of the supporting garment on the electrical properties of the fabrics is investigated and compared to samples' behaviour in the tensile machine. A comparison of the outcomes of the two measurement systems, advantages and disadvantages are also provided.

*Chapter 7* contains the overall discussion and conclusions of the work and recommendations for further work.

# Chapter 2

# Literature Review

## 2.1 Introduction

The analysis of human motion is an important area of research. In the bio-engineering and rehabilitation fields, it is motivated by different goals, such as comparing normal with pathological movements, planning and evaluating treatment protocols and assessing the design of orthosis and prosthesis. In sports medicine, motion analysis plays a key role in professional training, improving athletic performance and preventing injuries.

To measure human motion, image-based methods have been developed, such as: photogrammetry, the optoelectric technique and video analysis. Photogrammetric systems have been used to record two or three-dimensional images of posture by either light-reflective markers or light-emitting diodes affixed to the human body while films capture data for measuring the orientation of body segments. The same principles have been applied by both optoelectric and video systems, with optoelectric sensing units and cameras of high sampling rate being used, respectively, for collecting the data instead of films. Nonetheless, these methods are complicated to set up, time-consuming to operate and can only be applied

within laboratory environments.

To solve the relevant application problems of the image-based methods, electronic sensors and systems with advanced technology have been employed. For instance, inertial sensors (accelerometers, gyroscopes or a combination of the two) and flexible angular sensors (e.g. strain gauges) have been widely used as *wearable sensors* to gather data about locomotion (acceleration of the joint, joint angle, joint torque, velocity, angular displacement, etc.).

Nowadays, the convergence of electronics and textiles (e-textiles) has developed smart materials, whose sensing properties represent a new and interesting field to investigate.

## 2.2 Human motion

Human movement is the results of complex and highly coordinated mechanical interaction between bones, muscles, ligaments and joints within the musculoskeletal system (Lu and Chang 2012). Any movement derives from the action of forces (internal and external) applied to an object, whose changes in position and velocity depend on the magnitude and direction of the applied forces. Newton's laws of motion describe the relationship between the changing force and the resultant change in movement, and are applicable to all forms of movement, including human locomotion.

Human motion analysis is the study of human motion in terms of body movement, body mechanics and activity of the muscles. A special area of investigation of human motion is gait analysis which studies specifically human walking and any condition causing degradation, instability or disability of movement.

## 2.3 Techniques for human motion analysis

Monitoring motor activities is one of the first goals of many researchers interested in clinical applications of wearable technology. Several methods of collecting and analysing movement data have therefore been proposed over the last few centuries. Figure 2.1 outlines two techniques used for human motion analysis: static and wearable platforms. Examples of motion analysis for both categories are reported in 2.3.1 and 2.3.2, respectively.

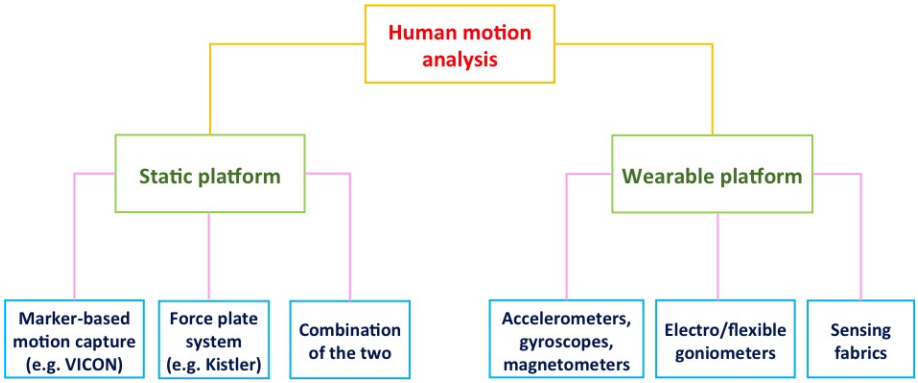


Figure 2.1: Scheme of the platforms used for human motion analysis

### 2.3.1 Static platform for human motion analysis

Patterns of locomotion for both humans and animals were recorded with the first motion picture cameras in the late 19th century. Eadweard Muybridge (1830-1904) improved photography by creating a camera with a shutter speed of up to 1/100 of a second to capture the rapid limb movements of horses in motion and, afterwards, of birds and humans (Allard, Stokes, and Blanchi 1995). Muybridge's invention continued to develop in the 20th century with the aid of computer vision, techniques of pattern recognition, photogrammetry and, in particular, with stereophotogrammetry (i.e. technique of measuring 3D landmark coordinates from photographs, radiographs and video images).

The combination of photogrammetry and the geometrical properties of central projection from multi-camera observations brought Braune and Fisher to estimate the 3D position data from digitised and noisy image data (Chiari et al. 2005). In the 1890s, Braune and Fisher used stereophotogrammetry and ground reaction force (GRF) measurements to study the biomechanics of human gait under loaded and unloaded conditions with the 3D mathematical technique based on Newtonian mechanics (Sutherland 2001). GRF is the force exerted by the ground on a body in contact with it and relates to Newton's third law of motion (relating to an equal and opposite reaction force), and to the second law of motion (relating to deceleration during an impact or acceleration during propulsion).

From the 20th century onwards, the knowledge of anatomy and mechanics increased, as well as the measurement technology, resulting in an improvement of the human motion analysis. In particular, 3D analysis of human motion became feasible with the collocation of video camera systems and high-speed computers. One of the first systems to become commercially available was the *Ariel Performance Analysis System (APAS)*, which is a video-based 3D motion analysis system that captures video from multiple cameras simultaneously and performs a biomechanical analysis automatically.

The need of automating the processing and analysing led to the development of the *3D Vicon motion capture system* thanks to Professor J. Paul, M. Jarrett and B. Andrews. This system was created to capture human movement data in numerical digits instead of analog data and continues, nowadays, to be widely used in the study of human motion (Figure 2.2).

Another way to perform gait analysis and provide both kinematic and kinetic information in spatial coordination is the combination of motion capture system and force plate system, such as the VICON motion capture

system and the Kistler force plate system. The motion capture system is marker-based, requiring the subject to be placed with numerous markers on the body. This system can be very accurate but also expensive, impractical to move and only suitable for laboratory settings. The force plate measures and records the ground reaction forces and their point of application (centre of pressure, COP). For this reason, force platforms are mounted on the floor and need to be stepped correctly by the subject to obtain good results. This system is costly, only found at laboratories and clinics and suitable for measuring the dynamics of the lower limbs only.
All the disadvantages related to the static platforms pushed researchers to investigate wearable sensors (Wong, Wong, and Lo 2007). In fact, compared to the systems mentioned above, these wearable systems are smaller, lightweight, mobile and a generally less expensive solution for measurements in home settings (Greene 2010, Bamberg 2008).

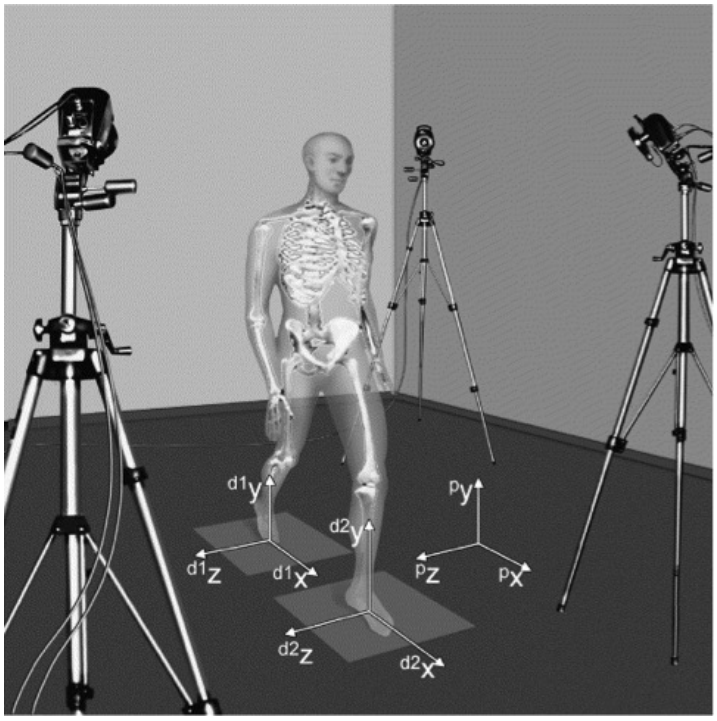


Figure 2.2: Example of motion camera system used in a movement analysis laboratory (Cappozzo et al. 2005)

### 2.3.2 Wearable platforms for human motion analysis

Motion analysis based on wearable platforms constitutes an alternative solution to stationary devices, that are expensive, time consuming and cannot be applied outside the laboratory environment (2.3.1). To enable this, motion sensors are worn or attached to various parts of the human body and thus recorded movement signal used to analyse motion. In this way, electronic positional sensors and other systems are used to track human posture and movement, measure gait parameters (Mayagoitia, Nene, and Veltink 2002), predict falls (Bourke, OBrien, and Lyons 2007) and detect activities of daily living (Atallah et al. 2010, Yang C-C 2010). The basic sensors and their features are described in the following.

#### Accelerometers, gyroscopes and magnetometers

*Accelerometer* is a type of positional sensor that measures applied acceleration acting along its sensitive axis. The common operation principle is based on a mechanical sensing element that comprises a proof mass attached to a mechanical suspension system, with respect to a reference frame. The proof mass can be forced to deflect by the inertial force due to acceleration or gravity according to Newton's second law. By using the displacement of the proof mass relative to the reference frame, acceleration can be electrically measured.

Accelerometers can be used for long-term monitoring of human movements, physical activity, fall detection (Bourke, OBrien, and Lyons 2007), postural orientation (Takeda et al. 2009b), activity classification and estimation of temporal gait parameters (Yang et al. 2011; Takeda et al. 2009a). The disadvantages are computational problems for determining the angles (Mayagoitia, Nene, and Veltink 2002). In fact, the double integration of the measured angular acceleration (required for calculating the angular po-

sition) is usually a source of drift if the offset in the signals being integrated is not properly compensated.

*Gyroscopes* are angular velocity sensors based on the concept of measuring the Coriolis force, which is an apparent force proportional to the angular rate of rotation in a rotating reference frame. By detecting the linear motion from the Coriolis force and performing an integration of the gyroscopic signal, the angular rate can thus be obtained.

Gyroscopes can be applied for motion classification (Tunel, Altun, and Barshan 2009), posture (Takeda et al. 2009b) and spatio-temporal parameters estimation (Aminian et al. 2002). In gait analysis, a gyroscope is usually combined with an accelerometer to construct a complete initial sensing system (Figure 2.3).

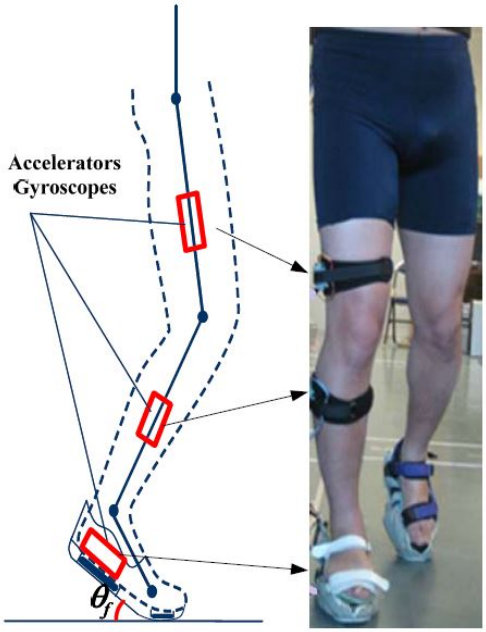


Figure 2.3: Angular displacements based on three pairs of accelerometers and gyroscopes attached on the foot, calf and thigh (Tao 2012)

*Magnetoresistive sensors* are based on the magnetoresistive effect, which refers to the change in the resistivity of a current carrying ferromagnetic material resulting from a magnetic field. The resistance change is proportional to the tilt angle in relation to the magnetic field direction. Based on this magnetoresistive effect, magnetoresistive sensors can estimate changes in the orientation of a body segment in relation to the magnetic North or the vertical axis in the gait analysis (Graham 2004).
The electromagnetic tracking system has been used in human posture and movement analysis (Finley and Lee 2003) and spinal motion (Bull and McGregor 2000).

**Electro-flexible goniometers**

*Electrogoniometers* are very thin pieces of wire, sensitive to bending (the amount of bending changes the output voltage). Due to the direct proportionality between the angle and their output, electrogoniometers can be used to measure joint angles (Legnani et al. 2000) and track human motion (Zheng, Black, and Harris 2005). Particularly convenient are *flexible goniometers*, which output a voltage related to the angular position of two small blocks fixed to the body segments. Then, by using a manufacturer supplied scale factor specific to the transducer, the voltage is converted to an angle that can be displayed in real time or stored on a computer equipped with an analog-to-digital data acquisition card.
Among the flexible goniometers used in gait analysis we find *strain gauges*. They are lightweight, portable, easily applicable and adaptable to different body segments. Moreover, they provide an output directly proportional to the angle, do not restrict movements and thus overcome the major drawback of fixed-hinge electrogoniometers, namely the presence of a fixed centre of rotation, in contrast with the variable rotation centre of human joints.

Nonetheless, strain gauges are not sufficiently robust for daily clinical usage.

Figure 2.4(a) shows an example of an electrogoniometer consisting of two bases (which must be fixed to the two bodies whose relative orientation is required) and a measuring cable. The measuring cable has a core made of four strain-gauges (two in case of a planar electrogoniometer) constituting the branches of a Wheatstone's bridge. The difference of the gauge lengths has an effect on the output of the bridge and, thus, on the flexion angle.

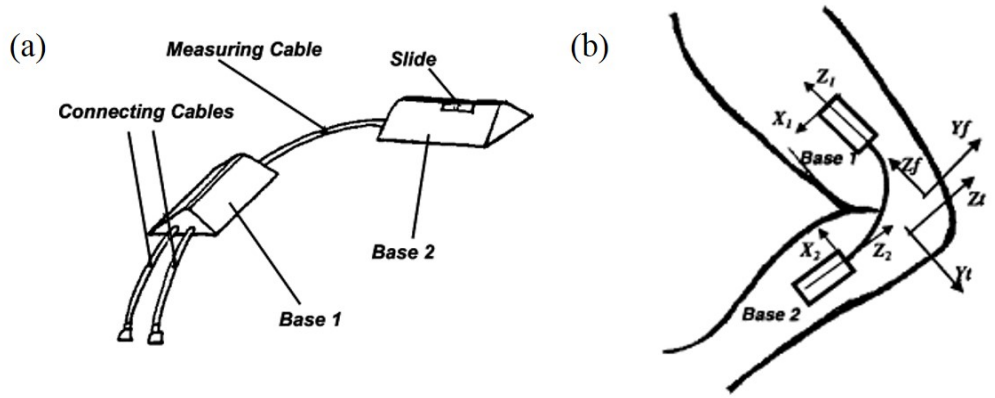


Figure 2.4: Example of (a) a biplanar electrogoniometer and (b) its application along the knee joint (Legnani et al. 2000)

### Sensing fabrics

Despite their advantages, wearable sensors suffer from some drawbacks. Sensors must be placed correctly and securely to prevent any unwanted movement (Kavanagh and Menz 2008) and, depending on the type of sensor used, the related signal processing must be corrected for gravity, noise and signal drift (Luinge and Veltink 2005). Moreover, wearable sensors may influence the subjects' behaviour during the measurements of interest.

An unobtrusive solution, comfortable to wear, easy to use, and with no long preparation requirement, is using *smart fabric sensors*. They can provide the same measurements of standard systems by using only the electrical

properties of the threads they are made of. Compared with other wearable sensors, sensing fabrics are more flexible and comfortable, especially when measuring human posture and movement.

### 2.3.3 Comparison between static and wearable platforms and areas of application

A comparison between the general advantages and disadvantages of static and wearable platforms is presented in Table 2.1. The areas of application of each system is reported in Table 2.2.

Table 2.1: Comparison between static and wearable platforms

| **Platform** | **Advantages** | **Disadvantages** |
|---|---|---|
| *Static* | • Accuracy<br>• Non restriction by power consumption<br>• Simultaneous analysis of multiple gait parameters<br>• Better repeatability, reproducibility<br>• Less external factor interference | • Expensive equipment and tests<br>• Motion restriction due to the measurement system<br>• Limitation to laboratory settings<br>• Complicated set-up<br>• Time-consuming operations<br>• Bulkiness |
| *Wearable* | • Cheaper systems<br>• Easy motion tracking due to high body contact<br>• Deployment in any place<br>• Increasing usability with wireless systems<br>• Increasing availability of miniaturised sensors<br>• Small, lightweight dimensions<br>• Comfort to body shape<br>• Flexibility | • Power consumption restrictions due to limited battery duration<br>• Susceptible to noise and interference of external factors<br>• May require a cable connection to a base unit (not all wireless)<br>• Limited repeatability if not properly secured to the body |

Table 2.2: Area of investigation of static and wearable platforms and relative reference

| **Platform** | **Application** | **Reference** |
|---|---|---|
| *Accelerometer* | • Posture<br>• Temporal gait parameters<br>• Gait analysis<br>• Fall detection | • Takeda et al. 2009b<br>• Yang et al. 2011<br>• Takeda et al. 2009a<br>• Bourke, OBrien, and Lyons 2007 |
| *Gyroscope* | • Motion classification<br>• Posture<br>• Spatio-temporal parameters | • Tunel, Altun, and Barshan 2009<br>• Takeda et al. 2009b<br>• Aminian et al. 2002 |
| *Electromagnetic sensor* | • Posture<br>• Spinal motion | • Finley and Lee 2003<br>• Bull and McGregor 2000 |
| *Flexible angular sensor* | • Motion tracking<br>• Joint angle | • Zheng, Black, and Harris 2005<br>• Legnani et al. 2000 |
| *Sensing Fabrics* | • Joint flexion angle<br>• Physiological and biomechanical variables<br>• Health care system<br>• Injury prevention | • Shyr et al. 2014<br>• Scilingo et al. 2005<br>• Paradiso et al. 2005<br>• Munro et al. 2008 |

## 2.4 Smart fabric sensors

Smart fabric sensors (SFS) are fabrics that have been treated or modified to generally act as sensors. As reported in Castano and Flatau 2014, modifications enabling sensing features can be introduced at any level of the fabric structure represented in Figure 1.1:

- At a *fibre level* by making the fibre out of conductive materials;
- At a *yarn level* by interlacing sensing fibres with non-sensing fibres;
- At a *fabric level* by introducing sensing fibres (by knitting, weaving and embroidering) or by coating the fabric surface with sensing materials.

Thus, smart fabric sensors can be made sensitive to multiple stimuli, including mechanical, chemical, electrical, magnetic, thermal and optical (e.g. changes in pressure, force, electrical current, temperature and so on).

The investigation of the parameters and properties influencing the fibre, yarn and fabric level is therefore important to discuss. For instance, the *nature of fibres* determines the characteristics of the fabrics. Synthetic fibres (e.g. polyester) are hydrophobic, with less water absorption than natural fibres (Castano and Flatau 2014). This means that the fibre diameter does not increase upon wetting. This property can be preferred, for instance, when metalised connective elements are to be integrated with the fabric structure as this might reduce the possibility of changes in the overall fabric conductivity due to sweat. More generally, the presence of polyester will be useful in case of fabric employed in wearable applications where the close contact with skin implies not only sweat but also washing cycles. Also, when compared with natural fibres (e.g. cotton), polyester guarantees good wrinkle recovery for the garment they are integrated in.

The properties of textile yarns can be described in terms of:

1. *Linear density*, expressed in denier (weight in grams per 9000 m), tex or decitex (weight in grams per 1000 or 10000 m);
2. *Strength*, expressed in tenacity (i.e. measure of force required to break a yarn or the individual fibre);
3. *Percentage of elongation at break*.

Knitting yarns have a higher percentage of elongation at break, are more resilient and easily deformable when compared with woven, which are stable fabrics and hard to deform.

According to the application of the fabric sensors, the yarn should fulfil specific requirements. For instance, for a fabric sensor to be incorporated into a joint section (e.g. knee) of a garment, the yarn should have:

- Lower linear density to guarantee a small mechanical bending resistance. In fact, increasing fibre linear density or decreasing fineness increases bending rigidity;
- Machine sewability;
- A high percentage of elongation at break;
- Good tenacity.

*Yarn fineness* determines not only flexibility but also resistance to permanent deformation. *Wrinkling* may be defined as the unwanted residual deformation that can make the fabric loose after strain or wear. As explained in Sinclair 2014, when fibres are subjected to strain, they retain a certain degree of residual deformation after removing the deforming forces. The residual deformation depends on the fibre's viscoelastic properties and on the frictional force, which is related to the inter-fibre and inter-yarn

friction and pressure. Thus, the yarn and fabric construction affect the frictional force and also the nature and severity of the fibre deformations when the fabric is deformated. Also, the residual deformation depends on the degree and duration of the original deformation and on temperature and moisture during and after deformation. Therefore, fibres cannot be considered perfectly elastic but viscoelastic. This means that during stretching they undergo stress relaxation; when recovering, they show an instantaneous partial recovery followed by a slow time-dependent recovery, that is characteristic of viscoelastic materials.

According to Castano and Flatau 2014, the degree of *yarn twist* affects the tensile properties, low load deformations (e.g. wrinkle, recovery) and stiffness. Sinclair 2014, on the other hand, reports that changing the yarn twist does not appear to be an effective way of reducing wrinkling although very high twist levels are considered to effect some improvement. Sinclair 2014 considers that the fabric wrinkling performance is affected by two main fabric parameters: the state of relaxation (i.e. stress relaxation) of the fabric and the freedom of *yarn mobility*, both depending upon the recovery properties of the fibres. Thus, *fabric wrinkling* improves with an increase in fabric mass, fabric thickness and relaxation, and with an increase of yarn mobility which is related to the fabric' state of relaxation, tightness and number of yarn intersections per unit area (i.e. yarn float length).

The wrinkle recovery of a fabric can be achieved by:

- changing the fibre at molecular level (e.g. by changing fibre type and by chemical treatment);
- constructing the yarn, fabric and garment in a way that minimises the strains during bending and the interaction between fibres and yarns.

Table 2.3: Fibre, yarn and fabric parameters influencing wrinkling (Leeder and Shishoo 1977)

| **Fibre** | **Yarn** | **Fabric** |
|---|---|---|
| • Type | • Type | |
| • Viscoelastic bending parameters | • Ply and twist level | • Structure and crimp |
| • Viscoelastic torsional parameters | • Twist direction | • Mass per unit area |
| • Cross-sectional shape | • Crimp | • Thickness |
| • Crimp | • Cross-sectional shape | • Surface hairiness |
| • Diameter | • Linear density | • State of relaxation |
| • Diameter distribution | • Diameter | • Sett |
| • Friction | • Lateral pressures | • Compactness |
| • Chemical or physical treatment | • Construction | • Mechanical finishing |

Table 2.3 lists the fibre, yarn and fabric parameters (some of which are discussed in this section) that play a role in wrinkling and wrinkle recovery (Leeder and Shishoo 1977). It is important to notice that parameters influencing wrinkling and causing, therefore, loosening of the fabric are many and belong to the three levels of the fabric structure. This indicates the complexity of the phenomenon, which affects any fabric undergoing strain.

## 2.5 Techniques to enable sensing functionality into fabrics

Sensing functionality can be created at any level of the fabric structure (Figure 1.1) by intrinsic and extrinsic modifications to textile substrates. *Extrinsic* modifications can be achieved:

- By attaching sensing elements (e.g. sensors and electronic components) to the surface of a fabric. Fabrics that are modified in such a manner are referred to as *electronic textiles* or *e-textiles*. In e-textiles, conductive lines are established by attaching conventional wires or sewing conductive threads, by replacing non-conductive fibres with conductive ones or by printing stretchable conduction lines (i.e. inks, polymers). Typical interconnects to data acquisition systems are conductive yarns (e.g. stainless steel staple fibres).

- By coating piezoresistive (Sawhney et al. 2006), piezoelectric (Kim et al. 2009), or piezocapacitive materials (Taya, Kim, and Ono 1998), usually in the form of polymers for their elastic properties. In case of piezoresistive coating, the application of strain to the substrate changes the electrical resistance. Coatings are either externally modified by conductive fillers or intrinsically sensitive to changes in elongation, pressure and so on. The coated sensor characteristics will depend on several factors, such as: the composition of the coating, the geometry of the yarn or fabric substrate and how the coating permeates the substrate.

*Intrinsic* modifications enabling sensing features relate to fibres and yarns made of materials which are sensitive to different mechanical or electrical stimuli. Conductive properties can be given to thread by different tech-

niques during and after the manufacturing process, as illustrated in Figure 2.5. During manufacturing, conductive threads are created, for instance, by coating at a fibre or yarn level, by twisting metal wire with base material (Figure 2.6) or with an extruded wire. After manufacturing, conductivity is enabled by coating techniques: film coating (e.g. sputtering), electrochemical (e.g. vapor coating) and dipping or, alternately, by integrating conductive yarns into a textile structure by knitting, weaving or embroidering (Wijesiriwardana, Dias, and Mukhopadhyay 2003).

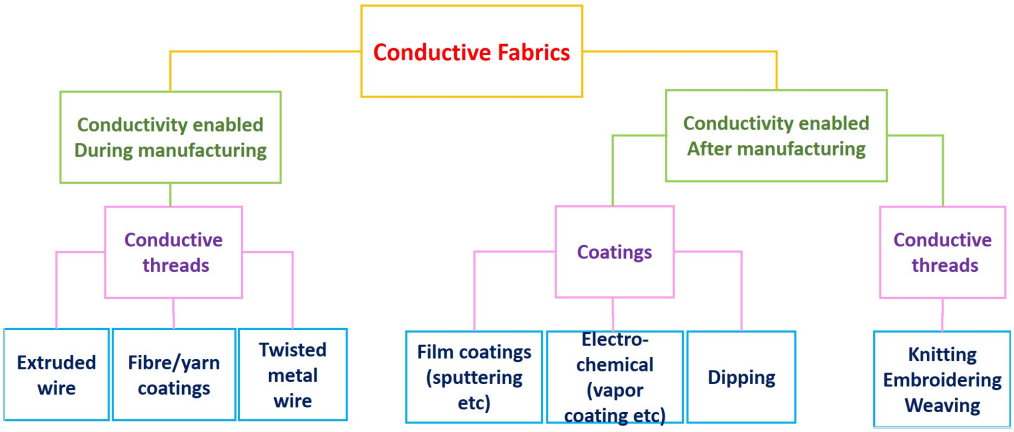


Figure 2.5: Scheme of techniques enabling conductivity in fabrics (Modified from Castano and Flatau 2014)

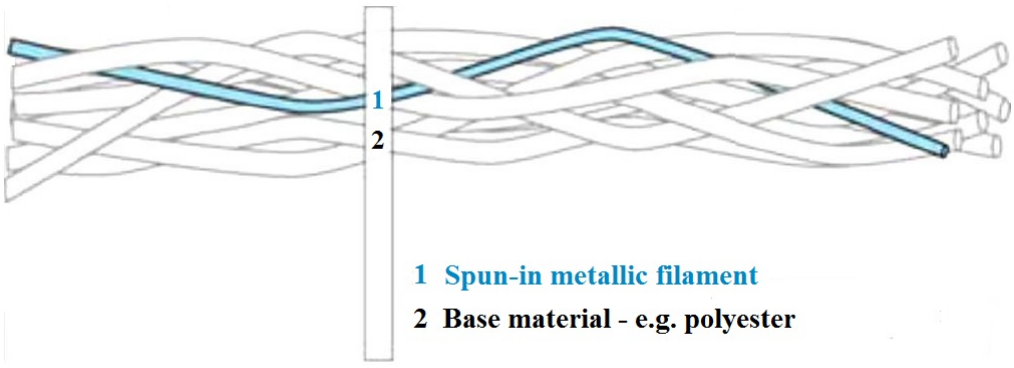


Figure 2.6: Schematic of conductive fibre twisted with normal fibres (e.g. polyester) (Modified from Stoppa and Chiolerio 2014)

Conductive polymers can be used to make fibres with sensing properties. Conductive polymers are obtained by adding doping particles to provide enough conductive contacts to enable the passage of current or due to electron tunneling effect (case of nanotubes and nanoparticles). Polymers can be intrinsically or extrinsically conductive. Intrinsically conductive polymers (ICPs) do not need to be doped to achieve high conductivity (e.g. polypyrrole). Extrinsically conductive polymers (ECPs) are obtained by doping with conductive fillers such as carbon (carbon black, CB), carbon nanotubes (CNTs) or inorganic particles (e.g. metal). In particular, carbon doped polymers can achieve very high conductivity. However, by incorporating, for instance, at least 10% concentration of carbon nanotubes or a smaller concentration of graphene, fibres become stiff and fabric construction is made more difficult compared to metal blended yarns (Skorobogatiy and Qu 2015). Conductivity range of materials are illustrated in Figure 2.7 (Kaur et al. 2015).

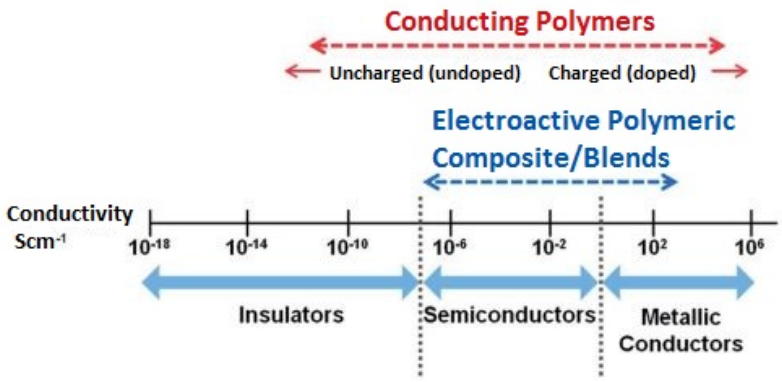


Figure 2.7: Conductivity range of materials (Kaur et al. 2015)

Sensing functionality enabled into fabrics makes it possible to measure many parameters including force, pressure and strain variations. For instance, the sensing mechanics of a pressure sensor is that the pressure applied to conductive yarns changes the contact resistance of intersecting yarns. By detecting the position where the change of the resistance oc-

curs, the location of the applied pressure can be identified. The samples used in this thesis belong to the category of fabric strain sensors, which are discussed in section 2.6.

## 2.6 Fabric strain sensors

Strain sensors (or strain gauges) are devices that convert physical deformation into electrical signals. What is required for materials to be employed as flexible strain sensors is the *piezoresistive effect*, according to which the electrical resistance of the material changes with stress or deformation. In other words, the change in resistance is correlated with the change in strain amplitude.

Fabrics can be made sensitive to mechanical strain according to the techniques described in section 2.5. Metal fibres (e.g. stainless steel fibres) can be knitted to construct a piezoresistive textile. The piezoresistive behaviour of knitted fabrics is explained as the change of conductive contacts (due to local deformation of textile structure) affecting the charge path. This is due not only to the different interaction among the single filaments inside the yarn but also to the deformation of the loops of the knitted fabrics during the stretch-recovery phases (Wijesiriwardana, Dias, and Mukhopadhyay 2003).

Polymers are also interesting when developing strain sensors but, especially, in case of large strain (Mattmann, Clemens, and Trster 2008). For instance, elastomeric polymers have been largely used for strain sensor applications thanks to their ability to deform elastically to large strains while providing electrical conductivity (De Focatiis, Hull, and Sanchez-Valencia 2012).

Key factors for textile strain sensors are:

- Large gauge factor (i.e. the change in electrical resistance, $\Delta R$, rel-

ative to the resistance at zero strain, $R_0$, with respect to the change in length, $\Delta l$, relative to the original lenght, $l_0$);

- High stability (repeatability of the sensing signals over many cycles);
- Large sensing range (to cover the applied strain of the desired applications);
- The sensing response of the textile must be easily measurable (without requiring complex circuits or processing techniques);
- The electrical properties should correlate well to the magnitude of the applied strain (to allow computation of strain based on measurement of resistance) (Seyedin et al. 2015).

The possibility of using textiles as strain sensors is beneficial for those applications for which conventional sensors are not suitable due to their rigid mechanical properties. In fact, traditional strain sensors are made of metals or rigid materials that offer limited stretchability and sensing range. Thus, once embedded in a textile structure, they are unsuitable for practical applications. On the other hand, textile-based strain sensors are flexible, wearable and capable of large sensing range.

Integrating strain sensors into textiles leads to new applications. For instance, when attaching the sensor in the knee or elbow region, the bending angle of the joint can be measured (Figure 2.8). Other applications are: monitoring of biomedical parameters (Figure 2.9) and sport rehabilitation/injury prevention (Figure 2.10).

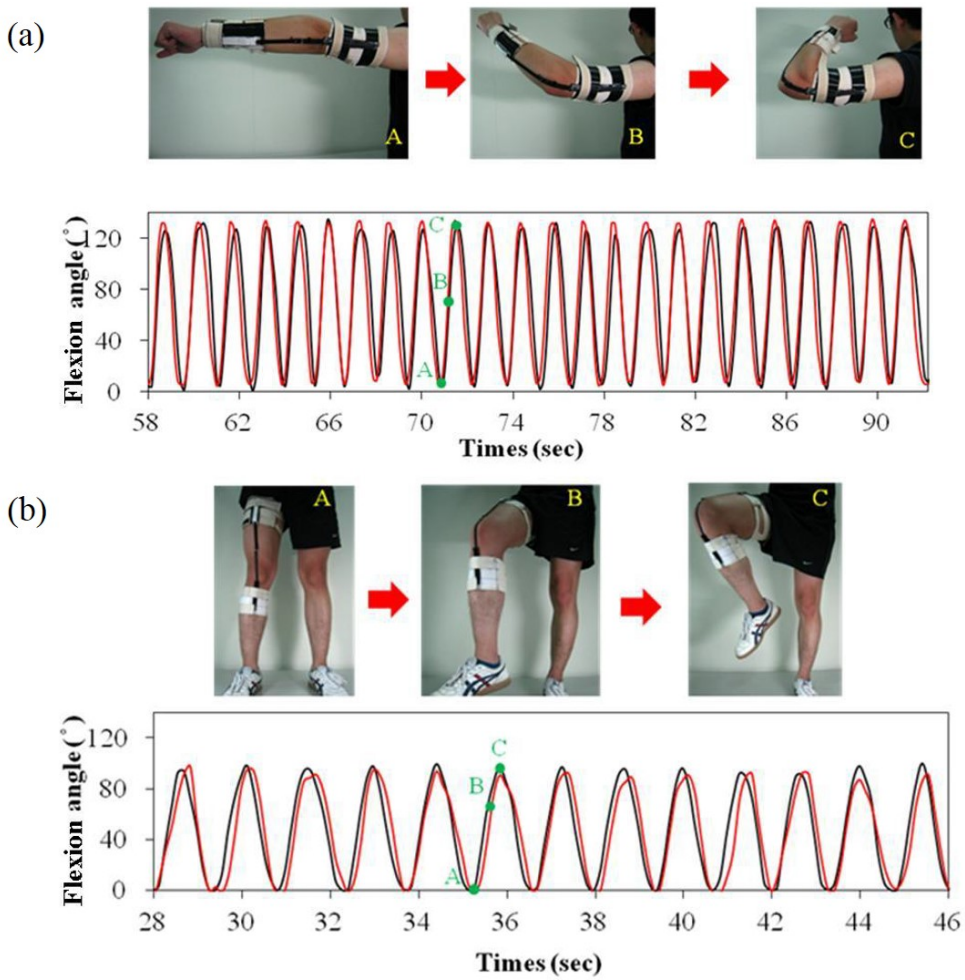


Figure 2.8: Example of flexion angle-resistance measurements proposed by Shyr et al. 2014 for (a) elbow and (b) knee movements. The strain-resistance sensor is an elastic conductive webbing made of polyamide fibre coated with carbon particles and polyester yarn. The flexion angle measured by the wearable gesture sensing device (red line) was compared with a variable resistor and a protractor (black line). The resistance of the elastic conductive webbing to the flexion angle showed a good linear relationship during the stretch-recovery cycles within 30% strain.

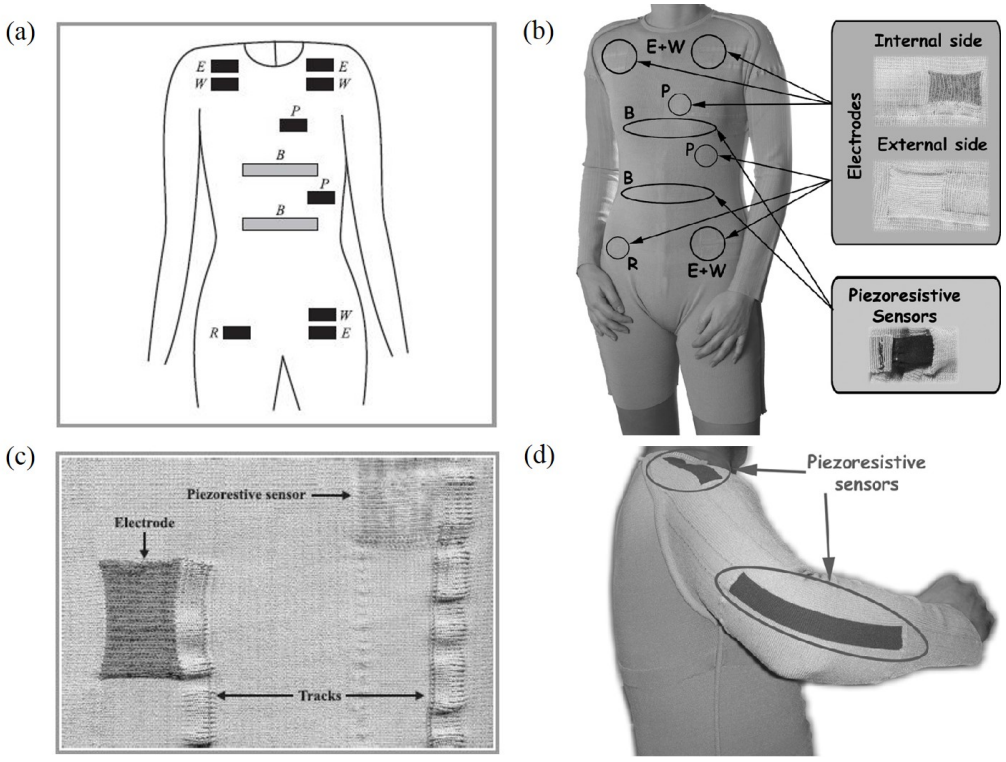


Figure 2.9: Example of wearable instrumented garment (named WEALTHY) based on knitted integrated sensors and conceived for electrocardiogram (ECG), respiration, activity and respiration monitoring (Paradiso et al. 2005). The fabric electrodes are realised with stainless-steel based yarns, whereas the piezoresistive fabric sensors are made of lycra fabric coated with carbon-loaded rubber and commercial electroconductive yarn (Scilingo et al. 2005). (a-b) Prototype model with: E-Einthoven, W-Wilson, R-reference, P-precordial leads for ECG measurement and B-breathing sensor (c) Part of the WEALTHY interface (d) Movement sensors



Figure 2.10: Example of wearable biofeedback system (called the Intelligent Knee Sleeve) formed by polypyrrole-coated nylon-lycra sensor integrated into a base sleeve together with appropriate electronic circuitry (provided by CSIRO Textile and Fibre Technology). The system is conceived to alert the wearer that the desired knee flexion angle (i.e. a predetermined threshold resistance based on the stretching of the fabric sensor) is achieved according to a preventing injury program (Munro et al. 2008)

## 2.7 Influencing factors of the fabric resistance

The overall electrical characteristics of the fabric sensors are determined by the electro-conductive area (ECA) embedded in the textile. In addition to the material properties, the size, shape and the binding elements of the fibres (namely different types of stitches) determine the electrical resistance of the ECA and its response to structural deformation (e.g. stretching, bending, twisting and compression). When knitted fabrics are subjected to strain, fibre/yarn deformations and slippages between the fibre contact areas of stitches occur (Wijesiriwardana, Dias, and Mukhopadhyay 2003). In particular, knitted strain sensors are electrically affected by the deformation caused by stretching (and recovery), which changes their conductivity.

Many works have investigated the relationship between the resistance and the elongation of conductive fabrics. For instance, Zhang et al. 2005 studied the electrical conductive fabrics as resistive circuit network, whose basic element (i.e. the unit loop) comprised the resistance contributions due to the contact force of the interlapped yarns and the intrinsic resistance of the metallic yarns used. In particular, the dependence of the resistance on the elongation was associated to the change of contact resistance (i.e. related to the contact force between yarns) during stretching. Afterwards, Li et al. 2010 modelled the resistive network of conductive knitted stitches with analytical equations for different numbers of courses and wales and described with empirical equations the different electrical contributions for fabrics unidirectionally extended (Li et al. 2012). The elongation dependent behaviour of fabrics knitted with different stitch dimensions, yarns and elongation directions was also investigated (Ehrmann et al. 2014).
Nonetheless, to apply knitted conductive textiles as wearable motion sen-

sors, the electrical response of such fabrics should be studied considering a large number of cycles of fabric deformation (i.e. hundreds of cycles of stretch-recovery and not tens, as reported in the literature so far). This is the novel contribution discussed in this thesis in which the effects of an extended cyclic mechanical loading (preconditioning) on the electrical properties (e.g. stabilisation and repeatability after a period of rest) were investigated for knit patterns made of 20% stainless steel fibres and 80% polyester.

According to the methods described in literature, the variation of fabric electrical resistance is due to factors correlated to each other:

- The length variation of the conductive yarn in the knitted structure, which results in a variation of resistance. This contribution is called *length-related resistance*, $R_l$ (subsection 2.7.1);
- The variation of the contact forces between stitches in the conductive area which leads to a variation of the *contact resistance*, $R_c$, between loops (subsection 2.7.2);
- The parameters affecting the mechanics and the condition of the fabrics (subsection 2.7.3);
- The geometry of the loop (subsection 2.7.4) and the phenomenon of fibre-to-fibre slippage (subsection 2.7.5).

### 2.7.1 Length-related resistance

The *length-related resistance* can be described according to Ohm's law (Shedd and Hershey 1913) by Equation 2.1:

$$R_{\mathrm{l}} = \frac{L}{\sigma A} \tag{2.1}$$

According to Ohm's law, the resistance of a conductive yarn changes when it is stretched as it is directly proportional to the wire length, $L$, and inversely proportional to its conductivity, $\sigma$ and cross-sectional area, $A$. When a knitted textile is subjected to a uniaxial strain the length of a stitch increases and the cross-sectional area of the conductive fibres decreases (opposing increasing resistance to any flow of current). This thesis shows that this is due to the slippage of the yarns in the loop during the extension and the overall loosening of the fabric after extended use. Thus, when considering only the effect of the length-related resistance, the fabric resistance increases with elongation according to Equation 2.1.

Nonetheless, when the elongation further increases, it is also necessary to take into account the contact resistance $R_c$ as the contact forces between adjacent loops increase. This results in better contact, adds parallel conductivity paths and leads to a decreased overall resistance.

### 2.7.2 Contact resistance

To account for the effects of the oxidation at the fibres' surfaces (described in section 4.5.2), the *contact resistance* between two conductive fibres (e.g. stainless steel fibres) can be described by using a modified formula very similar to the one originally proposed by Holm in his contact theory (Holm 1967):

$$R_{\mathrm{c}} = \frac{\rho_{\mathrm{c}}}{2}\sqrt{\frac{\pi H}{nP}} \tag{2.2}$$

Where: $\rho_{\mathrm{c}}$ is the *contact* electrical resistivity, $H$ represents the material hardness, $n$ the number of contact points and $P$ is the contact pressure, both depending on the sensor design. Differently from the original formula by Holm, $\rho_{\mathrm{c}}$ is not only the electrical resistivity of the conductive materials but it is the resistivity of the whole contact (conductors and contact

surfaces) and, consequently, it takes into consideration all the factors that influence the contact resistivity (e.g. $\rho_c$ is dependent on the current flowing through the fabric). The contact surfaces of the metallic fibres are not affected by the stretching of the fabrics and the applied tension but by the presence of oxidation layers or environmental humidity (Yin, DHaese, and Nysten 2015). The material hardness is assumed constant for a given conductive yarn and not influenced by the fabric elongation, whereas the number of contact points and the contact pressure depend on the applied strain. Thus, while the knitted fabric is under strain, changes in $R_c$ are caused by the change of the contact force acting on the two overlapped yarns during the deformation process of the fabric. In particular, the contact resistance decreases with higher contact pressure or increased number of contact points. For instance, by stretching the textile in the wale (i.e. vertical) direction the contact pressure between the interlocked fibres increases and, hence, the contact resistance of the fibres at the interlocks decreases.

### 2.7.3 Fabric mechanical parameters

The overall electrical resistance of conductive fabrics is related to the yarn length (according to Equation 2.1) and contact force between yarns (Equation 2.2). Thus, when electrically conductive textiles undergo strain (e.g. elongation-recovery cycles) their electrical properties are influenced by the effect of loading on the mechanics of the fabrics. In particular, contact pressure, number of contact points as well as loop length and cross-sectional area are the mechanical and geometrical parameters affected by fabric deformation and whose changes influence the electrical behaviour. The effect of mechanical properties on the electrical behaviour of knitted conductive textiles during cyclic stretch-recovery trials is discussed in more detail in

Chapter 4.

### 2.7.4 Loop geometry

The geometry of the fabric's loop affects the overall loop length and, thus, the fabric electrical resistance (according to Equation 2.1). Moreover, the way such loops are interconnected to each other determines the interaction between contact and length-related resistances during elongation and, thus, the overall electrical behaviour of the fabric.

An equivalent electrical model can be associated to the structure of the fabrics. Knitted textiles are interconnections of loops of courses and wales (defined in section 1.3), with each loop consisting of a head, two legs and two sinker loops joining the adjacent loops (H, L and S, respectively in Figure 2.11(a)). The conducting fibre makes contacts at the intersection of the head of a stitch with the sinker loops of the stitch above in the same wale and side by side between two stitches on the same course. In practice, this leads to four contact areas between the loop under consideration and the adjacent loops. Depending on the loop geometry and the applied strain, each contact area comprises one or more contact points, influencing the contact resistance and the equivalent resistance model. For simplicity, Figure 2.11 (a) illustrates in bold a loop with no strain applied and with two contact points (red circles) for each contact area. Figure 2.11 (b) represents the associated electrical network consisting of interconnected contact resistances $R_c$ (highlighted in red) and length-related resistances $R_l$ (drawn in black or gray depending if related to the loop under consideration or to the adjacent loops). When a voltage (current) is applied (sourced) to the fabric, the current flows through the paths with the lowest resistance. In case of low strain applied to the textile, the preferred path is represented by the length-related resistances (black resistances) as the pressure between yarns

is low and, thus, the contact resistances are high. On the other hand, when the fabric is subjected to a higher strain, the contact pressure between the interlocked fibres increases causing a decrease of the contact resistance at the interlocks. This means that the current flow path is reduced in length thanks to the shortcuts provided by the red contact resistances.

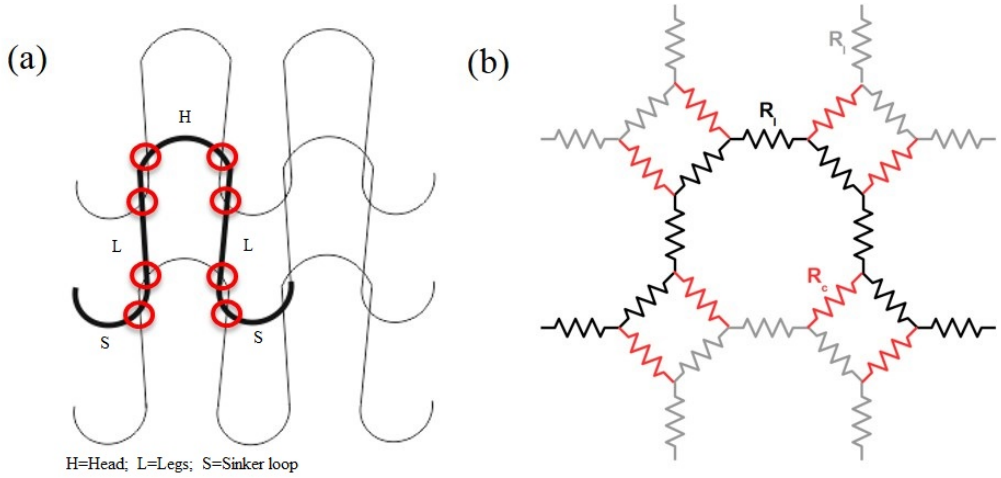


Figure 2.11: (a) Single loop (represented in bold) -consisting of a head (H), two legs (L) and two sinker loops (S)- and contact points (red circles). (b) Corresponding resistive network model (modified from Isaia et al. 2018)

This is just a simplified discussion about the complex electrical network of interconnected resistances representing a knitted conductive textiles. To build a fabric model describing more than one level at a time (i.e. the fibre or yarn level) information on multiple structural levels should be provided, such as fibre and yarn spacing, number of fibres in the cross-section, interlacing topology and geometry, friction coefficient, torsional and bending curvature.

### 2.7.5 Fibre-fibre slippage

Another phenomenon to take into account when considering the factors influencing the fabric resistance is the fibre-fibre slippage.

As presented in section 1.3, fabrics are fibrous materials, whose smallest

unit is the fibre. Under deformation, any fibrous assembly undergoes large and significant slippage between fibres, often irreversible. This mechanism results in the change in dimensions of the assembly, as reported in the analysis conducted by Carnaby and Pan 1989.

Grosberg and Smith 1966 described theoretically the interaction of two fibres at a contact point by Equation 2.3:

$$WF = \mu^{'} P + WF_0 \tag{2.3}$$

where: $WF$ is the withdrawal force per unit length of fibre (necessary for producing a slippage between the two fibres), $P$ is the external pressure, $\mu^{'}$ is the proportionality factor (with dimensions of length) and $WF_0$ is the value of the withdrawal force when $P$=0.

According to Equation 2.3, when $P$ is reduced to zero, there is still a non-zero force at the contact points. This means that even without external load, contact forces exist within a fibre assembly. Thus, a non-zero withdrawal force must be exert to cause a slippage even if no external pressure or load is applied to the fabric.

Figure 2.12 illustrates the interaction between two fibres in terms of forces applied at a contact point. When considering two fibres in contact and an external load applied (for instance in the j direction), the fibre contact point sustains a contact force $C_j$ which can be split in a normal component ($C_{jn}$) and one tangential ($C_{jp}$) to the contact surface.

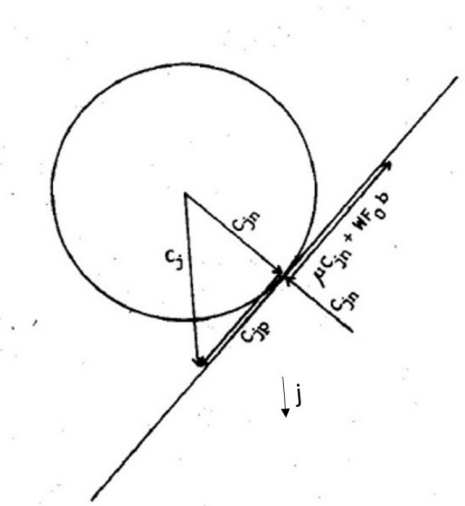


Figure 2.12: Interaction between two fibres at a contact point (modified from Carnaby and Pan 1989)

The magnitudes of these components are a function of the angle between the compression direction of the fibre assembly and the normal to the contact surface. The slippage of the top fibre starts when the tangential force exceeds the required withdrawal force:

$$C_{\mathrm{jp}} \geq C_{\mathrm{jn}}\mu + WF_0 b \tag{2.4}$$

where: $\mu$ is the coefficient of friction between two contacting fibres and $b$ is the mean free fibre length. After an external load applied to the fibre assembly (which caused slippage) is removed, the assembly does not return to its original state as irrecoverable energy is lost due to inter-fibre friction. In other words, the presence of friction forces, even with zero externally applied load, makes the application of an additional external load necessary to bring the fibres to their original position. The inclusion of the fibre slipping justifies the hysteresis effect of the fibre assembly (Sherburn 2007). A study of hysteresis is thus important as the magnitude of such effect can affect the employability of knitted conductive textiles as sensors.

## 2.8 Conclusions

In this chapter different methods for human motion analysis were discussed. Firstly, a distinction between *static and wearable platforms* was reported, together with some applications found in literature (e.g. image-based methods, force plates and a combination of the two as examples of stationary devices; inertial sensors, electro-goniometers and sensing fabrics as wearable sensors). Advantages and disadvantages of both methods were listed, with the wearable technology constituting an alternative solution to the expensive, time-consuming and laboratory-restricted stationary devices.
Secondly, the focus of the description was on *smart fabrics sensors*: starting from the modifications enabling sensing features into fabrics (i.e. intrinsically and extrinsically at any level of the fabric structure), the parameters and properties influencing the fibre, the yarn and the fabric were presented. In this way, the reader becomes familiar with terms, phenomena and issues that will be used when describing the electrical characterisation of the knitted conductive fabrics used in the thesis (Chapter 3) and when discussing the results of the tests conducted (Chapter 4). For instance, the *nature of fibres* determines the characteristics of the fabrics (e.g. using polyester fibres implies samples not affected by sweat/washing cycles). Also, specific *yarn requirements* depend on the application of the fabric sensors (e.g. for fabric sensor incorporated into a joint section the yarn should have lower linear density to guarantee a small mechanical bending resistance). A particular attention is given to parameters causing *fabric wrinkling* (i.e. unwanted residual deformation that can make the fabric loose after strain or wear). Such parameters belong to the three levels of the fabric structure, proving the complexity of the phenomenon, which affects any fabric undergoing strain. For the purpose of the thesis, the origin of the wrinkling

will be not investigated but only described in terms of the electrical effects of loose fabrics on the textile-sensor performance (section 4.3.1).

Thirdly, a special section is reserved to the *fabric strain sensors*, as they will be the ones described in the thesis as wearable motion sensors. The electrical behaviour of knitted conductive samples made of conductive yarn (e.g. stainless steel) is strain sensitive. This means that, when such fabrics are subjected to stretching (and recovery), fibre/yarn deformations and slippages between the fibre contact areas of stitches occur and this changes their conductivity. An equivalent electrical model can be associated to the fabric structure under deformation but any further investigation (e.g. electro-mechanical model or simulation) is outside the scope of this thesis. Influencing factors of the fabric resistance are: length variation of the conductive yarn (contributing to the *length-related resistance*, $R_l$), structural deformations of the stitches causing variation of the contact forces (affecting the *contact resistance*, $R_c$), *fabric mechanical parameters* (such as contact pressure, number of contact points, loop length and cross-sectional area), *loop geometry* and *fibre-fibre slippage*. In particular, the fibre slipping is included in the analysis of the fabric behaviour as it justifies the hysteresis effect which affects any fibre assembly. A study of hysteresis will be therefore important for the employability of knitted conductive textiles as wearable motion sensors, as discussed in 4.8.1.

# Chapter 3

# Characterisation of Knitted Conductive Fabrics

## 3.1 Introduction

A yarn can be given conductive properties by knitting conductive fibres into non-conductive knits, for instance by using a combination of stainless steel and polyester fibres. Fabrics knitted from such yarns develop sensing properties as structural deformations of the fibres (e.g. stretching) will cause changes in the conductivity of the fabric (as described in section 2.5). Such textiles are employable as smart fabric sensors and used, for instance, as wearable devices to detect movements of a subject wearing them (section 2.4).

To improve the performance and the reliability of fabric-based sensors the electrical properties of conductive textiles require an attentive investigation during deformation.

## 3.2 Objectives

This chapter will present the method used for the electrical characterisation of the knitted conductive samples, whose outcomes will be discussed in Chapter 4. Experiments are outlined to study changes in the electrical properties exhibited by knitted conductive textiles made of 20% stainless steel and 80% polyester fibres in various knit configurations, during unidirectional elongation in an Instron Fatigue machine.

The electrical characterisation will comprise how conductive fabrics knitted with four different stitch patterns behave under strain, various elongations, different input currents, varying elongation rates and, particularly, after a considerable number of stretch-recovery cycles of mechanical preconditioning.

## 3.3 Description of the knitted conductive samples

Conductive samples knitted according to four different stitch patterns, Single Jersey, SP27, SP29 and SP31 (©Footfalls & Heartbeats (UK) Limited)[1], were employed for this investigation (Figure 3.1).

Single Jersey, SJ, (Figure 3.1(a)) is a control stitch structure composed of a series of interconnecting loops creating 100 % of the sensor area.

SP27 (Figure 3.1(b)), SP29 (Figure 3.1(c)) and SP31 (Figure 3.1(d)) consist of a minimum of 50 % SJ and a combination of miss or tuck stitches that constitute the balance percentage. A tuck stitch is composed of a held loop, one or more tuck loops and knitted loops and is produced when a needle holding its loop also receives the new loop (Figure 3.2).

[1] http://www.footfallsandheartbeats.com/

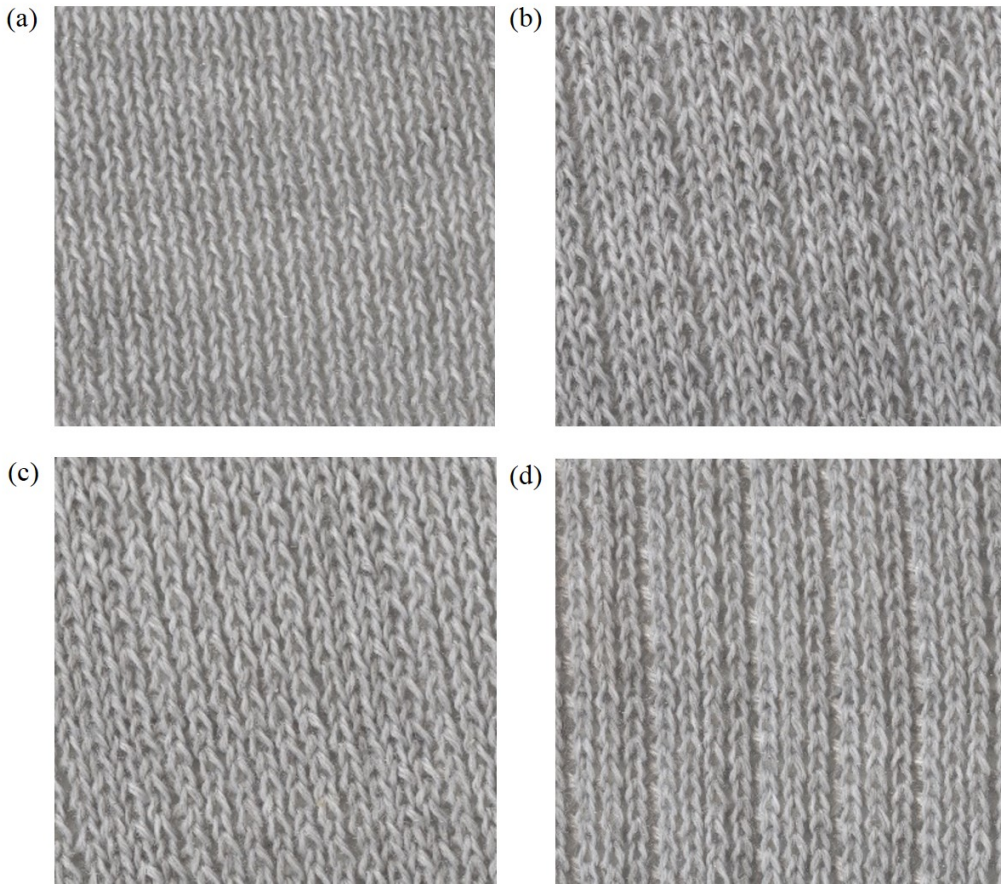


Figure 3.1: Knitted conductive samples used in the study: a) Single Jersey b) SP27 c) SP29 and d) SP31.

A miss stitch or float stitch is composed of a held loop, one of more float loops and knitted loops. It is produced when a needle holding its old loop fails to receive the new yarn that passes, as a float loop, to the back of the needle and to the reverse side of the resultant stitch.

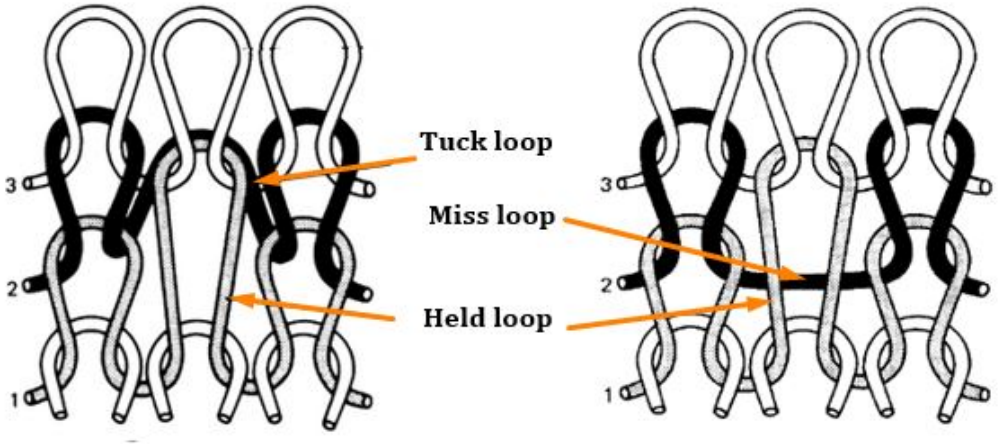


Figure 3.2: Type of stitches (Sarker 2016)

Each of the four samples was 250 mm x 50 mm (height x width) and made of conductive (150 mm x 50 mm) and non-conductive yarns (Figure 3.3).

The difference between the four stitch patterns are illustrated in Tables 3.1 and Table 3.2 in terms of:

- *Fabric density*, indicating the number of wales per inch (WPI) and courses per inch (CPI). These data were counted in an inch of each sample with the aid of a magnifying glass.
- *Stitch density*, measuring the product of wales per inch and courses per inch (WPI * CPI).
- *Loop width (wale spacing)* and *loop height (course spacing)*. The former is represented by the maximum width of the stitch in a singular wale, the latter is the distance between the stitch heads in two consecutive courses.

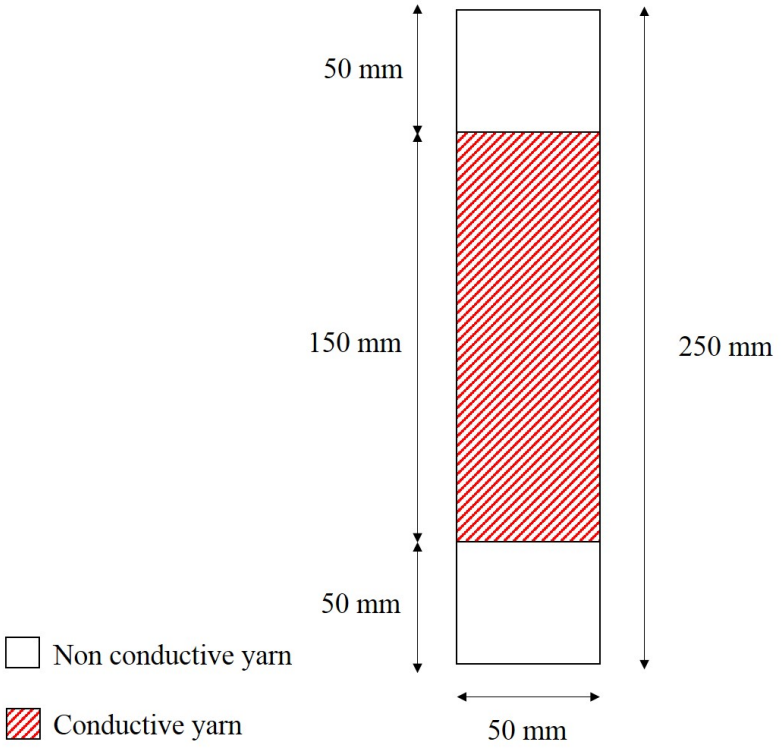


Figure 3.3: Fabric scheme

These features were measured by means of a Nikon Eclipse LV100 ND optical microscope and NIS- Elements image analysing software (Figure 3.4).

- *Yarn thickness*, equal to yarn diameter assuming that the cross-section of the yarn is circular. The method used to measure the yarn diameter was by microscopic observation and optical-projection involving subjective determination of the yarn boundaries (Figure 3.4). Higher measurement accuracy achievable with mechanical methods (Mahmoudi and Oxenham 2002) is beyond the scope of this thesis.

- *Loop length*, calculated with the equation (3.1) provided by Cuden, Hladnik, and Sluga 2013 for conventional knitted fabrics:

$$L = 1.92 * \textit{Loop width} + 1.41 * \textit{Loop height} + 4.59 * \textit{Yarn thickness} \quad (3.1)$$

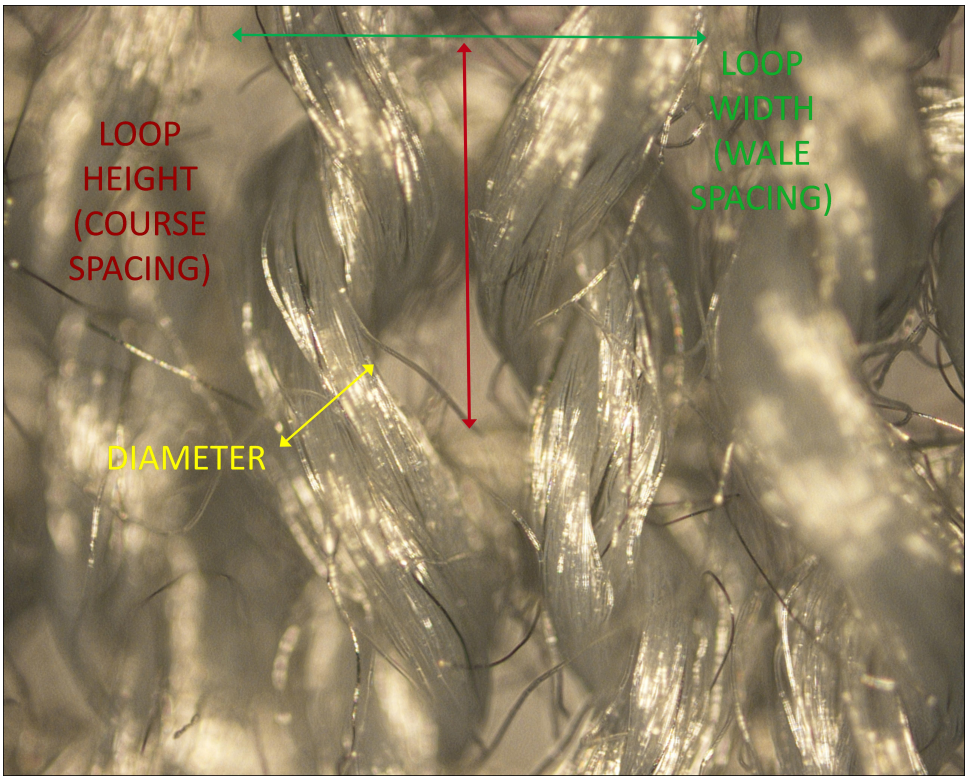


Figure 3.4: Loop geometrical parameters: loop height (red), loop width (green) and yarn diameter (yellow)

Table 3.1: Fabric and stitch density counted in one inch (equivalent to 2.54 cm) of the four samples under investigation

| Sample | Wale/cm (WPC) | Course/cm (CPC) | Stitch density ($/cm^2$) |
|---|---|---|---|
| Single Jersey | 6.7 | 9.0 | 60.3 |
| SP27 | 6.3 | 6.7 | 42.2 |
| SP29 | 5.5 | 7.1 | 39.1 |
| SP31 | 5.1 | 7.5 | 38.3 |

Table 3.2: Mean values and standard deviations of the fabric parameters for the four samples under investigation considering 10 measurements

| Sample | Loop width (mm) | Loop height (mm) | Yarn diameter (mm) | Loop length (mm) |
|---|---|---|---|---|
| Single Jersey | 1.42 ±0.05 | 1.10 ±0.04 | 0.50 ±0.05 | 6.58 ±0.24 |
| SP27 | 1.41 ±0.03 | 1.29 ±0.02 | 0.54 ±0.03 | 7.00 ±0.10 |
| SP29 | 1.43 ±0.03 | 1.37 ±0.01 | 0.51 ±0.01 | 7.01 ±0.10 |
| SP31 | 1.59 ±0.10 | 1.34 ±0.08 | 0.55 ±0.02 | 7.44 ±0.32 |

The samples under investigation were formed by a 'course'of knit, which means that a horizontal row of needle loops was produced by adjacent needles during the same knitting cycle.

The choice of evaluating the electrical properties of these specific knitted textiles along the course direction was due to their limited resistance variation (kiloohms instead of megaohms measured along the wale direction). This leads to the possibility in applying them in a circuitry with a Wheatstone Bridge, in case only limited resistance variations need to be measured in future.

### 3.3.1 Conductive yarn

The conductive yarn used in the samples was a spun staple fibre yarn made by Schoeller (Bregenz) with 2 yarns of 50 m each, whose weight and composition were, respectively, 2 g and 20 % stainless steel staple fibres (AISI 316L, conductivity $1.351 * 10^6$ S/m, $8\mu m$ in diameter) and 80% polyester (PES) low pill fibres ($16\mu m$ in diameter). These staple fibres were >80 mm long and co-mingled when spun together into the yarn, integrating the sensing part during the manufacturing stage of the fabric (in contrast with coated sensors). According to the Schoeller yarn specification the number of twists per meter (t/m) for the single yarn was 600, with the yarn appearing twisted together as the diagonal of a Z. The

number of twists per meter for the folded yarn was 425 t/m, appearing as the diagonal of an S. The tenacity of the yarn (breaking force measured in Newtons per weight unit of yarn) was 916.4 cN/tex (mass in grams per 1000 meters). The extension (elongation) at break was 19%.

### 3.3.2 Non conductive yarn

The non-conductive yarn was a 150 dtex filament yarn consisting of 48 filaments of polyester constructed by texturing processes, which means by introducing bulkiness into continuous filaments.

### 3.3.3 Sample preparation

The samples were knitted on a flatbed Shima Seiki 122S 10 gauge weft knitting machine (according to the specifications illustrated in Figure 3.3) at The School of Materials Textile Laboratory at the University of Manchester.

## 3.4 System for electrical characterisation of the conductive samples

To investigate the electrical properties of the conductive textiles described in section 3.3 a measurement system was arranged and illustrated in Figure 3.5.

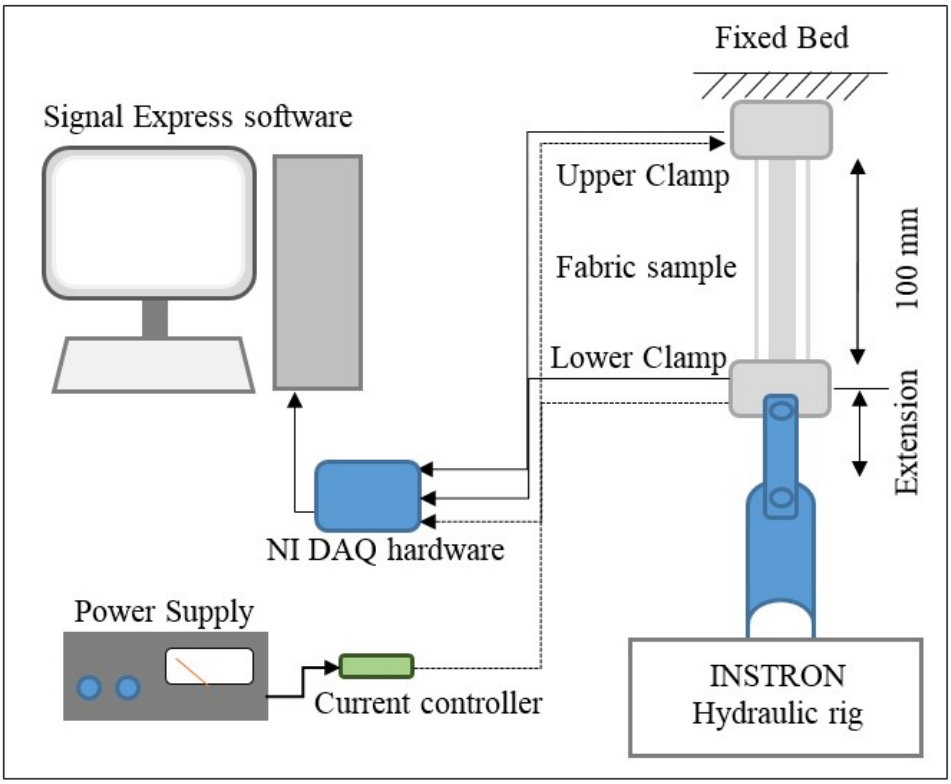


Figure 3.5: Experimental set-up scheme

The experimental set-up comprises:

- Electronic system, represented by the power supply and the current controller;
- Mechanical system, constituted by a tensile machine, the clamps and the fabric sample;
- Acquisition system, represented by the hardware acquisition device (NI DAQ) and the software (Signal Express).

The electrical characterisation carried out with the proposed measurement system regarded the fabric electrical resistance variation during stretch-recovery cycles, the effect of different currents, elongations and elongation rates on the resistance measurements and the consequence of an extended mechanical preconditioning on the electrical properties.

### 3.4.1 Electronic system

To measure the electrical resistance of conductive textiles and the effect of current on the resistance variation during cyclic loading, a purposely designed and manufactured circuit was employed (Figure 3.6).
Figure 3.7 is the schematic of the circuit illustrated in Figure 3.6, with the functioning of the components being highlighted.

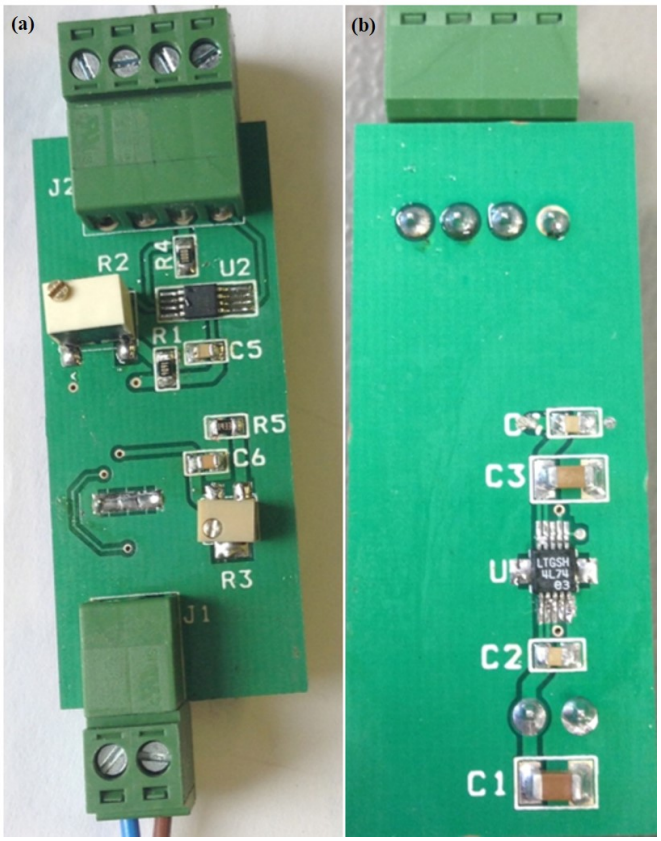


Figure 3.6: The printed circuit board: a) top of the board, b) bottom of the board

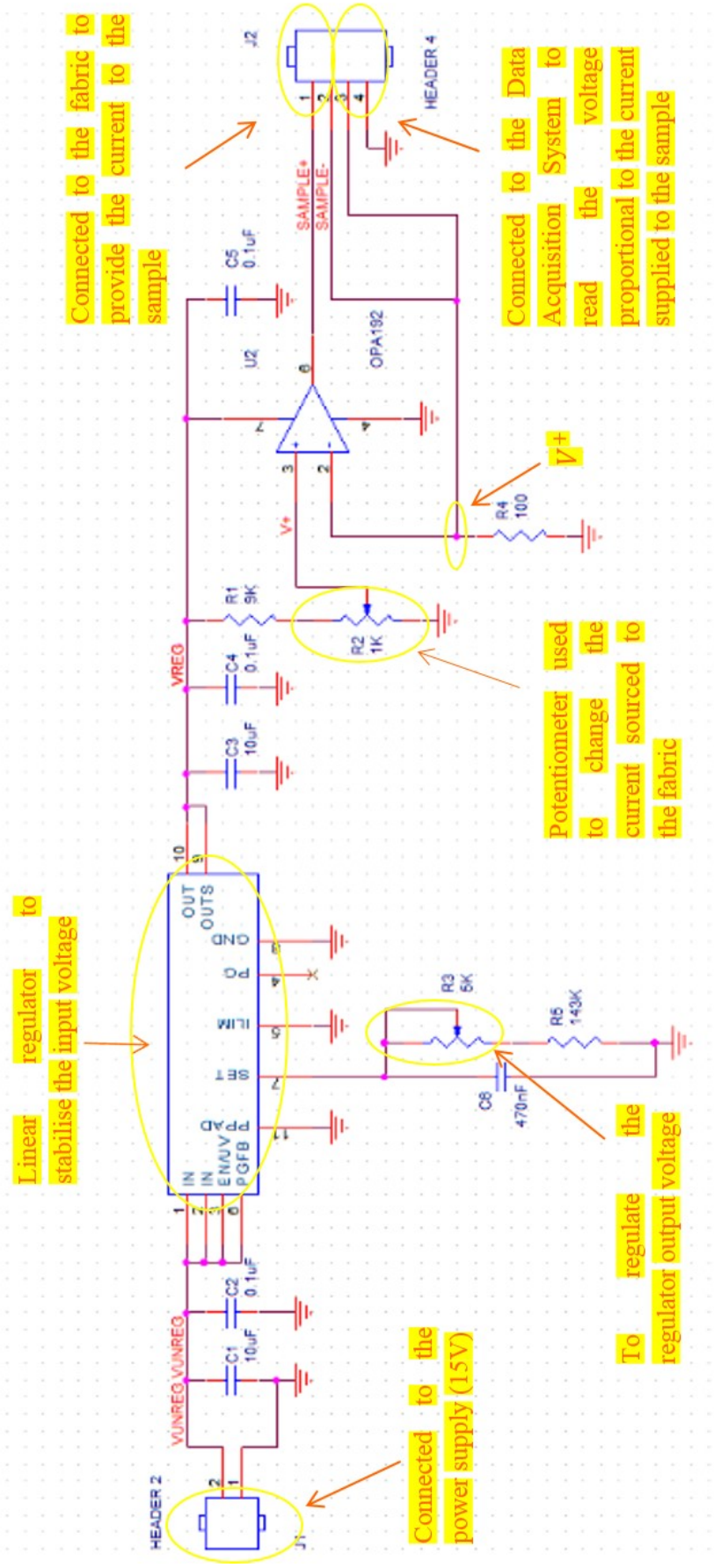


Figure 3.7: Schematic of the controlled current generator circuitry

The circuitry worked as a controlled current generator and sourced the conductive fabric under investigation with the current value manually set by a potentiometer ($R_2$).

The voltage $V^+$ at the non-inverting input of the operational amplifier (Figure 3.7) divided by the feedback resistance (represented as $R_4 = 100\Omega$ in the schematic) sets the current sourced to the fabric:

$$I_s = \frac{V^+}{R_4} \tag{3.2}$$

The voltage $V^+$ is derived from the power supply voltage by means of a voltage divider and can be manually adjusted by acting on the potentiometer $R_2$. By providing a 15 V voltage with a power supply (EMS Power A405) connected to the circuit, the maximum input voltage $V^+$ for the operational amplifier was 1.5 V due to the chosen resistance values in the voltage divider. Hence, the maximum current that was provided to the sample was 15 mA.

The ratio between the floating voltage across the fabric during the stretch-recovery cycles, $V_m$ (described in sections 3.4.2 and 3.4.3), and $I_s$ is the fabric resistance corresponding to the elongation-recovery accomplished.

$$R_{\text{fabric}} = \frac{V_m}{I_s} \tag{3.3}$$

$V_m$ was measured by the acquisition system by using different wires with respect to the ones providing the test current to the fabric sample.

Different current values were sourced to the specimens and, correspondingly, different electrical characterisations of the conductive fabric were carried out. The voltage across the feedback resistor (and thus the current sourced to the samples) was totally unaffected by the stretching of the specimens in the tensile machine. This was due to the fact that the

bandwidth of the operational amplifier used for current control was several orders of magnitude higher (megahertz) than the highest harmonic effectively present in the fabric resistance variation as a consequence of the stretching (described later on in section 4.9).

The choice of using the constant current control method for supplying the conductive textiles (in contrast with the universally used constant voltage method) was made for evaluating the fabric electrical behaviour under constant and repeatable conditions and individuating possible reasons for non-linear phenomena. In fact, such method resulted in the discovery of the non ohmic contact between stainless steel fibres, which is widely discussed in section 4.5.2.

### 3.4.2 Mechanical system

To electrically characterise the knitted conductive samples during deformation the fabric specimens were tested in two different tensile machines: the Instron 5969 (Figures 3.8 (a) and (b)) and the hydraulic Instron 8801 for high-cycle fatigue testing (Figures 3.9 (a) and (b)).

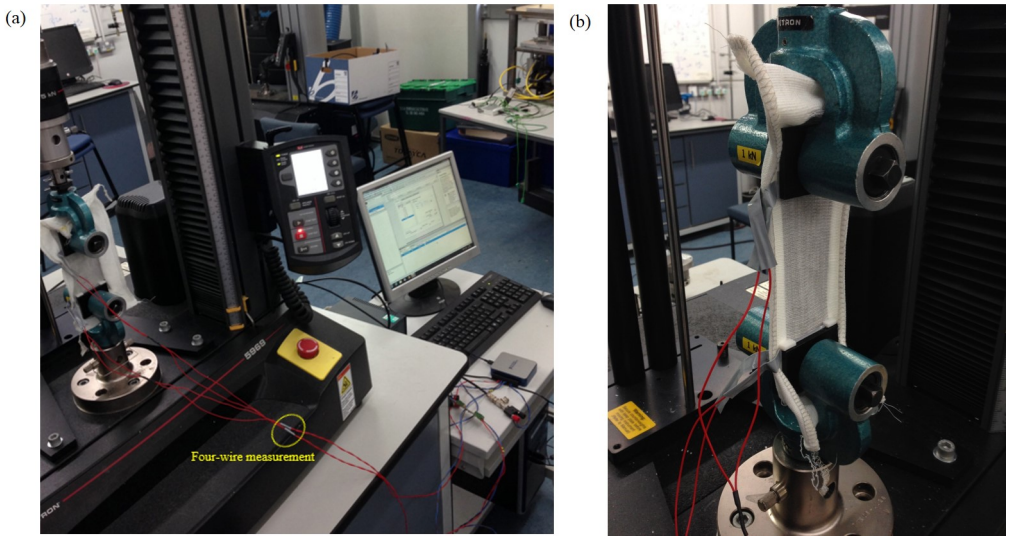


Figure 3.8: a) Instron 5969 testing machine b) Specimen in the customised clamps

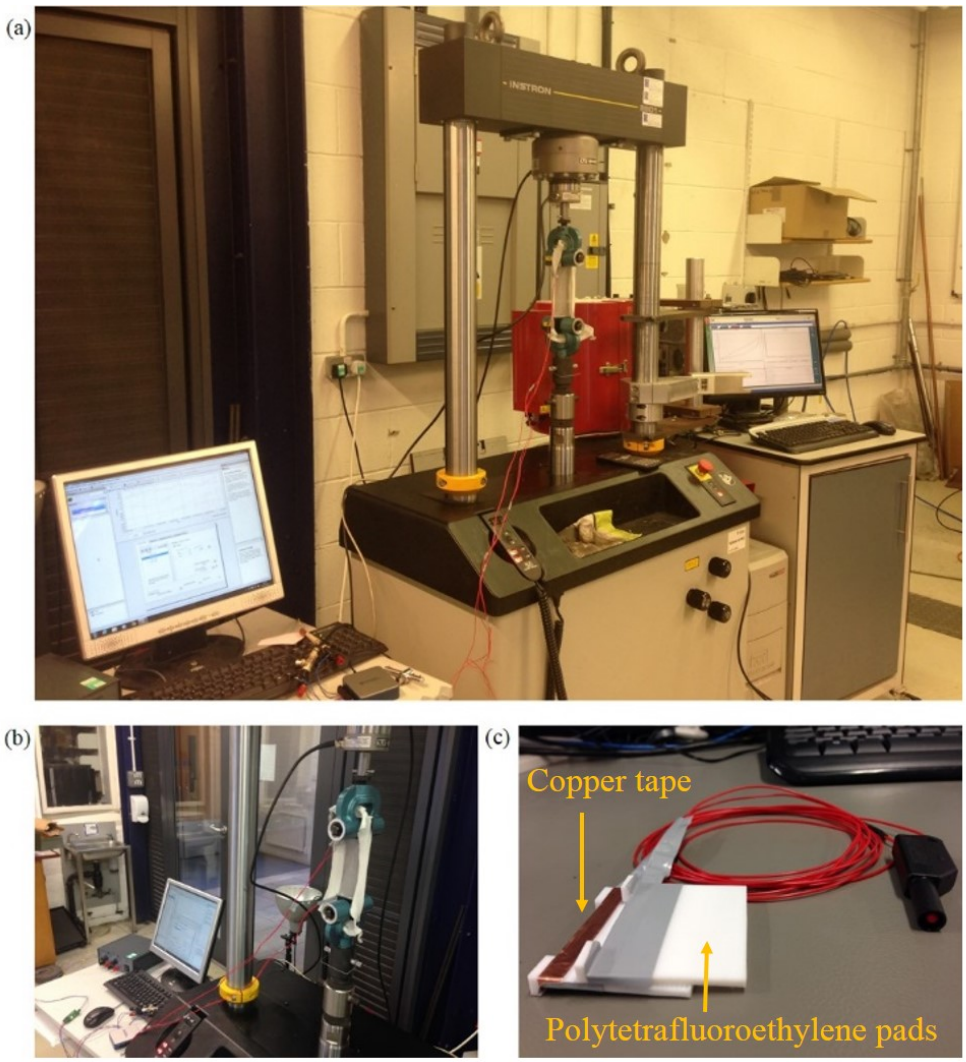


Figure 3.9: a)- b) Instron 8801 hydraulic machine c) Customised clamps

To gather the electrical signal coming from the conductive fabrics during cyclic loading customised clamps were employed (Figure 3.9 (c)). They were polytetrafluoroethylene (PTFE) insulating pads used to avoid any contact between the conductive knitted samples and the metallic grips of the tensile machine. A conductive (copper) tape was positioned to touch the conductive area of the sample and an insulator tape to prevent any contact between the metallic grips of the machine and the copper tape. The same clamping force (2N) was applied with a torque wrench to all samples to ensure the same test conditions, while not affecting electrical-wise the specimens by providing different contact pressure in correspondence of the clamps.

A four-wire resistance measurement was chosen to measure the electrical resistance of the conductive textiles. This means that the current and voltage wires were separated by connecting four wires to the clamps holding the test specimen: two wires (connected to SAMPLE+ and SAMPLE- terminals on J2 connector of Figure 3.7) provided the sample with the current sourced by the fabricated circuit shown in Figure 3.6, the other two wires read the voltage across the specimen during the stretch/recovery trials ($V_m$).

### 3.4.3 Acquisition system

The electrical signals gathered from the conductive fabrics clamped in the tensile machine were collected by a National Instrument data acquisition device, the NI USB 6003, at 1000 Hz.

In particular to measure the fabric resistance variation during cyclic loading two signals were essential:

- The floating voltage across the fabric during the stretch-recovery cycles, $V_m$. This is a differential signal collected by connecting the

positive clamp's lead of the voltage signal to the positive analog terminal AI+ of the DAQ and the negative lead of the clamp to the negative analog input AI- .

- The voltage proportional to the current supplied to the sample, $V^+$. This is a referenced single-ended (RSE) voltage signal measured by connecting the positive voltage signal from the circuit (pin 3 in the schematic of Figure 3.7) to an AI+ terminal and the ground signal (pin 4) to an AI GND terminal.

The detailed description of the fabric resistance variation during the stretch-recovery performed is described in section 4.3. For the analysis purpose the voltages proportional to the extension and to the load were gathered from the tensile machine and also collected by the acquisition system. The signals acquired simultaneously with the hardware data acquisition and recorded with the Signal Express software are represented in Figure 3.10.

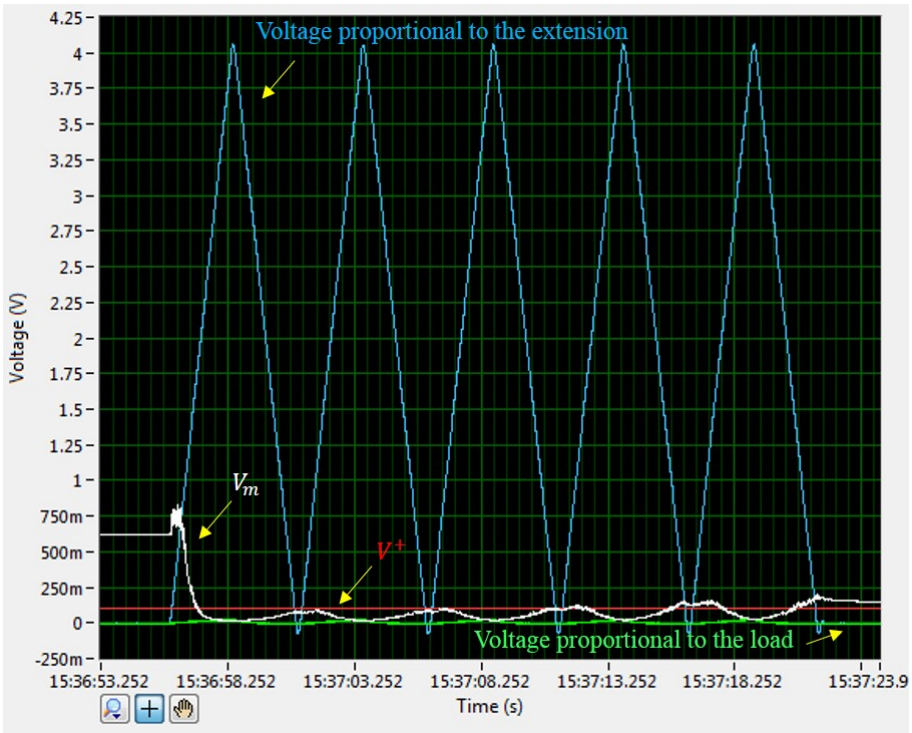


Figure 3.10: Signals captured with the Data Acquisition System

## 3.5 Testing of the knitted conductive fabrics

The experimental set-up described in Figure 3.5 was arranged to test the fabric specimens clamped in a tensile machine during stretch-recovery cycles. The tensile machine was different according to the use. For instance, for studying the electrical properties of the fabrics after an extended use (i.e. 250 cycles of elongation-recovery or more) and evaluating the effect of mechanical preconditioning, the Instron 8801 hydraulic machine was employed (Figures 3.9 (a) and (b)). Conversely, for limited use and initial electrical characterisation of the samples an Instron 5969 was chosen (Figures 3.8 (a) and (b)).

Before starting the tests the Single Jersey, SP27, SP29 and SP31 samples were kept for a minimum of 20 h in a tension-free state. Afterwards, the test specimens were handled carefully to avoid folds or wrinkles and minimise the effect of handling during positioning in the clamps. Each sample was gripped in the clamps under tension (without undergoing any pre-deformation/elongation); thus, the elongation started at exactly the beginning of loading. The test specimens were tested in the standard atmosphere for testing textiles described in the ASTM D1776 (temperature: $21 \pm 1°C$).

For all samples the elongation was along the course direction with the original –not stretched –length of the fabric between the clamps being equal to 100 mm. The tests were performed with a triangular elongation profile whose height corresponds to the fabric elongation (in mm) and whose gradient corresponds to the elongation rate (in mm/s). The extent of the elongation was chosen according to the study purpose (section 3.5.2) or application. For instance, for mechanical preconditioning of the conductive fabrics the elongation was set to 16 mm.

### 3.5.1 Mechanical preconditioning

The electrical properties of conductive textiles cannot be studied comprehensively without investigating the mechanical effect of cyclic loading since the overall fabric resistance is related to the length of yarn (Equation 2.1) and contact force between yarns (Equation 2.2).

From the literature it was evident that no studies have reported whether and in what manner the mechanical and electrical properties of knitted conductive textiles change after extended use or a considerable number of stretch-recovery cycles. In addition, there was no systematic analysis of the electrical behaviour of the conductive textiles after mechanical preconditioning with stretch-recovery cycles and of the effects of the current and the deformation rate on the fabric resistance variation.

The objective of the study on mechanical preconditioning is to assess its effect on the electrical behaviour of knitted conductive fabrics. In particular it was investigated whether the electrical properties shown by the textiles change during cyclic mechanical loading, after a rest period and if they are affected by the way the fabrics are mechanically loaded or electrically driven. To do so, cyclic unidirectional elongations were performed on the Single Jersey, SP27, SP29 and SP31 samples with the Instron 8801 Fatigue machine.

For each sample the testing was arranged in two sessions:

1. *Preconditioning test*: The preconditioning test was the first test performed whose aim was the evaluation of any change or stabilisation of the electrical properties of the fabric as a result of a certain number of stretch-recovery cycles. By preconditioning effect we mean the stabilisation of the electrical properties of the fabric resulting from the cyclic mechanical loading;

2. *Repeatability test*: The goal of the second session of tests was to study whether a short rest period reset the preconditioning effects. Without modifying the setting of the specimen in the clamps, the second test session was repeated at the same testing conditions of the preconditioning test after a rest time of 5 minutes. This time was chosen to electrically characterise the specimens in a way compatible as possible with a real application (e.g. fabric embedded in a garment at the knee and tested after a limited sitting/rest period).

Each session consisted of 250 stretch-recovery cycles, which were performed with a triangle wave of 16 mm amplitude and 0.3 and 0.375 Hz frequencies corresponding to the two elongation rates selected for the tests. This number of cycles was sufficient for evaluating the stabilisation of the electrical properties of all knit patterns.

The two sessions were repeated at three different currents (1 mA, 3 mA and 6 mA) and two elongation rates (9.6 mm/s and 12 mm/s), for a total of 48 trials. For instance, after an initial rest period of at least 20 hours, the Single Jersey was firstly mechanically preconditioned at 1 mA and 9.6 mm/s and, after 5 minutes rest period, tested again at the same conditions. Later on, the same sample was mechanically preconditioned at 3 mA and 9.6 mm/s and, after 5 minutes interval, stretched again with the same procedure. The same occurred at 6 mA and 9.6 mm/s. All samples followed this procedure for both elongation rates.

The elongation value (i.e. 16 mm) was chosen by mirroring typical human body extensions and considering a comparable fabric deformation on a garment during walking. In fact, as described in Chapters 5 and 6, the next application of the conductive fabrics is as sensors for monitoring human body movements. The choice of the current values was mainly related to considerations about the design constraints in battery operated wearable

applications. In fact, most of the low voltage operational amplifiers used in small-signal applications have limited current sourcing capability, typically below 8 mA. Consequently, 1 mA, 3 mA and 6 mA can be respectively considered as low, medium and high current values when considering the above current limit. Finally, the chosen elongation rate values (i.e. 9.6 mm/s and 12 mm/s) cover a range of possible deformation rate during walking.
The sequence of tests conducted on the four samples for mechanical preconditioning and repeatability is listed in Table 7.1 of Appendix I (7.3.4).

### 3.5.2 Tests at different elongations

Many studies have proved the strong dependence of the electrical resistance exhibited by knitted conductive fabrics on elongation. Such dependence is mainly caused by the change of contact resistance within the yarns during stretching (Li et al. 2012). This dependence will be studied in section 4.8 considering 4 different elongation cases (4 mm, 8 mm, 12 mm and 16 mm) of the same sample taken as an example (SP29 sourced with 1 mA and tested at 9.6 mm/s). The aim is to discover the relationship between the extensions performed and the resistance measured for the conductive sample under investigation. Moreover, the contribution of the contact and length-related resistance to the overall equivalent resistance will be examined as the extent of their effect changes at different elongations.

## 3.6 Data Postprocessing

An important stage after the acquisition with the experimental set-up described in Figure 3.5 was the data postprocessing. The raw data collected from the conductive fabrics were analysed in Matlab with the aim of extracting meaningful electrical features for the fabric analysis. The steps are summarised in the following :

1. Filtering;
2. Peak analysis;
3. Interpolation;
4. Extraction of features of interest.

SP29 is the sample taken as an example to describe the post processing, whose procedure is the same for all conductive fabrics and, for this reason, is illustrated only for one sample. The reason why a post processing of the gathered data was necessary is explained below.
The Matlab code purposely written for the data postprocessing is reported in the Appendix II (7.3.4). The values of the extracted features are collected in Table 7.2 of Appendix III (7.3.4).

### 3.6.1 Filtering of the raw data

During the cyclic elongation-recovery of the fabric in the tensile machine the contact force acting on overlapped yarn fibres changed, causing a change of the contact resistance (as described in Equation 2.2) and consequently of the total resistance. As a consequence of the non-linear behaviour of the friction forces and the unavoidable imperfections of the fibres in each fabric, a high frequency electrical noise was superimposed on the total resistance

measured during deformation.

To reduce this electrical noise and make it easier to evaluate the fabric resistance variation overtime, a Savitzky-Golay (SG) filter was applied to the signal. The SG filter is also called least-squares smoothing filter as the filter coefficients are derived by performing an unweighted linear least-squares fit using a polynomial of a given degree which minimises the least-squares error.

The Savitzky-Golay filter was considered suitable for the fabric analysis as it can adapt its frame size to the stretch-recovery speed of the specimens and the polynomial order to the observed shape of the signal. In particular the values chosen for the analysis were a polynomial order, N, equal to 3 and a frame size (or window length), f, equal to 151 (Figure 3.11), which corresponds to 151 ms window length whereas the resistance signal period is 3333 ms. This window was chosen sufficiently large to make it impossible for the low-order polynomial to follow fast changes in the signal due to the noise. At the same time the window was yet sufficiently small (compared to the period of the signal) to accurately follow the fabric resistance variation without introducing distortions or delays.

To validate the quality of the Savitzy-Golay filter in smoothing the data a FIR low pass is considered for comparison in Figures 3.12 and 3.13. The FIR low pass filter uses a least-squares approximation to compute the filter coefficients and then smooths the impulse response with window. The filter was designed in Matlab with these specifications:

- Sampling frequency: $fs = 1000Hz$;
- Filter order: N = 20;
- Cut-off frequency: $fn = 10Hz$ (considering the signal frequency equal to 0.3 Hz, as described in 3.5.1);

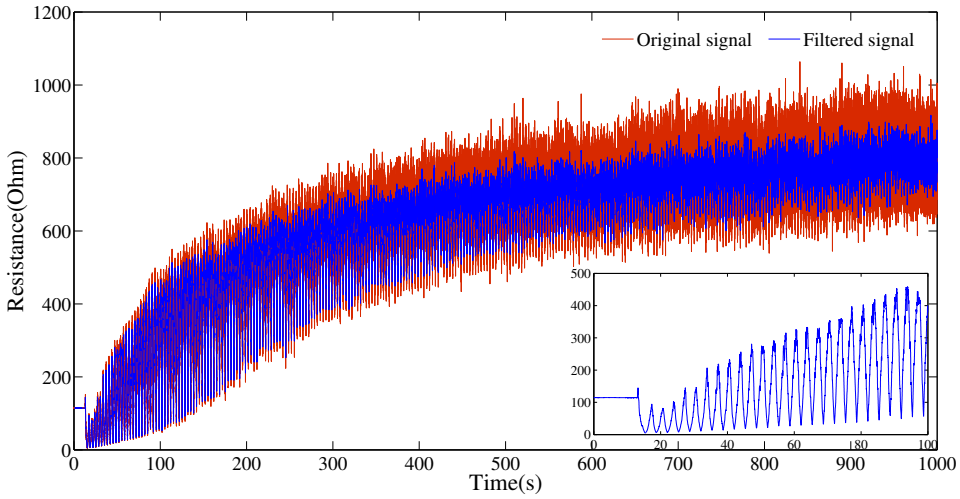


Figure 3.11: Original fabric resistance and Savitzky-Golay filtered resistance for the SP29 sample sourced with 3 mA and tested at 9.6 mm/s. In the box: zoom of the first 25 elongations for the filtered signal

- Normalised cut-off frequency: $\omega n = 0.02$

Figures 3.12 and 3.13 show the advantage of choosing the Savitsky-Golay filter in terms of following accurately the original signal and reducing the electrical noise, in particular in correspondence of the maximum resistance value, which is very important for the successive peak analysis.

In section 4.3, it will be discussed that the maximum resistance value occurs in correspondence of the minimum elongation of the fabric and this corresponds to a critical condition. In fact, the specimen which returns to the initial position (before being stretched) starts to become loose and this causes undesirable fluctuations of the electrical resistance. This critical condition will be discussed in more detail in section 4.3.1.

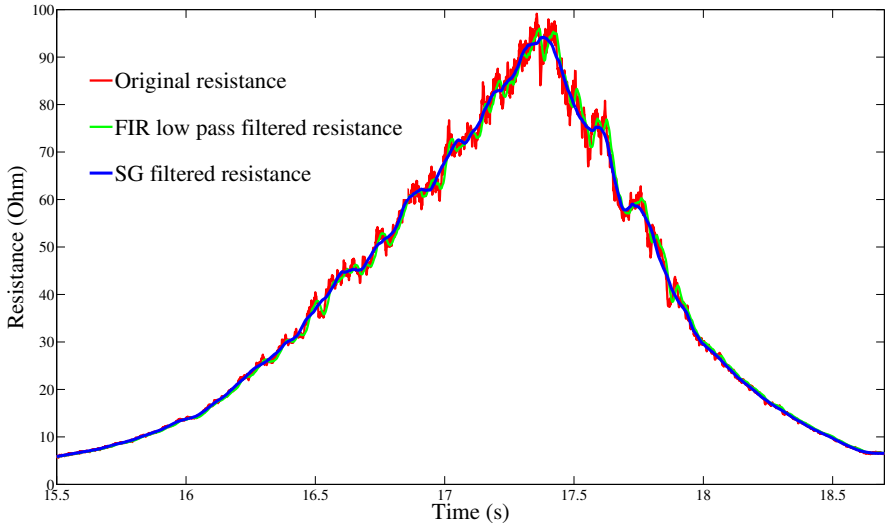


Figure 3.12: Original fabric resistance, FIR low pass and Savitzky-Golay filtered resistances on the same graph for the SP29 sample sourced with 3 mA and tested at 9.6 mm/s

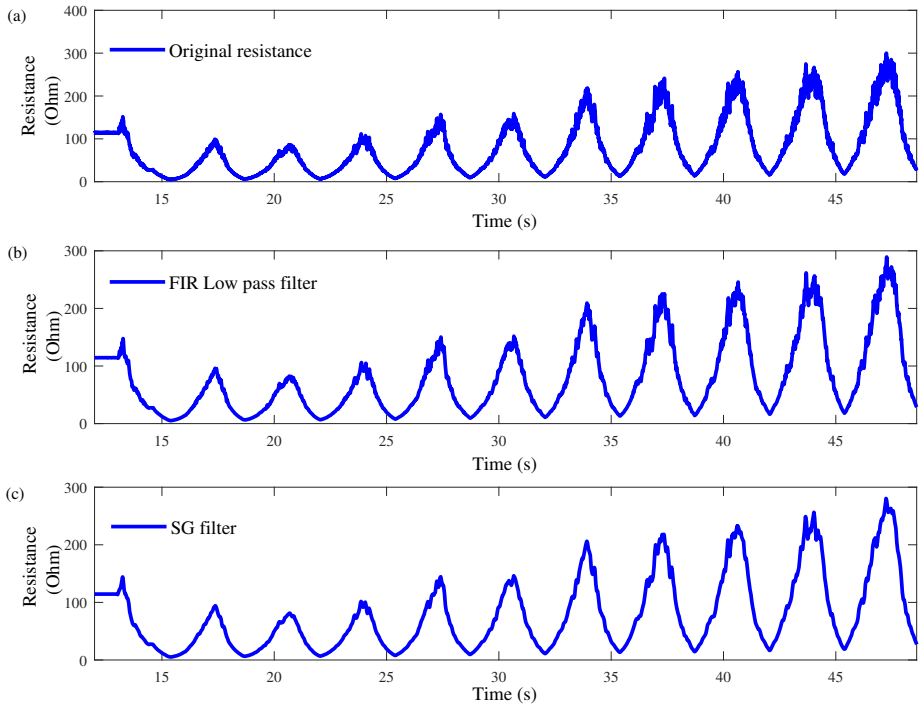


Figure 3.13: a) Original fabric resistance, b) FIR low pass and c) Savitzky-Golay filtered resistances in ten cycles for the SP29 sample sourced with 3 mA and tested at 9.6 mm/s

### 3.6.2 Peak analysis

The next stage after filtering the original fabric resistance was the peak analysis. This study was important to detect for each cycle the maximum and minimum resistance values of the filtered signal and associate them with the elongation performed. To do so the *findpeaks* command in Matlab was used twice (one for the maximum and one for the minimum values). The minimum values were obtained by finding peaks of an inverted version of the filtered signal. The required minimum peak distance in the Matlab command was set as the distance between a maximum and a minimum value in a cycle. The length of a cycle was calculated as the inverse of the test frequency, which was known after setting the elongation rate and the fabric elongation. In case of a triangular elongation profile, the fabric elongation corresponded to the height of the triangle and the elongation rate to the gradient. Thus, by dividing the elongation for the gradient the time between a maximum and minimum value was calculated. The maximum and minimum values detected with the peak analysis are in Figure 3.14.
To reduce the variability of the maximum and minimum values obtained with the peak analysis a new filtering was necessary. A Savitzky-Golay filter was used again, with polynomial order N=3 and window length f=21. The results of the filtering together with the original peaks are illustrated in Figure 3.15.

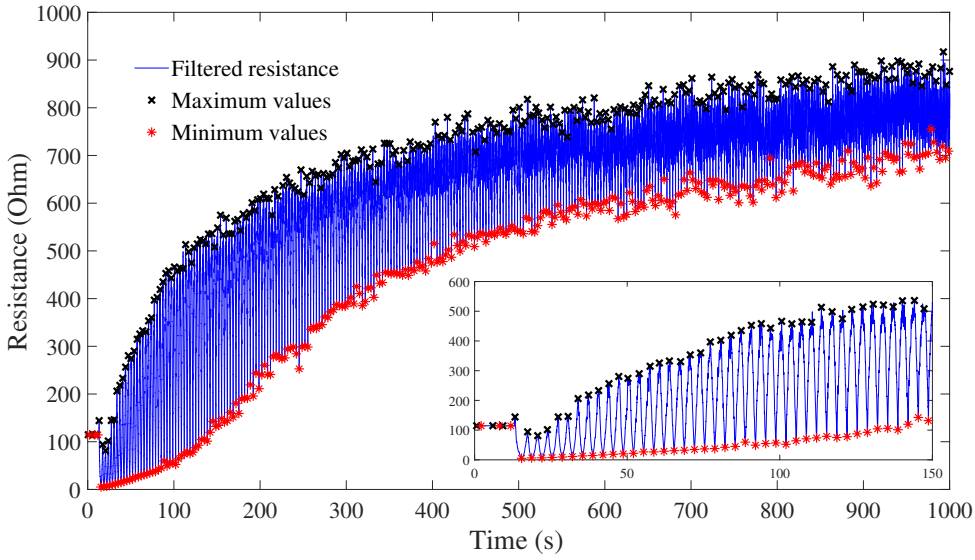


Figure 3.14: Detection of the maximum and minimum values of the filtered resistance for the SP29 sourced with 3 mA and tested at 9.6 mm/s. In the box: zoom of the detected peaks during the first 40 cycles

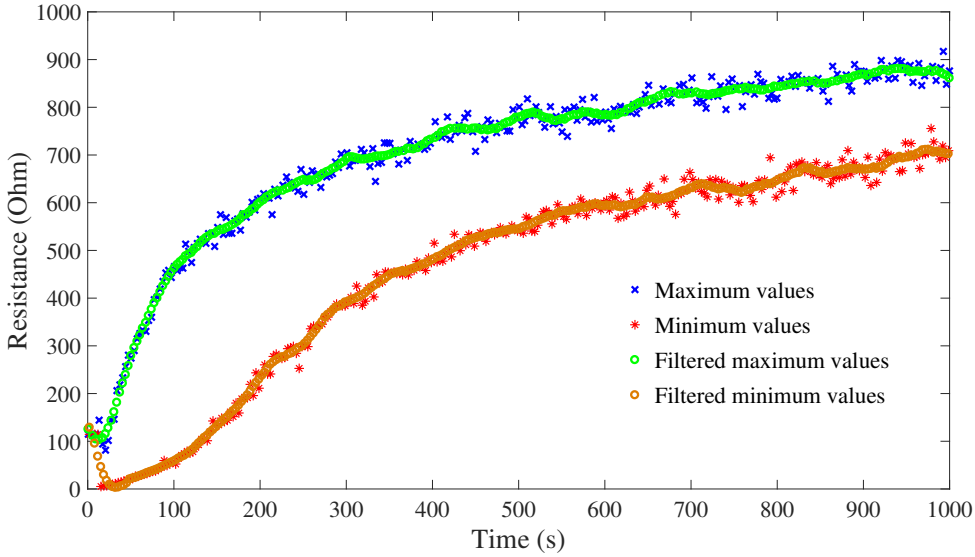


Figure 3.15: Maximum and minimum values obtained with the peak analysis and filtered maximum and minimum points using the Savitsky-Golay filter for the SP29 sample sourced with 3 mA and tested at 9.6 mm/s

### 3.6.3 Interpolation

To be able to compare in the time domain maximum and minimum points obtained with the peak analysis (section 3.6.2) and separated from each other by half a period, an interpolation method was used. This procedure constructed new data points within the range of a discrete set of known data points. In particular, a spline interpolation was chosen, with the interpolant being a low-degree piecewise polynomial. In this way, oscillations between points (Runge's phenomenon) were avoided, making the determination of interpolation curves more effective.

The results of the process, which was achieved with the *spline* function in Matlab, are described in Figure 3.16, with the interpolation curves being established passing through the filtered maximum and minimum values evaluated in section 3.6.2.

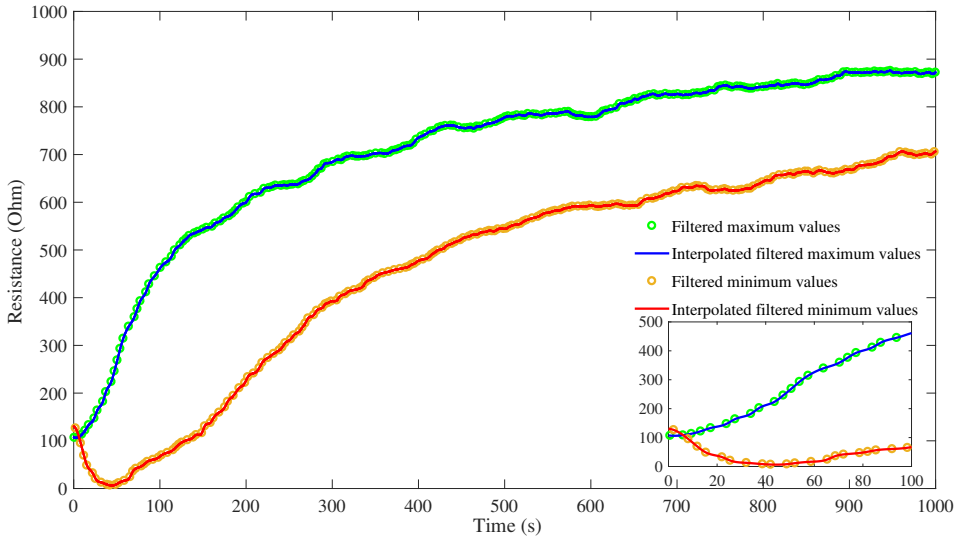


Figure 3.16: Maximum and minimum filtered values and interpolation curves of the filtered maximum and minimum points for the SP29 sample sourced with 3 mA and tested at 9.6 mm/s. In the box: zoom of the first 100 seconds

### 3.6.4 Extraction of features of interest

The last stage of data processing regarded the extraction of features of interest for describing the fabric electrical behaviour under cyclic deformation. The features used for presenting the results in Chapter 4 are:

- Peak-to-peak span;
- Settling time;
- Number of cycles for electrical stabilisation;
- Stabilised average resistance;
- Stabilised peak-to-peak span.

#### Peak-to-peak span

One of the main features for describing the electrical behaviour of the samples, independent of the fabric design and composition, was the peak-to-peak span (Figure 3.17). It was determined from the interpolated curves of Figure 3.16 by subtracting the interpolated filtered minimum curve from the interpolated filtered maximum one. The initial low value of the peak-to-peak span was due to the post-processing (described from section 3.6.2 onwards), which took into account also the interval prior to the elongation of the specimen.

The peak-to-peak span will provide information in terms of sensitivity of the fabric-transducer in section 4.6.

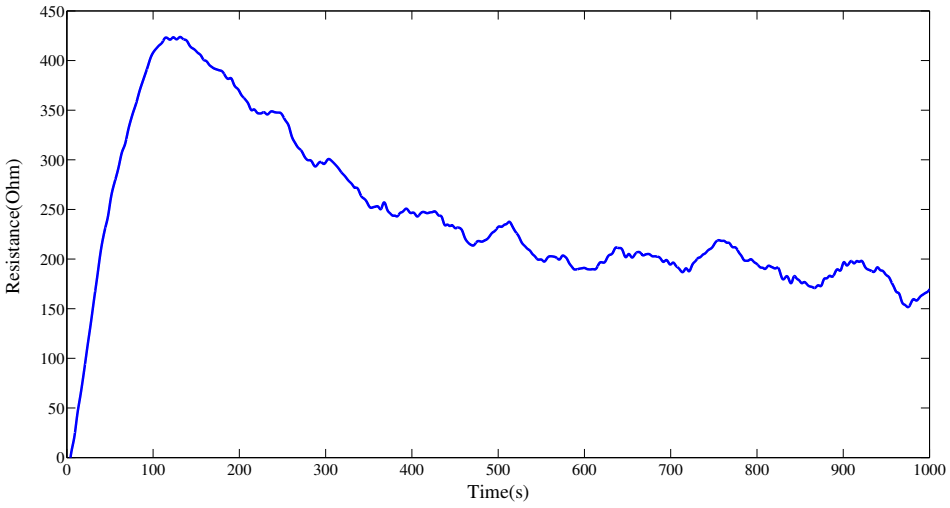


Figure 3.17: Peak-to-peak span for the SP29 sample sourced with 3mA and tested at 9.6 mm/s

### Settling time

One property to investigate when the specimens were elongated for a considerable number of cycles was the stabilisation of the fabric resistance. The settling time was studied during preconditioning and repeatability tests (described in section 3.5.1) as the instant since when the peak-to-peak span stabilised to a constant value.

To calculate the settling time a change point analysis (Picard 1985) was used for all samples. Change-point detection identifies times when the probability distribution of a stochastic process or time series changes. This method provides information in terms of a confidence level (indicating the likelihood that a change occurred) and a confidence interval (indicating when the change occurred). In other words, such analysis distinguishes the instant and extent to which change in the characteristics of interest occurs to a statistically significant degree.

The settling time $T_s$ was calculated in Matlab with the *findchangepts* function applied to the peak-to-peak span. This function is an estimation tech-

nique based on maximum likelihood of a parameter (e.g. mean, root-mean-square level and standard deviation). For determining the settling time of all samples, the chosen parameter was the standard deviation of the peak-to-peak span and the Gaussian Log Likelihood function was the estimation metric based on the maximum likelihood criterion. The reasons of this choice were the close match of the resulting estimates with the collected data and the shorter computation times being the likelihood problem reduced to a series of additions instead of multiplications.

The *findchangepts* function found that for all samples there was only one point in the data during which the standard deviation of the peak-to-peak span changed abruptly. Figure 3.18 illustrates the outcome of the presented analysis, with $T_s$ being the estimate of the settling time since the maximum value of likelihood occurs there. The red dash lines show, in fact, how in correspondence of such value the span changed to the most significant degree and started to settle to its mean value.

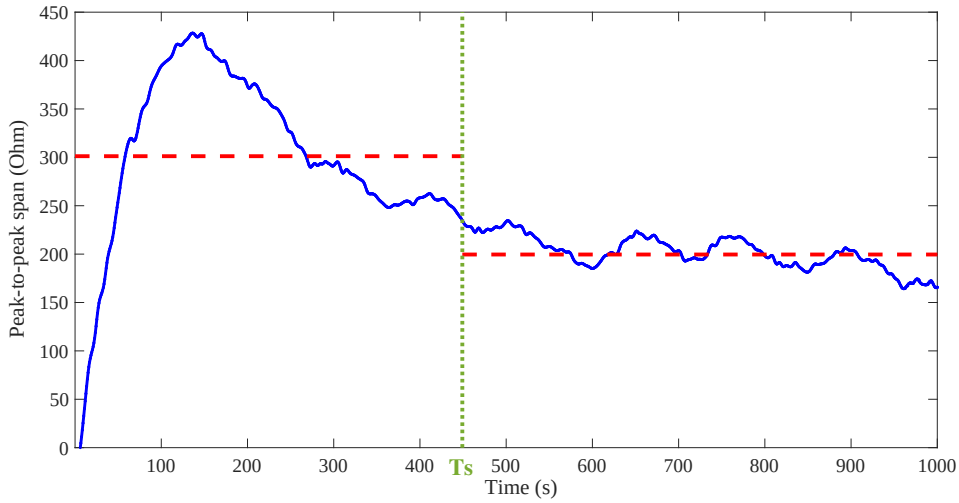


Figure 3.18: Change point analysis applied the peak-to-peak span for determining the settling time of the SP29 sample sourced with 3mA and tested at 9.6 mm/s

### Number of cycles for electrical stabilisation

The number of cycles was introduced to compare samples' performance and quantify when the fabrics electrically stabilised during extended use.
The number of cycles was calculated as:

$$N = k(T_s - T_0) * l_r \tag{3.4}$$

where: $k = \frac{1}{2L}$ is a constant with L being the fixed elongation, $T_s$ is the settling time calculated with the change point analysis, $T_0$ is the time when the sample starts its elongation for the first time and $l_r$ is the elongation rate.

### Stabilised average resistance

Another feature describing the electrical properties of the fabrics was the mean filtered resistance calculated from the settling time onwards (as illustrated in Figure 3.19). It will be referred to as stabilised average resistance in the rest of the thesis and indicated as $R_{\text{settling time}}$ in Table 7.2 of Appendix III (7.3.4).

### Stabilised span

Another feature used for presenting the results of the fabric analysis was the value at which the peak-to-peak span stabilised. It was calculated as the mean span value from the settling time onwards (as illustrated in Figure 3.20) and indicated as $R_{\text{settled span}}$ in Table 7.2 of Appendix III (7.3.4).

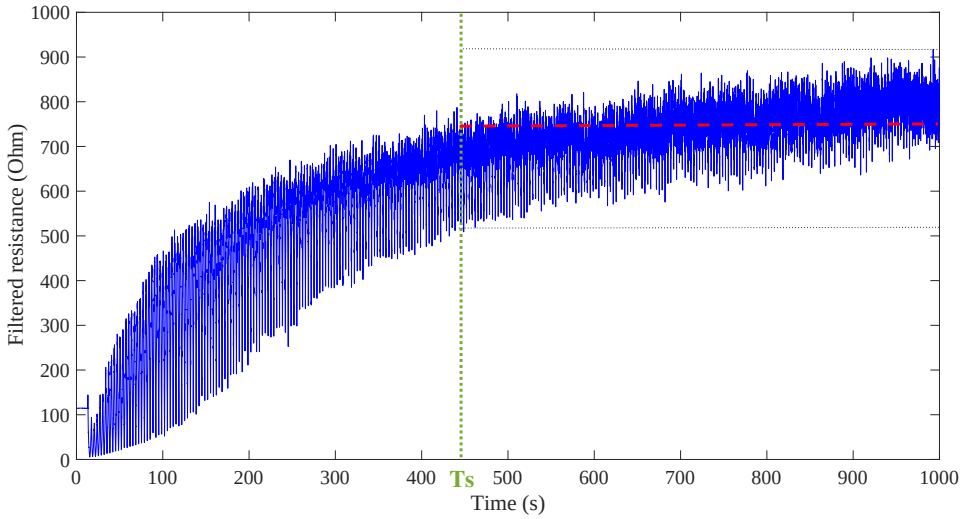


Figure 3.19: Stabilised average resistance (red dash line) determined as the mean filtered resistance from the settling time onwards for the SP29 sample sourced with 3mA and tested at 9.6 mm/s

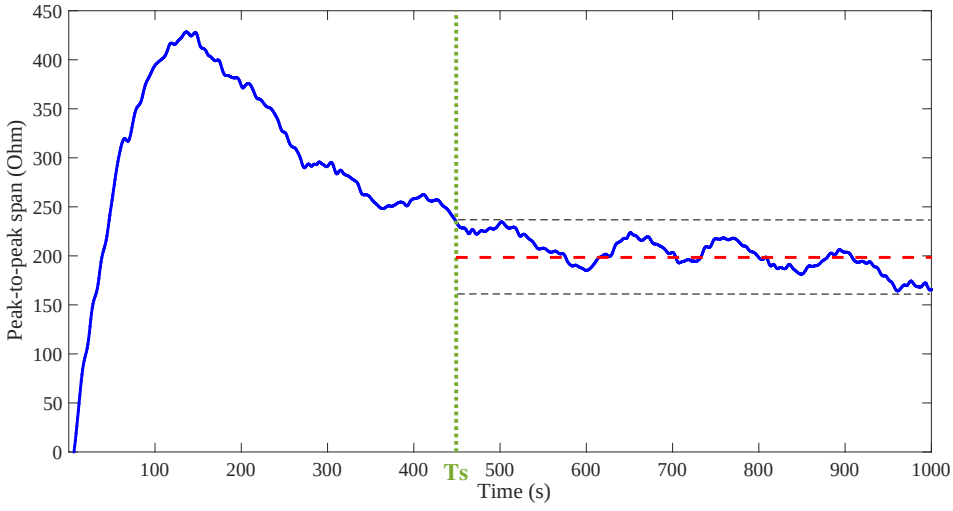


Figure 3.20: Stabilised span (red dash line) determined as the mean span value from the settling time onwards for the SP29 sample sourced with 3mA and tested at 9.6 mm/s

## 3.7 Conclusions

This chapter showed the methods used for the electrical characterisation of knitted conductive textiles during unidirectional elongation in two Instron tensile machines. Starting from the descriptions of the samples in terms of conductive and non conductive yarns composing the specimens, stitch patterns and fabric parameters, the chapter described the mechanical, electronic and acquisition systems employed for the fabric analysis. Test procedures for extended cyclic mechanical loading (preconditioning) were outlined considering different currents, elongation rates and varying elongations.

Lastly, the data post processing represented an important stage for studying the behaviour of the knitted conductive textiles under an electrical point of view and discriminating features of interest. In particular, the settling time (and associated number of cycles), the corresponding stabilised average resistance and the peak-to-peak span are the parameters chosen to present the results in Chapter 4.

# Chapter 4

# Analysis of the fabric electrical characterisation

## 4.1 Introduction

The electrical characterisation of knitted conductive textiles during cyclic loading on a tensile machine is a useful investigation prior to sewing them into garments to test as wearable sensors for human motion capture. For this reason, this chapter will evaluate the performance of different knitted fabrics in view of their possible application as knee-angle sensors, which will be described in Chapters 5 and 6.

Analysis of the fabrics electrical behaviour reveals sensing properties, whose potential and weakness are important to explore. In particular, once the aspect of electrical behaviour based on mechanical deformation has been investigated, it will then be possible to analyse special fabric treatments (e.g. embedding into supporting leggings) to improve the mechanical behaviour and thus electrical repeatability.

## 4.2 Objectives

The objective of this chapter is to examine the outcomes of the electrical characterisation (whose methodology was introduced in Chapter 3) carried out on knitted conductive samples during cyclic loading.

Firstly, the analysis of the fabric electrical behaviour during cyclic elongation-recovery will be discussed together with some critical conditions.

Secondly, the results of mechanical preconditioning will be presented as well as the influence of knitted fabric parameters, current and elongation rate on the resistance measurements.

Thirdly, the sensing properties of the four stitch patterns will be compared in terms of gauge factors.

Lastly, the time-dependent behaviour, the elongation-dependent behaviour and a time-frequency analysis will conclude the study on the fabrics.

## 4.3 Analysis of the electrical behaviour of the conductive samples

Stability, repetability, sensitivity, linearity and hysteresis of conductive samples undergoing cyclic deformation are the electrical features of interest that will allow the evaluation of the fabric's performance as a transducer in the rest of this Chapter.

The analysis of the electrical behaviour of samples undergoing cyclic stretch-recovery followed the post-processing described in section 3.6, with the SP29 sample being chosen to present the results of the study. Identical trends leading to similar considerations occurred for the other samples and, for this reason, they are not reported in the same detail.

Figure 4.1 shows the resistance variation with the elongation performed for

the SP29 sample sourced with 3 mA and tested at 9.6 mm/s during the preconditioning test.

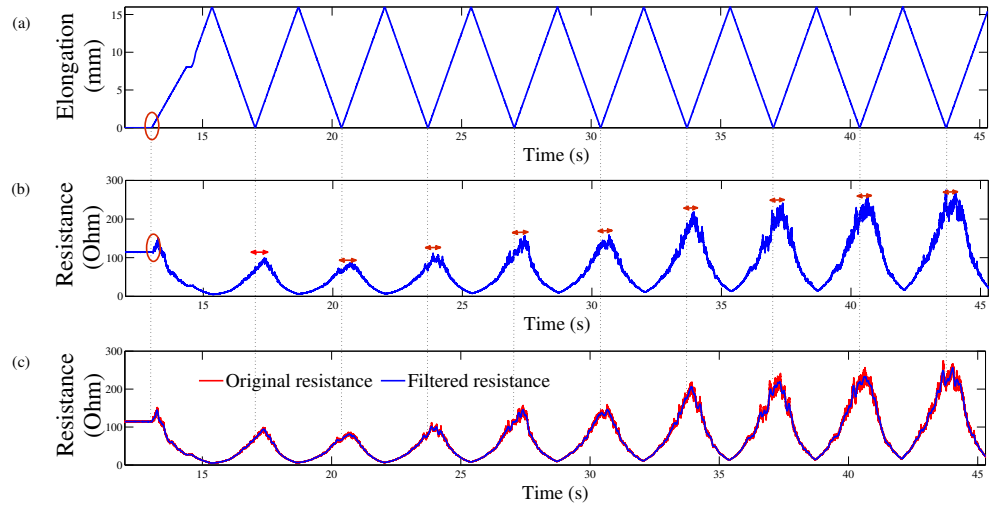


Figure 4.1: Analysis of the electrical behaviour of the SP29 sample sourced with 3 mA and tested at 9.6 mm/s during preconditioning test: (a) Elongation versus time (b) Original resistance versus time (c) Original and Savitzy-Golay filtered resistance versus time (N=3 and f=151). The red arrows show the delay between the maximum resistance and minimum elongation. The red ellipses indicate the instant when the specimen starts its elongation and, correspondingly, the fabric electrical resistance begins to increase

This behaviour can be explained by the fact that, for knitted textiles subjected to a uniaxial strain, the configuration of the loop changes and, consequently, so does the length of a stitch (as described later on in section 4.5.1). This is due to the slippage of the yarns in the loop during the extension (section 2.7.5) and the overall loosening of the fabric after extended use. Thus, when the specimen is initially elongated, its electrical resistance increases proportionally to L described by Ohm's law in Equation (2.1) as a result of the increased length of the stitch (red ellipses in Figures 4.1 (a) and (b)). This was possible because the elongation of the specimen (and thus of the yarn) started at exactly the beginning of loading thanks to the initial position of the fabric in the clamps (described in section 3.5). With

the increasing elongation a better contact within yarns causes a decreased contact resistance - for the appearing of multiple parallel conduction paths according to Equation (2.2) - and, therefore, a decreased resistance. This phenomenon explains why the minimum resistance value occurs at the maximum elongation, i.e. 16 mm.

Similarly, one would expect that the maximum resistance value is measured exactly in correspondence of the minimum elongation. Nonetheless, there is a delay between the maximum resistance and minimum elongation (red arrows in Figure 4.1 (b)) due to the fact that the mechanical characteristics of the fabric have a considerable impact on its electrical behaviour (as already explained in section 3.5.1). This delay is caused by the slow recovery time of the fibres composing the fabric (for the viscoelastic properties described in 2.4) when compared to the frequency of the stretch-recovery cycles. In fact, when the elongation reaches its minimum value (i.e. initial position of the clamps), the stitch length has not reached its minimum value as the loops shrink slowly in accordance with their own recovery time. Consequently, the maximum electrical resistance is measured with a delay, after the minimum elongation. This delay is not present when considering the maximum elongation/minimum resistance values as the fabric is elongated by the tensile machine and, thus, the length of the stitch forcibly changes with the timings imposed by the Instron.

The analysis of the fabric resistance presented in this section showed the electrical response of conductive samples during the first elongation-recovery cycles. More cycles provide the same information with only a difference in higher resistance values, as explained in the subsection 4.4.3. The examination of more cycles of fabric deformation is important, especially for the critical issues encountered, as discussed in subsection 4.3.1.

### 4.3.1 Fabric critical loosening

The analysis of the electrical behaviour of knitted conductive textiles undergoing cyclic loading shows some critical issues, as anticipated in section 3.6.1 when discussing the data filtering procedure. The most critical condition is when the sample returns to the position before being stretched (minimum elongation performed by the tensile machine) as the fabric structure starts to loosen, becoming more relaxed cycle after cycle (Figure 4.2).

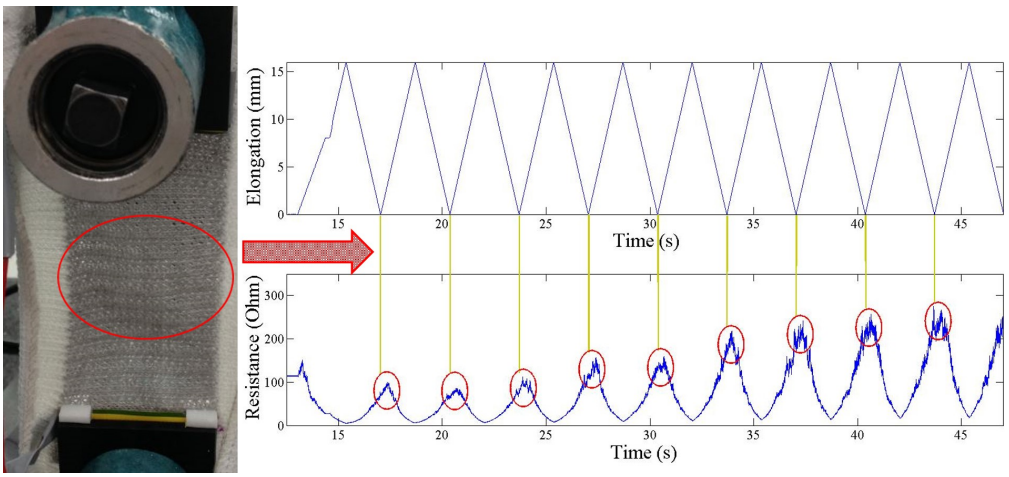


Figure 4.2: Loosening of the fabric during cyclic loading and its effect on the electrical resistance

The loosening of the conductive fabric due to the fibre-fibre slippage (section 2.7.5) causes unpredictable fluctuations of the electrical resistance in correspondence of the maximum resistance value measured (red ellipses in Figure 4.2). Such fluctuations are mechanically unavoidable, cannot be removed completely by filtering the original signal and, thus, they will not be excluded in the analysis of the electrical properties of the conductive textile. Moreover, such oscillations become numerous when the specimen undergoes hundred of cycles.

To illustrate how the loosening of the fabrics affects the electrical response progressively with cycles, two examples are given. Figure 4.3 analyses the electrical behaviour of the SP29 sample sourced with 3 mA and tested at

9.6 mm/s during the 50th-52nd cycles. In this interval, the minimum fabric resistance is still measured at the maximum elongation and the delayed maximum fabric resistance at the minimum extension. This means that the effect of the fabric relaxation is not critical.

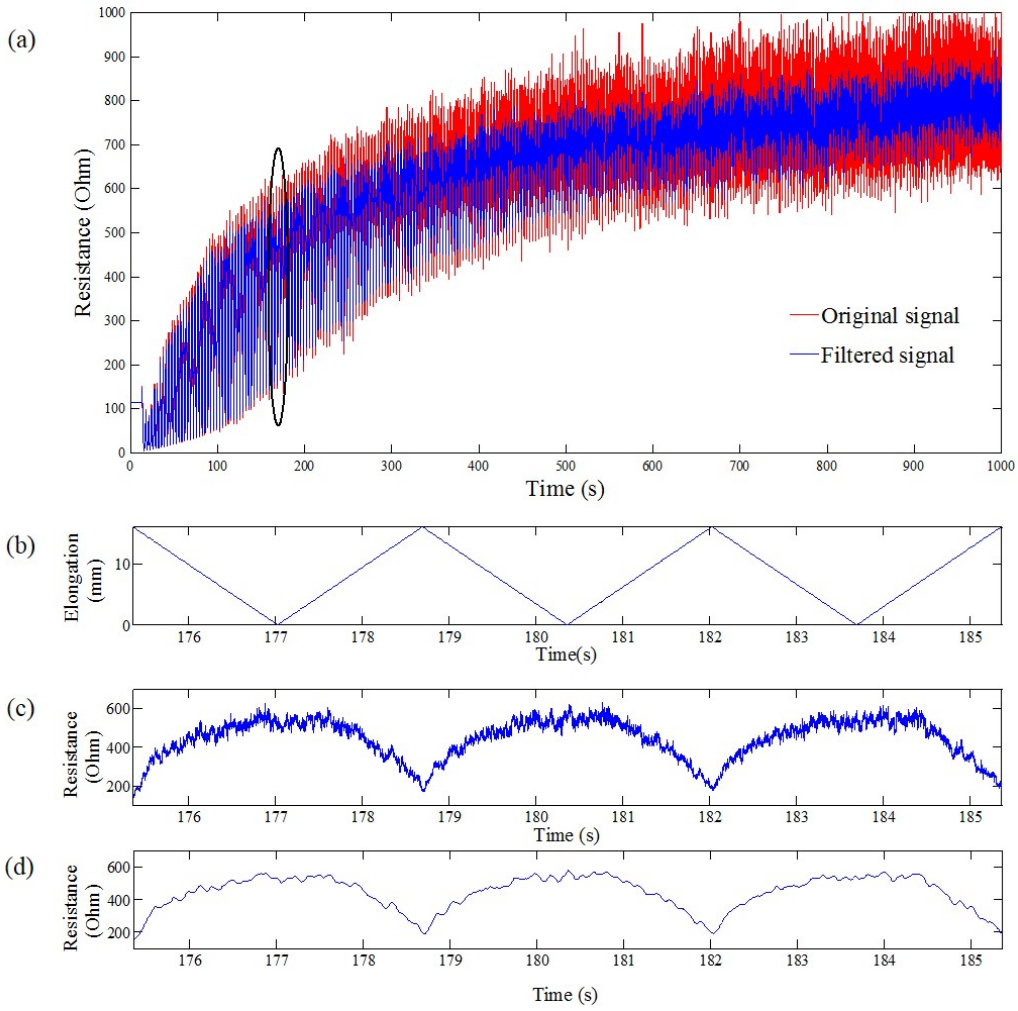


Figure 4.3: Analysis during the 50th-52nd cycles for the SP29 sample sourced with 3 mA and tested at 9.6 mm/s: (a) Area of investigation, (b) Extension, (c) Original resistance and (d) Savitzky-Golay filtered resistance

However, from the 200th cycle onwards (Figure 4.4), the loosening of the fabric affects massively the electrical behaviour, with the maximum and minimum resistance values being indistinguishable with the movement performed.

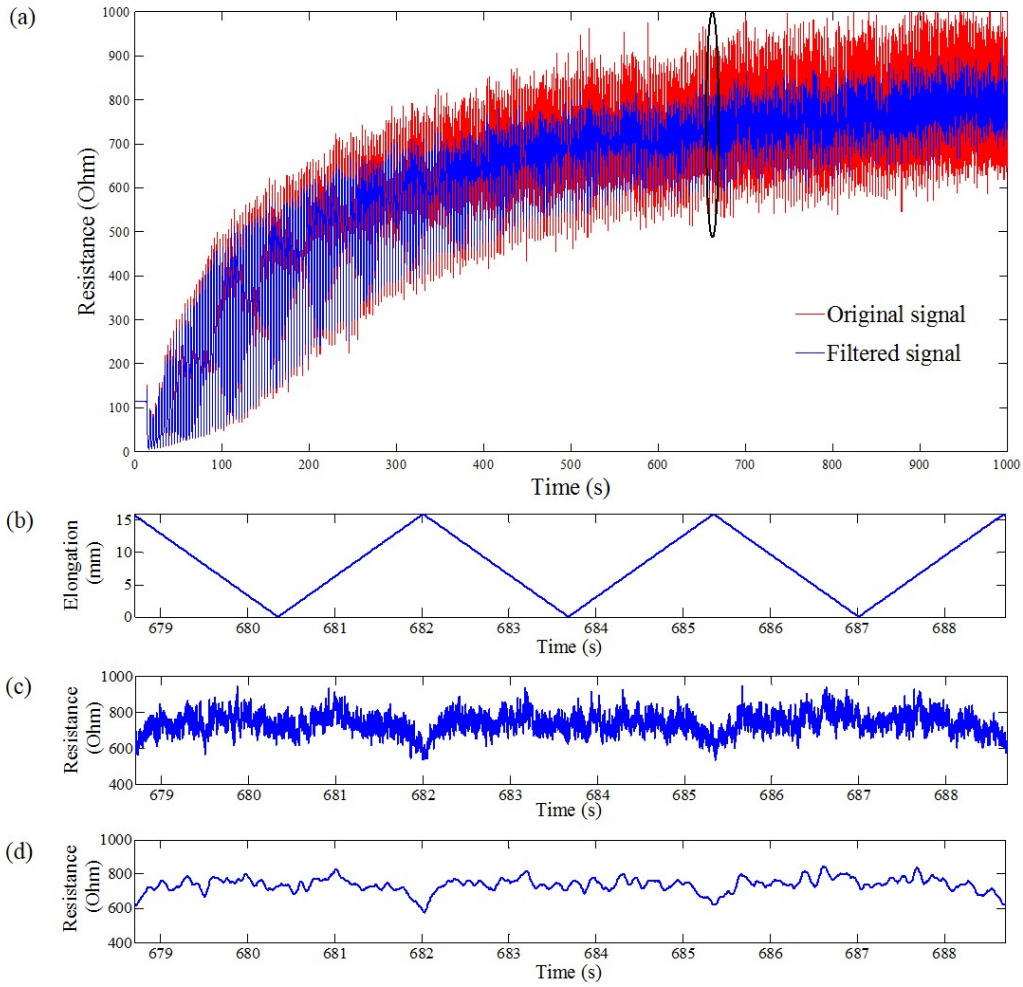


Figure 4.4: Analysis during the 200th-202nd cycles for the SP29 sample sourced with 3 mA and tested at 9.6 mm/s: (a) Area of investigation, (b) Extension, (c) Original resistance and (d) Savitzky-Golay filtered resistance

The analysis of the fabric electrical behaviour has therefore highlighted that all samples lose their ability in following promptly and accurately the movement performed after a considerable number of stretch-recovery cycles. This phenomenon occurs at any testing conditions (e.g. current and elongation rate) and will affect the over time reliability of the fabrics as a transducer (in particular as strain sensor in a wearable application) unless some remedies are arranged. The integration of samples in elastic supporting garments (discussed in Chapter 6) is the first step towards this goal. The loosening of the fabrics influences the performance parameters described in the rest of this chapter, including the gauge factor (4.6) and the signal to noise ratio (4.9.3).

## 4.4 Results and discussion of the mechanical preconditioning

The questions to answer when testing the knitted conductive textiles for a considerable number of stretch-recovery cycles (mechanical preconditioning described in section 3.5.1) were whether the electrical properties stabilised after a number of cycles and whether the effects of an extensive use were repeated after a rest period. The outcomes of this investigation provide a preliminary assessment on stability and repeatability of the electrical properties of conductive specimens prior to sew them across the knee joint of a pair of leggings and test for a considerable number of knee flexion-extension cycles (Chapter 6). The change in the electrical properties during cyclic mechanical loading is also discussed considering the way the fabrics are electrically driven (section 4.5.2) or mechanically loaded (section 4.5.3). The results of mechanical preconditioning described in section 3.5.1 are reported in Table 7.2 of Appendix III (7.3.4) in terms of:

1. Test number, which identifies the sample and the test conditions according to Table 7.1 of Appendix I (7.3.4).

2. Settling time, $T_s$, which is described in subsection 3.6.4;

3. Number of cycles to settle, which is calculated according to Equation (3.4);

4. Stabilised average resistance, which is introduced in subsection 3.3 and indicated as $R_{\text{settling time}}$ in Table 7.2;

5. Resistance value at which the peak-to-peak span settles, which is introduced in subsection 3.3 and named $R_{\text{settled span}}$ in Table 7.2.

The analysis of the results of Table 7.2 shows the effects of mechanical preconditioning in terms of:

- Stabilisation of the electrical resistance (subsection 4.4.1);
- Time to reach stability, in particular a decreasing number of cycles to settle during repeatability test (subsection 4.4.2);
- Increasing stabilised average resistance from preconditioning to repeatability tests (subsection 4.4.3).

### 4.4.1 Stabilisation of the electrical resistance

The first property of knitted conductive samples undergoing 250 cycles of mechanical preconditioning was the stabilisation of the fabric electrical resistance within the trial. To show the effect of mechanical preconditioning the peak-to-peak span is illustrated for the SP29 sample during preconditioning and repeatability tests (Figure 4.5), with the settling time ($T_s$) and standard deviation (SD) being determined by the change point analysis (described in section 3.6.4).

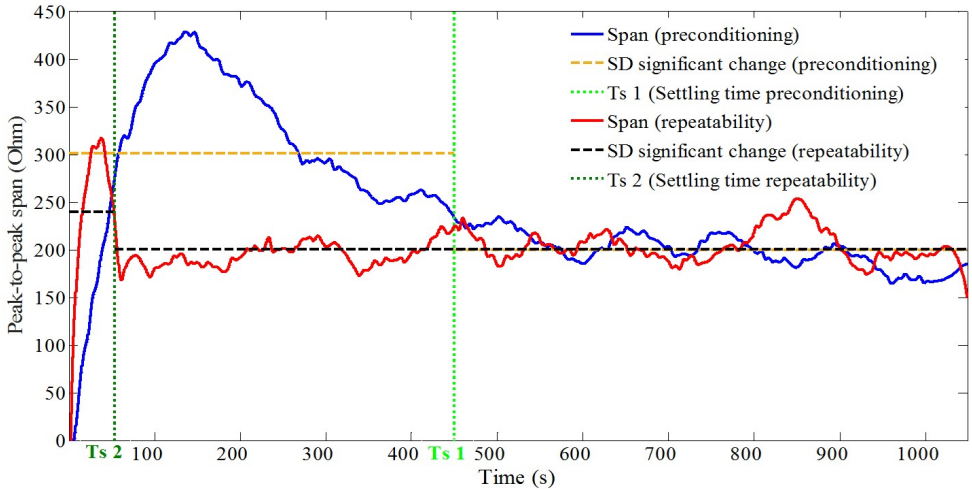


Figure 4.5: Effect of mechanical preconditioning on the peak-to-peak span for the SP29 sample sourced with 3 mA and tested at 9.6 mm/s during preconditioning (blue line) and repeatability tests (red line)

From Figure 4.5 it is evident how, after the initial cycles in which the electrical equilibrium was not reached, the peak-to-peak span settled to a constant value ($R_{\text{settled span}}$), which was conserved after a period of rest. In other words, the rest period between the first and second session did not cancel the effect of the preconditioning process. As a result, during the repeatability tests the samples showed again a stabilisation of the peak-to-peak span and, compared to the preconditioning session, it occurred in a shorter settling time ($T_{s_2} < T_{s_1}$ in Figure 4.5). Thus, the stabilisation of the electrical behaviour was faster when the samples underwent preconditioning. The time to reach stability is expressed in terms of number of cycles to settle in section 4.4.2 .

Some fluctuations around the stabilised value occurred, especially during the repeatability test. However, such fluctuations have a very low frequency when compared to the signal of interest (stretch-recovery cycles) and thus they can be removed by using a simple detrend algorithm.

### 4.4.2 Decreasing number of cycles to settle during repeatability test

The time to reach stability for conductive fabrics subjected to an extended cyclic mechanical loading (preconditioning) can be expressed in terms of number of cycles to settle and calculated with Equation 3.4. The mechanical preconditioning resulted in a decreased number of cycles for the electrical stabilisation during repeatability test, as can be seen in Figure 4.6 which compares the number of cycles to settle for each sample during preconditioning and repeatability tests. Each bar shows mean and standard deviation for a given sample at three different currents and two elongation rates and were calculated with formulas 7.11 and 7.12 of Appendix IX (7.3.4), respectively. The choice of representing results from different test conditions in the same bar is justified by the common tendency for all specimens (the reduction of number of cycles to settle occurs independently of the current provided and elongation rate performed). The consequence of the joint representation is a higher standard deviation in Figure 4.6.

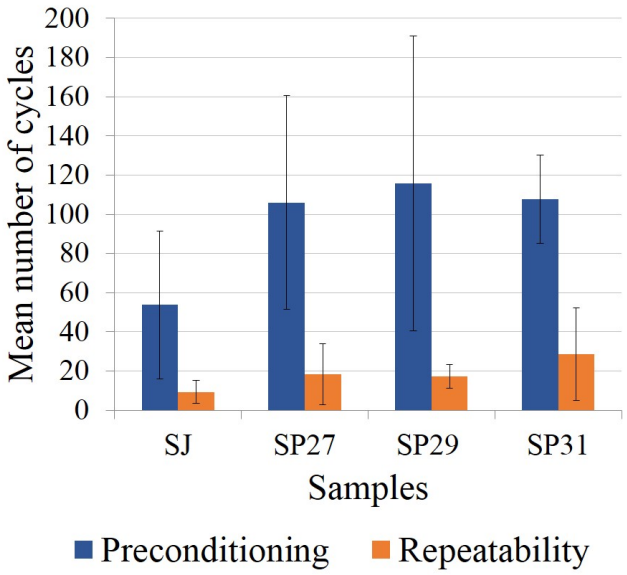


Figure 4.6: Mean number of cycles to reach the electrical stabilisation for all samples at three different currents and two elongation rates

As can be noticed, SP27 and SP29 were the samples that required the longest period of time to settle during the preconditioning, 106 and 116 cycles respectively. Nonetheless, they were also the samples for which the mechanical preconditioning had the most consistent effect, with the number of cycles being decreased to 18 and 17 cycles during the repeatability test.

To validate the effectiveness of mechanical preconditioning on the electrical properties of knitted conductive samples a statistical analysis was conducted. A paired-samples $t$-Test was chosen to determine whether there was a statistically significant difference between the means of number of cycles for the electrical stabilisation during and after preconditioning.

Figure 4.7 reports the $t$-test table calculated with the SPSS software and Figure 4.8 illustrates the difference of means between each pair of samples, the error bars corresponding to the standard error and the $p$-values.

Significant differences were found for all samples, being $p < 0.05$ for the four pairs. This confirmed that the average number of cycles to reach the electrical stabilisation was significantly larger during preconditioning test.

**Paired Samples Test**

| | | Paired Differences | | | | | t | df | Sig. |
|---|---|---|---|---|---|---|---|---|---|
| | | Mean | Std. Deviation | Std. Error Mean | 95% Confidence Interval of the Difference Lower | Upper | | | |
| Pair 1 | SJ_PRE-REPEAT | 44.50000 | 35.44432 | 14.47008 | 7.30346 | 81.69654 | 3.075 | 5 | .014 |
| Pair 2 | SP27_PRE-REPEAT | 87.66667 | 99.72094 | 40.71090 | -16.98405 | 192.31738 | 2.153 | 5 | .042 |
| Pair 3 | SP29_PRE- REPEAT | 98.33333 | 88.77762 | 36.24331 | 5.16693 | 191.49974 | 2.713 | 5 | .021 |
| Pair 4 | SP31_PRE - REPEAT | 79.00000 | 53.00943 | 21.64101 | 23.37001 | 134.62999 | 3.650 | 5 | .007 |

Figure 4.7: $t$-test table obtained from the difference between means number of cycles for the electrical stabilisation during and after preconditioning

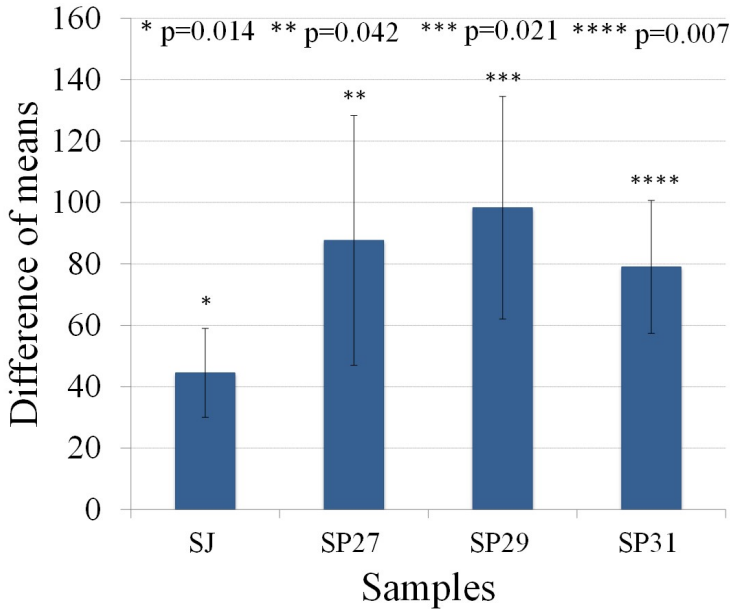


Figure 4.8: Difference of means of number of cycles, standard error and $p$-values between the four pairs of samples during and after preconditioning

### 4.4.3 Increasing stabilised average resistance from the preconditioning to repeatability tests

Another interesting effect of the mechanical preconditioning was that the stabilised average resistance increased from the preconditioning to repeatability tests, as illustrated in Figure 4.9. This tendency was likely due to an increase of the total resistance between trials related to both an increase of the contact resistance (due to the decreased contact pressure according to Equation 2.2) and an increase of the length-related resistance (due to the increased yarn length following the loosening of the fabric, according to Equation 2.1). Similarly to Figure 4.6, each bar in Figure 4.9 represents mean and standard deviation at three different currents and two elongation rates, as the tendency was common for all specimens independently of the current provided and elongation rate performed. Such comparison among values at different test conditions justifies, again, the higher standard deviation.

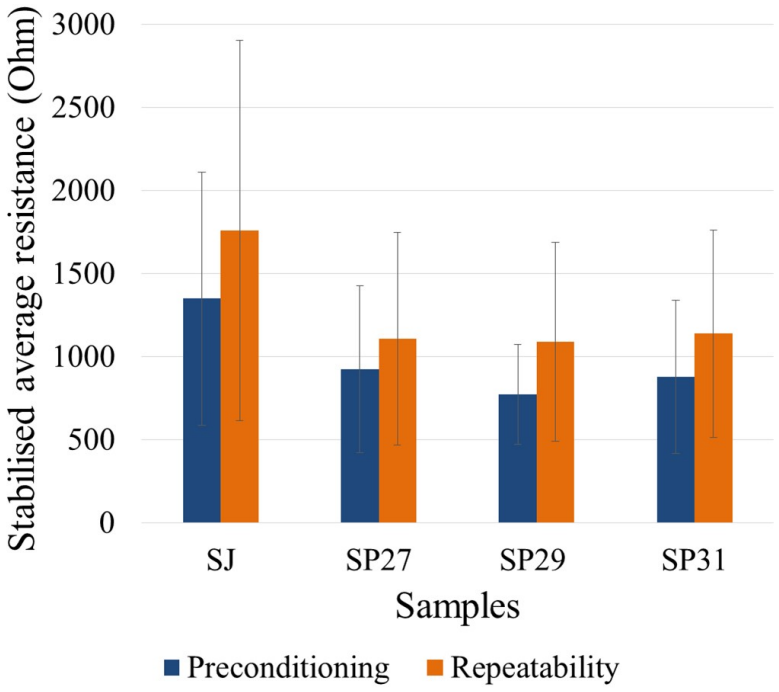


Figure 4.9: Stabilised average resistance for all samples during preconditioning and repeatability tests as mean at three different currents and two elongation rates

## 4.5 Effects influencing the electrical features of the samples

The electrical behaviour of the conductive samples is influenced by many causes:

- Change of the knitted fabric parameters between tests;
- The current provided to the samples;
- The elongation rates at which the tests are performed.

In the following sections each effect influencing the fabric electrical behaviour is analysed in detail.

### 4.5.1 Analysis of the knitted fabric parameters

An analysis of the fabric parameters was conducted with the same optical technique introduced in 3.3 on knitted conductive samples after the extended cyclic loading (subsection 3.5.1).

From this investigation, it was noticed that the shape of the stitch changed for all specimens. In particular, it was measured an increase of the loop width and the yarn diameter, whereas the loop height generally did not change considerably while the samples were elongated in the course direction. As an example, Figure 4.10 compares the dimensions of the stitch for the SP29 before and after fatigue. Between the preconditioning and repeatability tests the values of loop height, loop width and diameter passed from 1375 $\mu m$, 1490 $\mu m$ and 497 $\mu m$ to 1384 $\mu m$, 1607 $\mu m$ and 514 $\mu m$, respectively. The results of the optical analysis after preconditioning are reported for all samples in Table 4.1 in terms of loop width, loop height, yarn diameter and their percentages of variation with respect to the original measurements (Table 3.2).

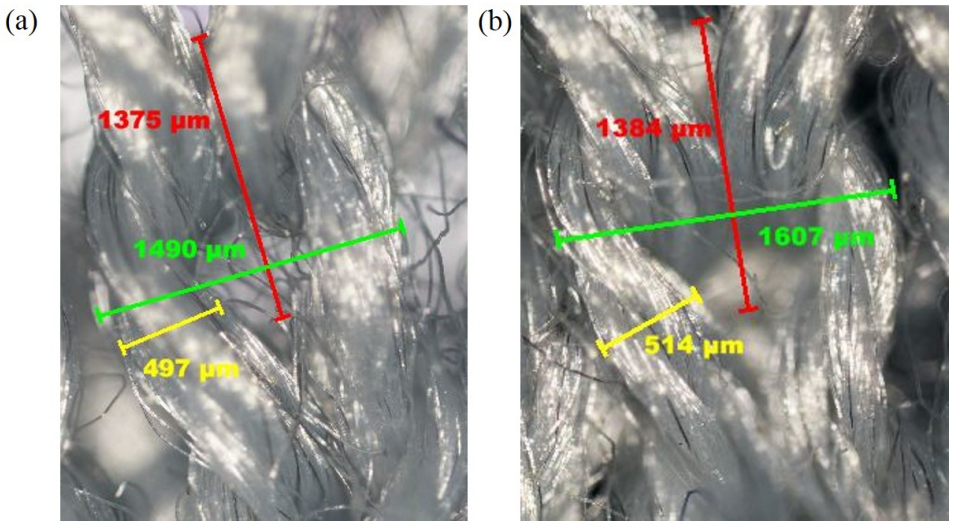


Figure 4.10: Analysis of the dimensions of the stitch for the SP29 before (a) and after preconditioning (b). Loop height, loop width and diameter are represented in red, green and yellow respectively.

Table 4.1: Mean values and standard deviations of the fabric parameters for the four samples under investigation considering 10 measurements after preconditioning

| Sample | Loop width after (mm) | Width variation (%) | Loop height after (mm) | Height variation (%) | Yarn diameter after (mm) | Diameter variation (%) |
|---|---|---|---|---|---|---|
| Single Jersey | 1.50 ±0.07 | 5.96 | 1.16 ±0.02 | 5.52 | 0.55 ±0.02 | 9.63 |
| SP27 | 1.65 ±0.06 | 16.88 | 1.54 ±0.05 | 19.05 | 0.60 ±0.02 | 11.01 |
| SP29 | 1.68 ±0.07 | 17.77 | 1.39 ±0.01 | 1.80 | 0.62 ±0.03 | 21.06 |
| SP31 | 1.67 ±0.13 | 2.16 | 1.35 ±0.13 | 6.94 | 0.55 ±0.03 | 0.32 |

These values were calculated as mean of the stitch parameters contained in an inch of fabric. It is noticeable that SP27 and SP29 were the samples with the highest variation in loop width (+ 16.88 and + 17.77, respectively) and diameter (+ 11.01 and + 21.06).

The loop length was therefore determined (Table 4.2) by using Equation 3.1 and the measurements of Table 4.1.

Table 4.2: Comparison of loop lengths before and after preconditioning considering 10 measurements

| Sample | Loop length (mm) | Loop length after (mm) | Percentage of variation (%) |
|---|---|---|---|
| Single Jersey | 6.58 ±0.24 | 7.05 ±0.19 | +7.14 |
| SP27 | 7.00 ±0.10 | 8.07 ±0.16 | +15.37 |
| SP29 | 7.01 ±0.10 | 8.02 ±0.29 | +14.48 |
| SP31 | 7.43 ±0.32 | 7.63 ±0.40 | +2.69 |

A comparison between loop lengths for new samples (Table 3.2) and samples already preconditioned (Table 4.1) is illustrated in Figure 4.11. Figure 4.11 shows that SP27 and SP29 were the samples that changed the most their loop lengths after preconditioning (i.e. +15.37 for SP27 and +14.48 for SP29), followed by Single Jersey (+ 7.14). Significant changes in the loop lengths after fatigue were confirmed by the paired-samples $t$-Test for Single Jersey ($p = 0.0420$), SP27 ($p = 0.0014$) and SP29 ($p = 0.0318$). In the overall, samples most affected by changes in their geometry after fatigue tests (SP27 and SP29) were also the ones which the highest variation of number of cycles for electrical stabilisation between preconditioning and repeatability tests (Figure 4.6).

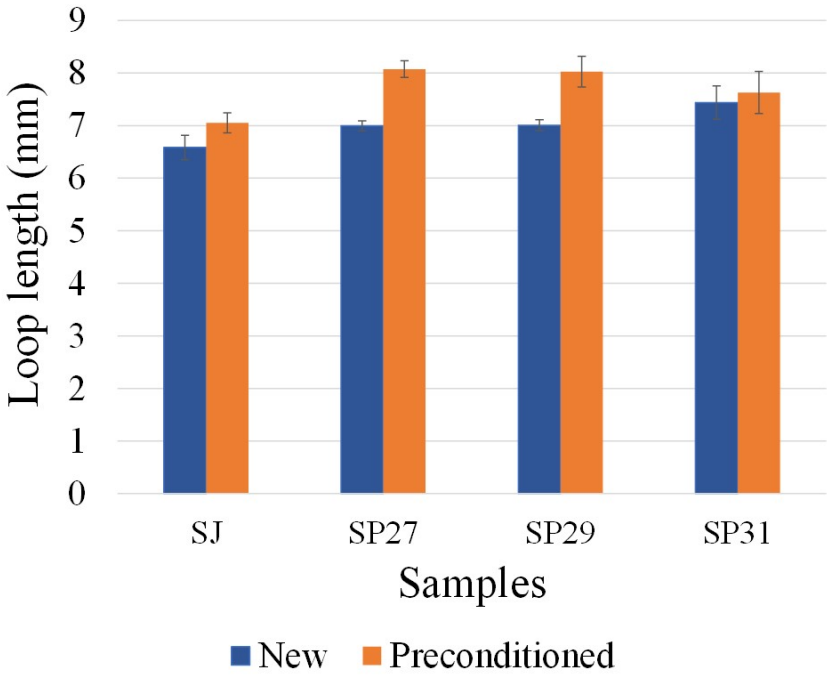


Figure 4.11: Loop length for new and preconditioned samples

### 4.5.2 Effect of the current on the electrical resistance of the fabrics

The electrical properties of the conductive samples changed with the currents provided. Preconditioning and repeatability sessions performed at three different currents (1 mA, 3 mA and 6 mA) demonstrated that the stabilised average resistance decreased for increasing currents sourced to the specimens (Figure 4.12).

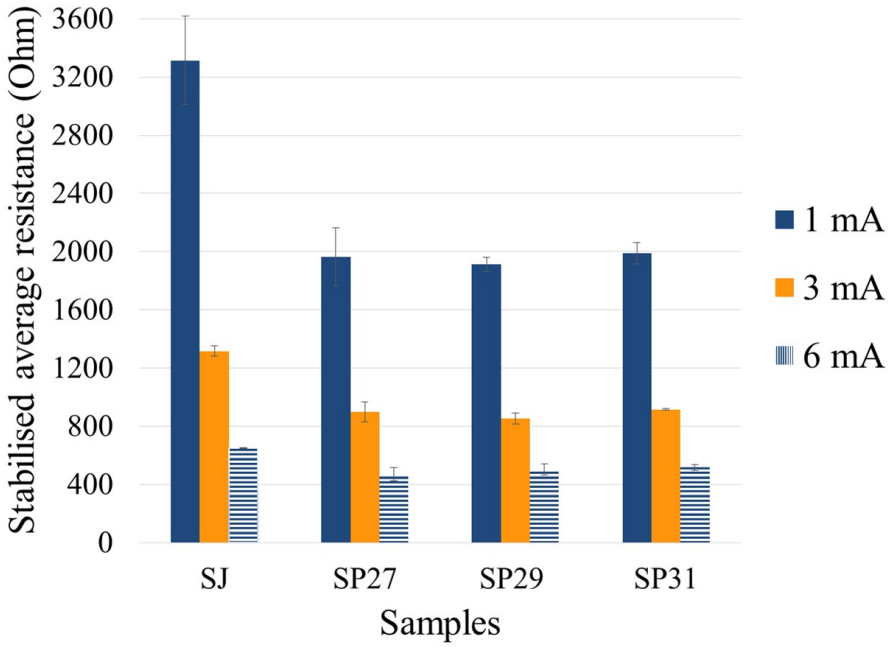


Figure 4.12: Stabilised average resistance for all samples at three different currents during repeatability test, as mean at two elongation rates

An explanation of this phenomenon was that on the stainless steel fibres' surface an oxide film (i.e. passivation layer) exhibited a p-type semiconducting behaviour (Yin, DHaese, and Nysten 2015). Thus, the contact between fibres behaved as a non ohmic contact, whose phenomenon of decreasing resistance with increasing current has been widely observed (Lee 1999). Hence, when the sourced current is increased, the contact resistivity $\rho_c$ in Equation 2.2 decreases, resulting in a decreased contact resistance

and, lastly, fabric resistance.

The effect of current on resistance is more pronounced on Single Jersey, as highlighted in Figure 4.13 with the stabilised average resistance being compared in relative terms among knit patterns and with respect to the stabilised average resistance at 1mA. This can be explained by the fact that Single Jersey is the specimen with the highest stitch density (Table 3.1) and thus, compared to the other samples, has more electrical contacts (Figure 2.11) between adjacent loops per $cm^{-2}$, leading to more numerous current flow paths.

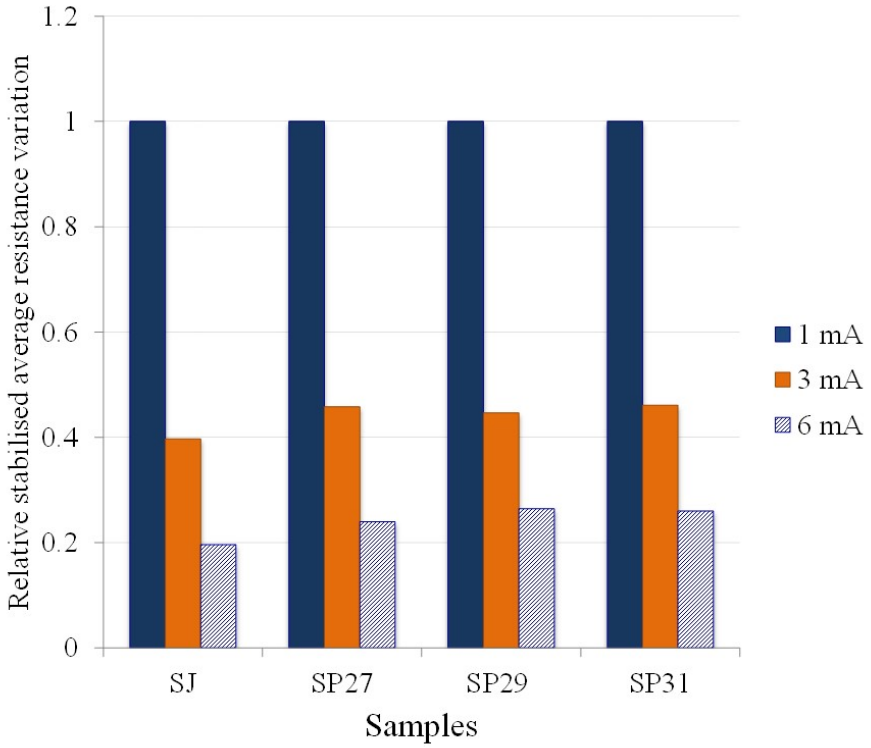


Figure 4.13: Variation of the stabilised average resistance at 1, 3 and 6 mA sourcing currents normalised with respect to the 1mA test

### 4.5.3 Effect of the elongation rate on the electrical resistance of the fabrics

In Chapter 3 Equation 3.4 described the linear relationship between the number of cycles (N) necessary for the stabilisation of the fabric electrical resistance and the elongation rate ($l_r$). The analysis of the results of Table 7.2 determined the effect of $l_r$ on N and, thus, on the stabilised average resistance of the fabrics.

In particular it was demonstrated that the difference between the mean number of cycles for preconditioning and repeatability tests increased with the elongation rate (Figure 4.14). Moreover, the specimens tested at the highest elongation rates (12 mm/s) stabilised in less cycles, independently of the current sourced.

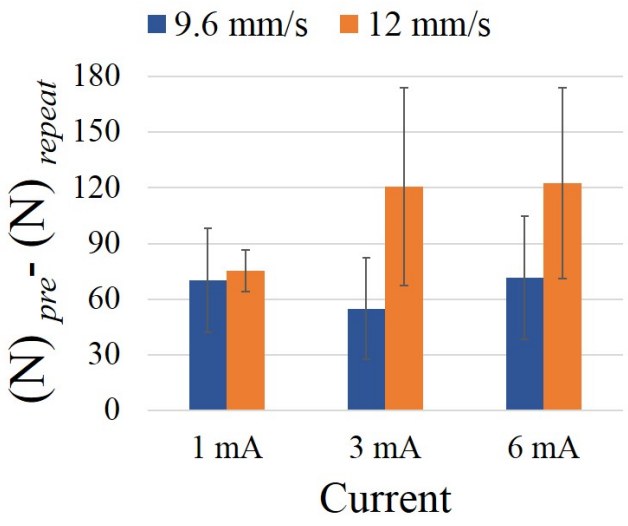


Figure 4.14: Difference of mean number of cycles (N) to settle between preconditioning and the repeatability test at different elongation rates. The error bars correspond to the standard error.

## 4.6 Gauge factor of the stitch patterns

To evaluate which fabric is a suitable basis for sensor design, it is important to compare the sensing property of the four stitch patterns. To do so, the variation of the gauge factor with the stretching-recovery cycles was calculated according to Equation 4.1:

$$GF = \frac{\frac{\Delta R}{R}}{\varepsilon} \tag{4.1}$$

Where: GF is the gauge factor, $\Delta R$ is the change in resistance, R the initial resistance and $\varepsilon$ is the strain value. In this study, the relative change in resistance is represented by the peak-to-peak span with respect to the average resistance ($R_{avg}$). $R_{avg}$ is the mean value of the unfiltered fabric resistance variation and is calculated with a Butterworth filter of order 2 and normalised cut-off frequency equal to $5 * 10^{-5}$ (Figure 4.15). These values were chosen to remove the ripple due to the loading cycles and, at the same time, to follow the mean variation of the original fabric resistance.

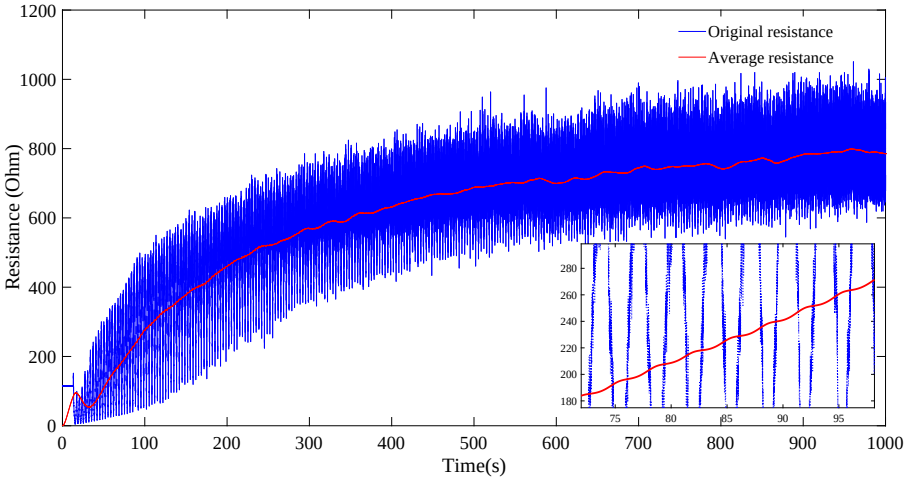


Figure 4.15: Original and average resistance for the SP29 sample sourced at 3 mA and tested at 9.6 mm/s. Zoom of the reduced ripple following the original signal

The strain $\varepsilon$ is the ratio between the absolute change in the specimen length ($\Delta L = 116 - 100 = 16mm$) and the original length of the specimen in the clamps (100 mm).

To specify which stitch pattern delivers the best sensitivity under the same test conditions (3 mA and 9.6 mm/s), the gauge factor variation with cyclic loading was compared for the four samples (Figure 4.16) during preconditioning (A) and repeatability tests (B). During the preconditioning test, SP29 (red line) is the sample that maintains the highest GF for the longest time interval showing, however, also the largest variation from 20 to 2 after 200 cycles. Conversely, the SP27 (blue line) exhibits the lowest gauge factor maintained over time and the lowest gauge factor variation, from 5 to 1 after 30 cycles. Both knit patterns have therefore interesting properties: the SP29 assures higher sensing performance but decreasing with cycles, whereas the SP27 guarantees stable but lower sensitivity. For these complementary characteristics, SP27 and SP29 were chosen for the application described in Chapters 5 and 6.

The common decrease of the gauge factor with time in Figure 4.16 is a confirmation of the effect of the loosening of the fabrics on all samples. This tendency was discussed in 4.3.1 and illustrated in Figure 4.4 according to which, after 200 cycles of cyclic loading, the SP29 (at 3 mA and 9.6 mm/s) loses accuracy with the movement performed due to the fabric relaxation. The 5 minute interval between tests has the effect of generally improving the sensing property of the samples. In fact, the gauge factor at the beginning of the repeatability test is higher than at the end of the preconditioning test (11, 10 and 8 for SP29, Single Jersey and SP27 respectively). Nonetheless, during the repeatability test, the gauge factor of all samples drops steeply with cycles, reaching the minimum value (i.e. 2) from the 20th cycle onwards.

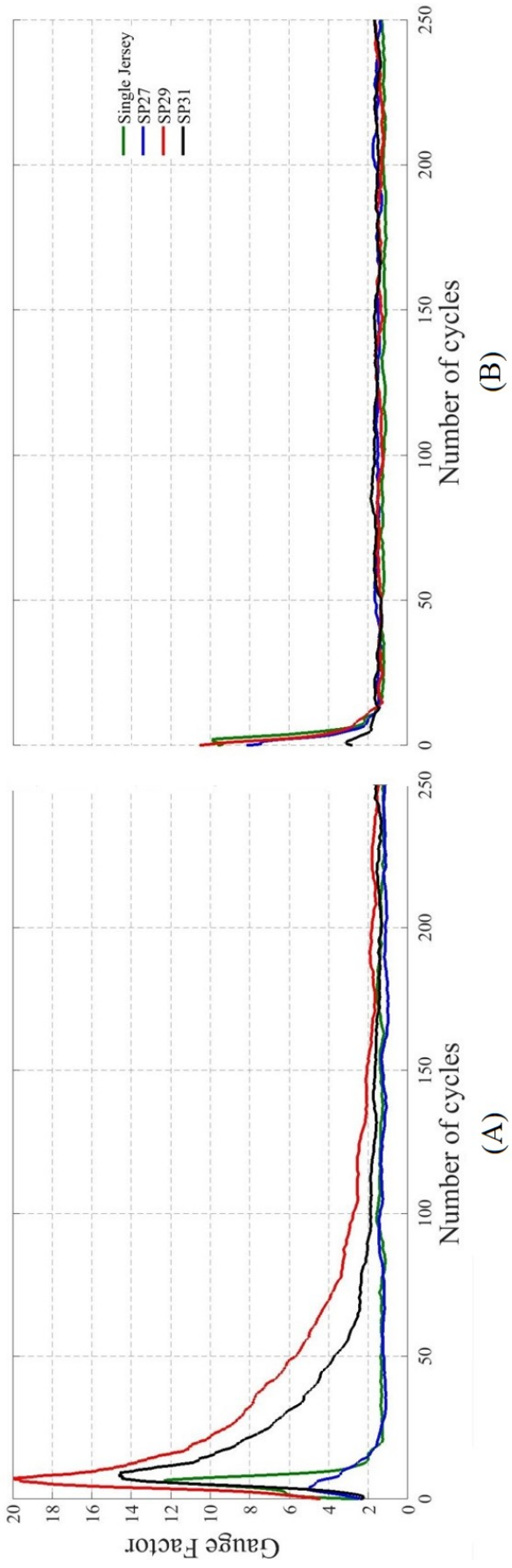


Figure 4.16: Gauge factor variation with number of cycles for Single Jersey, SP27, SP29 and SP31 under the same test conditions (3 mA and 9.6 mm/s) during (A) preconditioning and (B) repeatability tests

This indicates that the 5 minute rest is not enough for all specimens tested cyclically on an Instron machine under the same conditions to fully recover from the effect of relaxation, which affects them from the last 50 cycles of the preconditioning onwards.

All samples tested at 1 mA and 6 mA show a similar behaviour, with the gauge factor decreasing gradually with cycles during preconditioning and steeply during repeatability. These results are reported, respectively, in Figures 7.4 and 7.5 of the Appendix IV (7.3.4).

Another way of comparing the sensing properties of the samples is by considering the gauge factor variation with cycles for each specimen at different currents, as illustrated in Figure 4.17 for the SP29 sample (tested at 9.6 mm/s) during preconditioning (A) and repeatability tests (B). Figure 4.17 shows that the gauge factor of the SP29 at 1 mA (blue line) is the highest for the longest interval of both tests, followed by the 3 mA (red line) and 6 mA (green line) cases. In particular the GF at 1 mA decreases gradually from 20 to 2 within 180 cycles of preconditioning and rapidly from 20 to 3 after 50 cycles of repeatability. Again, the 5 minute rest improves the sensing properties of the sample but only for a limited number of cycles.

For completeness, illustrations of GF for Single Jersey, SP27 and SP31 at 1 mA, 3 mA and 6 mA are reported in Figure 7.6 of the Appendix IV (7.3.4). Similarly to the SP29, the gauge factor at 1 mA is generally the highest for the longest interval of both tests, followed by the 3 mA and 6 mA cases. Moreover, during the repeatability test, the GF drops to 2 for all samples at different currents since the 20th cycle onwards.

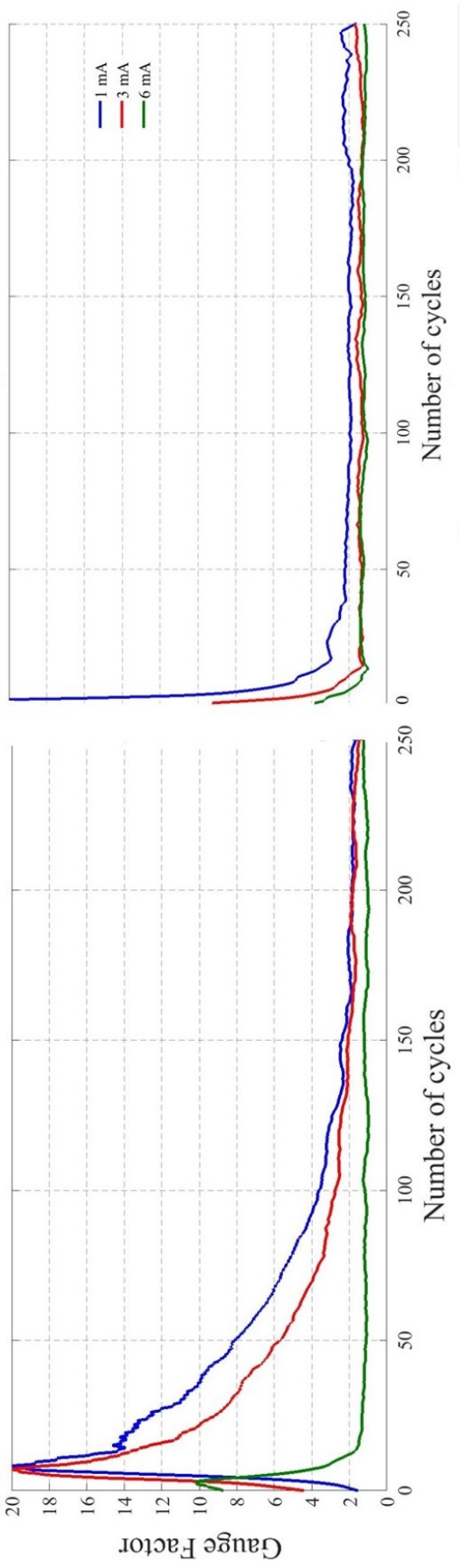


Figure 4.17: Sensitivity variation with current for the SP29 sample tested at 9.6 mm/s during (A) preconditioning and (B) repeatability test

## 4.7 Time dependent behaviour

An important requirement for materials to use as elongation sensors is that their electrical response is repeatable with elongation. The aim is to allow computation of elongation based on measurement of resistance. In terms of application, e.g. fabric embedded into garment for motion capture, the goal is to estimate joint angles based on resistance measurement.

A possible reason why the electrical response deviates from the ideal behaviour is its dependence on the loading path (e.g. stretching, recovery) or hysteresis. Hysteresis is typically caused by friction and structural change in materials (Fraden 2010). A study of hysteresis is therefore important as the magnitude of such effect can affect the employability of the conductive textiles as sensors.

Figures 4.18 and 4.19 illustrate the dependence of the electrical response on the elongation during the first three cycles of preconditioning and repeatability tests for the SP29 sample sourced with 3 mA and tested at 9.6 mm/s. The resistance values of both graphs were different, as they referred to different electrical conditions. Figure 4.18 corresponds to a sample never stretched before. Thus its resistance varied slowly during the first cycles of preconditioning, was dependent on the elongation cycle and, thus, affected by a considerable hysteresis. On the contrary, Figure 4.19 shows the electrical behaviour of a sample already preconditioned and tested after a 5 minute rest. From the y-axis range, it is possible to notice the increased average resistance caused by the loosening of the fabrics. The upward shift of the curves was due to the faster electrical stabilisation during the first cycles of the repeatability test. The hysteresis behaviour as well as the resistance span were also reduced as a result of the fabric loosening caused by the mechanical preconditioning.

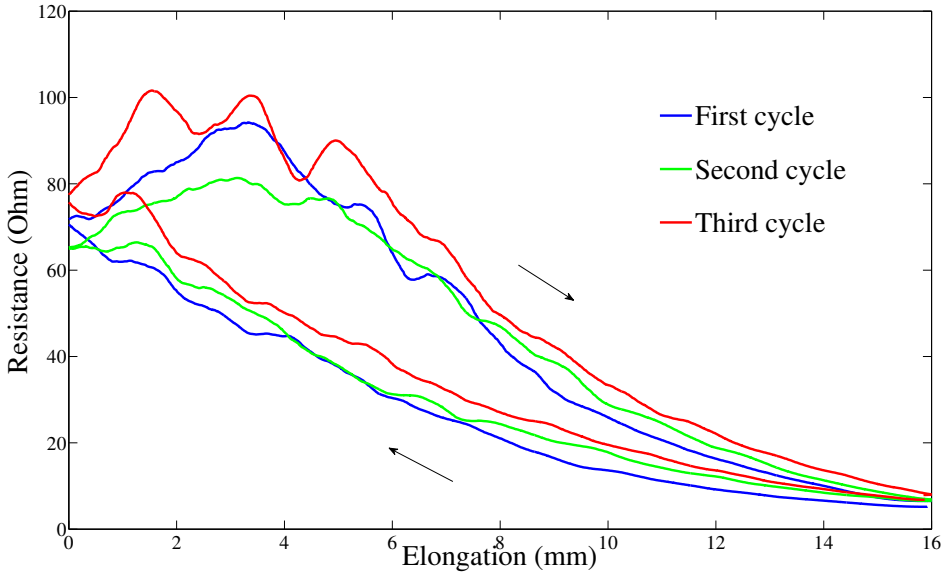


Figure 4.18: Hysteresis during the first three cycles of preconditioning test for the SP29 sample sourced with 3mA and tested at 9.6 mm/s

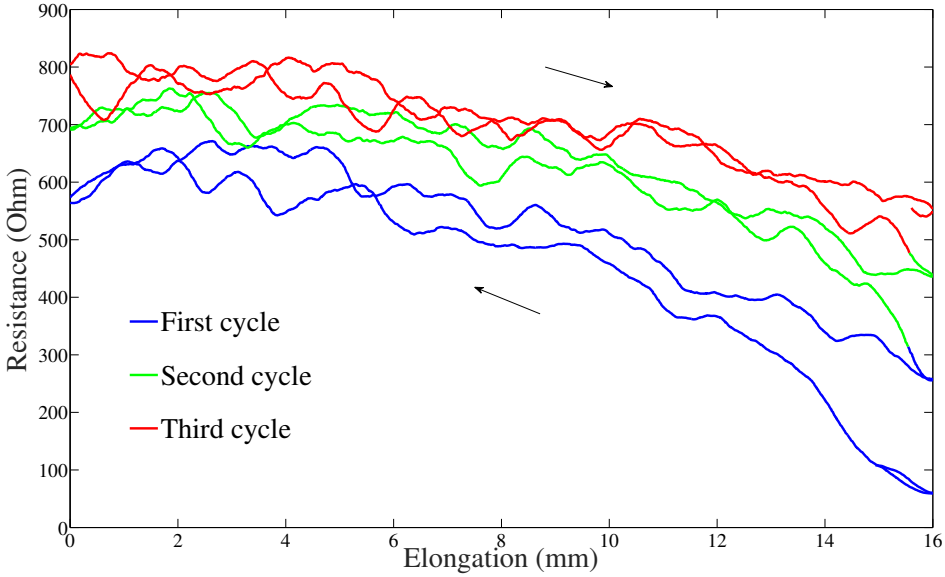


Figure 4.19: Hysteresis during the first three cycles of repeatability tests for the SP29 sample sourced with 3mA and tested at 9.6 mm/s

## 4.8 Elongation dependent behaviour

The elongation to which the conductive samples are stretched influences their electrical behaviour. In fact, as anticipated in section 3.5.2, the contribution of the contact and length-related resistances to the overall equivalent resistance varies with extension. This phenomenon was already observed in literature (Li et al. 2012) and establishes that the contact resistance dominates the overall equivalent resistance during the initial tensile process, whereas the length-related resistance determines the total resistance when further extensions are applied.

To illustrate the effect of contact and length-related resistances to the overall equivalent resistance, Figure 4.20 compares on the same graph the filtered resistance variation for the SP29 sample sourced with 1 mA and elongated of 4, 8, 12 and 16 mm. For the four cases the fabric resistance was filtered with the Savitzky-Golay of polynomial order 3 and window length 151 (according to section 3.6.1).

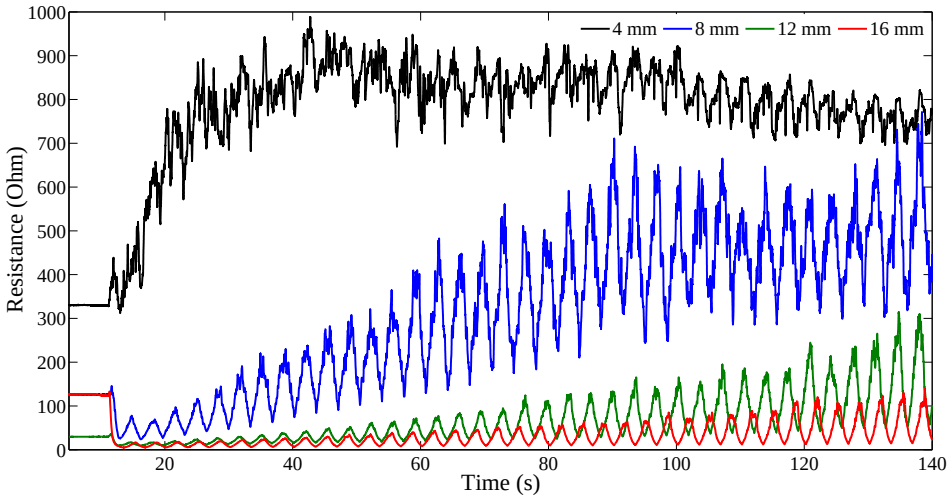


Figure 4.20: Contribution of contact and length-related resistances to the overall equivalent resistance for the SP29 sample sourced with 1 mA and elongated of 4 (black line), 8 (blue line), 12 (green line) and 16 mm (red line)

When the samples were elongated by a small amount (4mm, which corresponds to 4 % of the specimen's length), the contribution of the contact resistance overtook the one of the length-related resistance (black curve). This can be explained by the low pressure at the contact points that makes the contact resistance very high (Equation 2.2) and, thus, very sensitive to any small change related to the fibre-to-fibre contacts. The outcome is the resistance of Figure 4.21 whose variation with time does not accurately follow the movement performed, especially in correspondence of the minimum elongation when the contact pressures are the lowest. In correspondence of the maximum (4mm) elongation the contact resistance is generally lower as the reduction of contact area due to the stretching was largely superseded by the increase of the contact pressure.

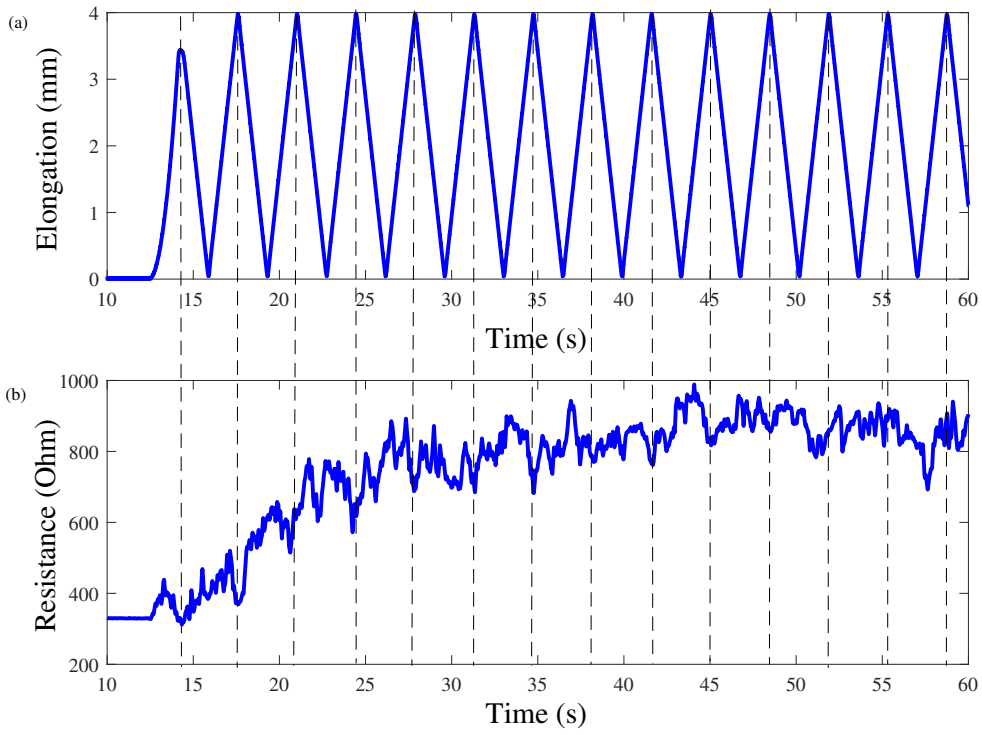


Figure 4.21: (a) Elongation and (b) filtered resistance variation with time for the SP29 sample elongated of 4 mm

On the other hand, the contribution of length-related resistance, which is proportional to the length of the conductive yarn (Equation 2.1), is noticeable when the specimen was elongated of a certain amount. For instance, when 8 mm elongation was applied to the sample, the contribution stemming from the length-related resistance rose, with the resistance starting to vary according to the elongation-recovery phases (blue line in Figure 4.20). Lastly, for 12 mm (green line) and, in particular, for 16 mm (red line) elongations, the length-related resistance dominates, with the electrical behaviour being clearly described cyclically. In particular, the last case was already illustrated in Figure 4.1.

As a result, all tests performed at different elongation values showed the dependence of the fabric electrical behaviour on the elongation.

### 4.8.1 Hysteresis at different elongations

Another way to investigate the elongation dependent behaviour of the conductive samples was studying the hysteresis at different elongations. The relationship between the fabric resistance (the dependent variable) and the elongation performed (the independent variable) was analised during the first cycle at 8, 12 and 16 mm elongations for the SP29 sourced with 1 mA and tested at 9.6 mm/s (Figure 4.22). The aim of considering the first cycle for different elongation cases was to determine the ideal relationship between the electrical resistance and elongation, without the specimen being affected by the loosening occurring cycle after cycle (section 4.3.1). As can be noticed, the fabric electrical response to the elongation performed is not linear. As confirmation, the regression analysis was conducted by studying separately the stretching and recovery phases at 8, 12 and 16 mm elongations during the first cycle. The 4 mm elongation case was excluded as the excessive resistance variation due to the contact resistance (Figure

4.20) would make the results not meaningful.

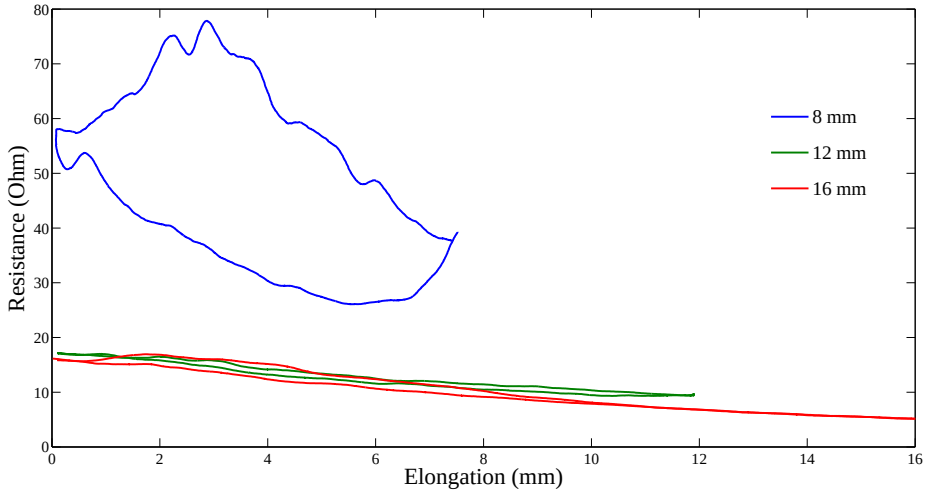


Figure 4.22: Hysteresis during the first cycle for the SP29 sample sourced with 1 mA, tested at 9.6 mm/s and elongated of 8, 12 and 16 mm

The results of the fit are illustrated in Figures 4.23 and 4.24 (with the experimental data represented in blue and the results of the fit in red) and summarised in Table 4.3. The goodness of the fit was estimated through the correlation coefficient $R^2$.

Table 4.3: Regression curves for the SP29 sample sourced with 1 mA, tested at 9.6 mm/s and elongated at 12 and 16 mm during the first cycle

| Phase | Elongation | Regression curve | $R^2$ |
|---|---|---|---|
| Stretching | 12 mm | $y = 0.0498x^2 - 1.3216x + 17.913$ | 0.994 |
| Recovery | 12 mm | $y = 0.0186x^2 - 0.9232x + 17.661$ | 0.988 |
| Stretching | 16 mm | $y = 0.0142x^2 - 1.0868x + 18.167$ | 0.971 |
| Recovery | 16 mm | $y = 0.0251x^2 - 1.1142x + 16.539$ | 0.997 |

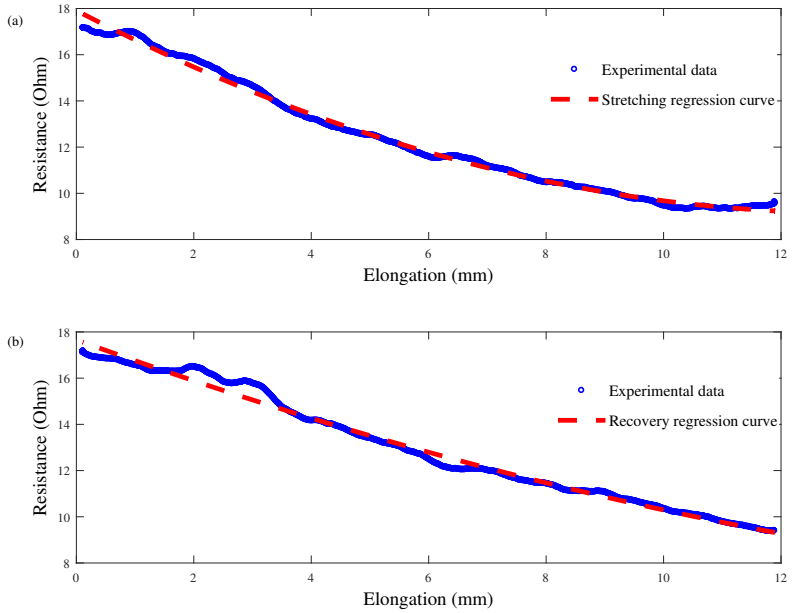


Figure 4.23: Characteristic curves for the stretching (a) and recovery (b) phases of the SP29 sourced with 1 mA, tested at 9.6 mm/s and elongated of 12 mm during the first cycle

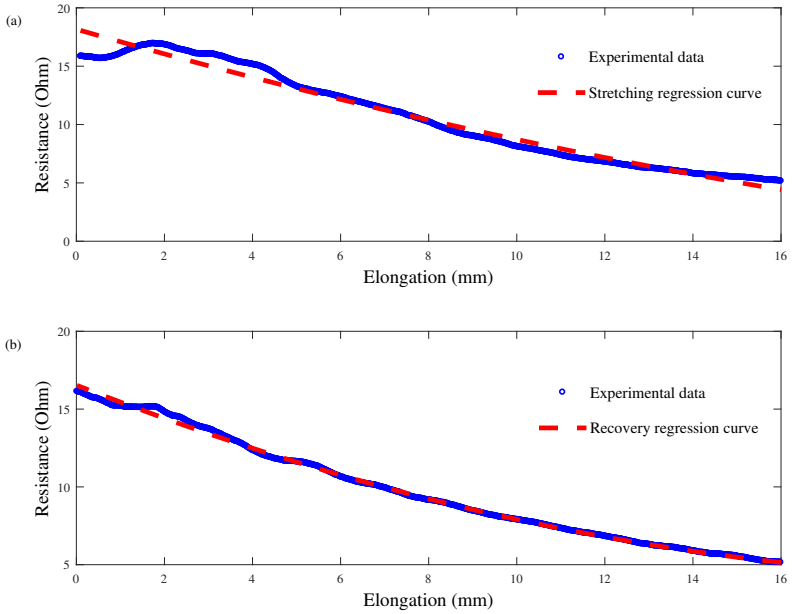


Figure 4.24: Characteristic curves for the stretching (a) and recovery (b) phases of the SP29 sourced with 1 mA, tested at 9.6 mm/s and elongated of 16 mm during the first cycle

Overall, the electrical behaviour of the conductive fabric elongated of 12 and 16 mm can be accurately modelled during the first cycle by quadratic curves for both the stretching and recovery phases. The electrical behaviour of the fabric elongated of 8 mm could not be described by a low order polynomial (linear or quadratic curve) and, for this reason, it is not reported. The non-linear and elongation dependent behaviours were shown for further cycles. Figure 4.25 compares the first and fiftieth cycles for the SP29 sample sourced with 1 mA, tested at 9.6 mm/s and elongated of 8, 12 and 16 mm. It is possible to notice the increased resistance for the three elongations during the fiftieth cycle caused by the fabric relaxation. Moreover, the 16mm elongation shows the smallest hysteresis.

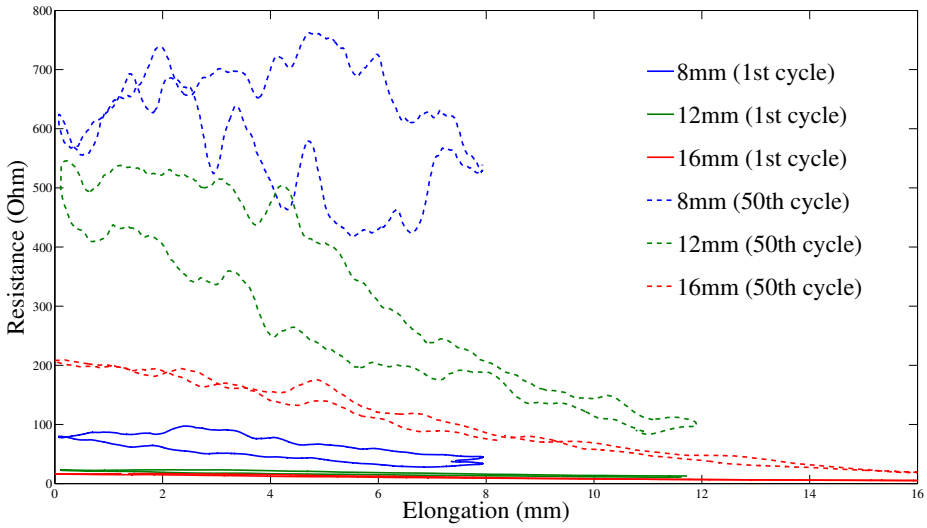


Figure 4.25: Hysteresis during the first and fiftieth cycles for the SP29 sample sourced with 1 mA, tested at 9.6 mm/s and elongated of 8, 12 and 16 mm

## 4.9 Time-frequency analysis

The loosening of the fabric during cyclic loading (described in section 4.3.1) introduces additional noise components to the harmonics spectrum of the fabric resistance signal. In particular, when considering a considerable number of elongation-recovery cycles (subsection 3.5.1), the effect produced might be significant. A time-frequency analysis is, therefore, a useful tool to represent how the frequency spectrum of the fabric resistance varies with time (subsection 4.9.1). Moreover, from such analysis the harmonics representing both the signal and distortion components and their variation with time can be described (subsection 4.9.2). Lastly, by studying the signal-to noise ratio (subsection 4.9.3), it is possible to determine the number of cycles after which the noise overtakes the signal of interest, making the extraction of useful features from the fabric resistance more difficult.
The Matlab code written for the fabric spectral analysis is reported in the Appendix II (7.3.4).

### 4.9.1 Spectrogram

To evaluate how the loosening of the fabric influenced the waveform of the resistance measured during 250 stretch-recovery cycles (at the same test conditions described in subsection 3.5.1), the MATLAB function spectrogram was used. This command computes a fast Fourier transform (FFT)-based spectral estimate over sliding windows overlapped by 50% and whose width was selected in order to have frequency resolution equal to 0.01 Hz. In this way it was possible to appreciate how the frequency content varied over time during cyclic loading.
As an example of the spectral analysis, Figure 4.26 represents the spectrogram of the SP29 sample during preconditioning (Figure 4.26 (a)) and

repeatability tests (Figure 4.26 (b)), with the maximum plotted frequency being 1.55 Hz. This value was chosen as the most relevant frequency content was found in the first five harmonics.

The frequency variation within the harmonics spectrum (horizontal axis) was represented as a function of time (vertical axis) with the amplitude (i.e. the power) of a particular frequency at a particular time depicted by the intensity/color of the corresponding rectangle in the spectrogram.

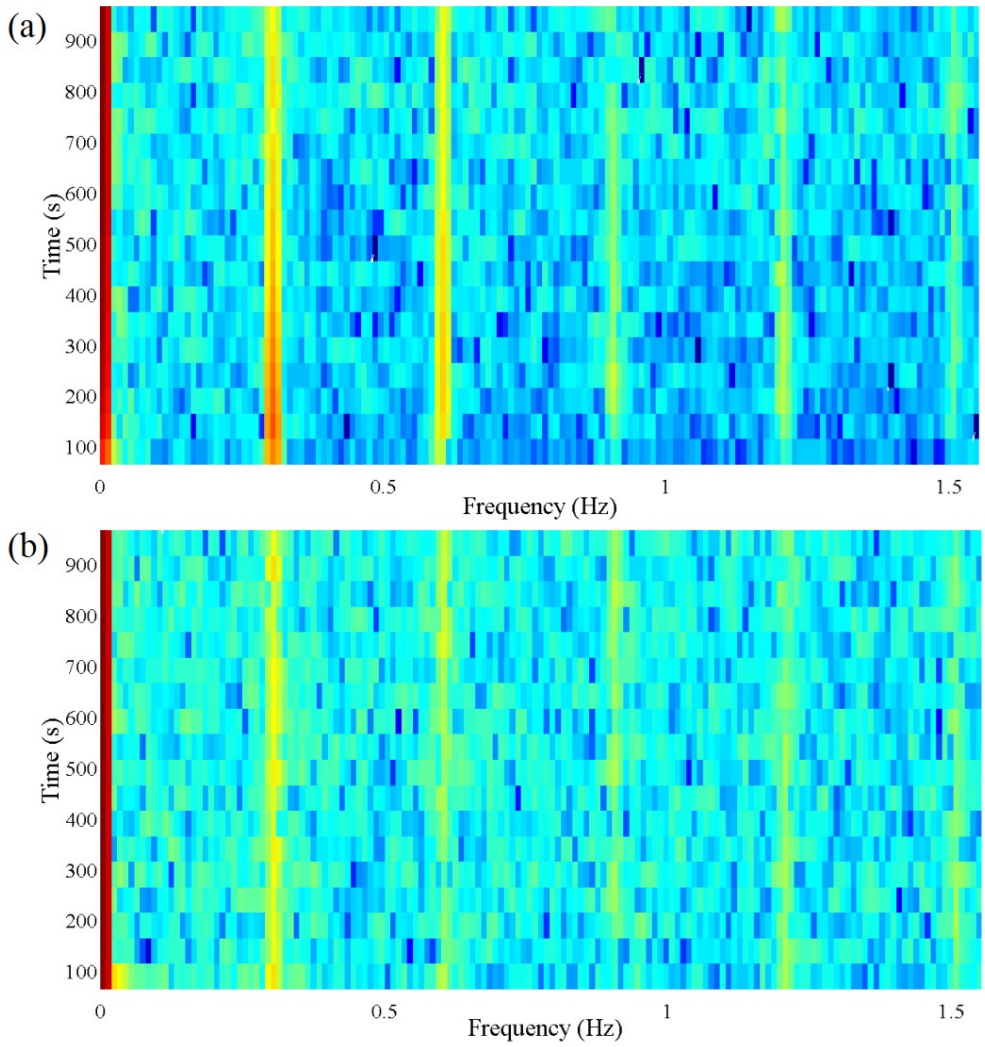


Figure 4.26: Spectrogram of the SP29 sample sourced with 3 mA and tested at 9.6 mm/s during (a) preconditioning and (b) repeatability tests

### 4.9.2 Harmonics amplitude

The harmonics amplitude for both the signal and distortion components and their variation with time are illustrated in Figure 4.27. As the most significant frequency content was found for the first five harmonics, the amplitude variations with time were depicted for 0.3, 0.6, 0.9, 1.2 and 1.5 Hz and for the direct current (DC) component. The odd harmonics of the fundamental (0.3 Hz) were the expected components approximating the input (a triangle wave). The even harmonics were instead the distortion terms, which were generated by the loosening of the fabric during cyclic loading.

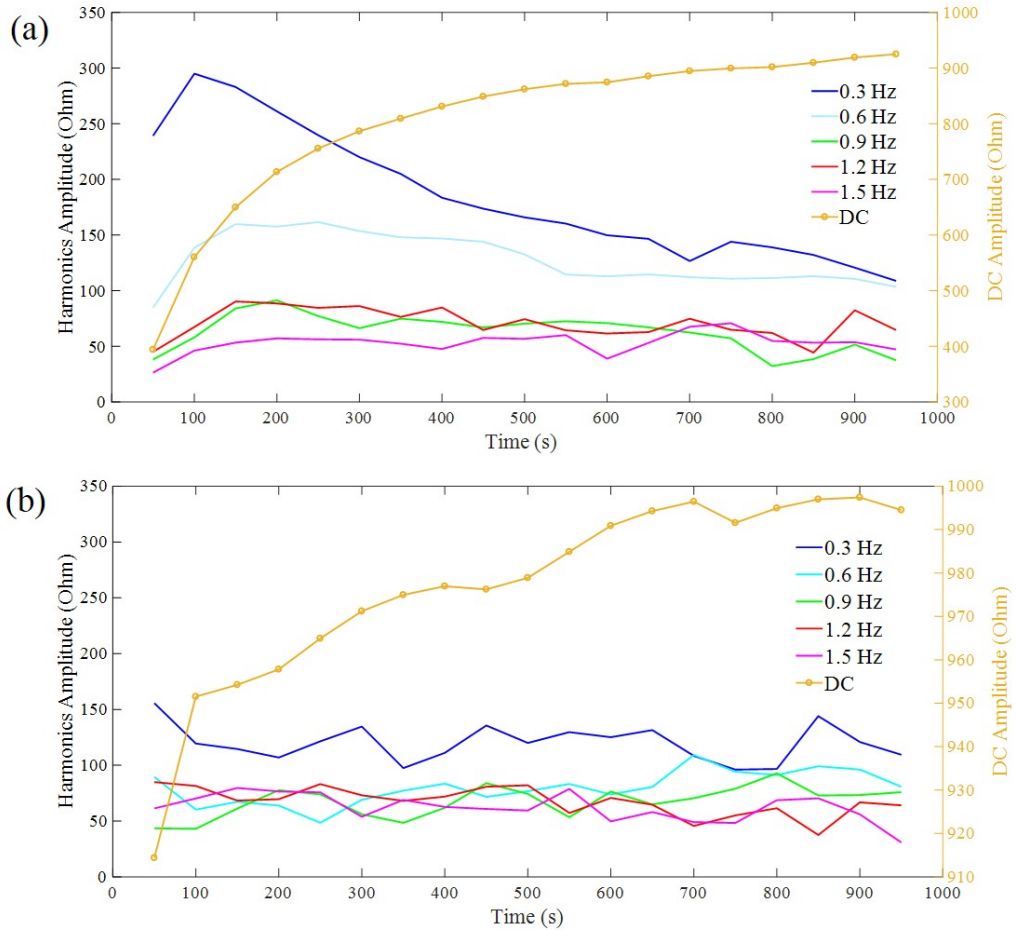


Figure 4.27: Amplitude variation of the most relevant components of the SP29 sample sourced with 3 mA and tested at 9.6 mm/s during (a) the preconditioning test and (b) the repeatability test

With regard to the evolution with time, it was noticed that the DC component (describing the fabric average resistance) increased over time. Moreover, during the preconditioning test, the harmonic at the fundamental frequency has seen its amplitude progressively reduced from the initial value of 300 Ω to approximately 120 Ω, the second-order harmonic (0.6 Hz) decreased from 160 Ω to 110 Ω, whereas no important variations were appreciated in the other harmonics (4.27(a)). During the repeatability test, no variation was appreciated in the fundamental frequency (almost stabilised since the beginning of the test) and in the other harmonics (4.27(b)).
Spectrograms and the harmonics amplitude are reported for Single Jersey, SP27 and SP31 under the same conditions (3 mA and 9.6 mm/s) in Figures Figure 7.7, 7.8 and 7.9 of the Appendix V (7.3.4). Common to all samples was the increasing DC component over time and the progressively decrease of the fundamental frequency during the preconditioning test (from 270  to approximately 130  for the SP31, 240  to 145  for the Single Jersey and from 240  to 50  for the SP27). Lastly, no important variations were appreciated in the fundamental frequency (almost stabilised since the beginning of the repeatability test) and in the other harmonics during both tests.

### 4.9.3 Signal-to-noise ratio

Lastly, the signal to noise ratio was determined for all samples at the same test conditions described in subsection 3.5.1. The signal was calculated as the power of the fundamental component (0.3 Hz) and the noise by the sum of the power of the components at 0.6, 0.9, 1.2 and 1.5 Hz. As an example, Figure 4.28 illustrates the SNR for the SP29 sample sourced with 1 mA and tested at 9.6 mm/s.
It is noticeable that for the SP29 sample the signal power remained over 0 dB during all the preconditioning test (signal power always greater than the

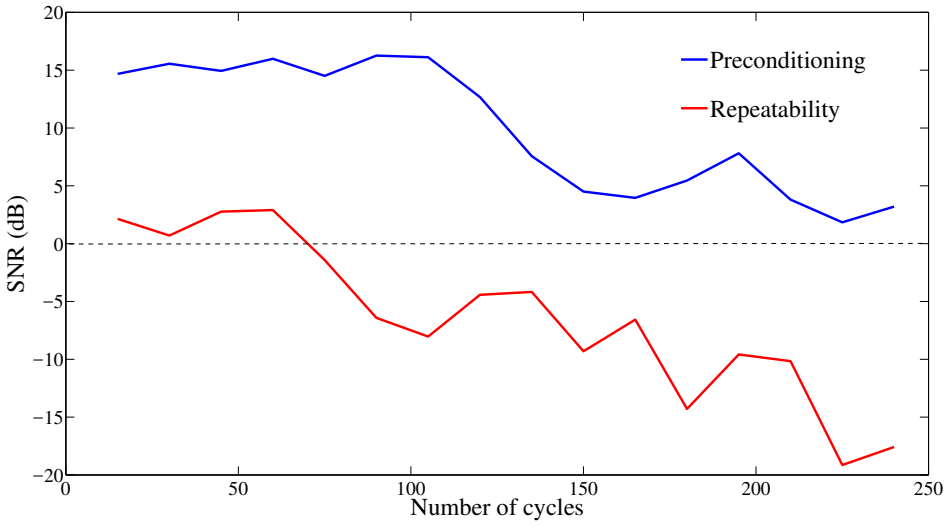


Figure 4.28: Signal to noise ratio for the SP29 sample sourced with 1 mA and tested at 9.6 mmps during preconditioning and repeatability tests

noise power). Along with the cycles the loosening of the specimen affected the fabric electrical behaviour, causing a decrease of the signal-to-noise ratio. During the repeatability test (occurring after five minutes rest from the preconditioning), the noise progressively increased and overwhelmed the signal from the 75th cycle onwards (SNR $\leq$ 0 dB).

The results for all samples are reported in Table 7.3 of Appendix III (7.3.4), whose first column indicates the specimen and test conditions according to Table 7.1. The second column shows the number of cycles N from which the noise overwhelms the signal power (SNR $\leq$ 0). N is expressed as an interval of 15 stretching-recovery cycles as it is related to the time resolution of the spectrogram. The third and fourth columns report the maximum and minimum values of the signal-to-noise ratio in dB. The obtained figures can be conceptually assumed as the values at the beginning and at the end of the tests, being SNR always decreasing with cycles.

Table 7.3 shows that SP29 tested at 9.6 mm/s and sourced with any current value is the sample less affected by the noise during preconditioning and

repeatability tests. In fact, from Figure 4.28 (corresponding to test 13 in the Table) it is evident that not only the signal power is dominant on the noise during the preconditioning test but also the recovery from the noise always occurs during the interval in between tests (cases 3 and 6 mA corresponding to tests 15 and 17, respectively).

The recovery from the noise before repeatability test is common for all samples tested at 9.6 mm/s (tests 1 - 24 in the Table). Conversely, for all samples at 12 mm/s, the signal-to-noise ratio is negative from the beginning of the preconditioning and repeatability tests (N=0 from the 25th test onwards). This means that higher elongation rates determined a noisy signal and no signal recovery from the noise was possible in between tests.

## 4.10 Discussion

Some of the findings presented in this Chapter can be connected to the literature. For example, during the cyclic loading the slow recovery time of the stainless steel fibres composing the fabric (discussed in section 4.3) finds justification in Sun, Cheng, and Zhang 2011 in terms of yarn-to-yarn friction and yarn-to metal friction for the stainless steel yarn. In fact, the stainless steel fibres show significant viscoelastic effects, which means that stainless steel is more likely to undergo stress relaxation over an extended service period compared to other metals (e.g. silver). As a result, the relaxation of the stainless steel yarn during an extended use can affect conductivity and, thus, the overall electrical behaviour.

The gauge factor discussed in section 4.6 drops to 2 for all samples at different currents. This behaviour is consistent with what presented in Guo, Berglin, and Mattila 2010 regarding the sensitivity value of a metal strain sensor (around 2).

Non-linearity and hysteresis in the response to applied strain were aspects encountered in the electrical characteristics of the textile sensor described in Atalay O 2014, as well as the effect of the elongation-dependent behavior of knitted fabrics (Ehrmann et al. 2014). It is due to the non-linearity and hysteresis in the response to applied strain if only few systems have been commercialised so far despite considerable research in the field of wearable strain sensors. Therefore, understanding the effects of the manufacturing process is important to produce knitted sensors suitable for specific target applications.

The increase of the average resistance as a consequence of the fabric loosening has been also recently observed (Atalay et al. 2017). However, there are also many novel results and methodologies arising from this Chapter. Firstly, the constant-current control method employed for the samples under test was an approach completely different from the universally used Wheatstone Bridge. Such method allowed the discovery of a phenomenon not highlighted so far in the literature, which is the non-ohmic behaviour of the contact resistances as a consequence of the presence of surface's oxidation layers.

Secondly, the use of time-frequency spectrograms was a powerful tool for analysing the behaviour of the samples during extended cyclic loading tests. This method permitted to characterise the degradation of the knitted sensor's performance over time in terms of change of the harmonic content shown by the measured resistance and to compare different samples over a much larger time window (with respect to the analysis techniques used so far, such as hysteresis plots showing only a few elongation cycles).

## 4.11 Conclusions

This chapter discussed the electrical response of conductive samples knitted with different stitch patterns to the tests illustrated in Chapter 3.

Firstly, the fabric resistance variation with stretch-recovery cycles was analysed. The most critical condition encountered was the loosening of the specimens when returning to the minimum elongation due to the fibre-fibre slippage. This affected the fabric electrical behaviour with unpredictable fluctuations in correspondence of the maximum resistance value and influenced the performance parameters, such as the gauge factor and the signal to noise ratio.

Secondly, after an extended cyclic mechanical loading (preconditioning test), fabrics tested again after a limited period of rest under the same conditions (repeatability test) showed a stabilisation of their electrical resistance, a decreased number of cycles to settle and an increased stabilised average resistance. Moreover, increasing sourced currents and elongation rates affected the resistance measurements by, respectively, decreasing the stabilised average resistance (proving the non linear behaviour of the metal-semiconductor contact between fibres) and reducing the number of cycles to reach the electrical stabilisation. In particular, specimens with the highest stitch density (Single Jersey) showed the most relevant dependence of the resistance on the current (due to the highest number of electrical contacts).

Thirdly, by comparing the sensing properties of all knit patterns, it was found that the gauge factors decreased gradually with cycles during preconditioning test (up to 20 times smaller) and steeply during repeatability session (reducing to the minimum value from the 20th cycle onwards). The 5 minute rest between tests was not enough for all specimens to fully re-

cover from the effect of relaxation when tested cyclically on an Instron machine. Particularly, it was found that SP29 was the sample that generally maintained the highest sensitivity for the longest time interval but with the variation decreasing with cycles, whereas the SP27 guaranteed stable but lower sensitivity.

Lastly, this chapter showed the time-dependence of the fabrics by means of hysteresis graphs and their non-linear behaviour thanks to a time-frequency analysis. As a result of the mechanical preconditioning, the hysteresis behaviour of the resistance curves was reduced. Moreover, the signal-to-noise ratio was decreasing with cycles for all samples. In particular, the SP29 tested at 9.6 mm/s was the sample less affected by the noise during preconditioning and repeatability tests. Conversely, for all samples at 12 mm/s, the signal-to-noise ratio was negative from the beginning of the preconditioning and repeatability tests. This means that higher elongation rates determined a noisy signal and no signal recovery from the noise was possible in between tests.

The next stage of the research presented in Chapters 5 and 6 will investigate the importance of the support in which the conductive textiles are embedded. In particular the samples electrically characterised on an tensile machine will be sewn across the knee joint of an elastic supporting garment (e.g. two pairs of leggings with different percentage of elastane) and tested during cyclic knee bending-recovery. The aim is to study whether the support will reduce considerably the effect of the loose fabrics and, at the same time, will result in a more accurate tracking of the movement. The choice of which samples to sew on the leggings stemmed from the study of sensitivity presented in this Chapter. In particular the effect of the supporting garment on improving and maintaining the sensing properties will be discussed in Chapter 6.

# Chapter 5

# Application of electrically conductive leggings for motion capture - Methodology

## 5.1 Introduction

The next stage of research on knitted conductive textiles regards the study of their application as wearable motion sensors. The electrical properties of new samples with the same knit patterns of those previously tested on a tensile machine were investigated when integrated into a garment and subjected to deformation. In particular, two conductive textiles were sewn across the anterior aspect of the knees of two pairs of leggings with different percentages of elastane and tested during knee flexion-extension cycles. As a consequence of the integration, the conductive samples underwent stretch-recovery phases that changed their conductivity. The knee motion and the associated fabric electrical resistance variation were recorded with two different measurement systems described in this Chapter. The analysis of the electrical properties of the fabric integrated into a garment and the

evaluation of their employability as motion sensors are reported in Chapter 6.

## 5.2 Objectives

To investigate the electrical behaviour of knitted conductive textiles integrated into garments, two customised methods were used to capture the human motion and the fabric electrical resistance variation. First, this chapter presents the supporting garments, embedded samples and the technique of integration employed in this thesis. Next, the first methodology for knee angle capture is described, called *Method One*, based on image acquisition of coloured markers' positions placed on the human body.
*Method Two* is an alternative acquisition system which uses an isokinetic machine to perform a range of knee motion controlled by a computer. For both methods, the fabric resistance variation was acquired from the garment with a procedure similar to the one described for samples tested in the tensile machine. Calibration and testing procedures are also illustrated, whereas the outcomes of both measurement systems are reported in Chapter 6.

## 5.3 Materials

The conductive samples chosen for the application, the supporting garments and the way the specimens were integrated into them are presented in the following subsections.

### 5.3.1 Description of the knitted conductive fabrics

The choice of which samples to sew on the leggings stemmed from the study of sensitivity presented in 4.6, from which it was found that the SP29 was the sample that generally maintained the highest sensitivity for the longest time interval but with the variation decreasing with cycles, whereas the SP27 guaranteed stable but lower sensitivity. In particular, by integrating such knit patterns in two pairs of leggings with different percentages of elastane it was desired to determine whether the sensitivity of SP27 improves and the SP29's one is maintained. The effect of the supporting garment on the fabrics' sensing properties will be discussed in Chapter 6.

### 5.3.2 Description of the leggings

To investigate the effect of the supporting garment on the electrical behaviour of the conductive textiles embedded in it, two running leggings with different elasticity were employed. In particular the leggings used in this work were made of 15% elastane - 85% Polyester (dhb Zelos Run Tight) and 18% elastane - 82% Polyamide (dhb Active Running Tight). The combination of elastane fibres, even in small amounts, and hard structure man-made fibres made the resulting garment permanently elastic, and this was functional for the extended stretch-recovery tests presented in this thesis.

### 5.3.3 How to embed the knitted conductive fabrics into leggings

The SP27 and SP29 specimens were sewn on the leggings over the anterior aspect of the left and right knees, respectively. Conductive contacts were

created with two copper tapes sewn on top and bottom of the samples (Figure 5.1) with a conductive thread (Figure 5.2), made of stainless steel (28 $\Omega/Ft$ resistance, distributed by Sparkfun for e-textile projects). Connections were soldered on the conductive tapes to collect the electrical signal from the conductive area of the fabrics according to the method discussed in section 5.5.



Figure 5.1: Copper tape sewn on top and bottom of the conductive area of the fabric to create conductive contacts



Figure 5.2: Conductive thread used to sew the sample into the leggings

## 5.4 Method One - *Visual Motion Tracking System*

To measure the electrical resistance variation exhibited by knitted conductive textiles sewn across the anterior aspect of the knee during cyclic flexion-extension, a customised method was developed (Isaia, McNally, and Branson 2017). This system was referred to as Method One or Visual Motion Tracking System as consisted of (Figure 5.3):

- A *camera* (Logitech B910 HD Webcam) and *coloured markers* for the motion tracking and the knee angle calculation;
- *Connections* soldered on the conductive contacts of the leggings for a four-wire resistance measurement (Figure 5.4);
- A manufactured *electronic circuitry* (already described in 3.4.1) to supply a constant current to the samples;
- A *Data Acquisition System* (National Instrument -USB 6003) to collect data from the camera and from the fabrics integrated into leggings.

For this method, a moving object can be tracked by a camera on the basis of its colour. This means that, human motion capture can be detected with the aid of coloured markers placed on the body, or (in this case) on the leggings. Thus, the Visual Motion Tracking System presented in this thesis is based on image acquisition and markers detection, whose working principle is illustrated in subsection 5.4.1. Issues encountered with the markers detection and solutions are reported in subsection 5.4.2.

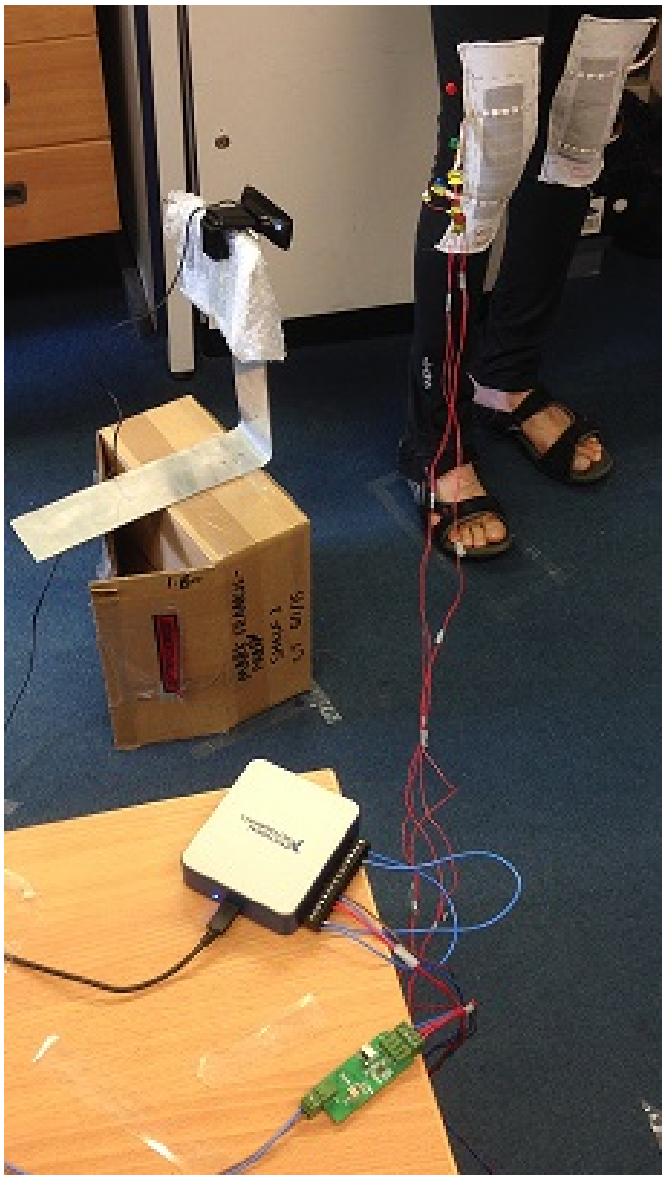

Figure 5.3: The Visual Motion tracking system

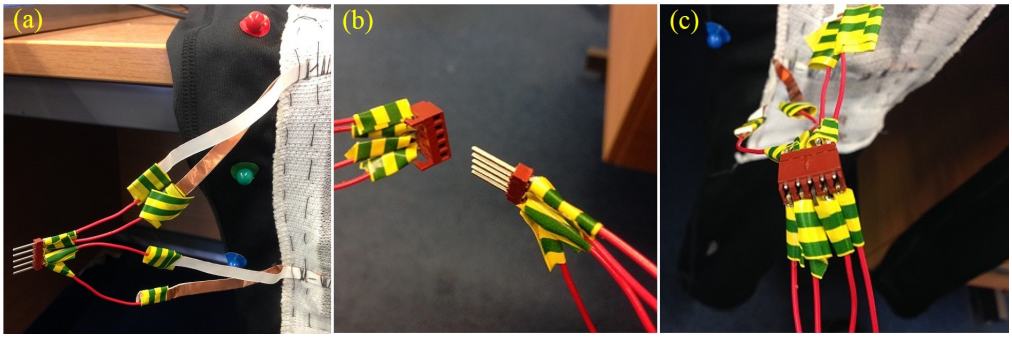


Figure 5.4: (a-c) Connections for the electrical acquisition from the fabric (4 wires measurement)

### 5.4.1 Image acquisition and objects detection

Any image is a matrix of pixel values that can be represented by using many colour models, such as gray-scale or RGB. In particular, the RGB model is used to detect the colours in an image, with red, green and blue components being added together in many ways to produce a wide range of colours (in the form of a MxNx3 matrix, with M rows and N columns of pixels for each red, green and blue colour components). Thanks to the image representation in the form of a matrix, mathematical operations can be applied to detect a particular colour in an image (Goel et al. 2017) and Matlab software can be used for image processing as it takes every input as a matrix.

The *Image Processing Toolbox* is a Matlab tool which provides a number of functions for colour detection and image analysis and, thus, was used in this thesis to distinguish and track real time motion of coloured markers acquired by a camera. In particular, red, green and blue (RGB) markers were placed in appropriate anatomical positions of the leggings (i.e. thigh, knee and shank) to follow the knee angle motion. An algorithm was written to distinguish the RGB markers by using the colour thresholding technique (with the thresholds for red, green and blue detections being set to 0.18, 0.05 and 0.15, respectively). In the following the code is explained step by step and the full code is given in Appendix VI (7.3.4).

First, video frames were captured using the *videoinput* function and a session with the data logger was created (*createSession*). From the video input object, an immediate single image frame was returned (*getsnapshot*) and displayed (*imshow*). Then, the *rgb2gray* Matlab function converted the RGB image object to grayscale, to increase the speed of processing and reduce complexity of the code (by converting a three-dimensional image into a two-dimensional one, the number of bits used to represent each pixel

is reduced). The resulting grayscale image was afterwards subtracted (*imsubtract* function) from the red band image for the detection of red colour in the image. Similarly for the detection of green and blue colours, the grayscale image was subtracted from green and blue bands, respectively.

To remove unwanted noise while maintaining the originality of image, a median filter was used (*medfilt2*). In this process, the pixel value was converted into a median value of 3x3 sampling window, while keeping the pixel value of the border of sampling window unchanged. To work only on the area of interest, the filtered image was consequently converted into a binary image (*im2bw* function) using the thresholding process. According to this, each pixel of the image was given a value of 1 (or 0) for pixel values greater (or lower) than the set threshold. Then, all the objects with less than 300 pixels were removed (*bwareaopen*). On the binary image, a set of properties (i.e. the bounding box and the centroid) for each labeled region was determined with the *regionprops* function (blob analysis). The bounding box drew the boundaries of the objects, whereas the centroid provided the (X, Y) coordinates of the centre of the bounding box and, thus, of the markers.

Lastly, by knowing the coordinates of the centre of the markers it was possible to determine two lines passing through the red, green and blue objects. An angle (and, thus, the knee angle) was calculated between these two lines (Figure 5.5), as described in subsection 5.5.1.

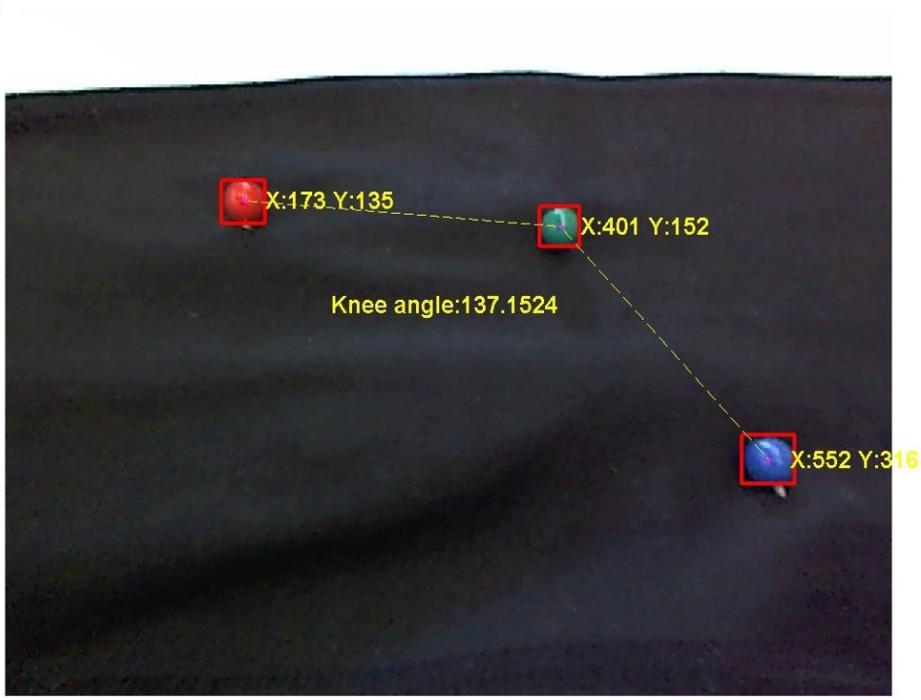


Figure 5.5: Screenshot of the knee angle measurement as the angle between two lines connecting the coordinates of red, green and blue markers. Position of markers is shown as text on the computer monitor

### 5.4.2 Issues with the markers detection and solutions

Reasons for failure in detecting the three markers at the same time were:

- Light condition (Figure 5.6 (a));
- The initial (rectangular) shape of the markers (Figure 5.6 (b)).

These elements, in fact, affected the identification and, thus, the distinction based on the colours thresholding technique (5.4.1).

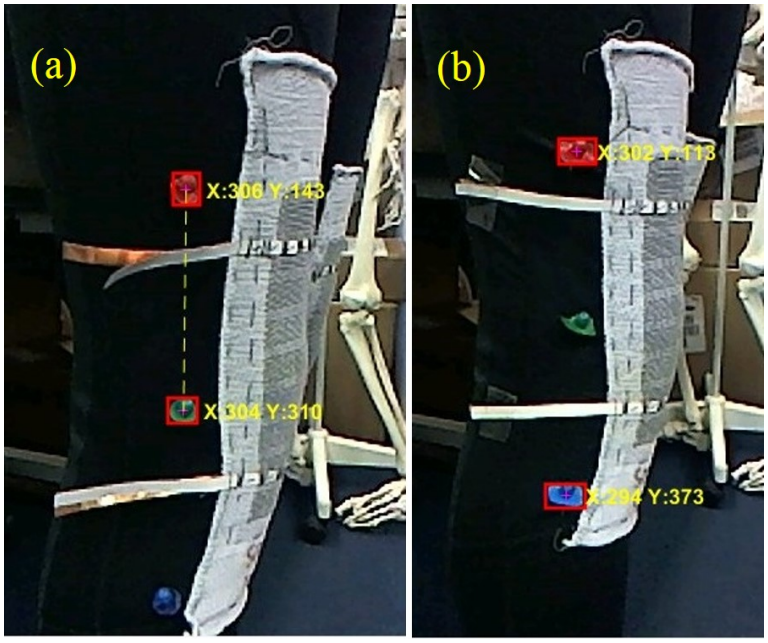


Figure 5.6: Issues with the markers detection: the blue marker is not detected for light condition (a) and the green for the initial (rectangular) shape of the marker (b)

To make sure the centre of the markers was correctly depicted and, as consequence, the knee angle was exactly represented, the chosen markers configuration consisted of (Figure 5.7):

- One flat round marker stuck to the leggings (to indicate the colourful boundary);
- One spherical marker placed in the centre of the flat one (to facilitate the objects detection and motion tracking).



Figure 5.7: Flat and spherical markers attached to anatomical positions of the leggings

## 5.5 Measurement system's objectives

The measurement system described in section 5.4 accomplished three different tasks:

1. Acquisition from a camera to track movement and calculation of the knee angle;

2. Acquisition from the leggings to measure the fabric resistance variation;

3. Synchronisation of knee angle and fabric resistance data.

These operations are described in subsections 5.5.1, 5.5.2 and 5.5.3, respectively.

### 5.5.1 Task 1: Acquisition from the camera

A Logitech camera, colourful markers and MATLAB Image Acquisition Toolbox were used to track movement and measure the knee angle. Red, green and blue markers were chosen to distinguish three different anatomical areas involved in the movement of the knee and, for this purpose, were placed in specific positions on the leggings: the red marker on the thigh, the green on the lateral condyle and the blue on the shank. The MATLAB algorithm described in 5.4.1 (Appendix VI, 7.3.4) identified the markers' actual location in the 2D space, with the (X, Y) coordinate values being provided at a given rate as resulting from the processing capabilities of the used PC. By knowing the coordinates of the centre of the markers, the knee angle was calculated as the angle between two lines, namely the line connecting the thigh-knee markers, $r_{thigh\text{-}knee}$, and the line between the knee-shank markers, $r_{knee\text{-}shank}$. Mathematically, such angle was identified as the one between the direction vectors of $r_{thigh\text{-}knee}$ and $r_{knee\text{-}shank}$ and found by subtracting the position vectors of two points on the line.

### 5.5.2 Task 2: Acquisition from the leggings

The electrical signals acquired from the conductive samples integrated into leggings were:

- The voltage across the specimen, $V_m$;
- The voltage proportional to the current provided to the fabric, $V_{current}$.

As described in 3.2 in Chapter 3, the voltage proportional to the current supplied to the sample ($V_{current}$) divided by the feedback resistance (i.e. R=100 Ω) is the current sourced to the fabric ($I_s$).

According to Equation 3.3, the fabric resistance corresponding to the movement accomplished is calculated as the ratio between $V_m$ and $I_s$.

To record data onto a computer, the NI USB-6003 acquisition system was used and Data Acquisition Toolbox and MATLAB technical computing environment were employed to communicate with this device by the session-based interface.

### 5.5.3 Task 3: Synchronisation

To study the electrical behaviour of knitted conductive fabrics embedded into leggings and relate it simultaneously to any knee flexion-extension performed by a user, data synchronisation is essential. This corresponds to provide at the same time the electrical signals coming from the fabric and the knee angle detected by a camera to the analog input channels of the NI-USB 6003 acquisition device. These data were generated by two MATLAB codes running at the same time (multitasking) and reported in Appendix VI (7.3.4) as:

1. *Image Acquisition from the camera.m*, which provides continuous and real time markers coordinates and the corresponding knee angle values;

2. *Acquisition data from the DAQ.m*, which detects the electrical signals from the leggings, adds the data obtained from the Image Acquisition (i.e. the voltage proportional to the knee angle) as a new input in a different analog input channel and plots the synchronised graphs, i.e. resistance versus time and knee angle versus time.

The NI-USB6003 does not allow to apply absolute temporal marking to the acquired samples but provides only the incremental sample number. So, on first instance, it would be impossible to synchronise the acquired analog signals with the knee angle, whose value is available as a floating number in MATLAB. To overcome this limitation, the knee angle (opportunely scaled)

was sent to an analog output channel and, at the same time, acquired by an analog input channel by means of a loopback connection.

## 5.6 Calibration of the tracking system

Prior to start any test with the motion tracking system, calibration was necessary. This process was firstly executed on a dummy (5.6.1) and, afterwards, on a participant (5.6.2).

### 5.6.1 Calibration on a dummy

The calibration on a dummy was an essential set-up operation (Figure 5.8), prior to start any experiment on a participant.



Figure 5.8: Parameters calibration by using a dummy

The parameters that have been calibrated were:

- **Camera-markers distance**

To effectively detect red, green and blue markers and track 2D movement with a MATLAB code, a number of measurements on a dummy has been carried out to determine the suitable distance between the camera and the markers (Figure 5.9(a)). The best value which guaranteed that the markers were distinguishable and with a clear visual definition was:
Camera-markers distance (upright position): **30 cm**.

- **Distance between markers**

Another important measurement to be evaluated prior to the testing on a participant was the distance between markers (Figure 5.9(b)).
This value was firstly determined by considering the anatomical positions on the thigh, knee and shank which are responsible for the knee movement. Secondly, this value together with the camera-markers distance should not exceed the limits of the working area. These considerations have brought to the value of:
Distance between markers: **9 cm**.

- **Alignment of the markers**

Before starting any testing on a participant in an upright position, the red marker (placed on the thigh) and the green (placed on the knee) should be aligned, namely the x value should be the same or pretty close (1% tolerance) for both markers. On the other hand, the blue marker (placed on the shank) starting from a position aligned with the other markers (Figure 5.9(c)), was free to rotate leading to the knee angle variation (Figure 5.9(d)).

- **Height of the camera from the floor**

The height of the camera from the floor (Figure 5.9(a)) was the parameter related to the height of the participant and, in particular, to the height of the knee from the floor. The investigation with the dummy has determined a value of:

Height of the camera from the floor: **60cm**

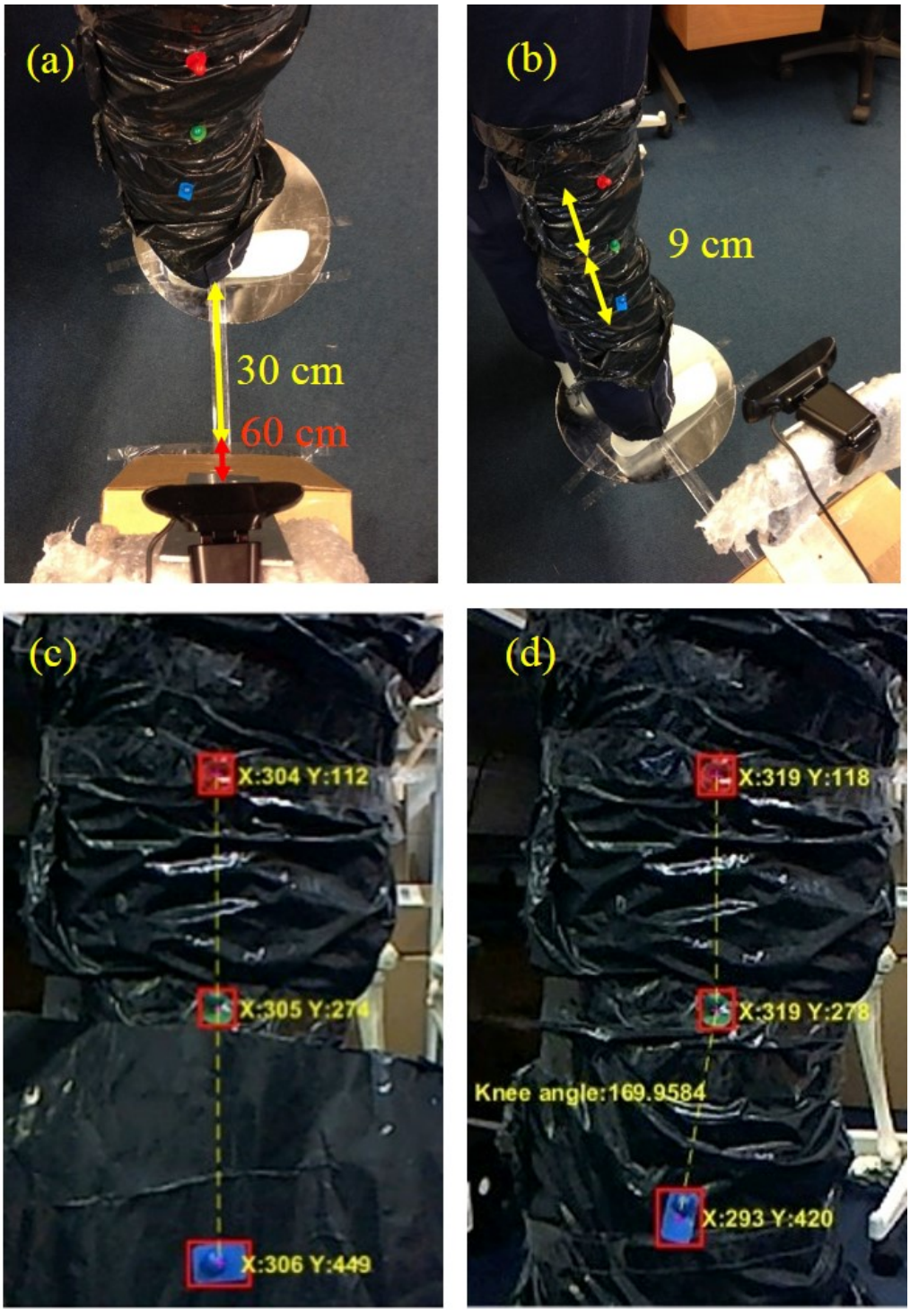


Figure 5.9: Parameters calibration on a dummy: (a) Camera-markers distance and height of the camera from the floor, (b) Distance between markers, (c) Matlab screenshot example of alignment of the markers in an upright position and (d) Matlab screenshot example of rotation of the blue marker determining the knee angle variation

### 5.6.2 Calibration on a participant

Another requirement before starting testing on a participant was the positioning of the markers in their appropriate locations on thigh, knee and shank and fulfill the values specified in the statement of requirements for the positioning system (subsection 5.6.1). This specifies that:

- The distance between the markers and the focus of the camera was set to 30 cm (Figure 5.10(a)):
- The distance between the markers was arranged to 9 cm (Figure 5.10(b));
- The markers should be initially aligned, with the x values being the same for the red, green and blue markers (Figure 5.10(c));
- The height of the camera from the floor was regulated according to the height of the participant's knee and become a required parameter for the rest of the testing sessions (Figure 5.10(d)).

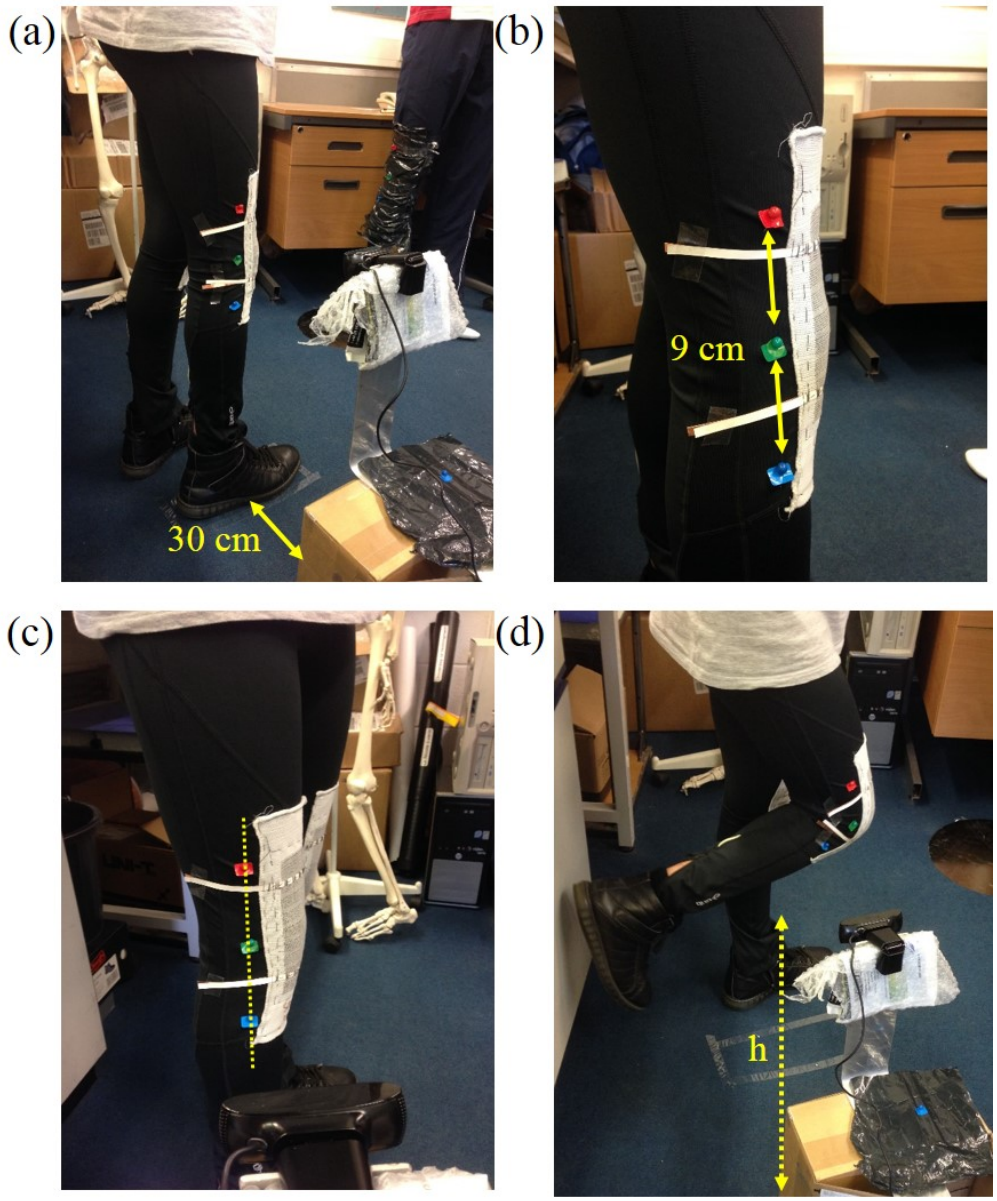


Figure 5.10: (a) Example of the distance between the markers and the focus of the camera, (b) Example of the distance between the markers on a participant, (c) Example of the alignment of the markers on a participant and (d) Example of the height of the camera from the floor and of the working area

## 5.7 Test procedure on a participant

After the calibration of the camera parameters on a participant (5.6.2), the measurement system was ready for testing (Figure 5.11). The aim of the tests was to investigate the electrical properties of knitted conductive textiles integrated into leggings during cyclic bending-recovery of the participant's knee. Method One recorded and analysed the fabric resistance variation of the SP29 sample sewn on two pairs of leggings with 15% and 18% elastane, with 1 and 3mA constant currents being provided.

The knee angle was determined by the image acquisition process described in 5.4.1 and collected by the data acquisition system (Figure 5.3) simultaneously with the electrical signals coming from the fabric. Examples of the working principle of the Visual Motion Tracking System are shown in Figures 5.12 and 5.13.



Figure 5.11: Test on participant with the Visual Motion Tracking System

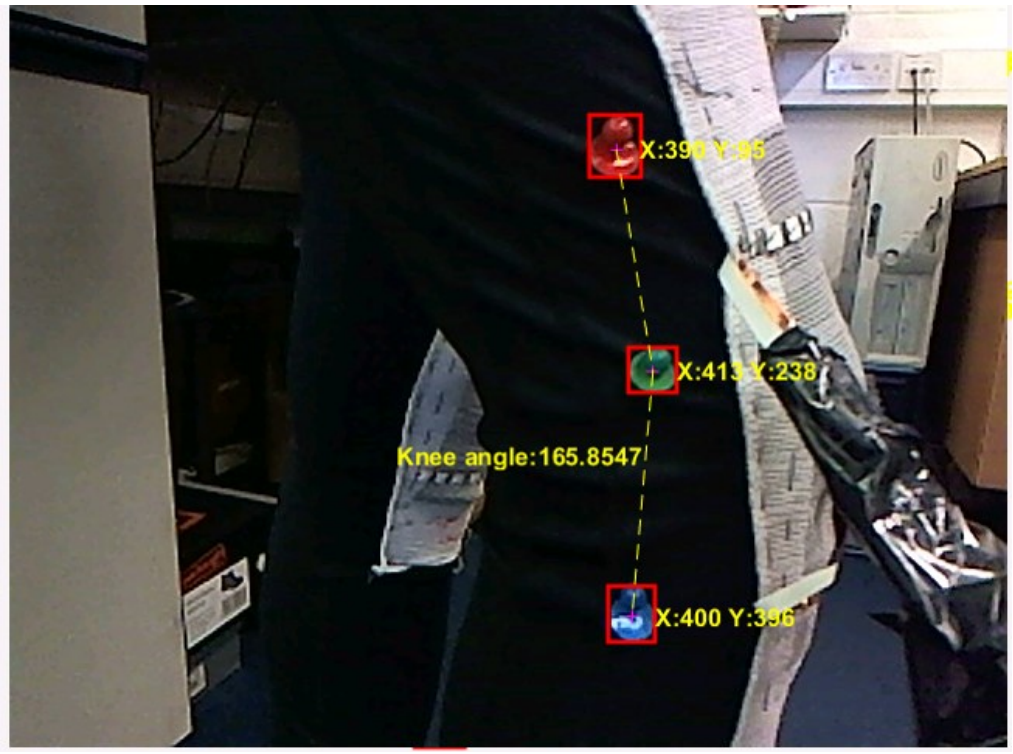


Figure 5.12: Screenshot of the knee angle measurement with the Visual Motion Tracking System

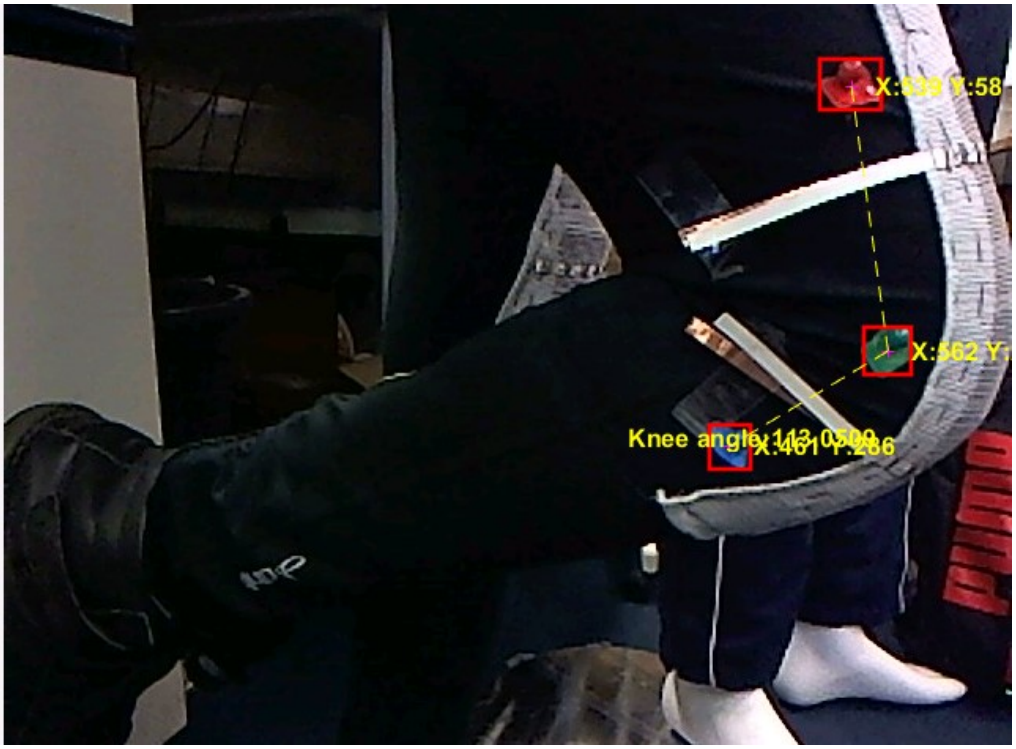


Figure 5.13: Screenshot of the knee angle variation with the Visual Motion Tracking System following the knee bending

### 5.7.1 Flexion-extension trials

Written consent was obtained by a participant (Appendix XI, 7.3.4) who was asked to perform as many cycles of knee flexion-recovery as possible in an upright position (Appendix X, 7.3.4). Ideally, the number of cycles the volunteer was asked to perform was hundreds but this was not possible for the reasons reported in subsection 6.5).
Knee flexion-extension tests were performed for:

1. Samples tested as soon as worn by the participant;

2. Samples preconditioned by previous trials (following after a five minute rest, similarly to the procedure described in subsection 3.5.1) or by wearing the leggings for one hour.

The aim of the first case was to investigate the electrical properties of fabrics once embedded into supporting garments with different percentage of elastane and compare their performance with the ones of the knit patterns previously tested on the tensile machine. The objective of the second case was to study the effect of preconditioning on the stabilisation and repeatability of the electrical properties of knitted conductive samples. The outcomes of these tests are reported in subsection 6.3.4.

## 5.8 Method Two - *HUMAC NORM System*

An alternative acquisition method was employed to measure the fabric electrical resistance variation of the SP27 and SP29 samples integrated into leggings with 15% and 18% elastane during knee flexion-extension cycles. Differently from Method One based on a camera and RGB markers to track the participant's unconstrained knee motion, the new method used the HUMAC NORM isokinetic machine for continuous knee rotation controlled by a computer. This system was called Method Two or the HUMAC NORM System from the name of the machine (Cybex Humac Norm model 770)) which allowed the user to perform repetitive knee motion at an agreed angle/speed.

The measurement system is represented in Figure 5.14 and comprises:

- The SP27 and SP29 samples integrated in two pairs of leggings with 15% and 18% elastane worn by a participant seated on the chair (A);
- The HUMAC NORM Isokinetic Machine and the dynamometer unit (B);
- The Auxiliary Outputs (C) of the HUMAC Interface accessible via the DB-9 connector (F);
- The power supply (D);
- The constant current generator (E) described in subsection 3.4.1;
- The NI USB 6003 acquisition system (G);
- The PC with the Matlab Data Acquisition Toolbox and customised code (H).

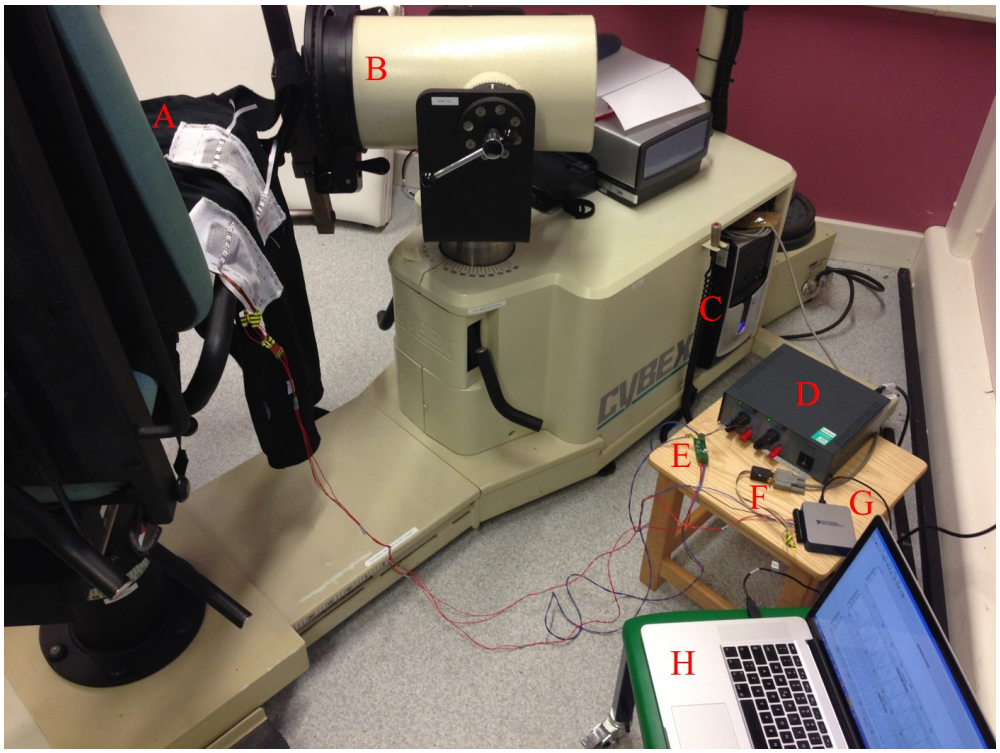


Figure 5.14: The HUMAC NORM measurement system

## 5.9 Description of the measurement system

The HUMAC NORM machine is a biomechanical isokinetic dynamometer generally used for functional assessment of the musculoskeletal system, for rehabilitation exercises and workout. In this thesis, such system was used for offering the participant repetitive knee joints movement according to a set pattern. The HUMAC machine is based on a dynamometer unit, whose functions are:

- Measuring the torque produced by the user during testing;
- Measuring position and speed of the input arm connected to the unit by means of an encoder.

Output torque and encoder pulses are read by an embedded firmware and used for controlling the input arm connected to the unit according to the desired motion profile. The maximum speed achievable in either direction

is 500 °/s. Analog signals corresponding to torque, speed and position are made available by digital-to-analog converters in the $\pm 10V$ range.
The test parameters defining the dynamometer's operation are: the operating mode, the operating speed and range of motion. These parameters were set before the first test session and are specified in section 5.10, together with the calibration procedure. Once the protocol was established and the tests started, the outputs of interest were gathered from the auxiliary outputs, as described in subsection 5.9.1. To measure the fabric resistance variation related to the movement performed, signals from the leggings (5.9.2) were acquired at the same time (5.9.3). All signals were acquired by the acquisition system (labelled G in Figure 5.14).

### 5.9.1 Acquisition from the dynamometer

The auxiliary outputs in the HUMAC Interface provide access to the machine's analog signals, such as position, velocity and torque. In this thesis, the acquired signals were:

- The voltage proportional to the position of the HUMAC, which indicated the knee angle performed by the user;
- The voltage proportional to the velocity of the HUMAC, which provided the velocity of the knee flexion/extension performed by the participant.

The range and the speed of movement were set in the machine before starting the tests (as described in section 5.11). In this way, the same test conditions were cyclically guaranteed and did not depend on the user's performance. At the same time, the fabric resistance variation was recorded with the acquisition system and related to the movement performed.

### 5.9.2 Acquisition from the leggings

The electrical signals collected from the leggings were the same of Method One (5.5.2), namely:

- The voltage across the specimen, $V_m$;
- The voltage proportional to the current provided to the fabric, $V_{current}$.

By dividing $V_m$ by the feedback resistance (R=100 Ω), the current sourced to the fabric ($I_s$) is known. Thus, the resistance along the knitted conductive textile was determined, again, as the ratio between $V_m$ and $I_s$.

### 5.9.3 Synchronisation

Similarly to Method One (subsection 5.5.3), to relate the fabric resistance variation to the knee flexion-extension performed by a user aided by the HUMAC machine, data synchronisation is crucial. A synchronous acquisition of the signals coming from the HUMAC machine (5.9.1) and from the fabrics (5.9.2) was obtained by a Matlab code reported in Appendix VII (7.3.4). The code created a new session with the NI USB 6003 and added four analog single-ended input channels from the acquisition device (i.e. ai1 for $V_m$, ai2 for $V_{current}$, ai3 for the voltage proportional to the position and ai4 for the voltage proportional to the velocity). In particular, the position and velocity signals were written in arrays after being appropriately converted. The conversion from sampled digital data to analog outputs used the equations provided by the HUMAC manual:

$$PositionOutput = (Gain * (SampledPosition + Offset)/1024) * (10v/32768) \tag{5.1}$$

$$VelocityOutput = (Gain * (SampledVelocity + Offset)/1024) * (10w/32768) \tag{5.2}$$

Where:

*Sampled position* and *Sampled velocity* were in units of 1/16 degrees;

*Gain* and *Offset* must be equal to the ones set in the HUMAC software, i.e. *Gain*=1024 and *Offset*=0;

$v$ is the analog position output;

$w$ is the analog velocity output.

Lastly, data representing the information of interest (i.e. Time, $V_m$, $V_{current}$, $I_s$, $R_{Fabric}$, Position, Velocity) were saved in an Excel file for Matlab post-processing.

## 5.10 HUMAC set-up and calibration

Many exercise modes can be performed by the HUMAC machine depending on the goals and the user's performance to improve (e.g. stability, strength, control). In this thesis, the purpose of the HUMAC NORM system was to allow the participant to perform the same range of knee motion repeatedly and at constant speed, to be associated to the fabric resistance variation recorded simultaneously. Thus, the set test parameters defining the dynamometer's operations were:

- *The Operating Mode*: continuous passive motion (CPM) which means that the dynamometer movement occurred regardless of whether the user was performing a concentric or an eccentric contraction (i.e. muscle shortening/lengthening). This choice stemmed from the research purpose, which was not a rehabilitative goal.

- *The Range of Motion*: 0° - 90°, with 0° being calibrated for the full extension position and 90° for the maximum flexion of the knee. These values were chosen considering the full range of knee motion possible in a real application and not achievable with the Visual Motion

Tracking System.

- *The Operating speed*: +60°/s constant rotation rate during the knee flexion (from 0° to 90°) and -60°/s constant rotation rate during the knee extension (from 90° to 0°). These values were acceptable for the elongation rate of the conductive fabrics integrated in the leggings as not affecting the specimens' structure (e.g. with a permanent deformation). Moreover, the chosen rotation rate was comfortable for the participant during repetitive tests.

## 5.11 Testing procedure on a participant

The participant was asked to sit in the HUMAC machine while wearing the electro-conductive leggings (with the SP27 and SP29 samples integrated in the left and right legs, respectively). According to section 5.10, the dynamometer was set in continuous passive motion (CPM) operating mode, which constantly moved the knee joint through a controlled range of motion (0° - 90°) and speed (60 °/s). The initial position of the leg before starting the tests was the full extension (0°), as shown in Figure 5.15. This was also the position where the dynamometer was stopped during the rest period between trials (to leave the textile in a not stretched position).

The testing procedure comprised 50 cycles of knee flexion-extension repeated for five trials. A rest interval of 5 minutes was planned between tests, to be consistent with previous cases (in the tensile machine and Method One). Each test session was repeated at the same conditions, without modifying the setting of the fabric in the leggings and the parameters in the HUMAC software. The first round of tests regarded the SP29 sample sewn along the right knee of the 15% elastane leggings (Figure 5.16). For comparison, the same knit pattern was tested afterwards on the leggings




Figure 5.15: Knee full extension position before starting the tests and during the rest interval

with a higher percentage of elastane (i.e. 18%).

During these tests, the opposite leg rested in a bent position, with the embedded SP27 sample being stretched.

To avoid that any preconditioning effect may alter the measurements, the specimens sewn in the unused leg, i.e the SP27 integrated in 15% and 18% elastane, were tested (Figure 5.18) on a different day from the SP29. Results of such comparison are discussed in 6.4.5.

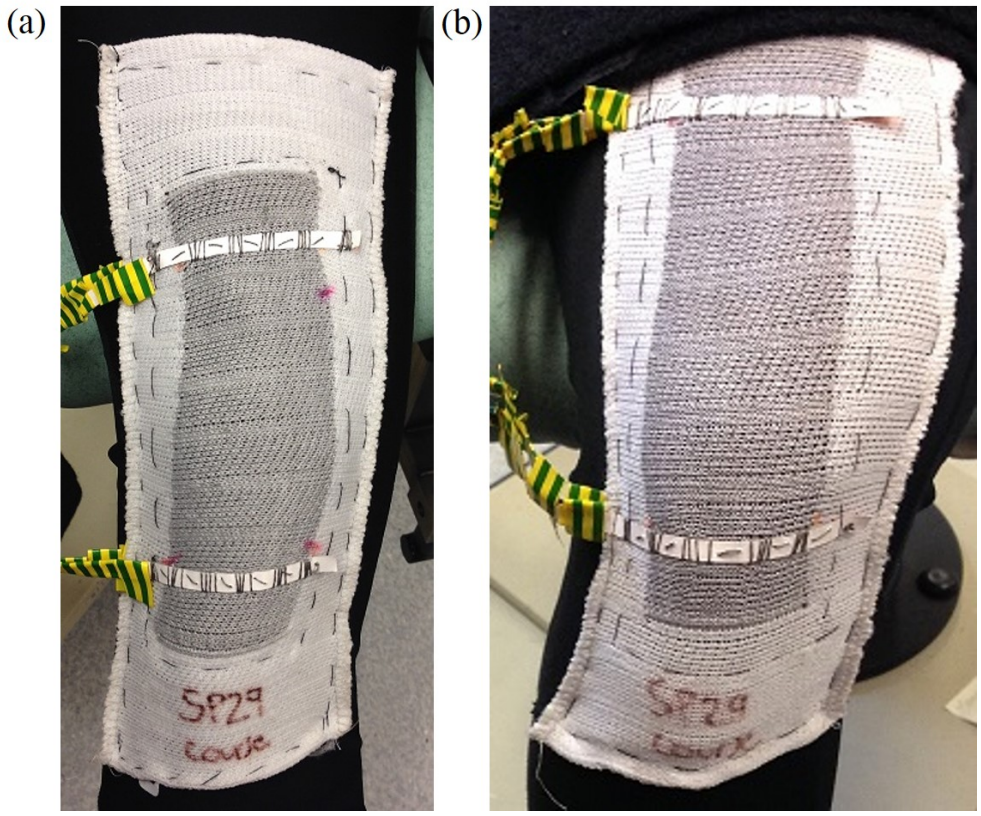


Figure 5.16: (a) Extension, (b) Flexion for the SP29 sample

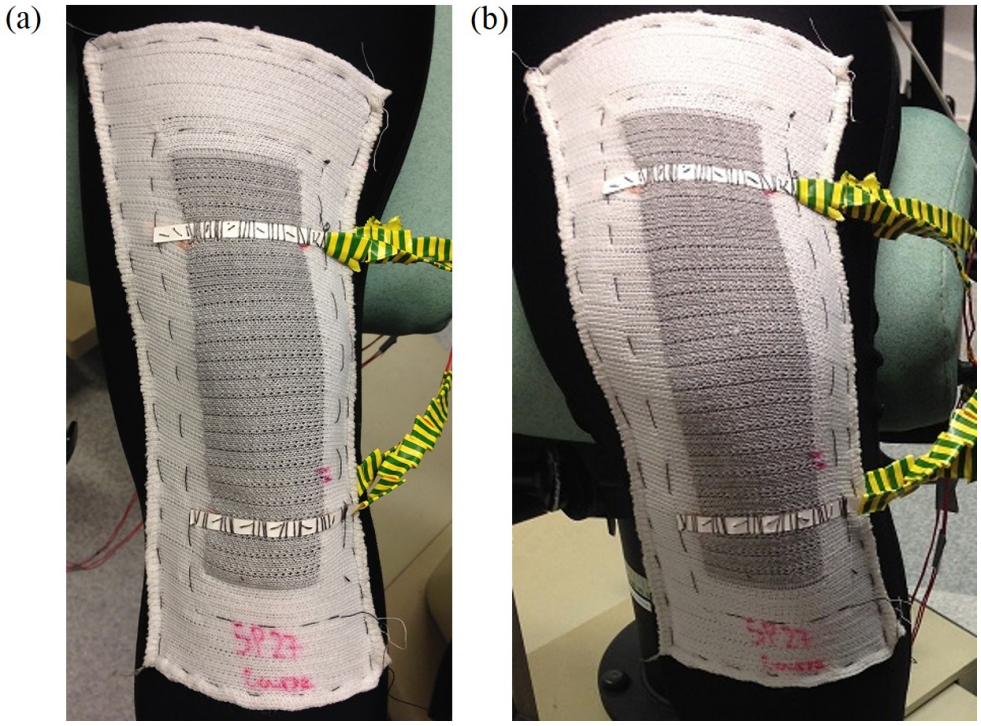


Figure 5.17: (a) Extension, (b) Flexion for the SP27 sample

## 5.12 Conclusions

This chapter described the integration of knitted conductive textiles into supporting garments for analysing their performances in view of their application as wearable motion sensors. First of all, the conductive samples chosen for the application, the leggings and the way the specimens were integrated into them were presented. The choice of which specimens to sew on the leggings stemmed from the study of sensitivity presented in Chapter 4, whereas the supporting garments were chosen with different percentage of elastane to compare electrical performance at different elasticity conditions.

Secondly, two measurement systems were arranged to investigate the electrical behaviour of knitted conductive textiles when they were integrated into garments and underwent cyclic stretch-recovery (corresponding to the knee flexion-extension). The first method, called Method One or *Visual Motion Tracking System*, used a customised procedure to capture human motion together with the fabric electrical resistance variation and was based on the principle that any moving object can be tracked by a camera on the basis of its colour. This means that, motion can be detected with the aid of coloured markers placed on specific anatomical positions of the body. An algorithm was written to detect red, green and blue coloured markers placed, respectively, on the thigh, knee and shank of the leggings with the help of the image processing toolbox in Matlab. The coloured objects were tracked at a fixed rate while enclosed inside a bounded region along with the centroid of that region. By knowing the coordinates of the centre of the markers (centroid), it was possible to determine the lines passing through them (connecting the thigh-knee and the knee-shank markers). The results of this implementation was successfully used in knee motion tracking as the

angle between those two lines.

The tasks accomplished by Method One used two customised codes which were described in detail: the image acquisition from the camera (for providing the markers coordinates and the corresponding knee angle values) and the acquisition from the data logger (for detecting the electrical signals from the leggings, adding the data obtained from the image acquisition and representing the fabric resistance variation synchronised with the knee angle versus time). Calibration and testing procedures were also illustrated.

Thirdly, the second method, called Method Two or *The HUMAC NORM System*, employed an isokinetic machine which allowed the participant to repeatedly perform the same knee motion range at a constant speed, to be associated to the fabric resistance variation recorded simultaneously. The measurement system, the signals acquisition from the dynamometer (position and velocity) and from the leggings (voltage across the leggings and voltage proportional to the current provided to the fabric) were described in detail, as well as the their synchronisation. Lastly, the machine set-up and calibration and the testing procedure on a participant conclude the presentation of Method Two.

Results of both the Visual Motion Tracking System and the HUMAC NORM System are discussed in Chapter 6.

# Chapter 6

# Analysis of the use of wearable sensors on a participant

## 6.1 Introduction

Stability, sensitivity, linearity, hysteresis of conductive samples undergoing cyclic deformation can be influenced by the garment in which they are embedded. This chapter, therefore, considers the application of fabric transducers as wearable motion sensors by analysing the electrical properties of knitted conductive textiles when integrated into a supporting garment. The outcomes are based on the testing methods and the measurement systems described in Chapter 5.

## 6.2 Objectives

The aim of this chapter is to characterise knitted conductive textiles in view of their application as wearable motion sensors, in particular as knee angle sensors. The electrical resistance exhibited by knitted conductive samples sewn across the knee joint of different leggings was measured during flexion-

extension together with the knee angle performed. Two measurement systems were used for the purpose: the *Visual Motion Tracking System* and the *HUMAC NORM System*. In this chapter, the outcomes of both methods will be presented. Next, the effect of the supporting garment and the elasticity on the fabric electrical properties will be investigated. Lastly, a comparison of the two methods, the results achieved and the advantages and disadvantages of their application will be discussed.

## 6.3 *Visual Motion Tracking System*: Results and Discussion

The outcomes of the Visual Motion Tracking System on the SP29 embedded along the knee joint of two pairs of leggings with 15% and 18% percentage of elastane are described in the following. The fabric resistance variation and the corresponding change of the knee angle with the movement performed were acquired with the experimental system described in section 5.4.

### 6.3.1 Data post-processing for conductive samples embedded into leggings

The analysis of the electrical behaviour of the conductive samples integrated into leggings was possible by post processing the data acquired with the system described in section 5.4. The fabric electrical resistance and the knee angle were the two signals which were gathered and analysed at the same time with a procedure similar to the one described in section 3.6 and reported in the Appendix VI (7.3.4). According to subsection 3.6.1, data were first filtered with a Savitzky-Golay filter of order and window length being N=3 and f=151 for the fabric electrical resistance, and N=1,

f=151 for the knee angle. The choice of these values stemmed, for the fabric resistance, from the necessity of reducing the electrical noise generated by friction and slippages among the conductive fibres without introducing excessive shape distortions. For this reason it was preferred to limit the size of the window length and increase the filter to obtain the desired filtering action. On the contrary, for the knee angle it was necessary to remove the staircase shape and the delay caused by the processing operations. To do so, the original staircase signal (red line in Figure 6.1 (b)) was firstly shifted left by the time duration of a step (green line) to account for the delay introduced by the camera processing. Then, another shift left by half the step's width was operated to account for the next filtering and, lastly, a low-pass filtering with a Savitzky-Golay filter (N=1, f=151) was used to reconstruct the original signal from its sample-and-hold replica (blue line). The outcome of the filtering is shown in Figure 6.1 for the first seven cycles of knee flexion-extension of the SP29 sample embedded into leggings with 18% elastane.

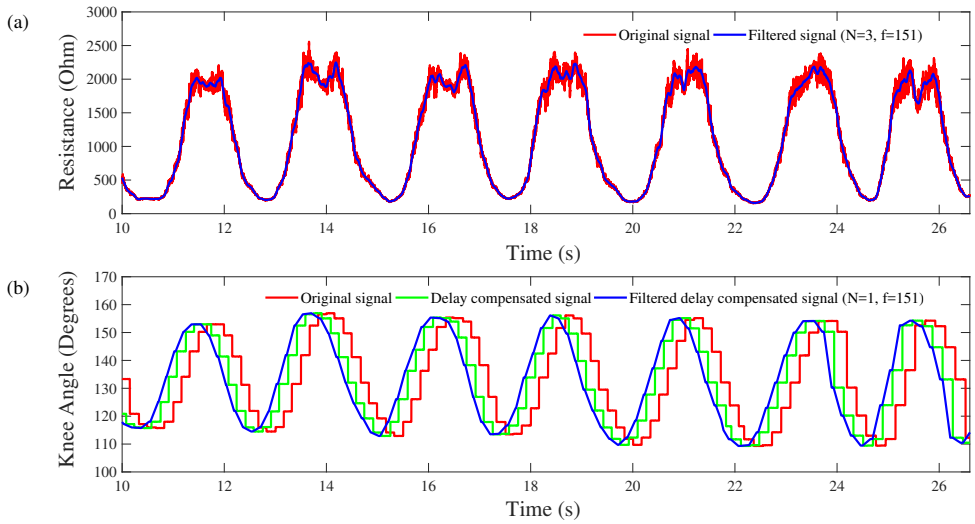


Figure 6.1: (a) Original and filtered resistance (N=3, f=151), (b) Original (red line), delay compensated (green line) and filtered delay compensated knee angle (blue line, N=1, f=151) for the SP29 embedded into leggings with 18% elastane and tested with the Visual Motion Tracking System

The range of motion varies from 155° (i.e. maximum extension, with 180° being the reference for full extension) to 110° (i.e. maximum flexion). One of the main differences between samples tested in the tensile machine (subsection 3.6.2) and in the tracking motion system was that, in the latter, the fabric elongation rate was variable cycle by cycle according to the free and unconstrained participant's knee bending movement. This led to a different approach for estimating the signals' cycle duration and detecting the peaks of the fabric electrical resistance and the knee angle, which did not recur at regular intervals. In particular, two parameters were specified in the *findpeaks* Matlab command applied to both signals:

- The *MinPeakProminence*, which worked comparing neighbouring peaks and returning the most relevant according to the level obtained by the *peak2peak* function (calculating the difference between the absolute maximum and minimum values);
- The *MinPeakDistance*, which guaranteed that the distance between any two maximum or minimum points was equal to the mean value of the peak's widths (returned by a previous execution of the *findpeaks* command).

After detecting the minimum and maximum values, interpolation curves and peak-to-peak spans were determined for fabric resistance and the knee angle utilising the same procedures described, respectively, in subsections 3.6.3 and 3.6.4. Examples of the sequential operations of post processing are illustrated for the fabric resistance (Figure 6.2) and for knee angle (Figure 6.3) of the SP29 embedded into leggings with 18% elastane. Interpolation and spans curves were considered from the first peak detected after the beginning of motion. The analysis of the electrical behaviour of the conductive samples embedded into leggings follows in section 6.3.2.

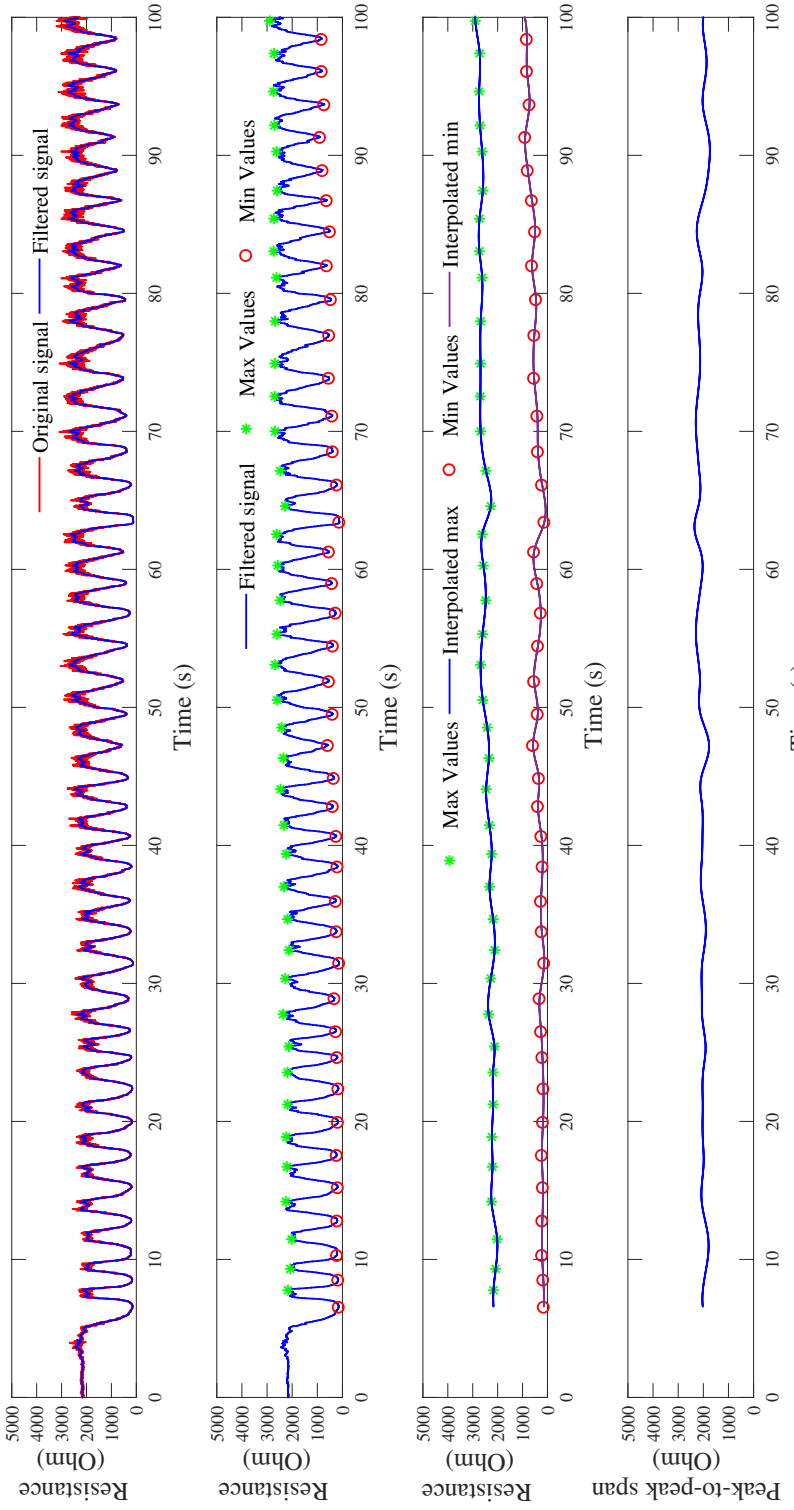


Figure 6.2: Resistance signal post-processing for the SP29 embedded into a pair of leggings with 18% elastane and tested with the Visual Motion Tracking System: (a) Filtering, (b) Maximum and minimum detection, (c) Interpolation curves, (d) Peak-to-peak span

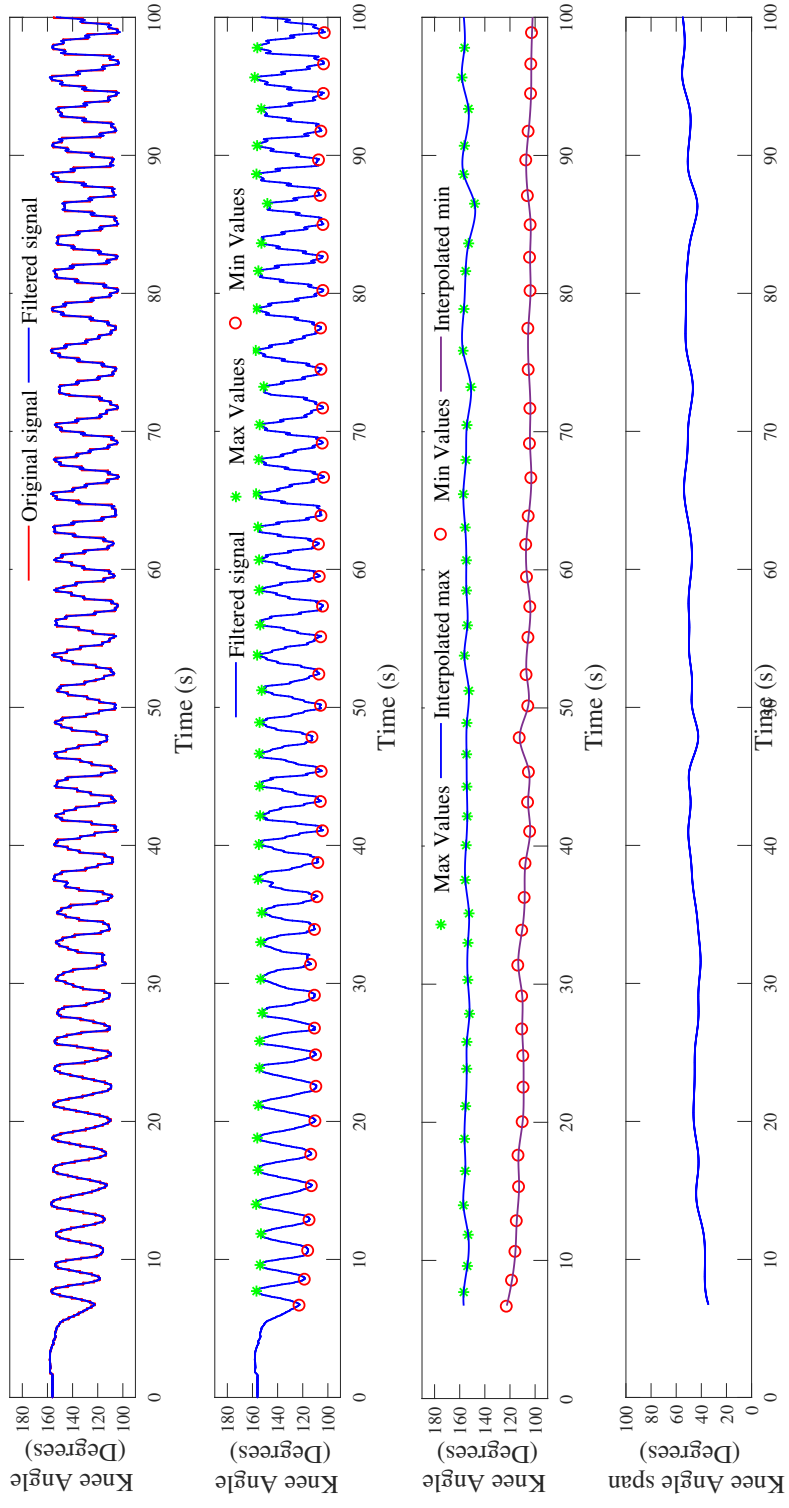


Figure 6.3: Knee angle signal post-processing for the SP29 embedded into a pair of leggings with 18% elastane and tested with the Visual Motion Tracking System: (a) Filtering, (b) Maximum and minimum points detection, (c) Interpolation curves, (d) Peak-to-peak span

### 6.3.2 Analysis of the electrical behaviour of conductive samples embedded into leggings

The application of fabric as a transducer requires investigation of the electrical properties in terms of linearity, stability, sensitivity and hysteresis. Similarly to the samples tested in the tensile machine (Chapter 4), such parameters were studied for the fabrics integrated into supporting garments with different percentage of elastane.

The electrical behaviour of conductive samples embedded into leggings followed the data post-processing described in section 6.3.1. The variation of the fabric resistance with the knee angle performed (Figure 6.1) is consistent with what discussed in section 4.3 in terms of the factors influencing the fabric resistance during extension-recovery cycles. In fact, in correspondence of the maximum knee bending (around 110°) and thus the maximum elongation of the fabric, a minimum fabric resistance value is measured as a consequence of better contact between the strands of yarn leading to an increased conductivity (Equation 2.1). Conversely, in correspondence of maximum knee extension (around 155°, with 180° being the reference for full extension) and minimum fabric elongation, a maximum fabric resistance value is recorded. This is explained by a decreased contact pressure causing an increase of the contact resistance and, therefore, an increase of the overall fabric resistance (Equation 2.2).

### 6.3.3 Linearity

The analysis of the fabric electrical response to the knee angle variation revealed the relationship between the sample resistance and the angle performed. Figure 6.4 gives an example of the two phases of the participant's knee movement: extension from 117° to 153° (red curve) and flexion from

153° to 115° (blue line). As can be noticed, the fabric electrical behaviour in a cycle was not linear with the knee angle variation.

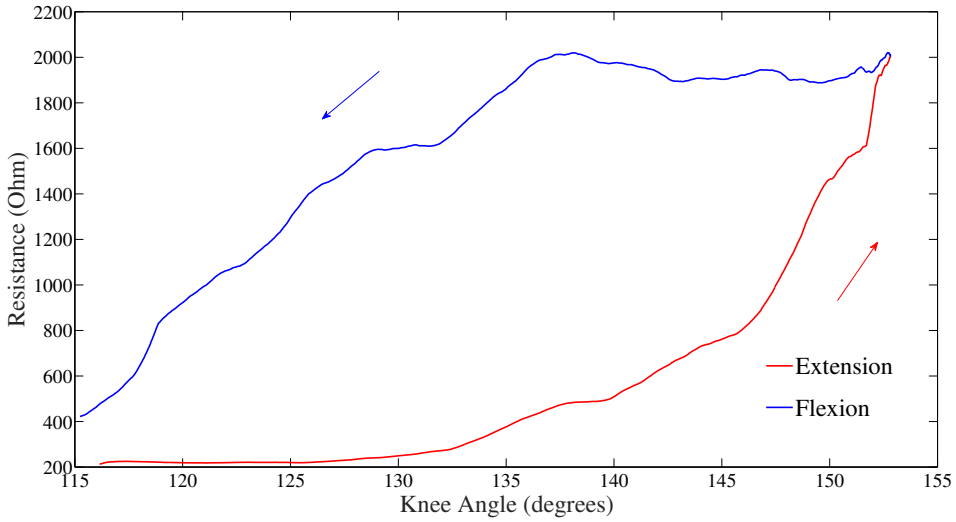


Figure 6.4: Extension and flexion curves for the SP29 embedded into a pair of leggings with 18% elastane during the first cycle with the Visual Motion Tracking System

As confirmation, the regression analysis was conducted separately for the flexion and extension phases, resulting in that the electrical behaviour can be accurately modelled by quadratic curves during both cases (especially during the flexion phase). The results of the fit are illustrated in Figure 6.5 (with the experimental data represented in blue and the results of the fit in red) and summarised in Table 6.1. This outcome is consistent with the response of the SP29 tested in the tensile machine (subsection 4.8.1). When considering further cycles, the higher order harmonics were not accurately followed by a second order polynomial but required more complex curve fitting, as shown in subsection 6.3.6.

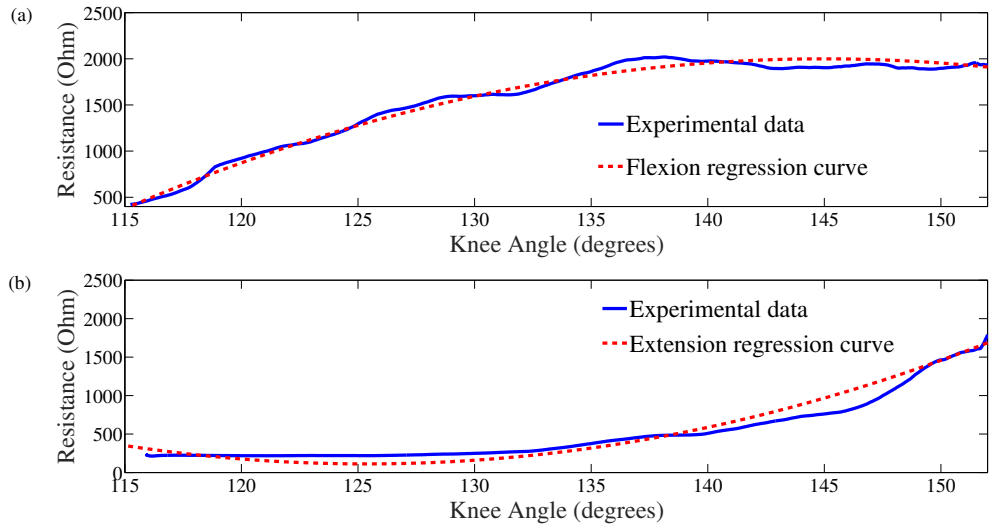


Figure 6.5: Characteristic curves for the (a) flexion and (b) extension phases of the SP29 integrated into a pair of leggings with 18% elastane during the first cycle with the Visual Motion Tracking System

Table 6.1: Regression curves for the SP29 sample embedded into leggings with 18%elastane with the Visual Motion Tracking System

| Phase | Characteristic curve | $R^2$ |
|---|---|---|
| Extension | $y = 2.263x^2 - 568.62x + 35834$ | 0.966 |
| Flexion | $y = -1.805x^2 + 523.38x - 35942$ | 0.988 |

### 6.3.4 Stability

The stabilisation of the electrical properties of knitted conductive textiles was discussed in Chapter 4 by considering for analysis purposes the peak-to-peak span of the electrical resistance. According to this definition (3.6.4), the peak-to-peak span measures the distance between the maximum and minimum filtered interpolated values of the fabric resistance occurring, respectively, at the maximum knee extension and maximum knee flexion. Once the stabilisation time for the resistance span was determined, other performance indicators were derived such as the number of cycles to reach stability and the stabilised average resistance. For samples integrated into garments, the same criteria for evaluating the electrical stabilisation of sub-

section 4.4.1 and the same procedure for calculating the settling time (and thus, the number of cycles to settle) of subsection 3.6.4 and stabilised average resistance of subsection 3.3 were used.

From such analysis, it was determined that the supporting garment had the effect of accelerating the electrical stabilisation of the conductive fabric embedded in it. In fact, the SP29 sample required on average $116 \pm 75$ cycles of stretch-recovery to reach stability when tested for the first time in the tensile machine (Figure 4.6). These values were calculated as the arithmetic mean and standard deviation (Equations 7.11 and 7.12 of Appendix IX (7.3.4), respectively) as all trials lasted the same number of cycles, namely 250. The high standard deviation was due to the joint representation of values obtained from different test conditions (three different currents and two elongation rates) preferred for emphasising the common tendency for all specimens (as explained in subsection 4.4.2).

Conversely, the SP29 integrated and tested for the first time into leggings needed only $23 \pm 11$ cycles of knee flexion-extension on average. In this case, the values were obtained by calculating the weighted arithmetic mean and weighted standard deviation (Equations 7.13 and 7.14) of the number of cycles to reach stability during the first tests. This was due to a different test length which implied a different weight to be considered when calculating the mean and standard deviation. Thus, the integration of conductive samples into a supporting garment makes a difference in terms of settling time of their electrical properties.

The time to reach stability depends on the condition of the samples at the moment of test and on the elasticity of the leggings used (as explained later on in this section). In fact, according to the mechanical preconditioning discussed in section 4.4, a different electrical behaviour occurred for:

- Samples tested as soon as the participant worn the leggings;
- Samples preconditioned by previous flexion-extension trials (following after a limited rest period) or by wearing the leggings for one hour.

In particular, samples tested immediately for the first time showed an increasing resistance span due to an increasing electrical resistance (according to subsection 4.4.3), which required a higher number of knee flexion-extension cycles to stabilise compared to the rest of the trials. Figure 6.6(a) is an example of the resistance variation for the SP29 integrated into 15% elastane leggings and tested as soon as the participant worn the leggings (the stabilised average resistance occurred from the 34th cycle onwards at 1020Ω).

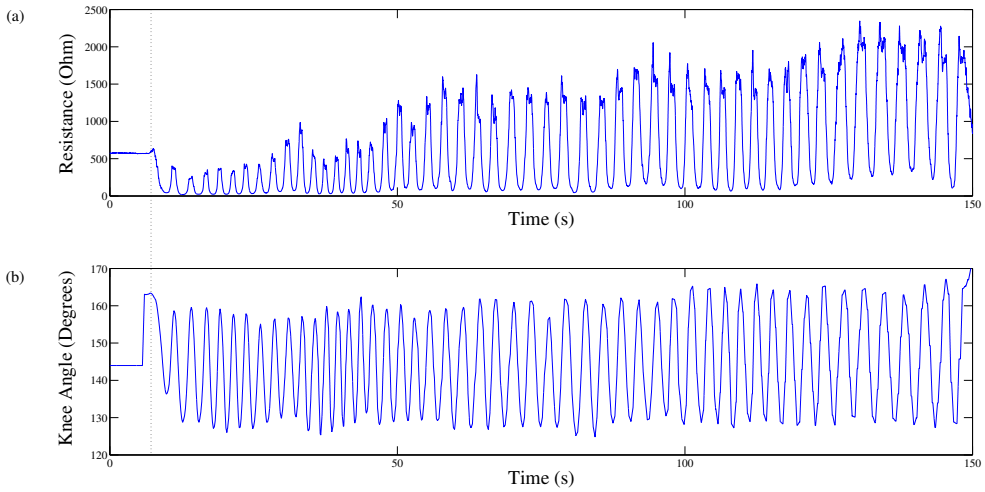


Figure 6.6: (a) Filtered resistance (N=3, f=151) and (b) Filtered knee angle (N=1, f=351) for the SP29 embedded into a pair of leggings with 15% elastane and tested with the Visual Motion Tracking System as soon as the participant worn the leggings

Conversely, preconditioned samples showed a quicker stabilisation. This is the case when considering 5 trials of knee flexion-extension separated by 5 minutes rest for the SP29 integrated into a 15% elastane leggings: the mean number of cycles to reach stability was $21 \pm 9$ (obtained by using Equa-

tions 7.13 and 7.14). An even quicker stabilisation was observed when the SP29 embedded into a 18% elastane leggings was preconditioned by the participant by wearing the leggings in a seated position for one hour: the outcome was in this case $11 \pm 5$ cycles on average (Figure 6.7(a) with the stabilised average resistance from the 16th cycle onwards at 1600Ω).
Thus, the composition of the leggings plays also an important role on determining the mechanical and, thus, the electrical behaviour of the resulting sensing garment. In fact, for leggings with the highest percentage of elastane (18%) the stabilisation occurs in less cycles.

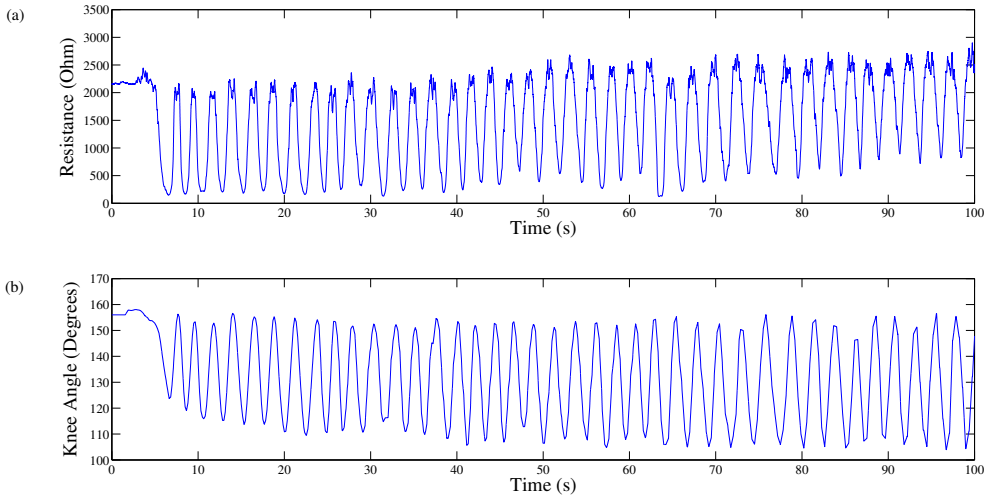


Figure 6.7: (a) Filtered resistance (N=3, f=151), (b) Filtered knee angle (N=1, f=351) for the SP29 embedded into a pair of leggings with 18% elastane and tested with the Visual Motion Tracking System after the participant worn the garment for one hour

The span of the fabric resistance provides information about the sensing performance of the fabric transducer cycle after cycle and trial after trial. For instance, a span that suddenly decreases during a trial while the knee range of motion remains almost constant or slightly decreases indicates the combined presence of fabric loosening and non-linear effects due to contact resistances. This is the case illustrated in Figure 6.8 for the SP29 embed-

ded into a pair of leggings with 15% elastane and tested for the fifth time after a 5 minute rest. This phenomenon is due to the elongation dependent behaviour of knitted conductive samples (discussed in section 4.8), according to which the contribution of the contact resistance overtakes the one of the length-related resistance during small elongations. In this case, when the knee range of motion (and, thus, the fabric extension) decreases under a certain angle (red dash line between 52 and 98 seconds), the non-linear effect of the contact resistance predominates. As soon as the angle variation becomes larger (black dash line around 100 seconds), the contribution stemming from the length-related resistance arises again, with the resistance starting to vary according to the knee flexion-extension phases.

Thus, by analysing the peak-to-peak span for the fabric resistance (which is included in the study of sensitivity described in section 6.3.5), it is possible to evaluate the performance of the fabric as a transducer. The SP29 integrated into 18% elastane showed good quality sensing-wise, as its span (Figure 6.2 (d)) remains constant over time $(2080 \pm 140)\Omega$ .

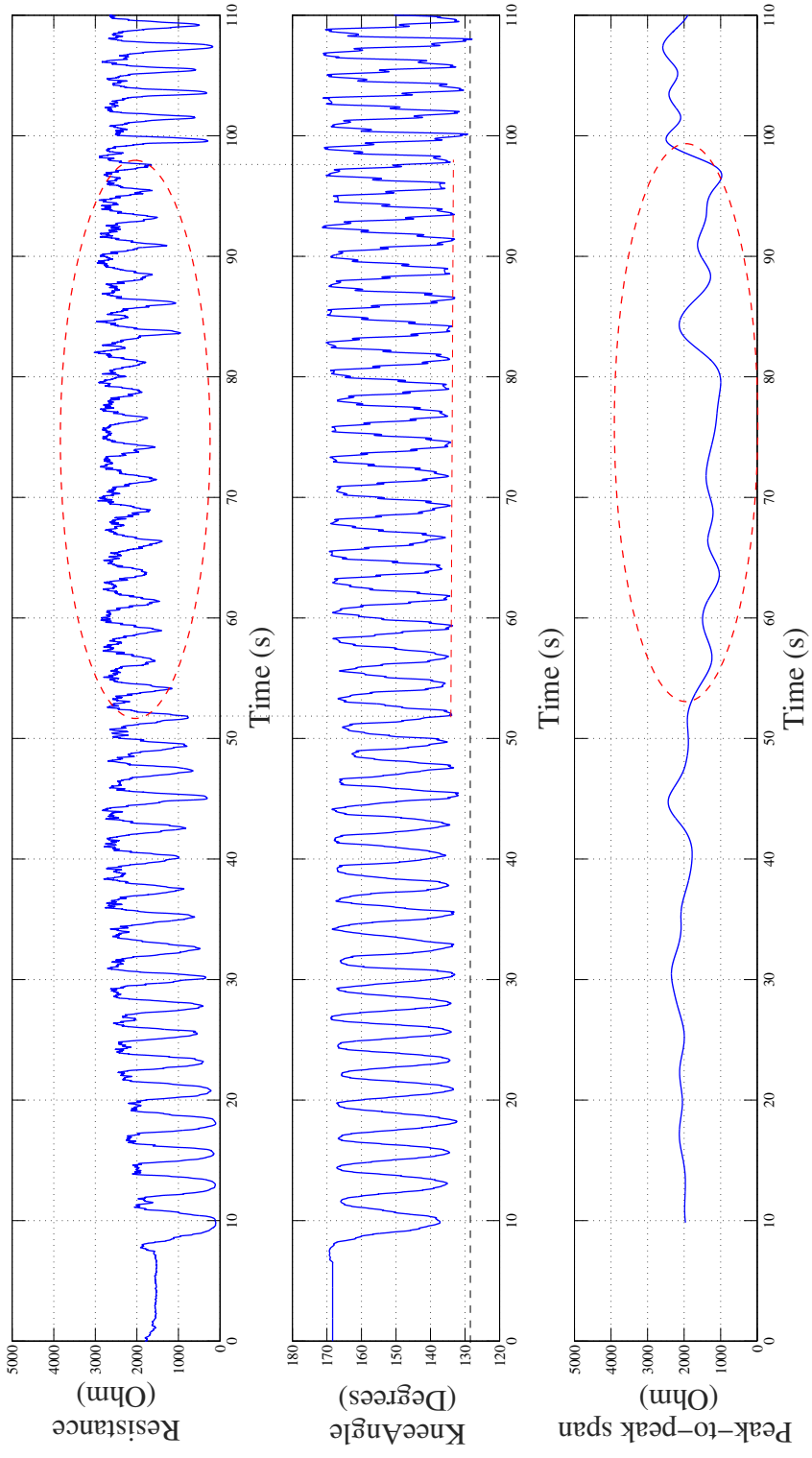


Figure 6.8: (a) Filtered resistance, (b) Filtered knee angle and (c) Peak-to-peak span for the SP29 embedded into a pair of leggings with 15% elastane and tested with the Visual Motion Tracking System for the fifth time after a 5 minute rest. The red ellipse shows when the non-linear effect of the contact resistance predominates on the length-related resistance (below a certain fabric elongation/knee angle) causing loss of accuracy in the electrical resistance and, correspondingly, the drop of span

### 6.3.5 Gauge factor and sensitivity

To evaluate the samples' performance once integrated into leggings with different percentage of elastane, the fabric sensing properties were first studied in terms of gauge factor during knee flexion-extension cycles. Similarly to section 4.6, the gauge factor was calculated according to Equation 4.1 as the ratio between the relative change in resistance (represented by the peak-to-peak span, $\Delta R$, with respect to the average resistance, $R_{avg}$) and the relative change in fabric length (the absolute change in the specimen length, $\Delta L$, with respect to the average fabric length, $L_{avg}$):

$$GF = \frac{\frac{\Delta R}{R_{avg}}}{\frac{\Delta L}{L_{avg}}} \tag{6.1}$$

$\Delta L$ and $L_{avg}$ were determined by the relationship between an angle and the length of its arc, as shown in Figure 6.9:

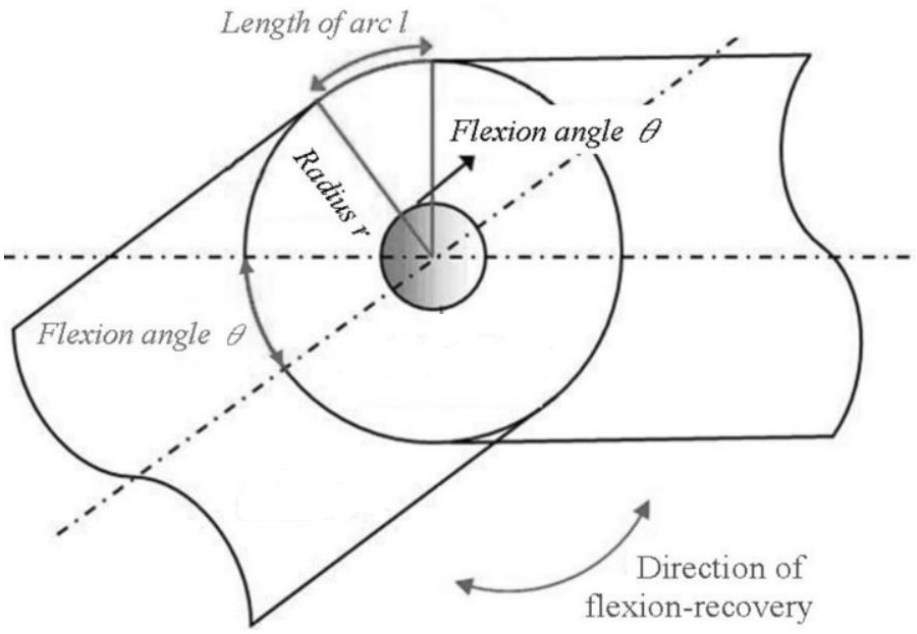


Figure 6.9: Relationship between the flexion angle $\theta$ and the length of arc $l$ (modified from Shyr et al. 2014)

$$l = 2\pi r \frac{\theta}{360} \tag{6.2}$$

In this case, $\theta$ is the knee flexion angle expressed in degrees (measured with the experimental system of section 5.4), $r$ is the distance between the centre of the knee and the lateral condyle (i.e. 60 mm on average) and $l$ is the length of the flexion arc, which can be considered the fabric length term for the specimen undergoing flexion under the assumption that the fabric follows the knee movement. Thus, the absolute change in the specimen length, $\Delta L$, was determined by Equation 6.2 with the peak-to-peak span for the knee angle ($\Delta\theta$, Figure 6.3(d)) in place of $\theta$.

The average fabric length, $L_{avg}$ was calculated by:

$$L_{\text{avg}} = 2\pi r \frac{(180 - KneeAngle_{\text{avg}})}{360} \tag{6.3}$$

Where: $KneeAngle_{avg}$ is the mean value of the unfiltered knee angle signal (considered from the beginning of the movement) and was calculated with a Butterworth filter of order 2 and normalised cut-off frequency equal to $5 * 10^{-5}$ (Figure 6.10). The $KneeAngle_{avg}$ values were obtained considering $180^{o}$ the full extension (thus, the numerator of Equation 6.3 was chosen to be consistent with the direction of rotation illustrated in Figure 6.9).

Similarly, $R_{avg}$ is the mean value of the unfiltered fabric resistance variation and was calculated with a Butterworth filter of order 2 and normalised cut-off frequency equal to $5 * 10^{-5}$ (Figure 6.11).

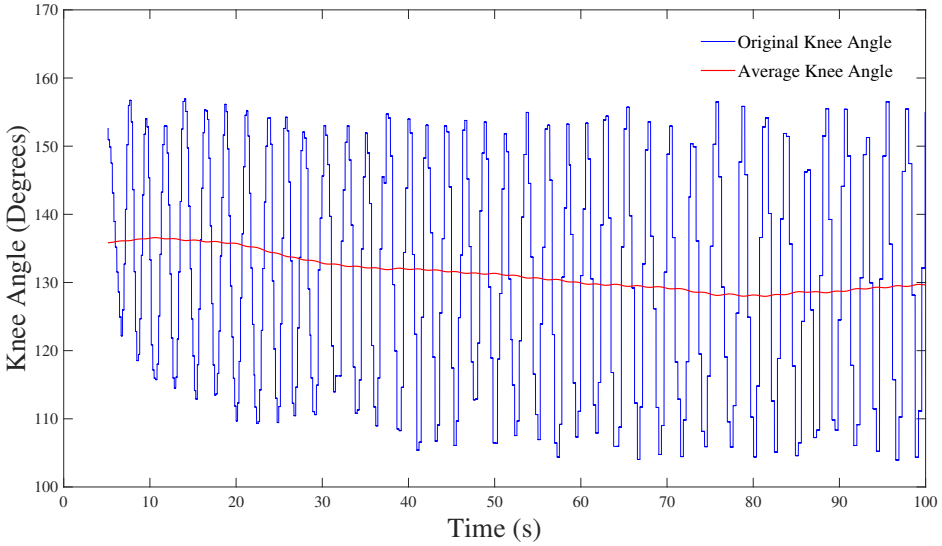


Figure 6.10: Original and average knee angle signals from the beginning of the movement for the SP29 integrated into 18% elastane leggings and tested with the Visual Motion Tracking System

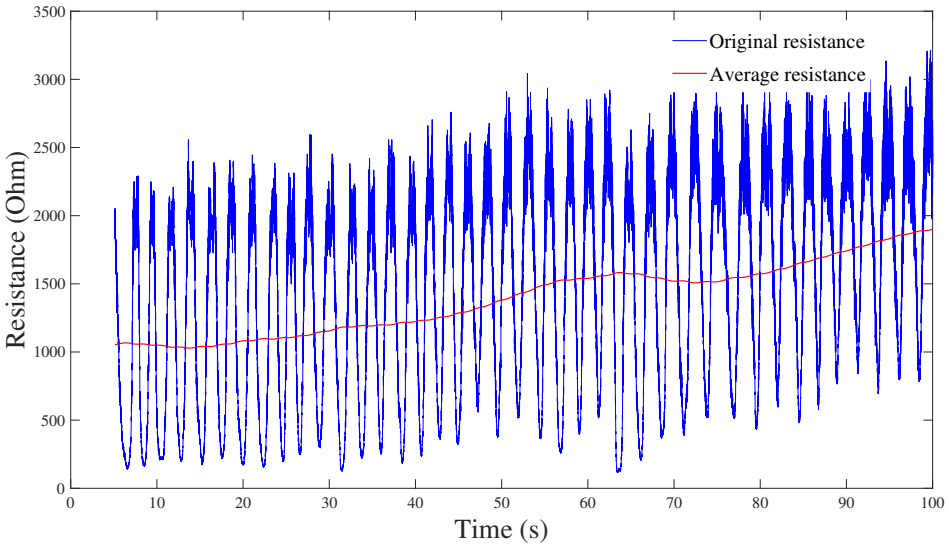


Figure 6.11: Original and average resistance signals from the beginning of the movement for the SP29 integrated into 18% elastane leggings and tested with the Visual Motion Tracking System

The gauge factor variation with cycles for the SP29 integrated into 18% elastane leggings is represented in Figure 6.12. The graph shows the decreasing behaviour with cyclic loading and this is a common tendency for samples integrated in leggings with different percentage of elastane. In particular, when comparing the values at the beginning and at the end of all trials, it was found that the gauge factor for the SP29 embedded into 15% elastane leggings decreased with an average variation equal to -35% and of -84% when embedded into 18% elastane leggings. This means that, although the more elastic garment was responsible of a quicker stabilisation of the electrical properties of the specimens integrated in them (6.3.4), the gauge factor worsened faster.

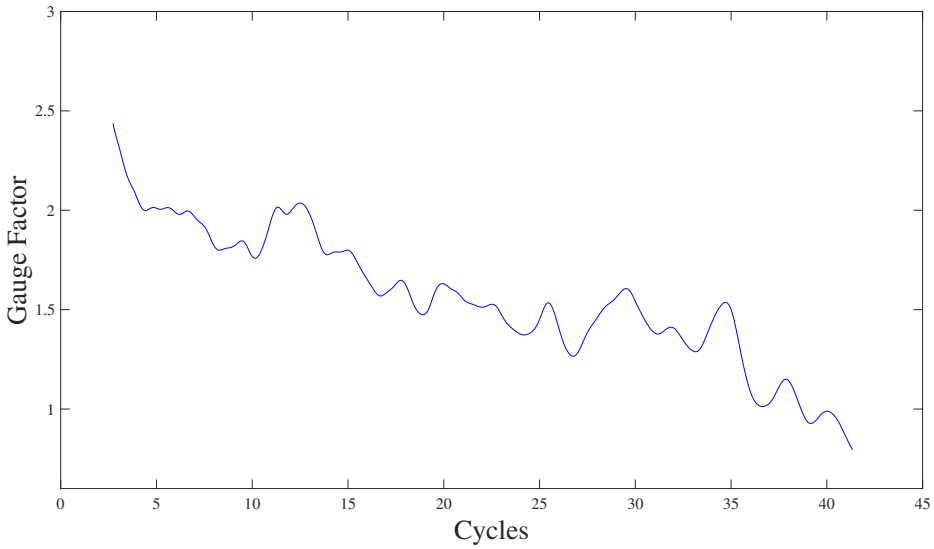


Figure 6.12: Gauge factor variation with cycles for the SP29 embedded into a pair of leggings with 18% elastane and tested with the Visual Motion Tracking System

The gauge factor calculated with Equation 6.1 was related to the $R_{avg}$ and $L_{avg}$ signals variation; in particular, the increase of $R_{avg}$ over cycles caused the decreasing trend observed in the gauge factor.

However, the gauge factor can be rewritten in terms of sensitivity:

$$GF = S_l * \frac{L_{\text{avg}}}{R_{\text{avg}}} = \frac{360}{2\pi r} * S_\theta * \frac{L_{\text{avg}}}{R_{\text{avg}}} (6.4)$$

Where:

$$S_\theta = \frac{\Delta R}{\Delta \theta} \tag{6.5}$$

is the sensitivity expressed as the ratio between the span of the fabric resistance ($\Delta R$) and the span of the knee angle ($\Delta \theta$).

To avoid the effects of $R_{avg}$ or $L_{avg}$ as sources of disturbing trends when studying the application of fabrics as angle sensors, the sensitivity was preferred to the gauge factor for comparison among samples. As the angle span does not vary consistently over cycles, the main factor affecting the sensitivity is the resistance span. This means that, for samples tested as soon as the leggings were worn, the sensitivity is higher as the loosening of the fabrics (that makes the distance between maximum and minimum values smaller) does not influence considerably. Also, sensitivity does not change/decrease for samples tested within a limited rest period (-2%). This means that, in an application, samples tested cyclically with a short interval between trials almost keep the initial sensitivity. Conversely, a longer rest period (e.g. in a seated position, corresponding to a stretched specimen) causes a consistent decrease of sensitivity (-47%). In the overall, to guarantee a high sensitivity of the integrated samples, the integrated specimens should be tested as soon as worn and with limited rest period in between trials or in a not stretched position.

The sensitivity together with both signals span are represented for the

SP29 embedded into a pair of leggings with 18% elastane in Figure 6.13, with their stabilisation being at: $(43.7 \pm 4.2)\Omega/^{o}$ for the fabric sensitivity, $(2054 \pm 136)\Omega$ for the resistance span and $(47.4 \pm 4.5)^{o}$ for the knee angle span. As can be noticed, the sensitivity is much less affected by trends. The residual decreasing behaviour is due to an effective decrease of the resistance span over cycles due to the loosening of the fabrics.

Moreover, a different sensitivity was found for the SP29 integrated into 15% and 18% elastane leggings. A comparison was carried out by calculating the weighted arithmetic mean and the weighted standard deviation of sensitivity among all trials of both cases (by using Equations 7.13 and 7.14 for the same reasons explained in subsection 6.3.4). The outcome of such a comparison is reported in Table 6.2 and illustrated in Figure 6.14, showing again that the SP29 samples embedded into the most elastic garment have the lowest sensitivity.

Table 6.2: Sensitivity for the SP29 integrated into 15% and 18% elastane leggings with the Visual Motion Tracking System

| Case | First trial sensitivity ($\Omega/^{o}$) | All tests sensitivity ($\Omega/^{o}$) |
|---|---|---|
| SP29 in 15% elastane leggings | 67.93 | 44.49 $\pm$14.13 |
| SP29 in 18% elastane leggings | 43.60 | 33.88 $\pm$12.53 |

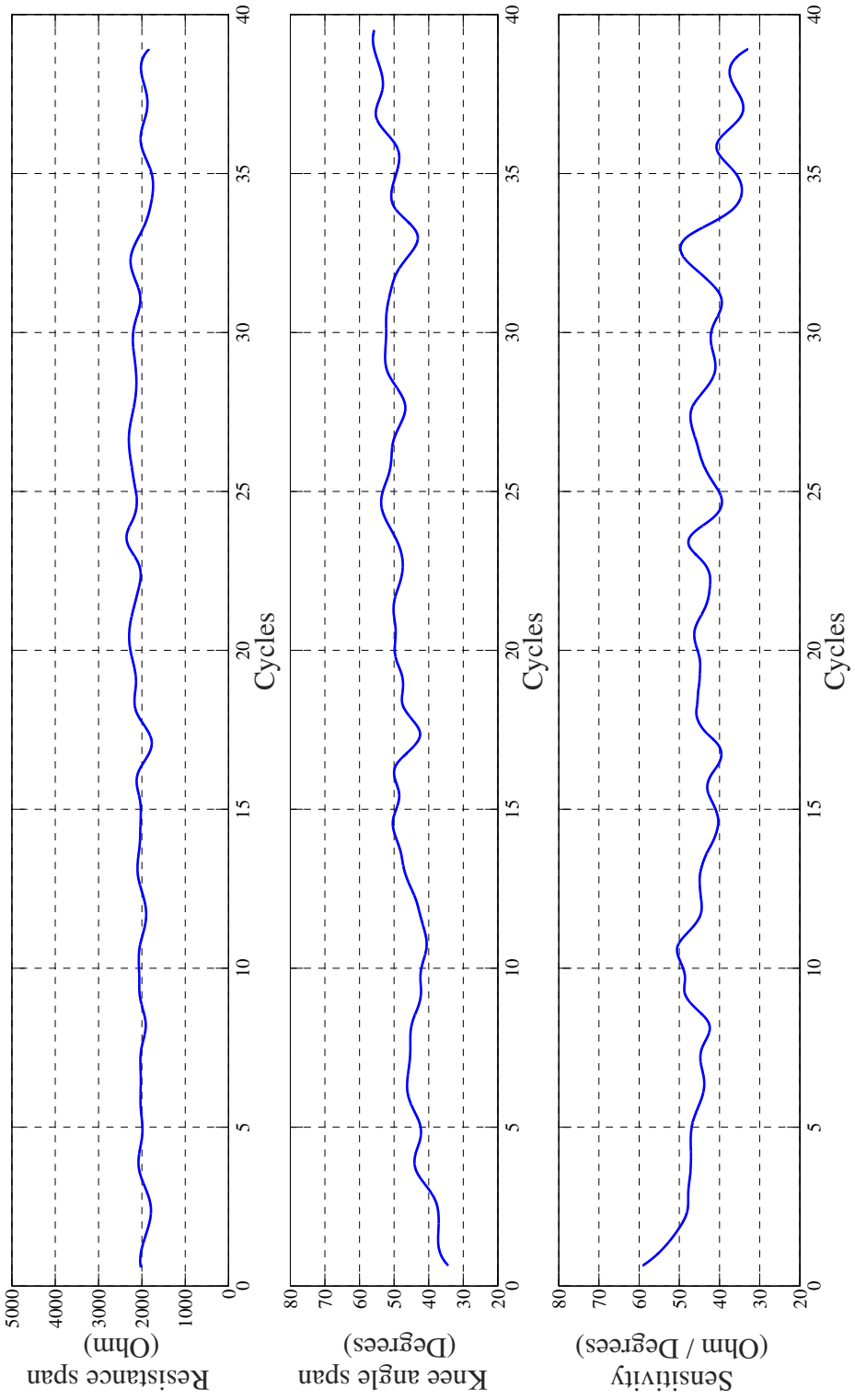


Figure 6.13: (a) Span of the fabric resistance, (b) Span of the knee angle and (c) Sensitivity for the SP29 embedded into a pair of leggings with 18% elastane and tested with the Visual Motion Tracking System after one hour preconditioning in a seated position

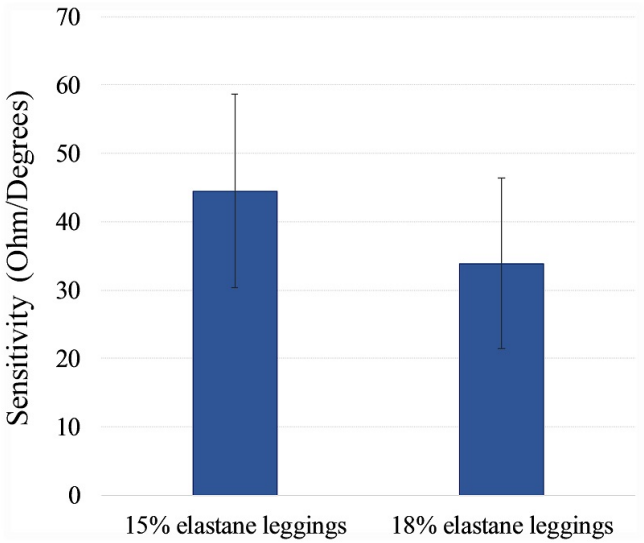


Figure 6.14: Sensitivity for the SP29 samples integrated into leggings with 15% and 18% elastane when studied with the Visual Motion Tracking System. The error bars represent the standard deviation

### 6.3.6 Hysteresis

The study of linearity (subsection 6.3.3) demonstrated that conductive samples integrated into leggings have a non-linear, elongation dependent electrical behaviour, as already discussed for the same knit pattern tested in the tensile machine (4.8.1). For completeness, the hysteresis behaviour of the SP29 integrated in 18% elastane leggings was considered over more cycles and, in particular, during the initial and last three knee flexion-extension cycles (Figure 6.15). As can be seen, the hysteresis was larger at the end of the trial. At this stage the fabric, being loose, was not able to promptly and accurately follow the knee angle accomplished. This is noticeable in the almost constant resistance variation from 115° to 155°, due to the increased delay between any knee movement and the resulting resistance. Therefore, the loosening of the fabric caused a change in the phase between resistance and knee angle, which resulted in an inversion of the hysteresis cycle: anti-clockwise during the first three cycles (solid arrows), clockwise during the last three cycles (dash arrows).

In terms of application, these results mean that the immediate estimation of the knee angle from the measured resistance is not straightforward.

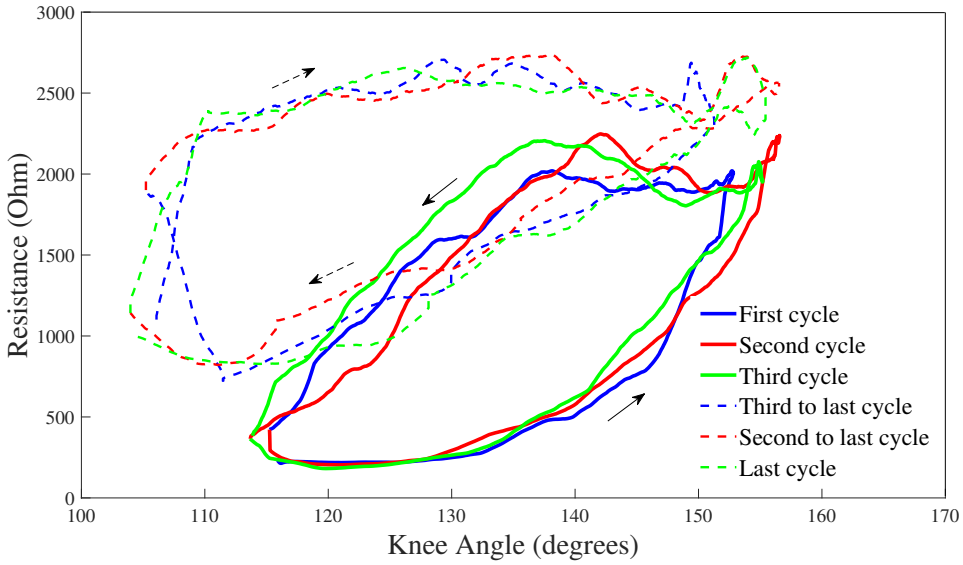


Figure 6.15: Hysteresis during the first and last three cycles of flexion-extension for the SP29 integrated into 18% elastane and tested with the Visual Motion Tracking System

### 6.3.7 Effect of the current on the fabric electrical resistance

The effect of the current on the electrical resistance of samples integrated into garment is the same of section 4.5.2, namely higher current values provided to the specimens resulted in lower stabilised average resistance values. To show this phenomenon, the 1mA and 3mA cases are reported (together with the knee angle performed) in Figures 6.16 and Figure 6.17, respectively. For the 1mA case, the stabilised average resistance is around 1700Ω versus the 750Ω of the 3mA case. These figures are in agreement with the analysis of the electrical properties of samples tested cyclically on a tensile machine (Figure 4.12), proving that the integration on a supporting garment does not affect the stabilised average resistance values.

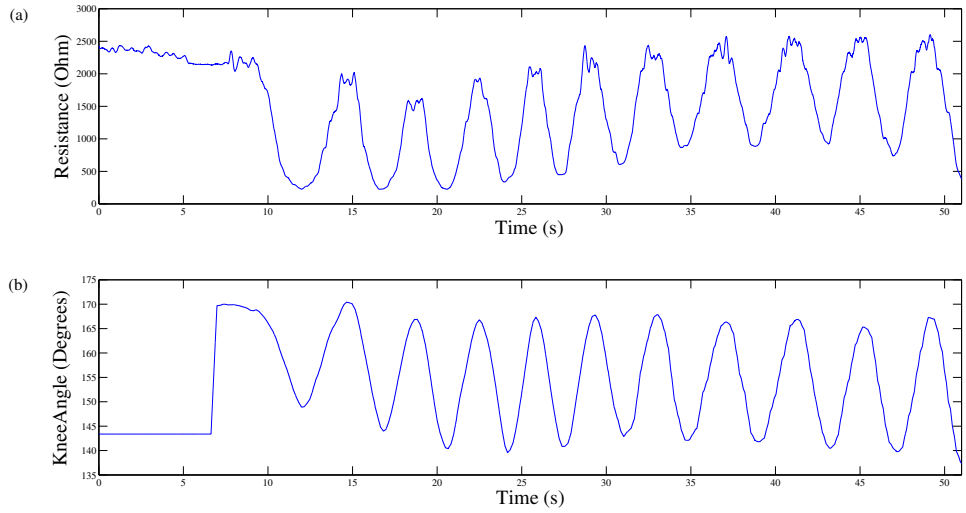


Figure 6.16: (a) Fabric resistance and (b) knee angle for the SP29 embedded into a pair of leggings with 15% elastane when sourced with 1mA constant current and tested with the Visual Motion Tracking System

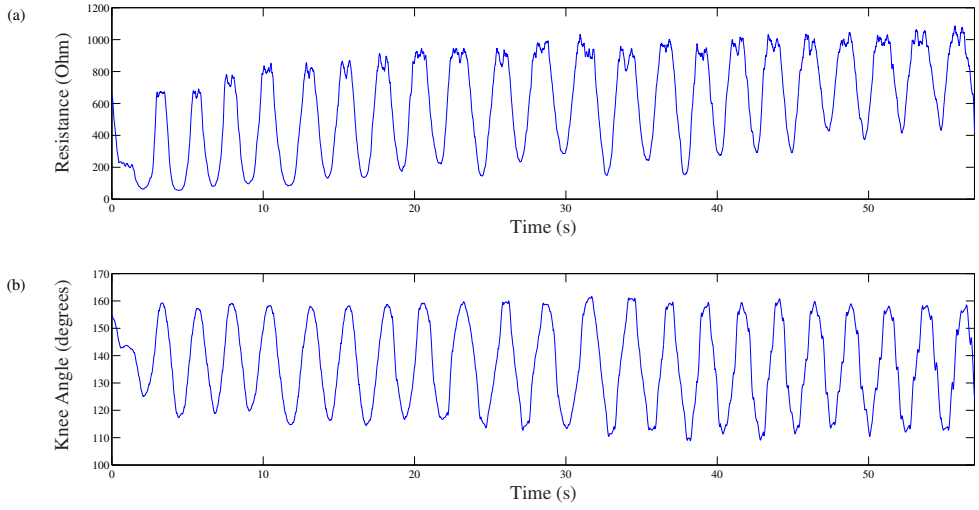


Figure 6.17: (a) Fabric resistance and (b) knee angle for the SP29 embedded into a pair of leggings with 15% elastane when sourced with 3mA constant current and tested with the Visual Motion Tracking System

## 6.4 *HUMAC NORM System*: Results and Discussion

The results of the tests conducted with the HUMAC NORM System (Method Two) are illustrated for the SP27 and SP29 integrated in leggings with 15% and 18% percentage of elastane in this section. The fabric resistance variation due to the change of the knee angle with the movement performed was acquired with the experimental system described in section 5.8.

### 6.4.1 Data post-processing

The analysis of the electrical behaviour of the conductive samples integrated into leggings was possible by post processing the data acquired with the system presented in section 5.8. The signals gathered from the HUMAC machine were the position and velocity outputs (subsection 5.9.1), whereas the fabric resistance was measured by collecting the voltage across the specimen ($V_m$) and the voltage proportional to the current provided to the fabric ($V_{current}$) from the leggings (subsection 5.9.2).

A procedure similar to the one described in section 3.6 and the code presented in subsection 6.3.1 (reported in Appendix VI (7.3.4)) were used for the post-processing of the fabric resistance signal. The only difference was the window length of the Savitzky-Golay filter, which was increased to f=651 to better reduce the electrical noise due to friction and slippages among the conductive fibres without introducing excessive shape distortions. The knee angle (obtained from $v$ of Equation 5.1) and the flexion-extension velocity (obtained from $w$ of Equation 5.2) were acquired without requiring further processing. The outcome of the filtering is shown in Figures 6.18 and 6.19 for the first three and fifty cycles, respectively, of knee flexion-extension of the SP29 embedded into a pair of leggings with 15%

elastane. The post-processing for the fabric resistance is illustrated in Figure 6.20 in terms of filtering (a), peaks detection and interpolation curves (b) and peak-to-peak span (c) for the SP29 in 15% elastane leggings.

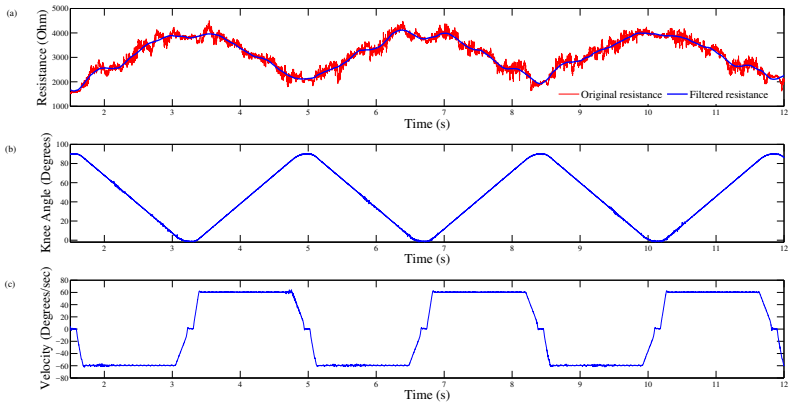


Figure 6.18: (a) Original and filtered fabric resistance (N=3, f=651), (b) Knee angle and (c) Velocity during the first three cycles for the SP29 embedded into 15% elastane leggings and tested with the HUMAC NORM System

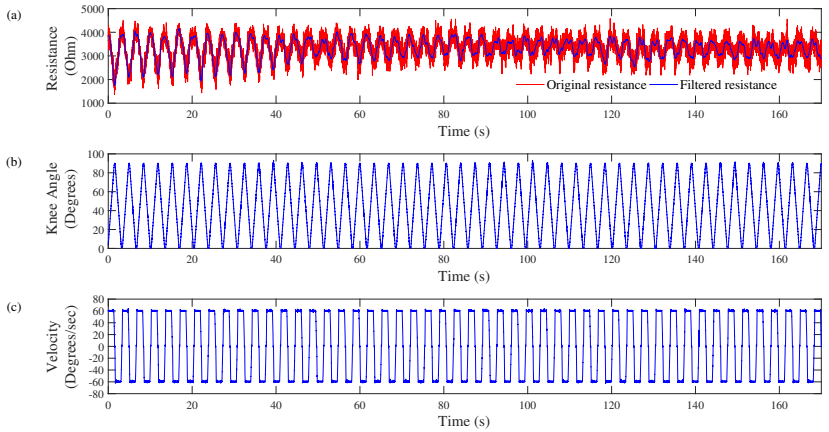


Figure 6.19: (a) Original and filtered fabric resistance (N=3, f=651), (b) Knee angle and (c) Velocity during the first fifty cycles for the SP29 embedded into 15% elastane leggings and tested with the HUMAC NORM System

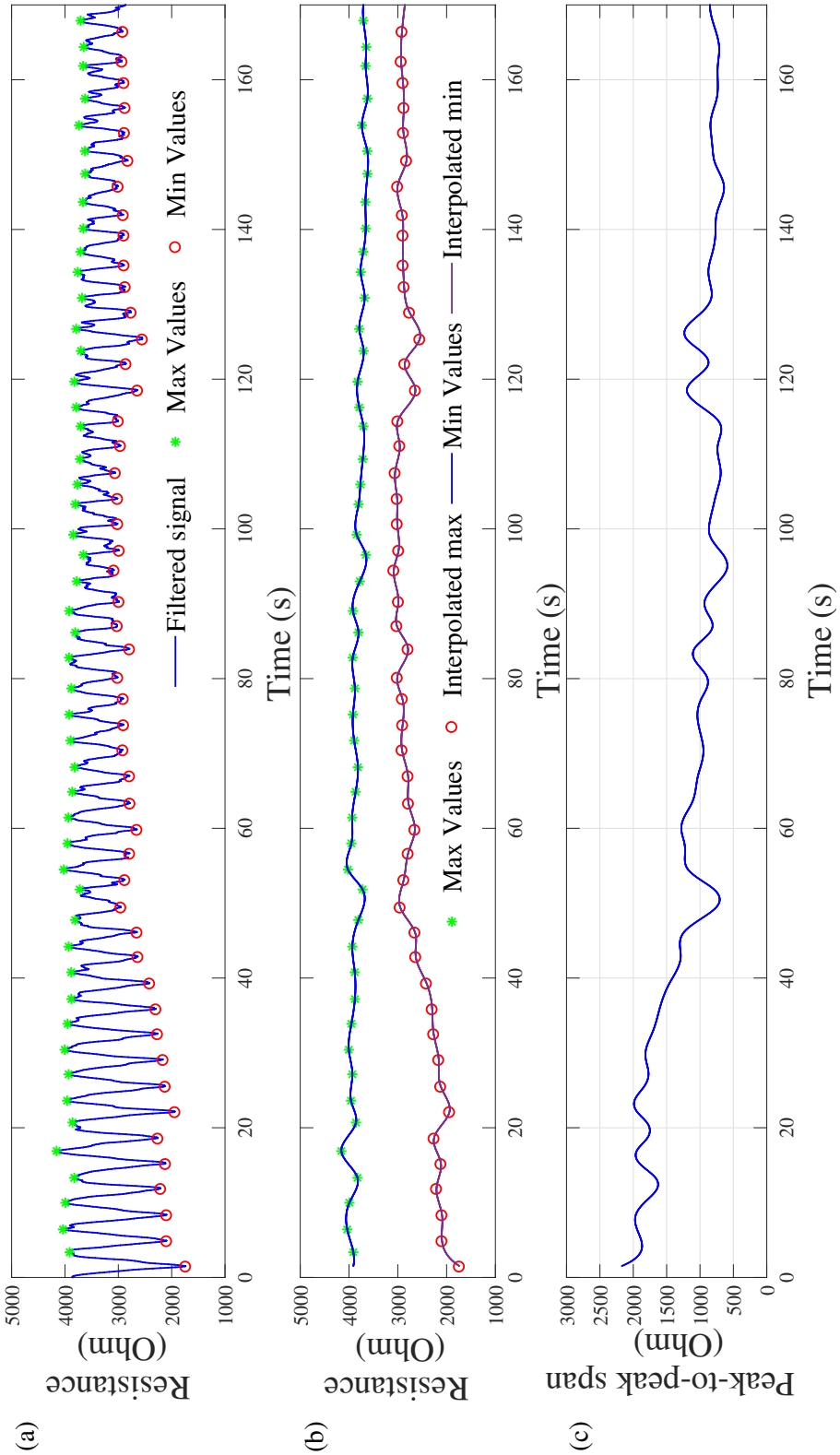


Figure 6.20: (a) Filtered fabric resistance (N=3, f=651), (b) Peaks detection and interpolation curves and (c) Peak-to-peak span for the SP29 embedded into 15% elastane leggings and tested with the HUMAC NORM System

For completeness, the post-processing for the other samples is shown in Figures 7.10, 7.11 and 7.12 for the SP29 in 18% elastane, SP27 in 15% elastane and SP27 in 18% elastane, respectively in the Appendix VIII (7.3.4)

### 6.4.2 Analysis of the electrical behaviour

The electrical behaviour of the conductive samples embedded into leggings and tested with Method Two was analysed thanks to the data post-processing described in subsection 6.4.1. Figures 6.18(a-b) and 6.19(a-b) show that the maximum fabric resistance occurred when the knee was fully extended (corresponding to no elongation of the fabric). From the calibration process the full extension was at 0°. On the other hand, the minimum fabric resistance was in correspondence of the maximum flexion of the knee (occurring at the maximum elongation of the specimen). From the calibration process this happened at 90°.

This behaviour is in agreement with what discussed both in section 4.3 and in subsection 6.3.2 regarding the factors influencing the fabric resistance during extension-recovery cycles. However, when comparing Figures 6.1(b) and Figure 6.18(b), the knee angle variation is opposite for the different convention used with the two acquisition systems: 180° for full extension and 90° for maximum flexion with Method One versus 0° and 90°, respectively, with Method Two.

### 6.4.3 Linearity

The fabric electrical response to the knee movement performed was not linear during the extension and flexion phases (Figure 6.21) but described by quadratic characteristic curves (Figure 6.22), whose equations are reported in Table 6.3 for the SP29 integrated into a pair of leggings with

18% elastane during the first cycle. Further cycles require a more complex curve fitting, which is not reported.

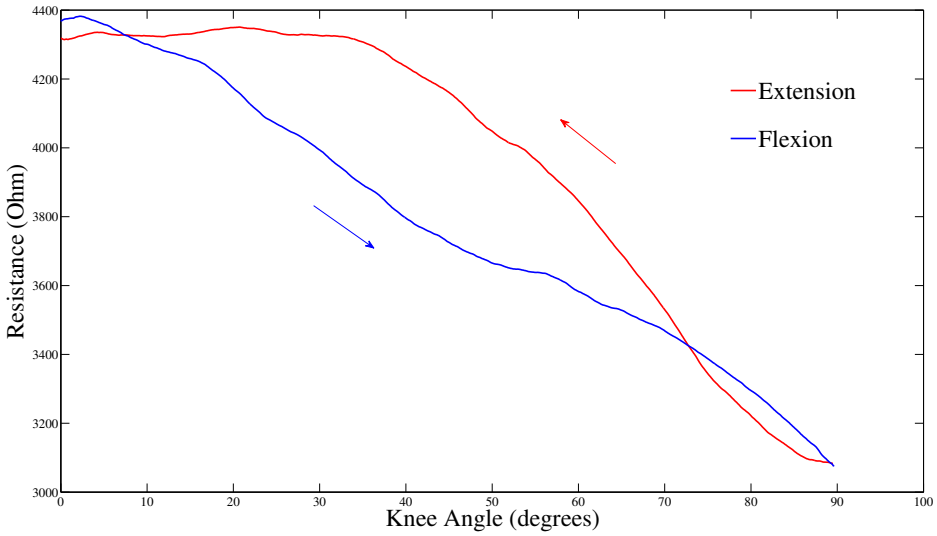


Figure 6.21: Extension and flexion curves for the SP29 integrated into a pair of leggings with 18% elastane during the first cycle with the HUMAC NORM System

Table 6.3: Regression curves for the SP29 sample embedded into leggings with 18%elastane and tested with the HUMAC NORM System

| Phase | Characteristic curve | $R^2$ |
|---|---|---|
| Extension | $y = -0.25175x^2 + 7.1286x + 4316.4$ | 0.991 |
| Flexion | $y = -0.0093x^2 - 13.408x + 4384.6$ | 0.992 |

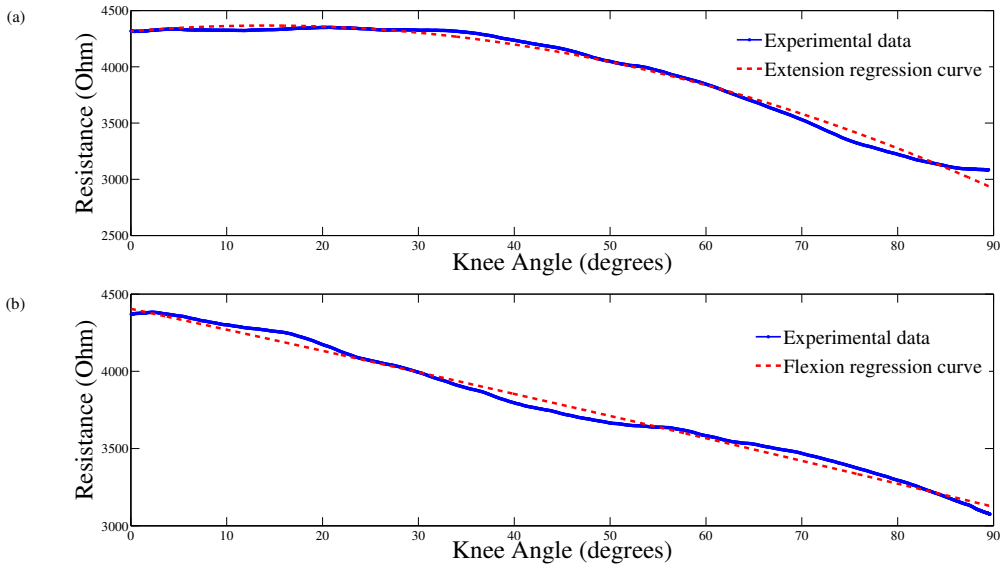


Figure 6.22: Characteristic curves for the (a) extension and (b) flexion phases of the SP29 integrated into a pair of leggings with 18% elastane during the first cycle with the HUMAC NORM System

### 6.4.4 Stability

Similarly to Method One in section 6.3.4, the stabilisation of the peak-to-peak span of the electrical resistance was studied for knitted conductive textiles integrated into garments and tested with Method Two by means of performance indicators, such as the number of cycles to reach stability. Such analysis confirmed that the supporting garment had the effect of accelerating the electrical stabilisation of the conductive fabric embedded in it. In fact, when compared to the results from the tensile machine (Figure 4.6):

- The SP27 sample required on average $106 \pm 55$ cycles of stretch-recovery to reach stability when tested for the first time in the Instron, whereas only $13 \pm 6$ cycles of knee flexion-extension when integrated and tested for the first time into leggings with Method Two.

- The SP29 sample required on average $116 \pm 75$ cycles in the Instron machine versus $11 \pm 2$ cycles of knee flexion-extension in the leggings.

The values in the leggings were obtained by using the arithmetic mean (Equation 7.11) and standard deviation (Equation 7.12) formulas, as all trials lasted the same number of cycles set by the HUMAC NORM machine (i.e. 50 cycles).

Figure 6.23 expresses these results with respect to the number of cycles for the SP29 in the tensile machine, showing that:

- The number of cycles to reach stability for the SP29 is reduced by 90% in the 15% elastane leggings and by 92% in the 18% elastane leggings;
- The number of cycles to reach stability for the SP27 is reduced by 93% in the 15% elastane leggings and by 86% in the 18% elastane leggings.

An explanation of this considerable reduction of the stabilisation time is provided by the way the samples were integrated into leggings. The specimens were sewn on the garment not only in proximity of the copper contacts but at fixed distance in several points along their lengths (Figure 5.1). As a consequence, during elongation or relaxation the supporting garment exerted a force distributed along the samples' lengths and not just in proximity of the contacts (as occurred during tests on the Instron machine). This means that the samples promptly followed the knee movement during the extension and flexion phases, being constrained by many stitches distributed all over their surface.

Moreover, it is noticeable that the SP29 integrated into the less elastic leggings (15%) exhibited the slowest stabilisation when compared to the SP27 in the same leggings. Conversely, the SP29 embedded into 18% elastane leggings showed a quicker stabilisation versus the SP27 that required the highest number of cycles to reach stability. This result will be discussed in

more detail when introducing the sensitivity in subsection 6.4.5.

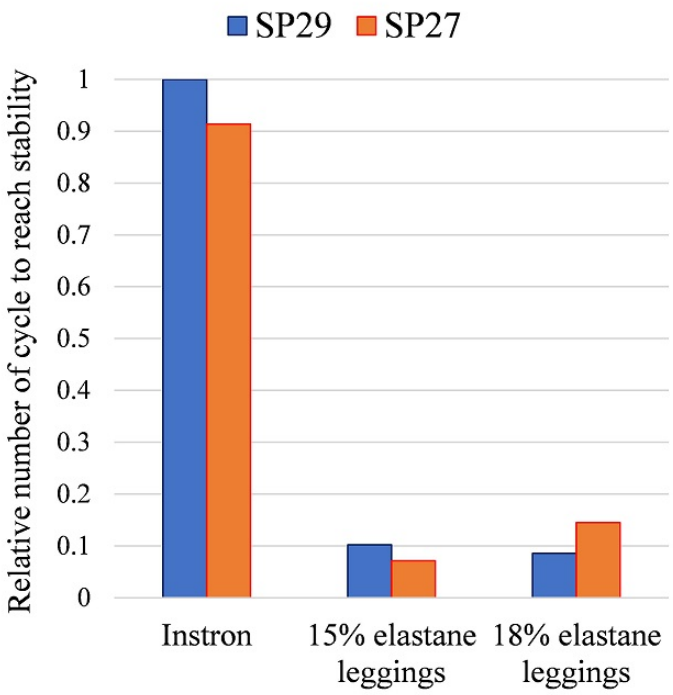


Figure 6.23: Comparison between relative number of cycles to reach stability for the SP27 and SP29 tested for the first time in the Instron tensile machine and integrated into leggings with 15% and 18% elastane

### 6.4.5 Sensitivity

To provide information about the sensing performance of the fabric transducer when tested with the HUMAC NORM System, the sensitivity was preferred to the gauge factor (as explained in subsection 6.3.5) and calculated as the ratio between the span of the fabric resistance and the span of the knee angle. As the knee angle span did not vary during repetitive flexion-extension cycles, the main factor affecting the sensitivity was the span of the fabric resistance. Thus, similarly to the resistance spans for the SP27 and SP29 samples integrated in 15% and 18% elastane leggings (Figures 7.11(c), 7.12(c)), 6.20(c) and 7.10(c), respectively), the sensitivity decreased with cycles as well (Figure 6.24).

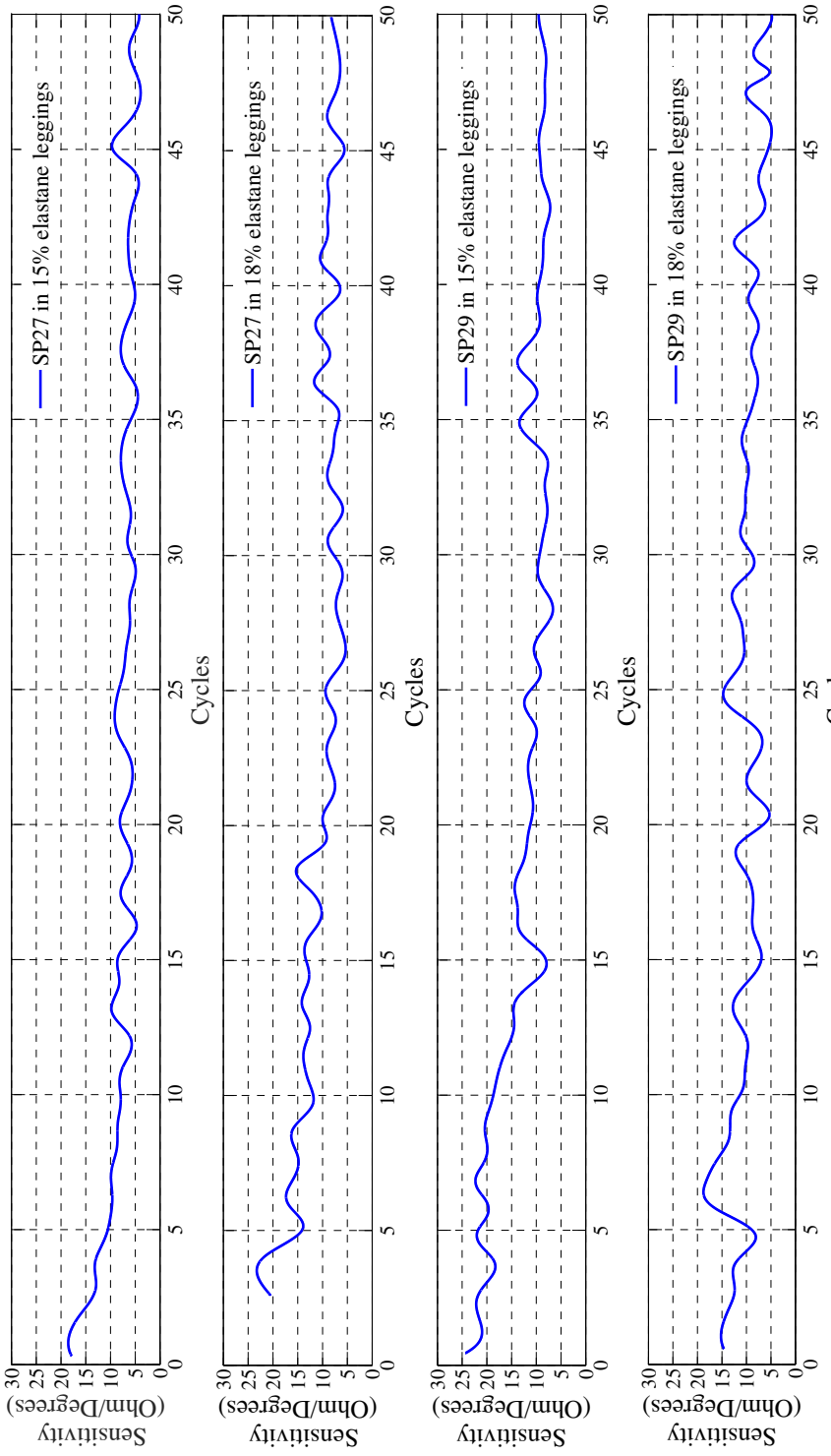


Figure 6.24: Sensitivity for: (a-b) the SP27 integrated into leggings with 15% and 18% elastane, (c-d) the SP29 embedded into 15% and 18% elastane leggings and tested with the HUMAC NORM System

By considering the mean values of sensitivity for each sample during all tests performed, Figure 6.25 was determined. The figure illustrates that the SP29 integrated into the less elastic leggings showed the highest sensitivity, whereas the SP27 in the same leggings exhibited the worst sensing properties. Conversely, the SP29 embedded into the 18% elastane leggings had the lowest sensitivity compared to the SP27. The worsening of the sensing properties for the SP29 in the more elastic leggings was already proved by Method One in section 6.3.5 in terms of gauge factor and sensitivity (Figure 6.14).

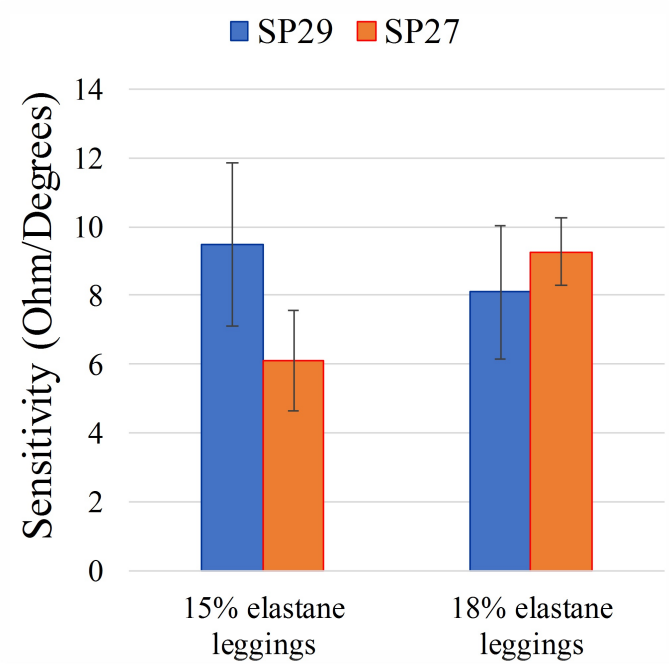


Figure 6.25: Sensitivity for the SP27 and SP29 embedded into leggings with 15% and 18% elastane when tested with the HUMAC NORM System. The error bars represent the standard deviation

The outcome of the study on sensitivity, together with what discussed in subsection 6.4.4 in terms of number of cycles to reach stability, provided an important general outcome: the samples which stabilised more quickly (Figure 6.23) were the ones that exhibited the worst sensing properties (i.e. SP27 in the 15% elastane leggings and SP29 in 18% leggings), whereas the

knit patterns which required more cycles to reach stability were the specimens with the highest sensitivity (i.e. the SP29 in 15% elastane leggings and SP27 in 18% elastane). This means that the loosening of the fabrics affected their sensing properties (with a decreasing resistance span) and, thus, their performance. As a result, a quicker electrical stabilisation does not guarantee a good fabric sensing-wise performance. On the contrary, the slower the stabilisation occurs, the most sensitive the fabric performance is.

Table 6.4 reports all the sensitivity values for the SP27 and SP29 at 15% and 18% elastane leggings for the first trial and all tests.

Table 6.4: Sensitivity for the SP27 and SP29 integrated into 15% and 18% elastane leggings when studied with the HUMAC NORM System

| Case | First trial sensitivity ($\Omega/^{o}$) | All tests sensitivity ($\Omega/^{o}$) |
|---|---|---|
| SP29 in 15% elastane leggings | 12.16 | 9.47 $\pm$2.39 |
| SP29 in 18% elastane leggings | 10.03 | 8.09 $\pm$1.93 |
| SP27 in 15% elastane leggings | 7.76 | 6.09 $\pm$1.46 |
| SP27 in 18% elastane leggings | 10.38 | 9.27 $\pm$0.97 |

### 6.4.6 Hysteresis

For completeness, the non-linearity of the fabric electrical behaviour (discussed in section 6.4.3) is illustrated for the SP29 integrated into 18% elastane leggings during the initial and last three cycles. Even if repetitive and accurate movements were performed by the HUMAC machine, the loosening of the fabrics caused a reduction of the resistance span or equivalently, a decrease of the fundamental component with respect to the amplitude of the higher order harmonics. This resulted in the down-shifting and increased distortion of the resulting hysteresis cycles (Figure 6.26). The opposite slope compared to the hysteresis graph obtained with the Visual Motion Tracking System (Figure 6.15) was due to the different convention used by the two acquisition methods for indicating the full extension and maximum flexion, as explained in subsection 6.4.2.

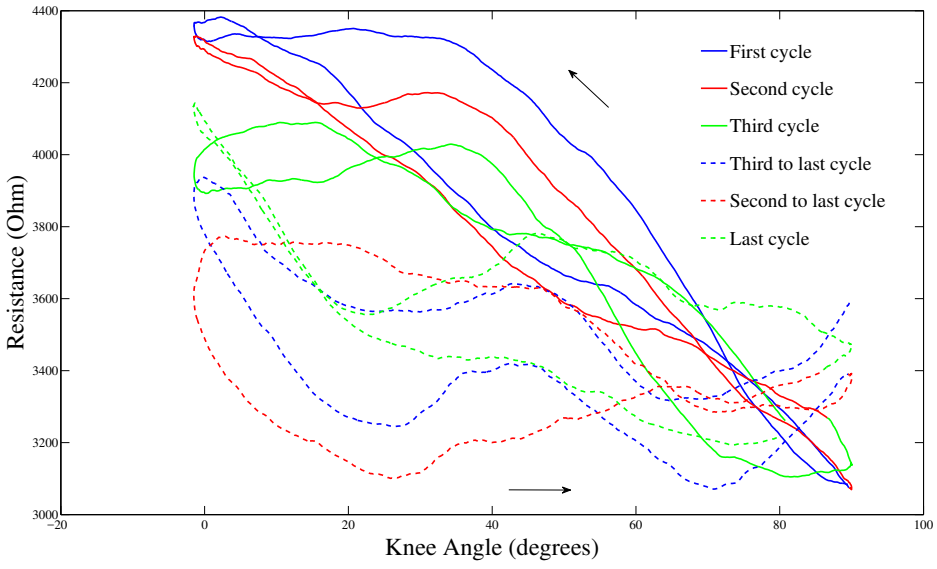


Figure 6.26: Hysteresis during the first and last three cycles of flexion-extension for the SP29 integrated into 18% elastane and tested with the HUMAC NORM System

### 6.4.7 Effect of the supporting garment on the fabric parameters

As a result of cyclic stretch-recovery of knitted conductive textiles a variation of the fabric parameters occurred (subsection 4.5.1). Once the same samples were integrated into leggings the effect of the supporting garment on the fabric parameters variation was investigated. The optical technique introduced in section 3.3 was applied to the SP27 and the SP29 before and after cyclic knee bending trials. From the microscope analysis, it was discovered that changes of loop lengths were more evident for samples embedded into a more elastic support (i.e. +15.33% and +14.45 in Figure 6.27 for the SP27 and SP29 in 18% elastane leggings versus +10.43% and +12.48% for the same samples in 15% elastane). The paired-samples *t*-Test confirmed significant changes in the loop lengths after tests for SP27 in 15% elastane (p = 0.029), SP27 in 18% elastane ($p$ = 0.001), SP29 in 15% elastane ($p$= 0.003) and SP29 in 18% elastane ($p$=0.031).

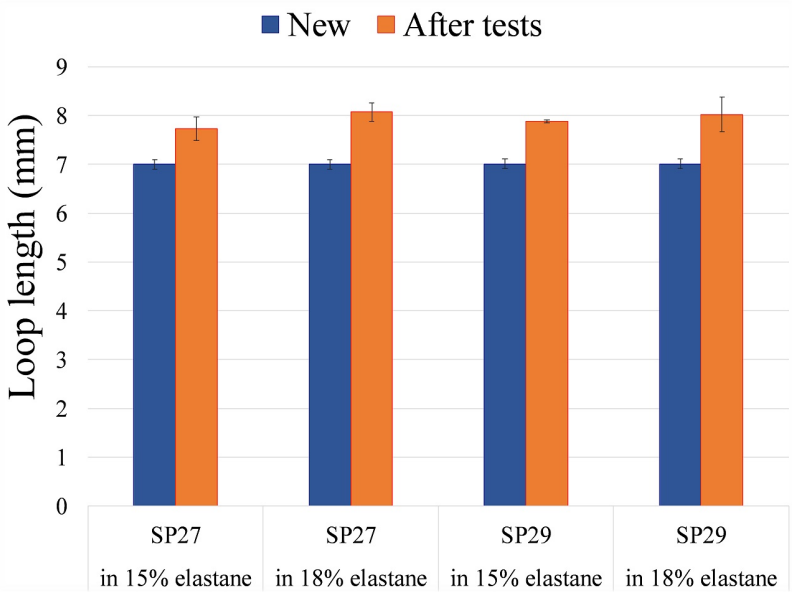


Figure 6.27: Loop lengths for the SP27 and SP29 embedded into leggings with 15% and 18% elastane in case of new specimens and samples tested with the HUMAC NORM System

## 6.5 Comparison of the two methods

Two different methods for motion capture were applied to the electrically conductive textiles integrated into a supporting garment, as described in Chapters 5.

Method One: The *Visual Motion Tracking System* (camera and red-green-blue markers) regarded a study case in which the user was free to perform knee flexion-extension at speed/angle which were not set but determined by his/her will and physiological factors, e.g. muscles strength/weakness, concentration, tiredness. This example represented a real case in which the user wore the electro-conductive leggings and led the tests arbitrarily and with no restrictions. In view of future applications of electrically conductive textiles (e.g. in rehabilitation), the question to address was whether the user could achieve meaningful results when performing on his/her own the movement with the electro-conductive leggings, without a machine ensuring repetitive movements. This explained the importance of discussing a method (and relative data collection) when physiological and external factors (e.g. light condition affecting the markers detection, working range restriction) play a significant role. Results of the fabric resistance variation due to the knee angle performed by the wearer were reported in 6.3.2.

Method Two: The *HUMAC NORM System* aided the user to achieve repetitive knee flexion-extension cycles thanks to a dynamometer which accomplished the movement at a set speed/angle. Thus, in this case, the measurements were not affected by the mentioned physiological and external factors and the conductive textiles were tested systematically by a machine for a longer and repeatable number of cycles.

On the basis of what discussed, advantages and disadvantages of using the two methods are summarised in Table 6.5.

Table 6.5: Comparison between method one and method two

| **Method** | **Advantages** | **Disadvantages** |
|---|---|---|
| *Tracking system* | • Freedom of movement<br>• Real working case<br>• Personalised application | • Influence of physiological factors (e.g. tiredness, distraction)<br>• Markers detection issues (e.g. light condition, working range) |
| *Humac machine* | • No influence of physiological/external factors<br>• Repeatability at the same angle/speed<br>• Longer cycles measurements | • The user does not lead the experiment<br>• The user needs the aid of a machine<br>• The method is not applicable at home |

When comparing the results obtained with both methods, a similar electrical behaviour of the conductive samples integrated into leggings was found whether the strain was provided either by the user or by a machine. In particular, both approaches confirmed the outcome of the study of conductive samples elongated in a tensile machine, namely a minimum fabric resistance value in correspondence of the maximum elongation of the fabric and maximum knee bending and a maximum fabric resistance value at minimum fabric elongation and maximum knee extension. Moreover, specimens elongated both arbitrarily (Method One) and systematically (Method Two) showed an electrical stabilisation occurring in a smaller number of cycles after preconditioning by previous trials or by wearing the leggings for a period of time. This proved the common effect of the supporting garment on the stability of conductive fabric embedded in it.

Another outcome of the analysis conducted by both methods was that the fabric electrical response to the knee angle variation was not linear but described by quadratic characteristic curves during the first cycle and more complex polynomial during further cycles. The elongation dependent behaviour was also highlighted by hysteresis graphs.

Both methods found that the SP29 integrated in the less elastic leggings had the highest sensitivity (Figure 6.14 for Method One and Figure 6.25 for Method Two). The difference in sensitivity values was due to the different knee angle range performed: 35° for method One and 90° for Method Two.

The application of two approaches provided also different feedback. For example, Method One was the methodology which highlighted the non-linear effect due to the contact resistance predominating over the length-related resistance. As shown in Figure 6.8, this phenomenon was identified by a sudden decrease of the resistance span once the knee range of motion performed by the wearer (and, thus, the fabric extension) decreased

under a certain angle. As soon as the angle variation became larger, the resistance (and, thus, the span) returned to vary according to the knee flexion-extension phases thanks to the contribution stemming from the arising length-related resistance. Conversely, the non-linear behaviour related to contact resistance was not evident during a constant knee span provided by the HUMAC NORM System. In this case, the cause of a progressive span decrease was the loosening of the fabrics cycle after cycle.

The reason why the Visual Motion Tracking System and the HUMAC NORM System were not employed at the same time was that the HUMAC machinery and the unused leg during tests were in the way of the camera and reference markers, as shown in Figure 5.15.

## 6.6 Discussion

Although only a few studies have been conducted on knitted fabric sensors for the measurement of joint angles, some of the findings presented in this Chapter can be linked back to the literature. Firstly, the loosening of the fabrics is one of the phenomenon to be taken into account when discussing the conductive textiles' performance for measuring joint angles. In this Chapter, the effect of the fabric relaxation was proved for samples integrated into garments by the decreased fabric sensitivity when subject to cyclic, larger knee rotations (90° with the *HUMAC NORM System*) compared to lower rotation angle (35° with the *Visual Motion Tracking System*). A similar issue was described by Cho et al. 2011 in terms of slow recovery time of the fabric shape for the textile-based sensor measuring the changes in the electrical resistance with the angle variation at the elbow joint. In this case, the authors' recommendation was to braid highly elastic yarn such as spandex with stainless steel yarn.

Secondly, the effects of change in sensitivity, non-linearity and hysteresis have been studied in Atalay 2014. To linearise the fabric response, the proposed solution was to avoid any electrical interaction between adjacent conductive courses by spacing and sewing them on a non-conductive knitted fabric. In this way, the contact resistances between courses were eliminated.

High sensitivity, low hysteresis, as well as high linearity and repeatability of the relationship between angle and resistance during elbow and knee movements were found by Shyr et al. 2014. In this study, a wearable gesture-sensing device consisted not of a knitted fabric but of an elastic conductive webbing made of polyamide fibre coated with carbon particles and polyester yarn. In the overall, polymer-based strain sensors are extremely competing in terms of stability and repeatability of the sensor response over a large number of cycles (e.g. 10,000) (Yamada et al. 2011). Although these features allow to precisely monitor rapid human motion, polymer-based strain sensors, when compared to knits, are not an ideal solution to bulkiness and discomfort as they cannot be simply integrated into garments but must be attached to them.

The results obtained in this Chapter are in agreement with those obtained in Chapter 4. In fact, the behaviour of the specimens under test remained consistent in terms of non-linearity, hysteresis and loosening, both for samples tested on the Instron machine and on a participant. In place of the gauge factor, the sensitivity has here been used as an indicator of the knitted sensor's performance to remove the influence of disturbing trends due to the loosening of the samples.

Quantities expressed in terms of angular displacement in this Chapter can be linked back to the corresponding ones presented in Chapter 4 as a function of linear displacement. The link between linear and angular dis-

placements was introduced in section 6.3.5 by Equation 6.2. The simplicity of such relation was adequate for performance evaluation and comparison among samples integrated into leggings. However, the angular sensitivity $S_\theta$ was preferred to the linear gauge factor for its effectiveness in presence of loosening and for being a more meaningful indicator in case of application of the fabric as an angular displacement sensor.

In a similar way, we could consider the relationship between the fabric resistance and the elongation, which was established in Table 4.3 during the first test cycle for, respectively, the stretching and recovery phases:

$$R_\mathrm{s} = A\Delta L^2 + B\Delta L + C \tag{6.6}$$

$$R_\mathrm{r} = D\Delta L^2 + E\Delta L + F \tag{6.7}$$

Where: $\Delta L$ is the absolute change in the specimen's length, A=0.00142, B=-1.0868, C=18.167, D=0.025, E=-1.0868 and F=16.539.

As $\epsilon = \dfrac{\Delta L}{L_\mathrm{o}}$ (with $L_o$ being the original length of the specimen in the clamps), the same equations can be rewritten in terms of strain:

$$R_\mathrm{s} = A(L_\mathrm{o}\epsilon)^2 + B(L_\mathrm{o}\epsilon) + C \tag{6.8}$$

$$R_\mathrm{r} = D(L_\mathrm{o}\epsilon)^2 + E(L_\mathrm{o}\epsilon) + F \tag{6.9}$$

At this point, based on the Equations 6.6 - 6.7 and on the relationship described in Equation 6.2, which links the rotation angle ($\theta$) to the length of the flexion arc $l$ (i.e. considered the fabric length term) and $r$ (i.e. the distance between the centre of the knee and the lateral condyle), we can assume a similar quadratic relationship between the fabric resistance and the knee angle during the first test cycle:

$$R_{\mathrm{s}} = A(\frac{2\pi r}{360})^2(\Delta\theta)^2 + B(\frac{2\pi r}{360})\Delta\theta + C = A^{'}(\Delta\theta)^2 + B^{'}(\Delta\theta) + C^{'} \quad (6.10)$$

$$R_{\mathrm{r}} = D(\frac{2\pi r}{360})^2(\Delta\theta)^2 + E(\frac{2\pi r}{360})\Delta\theta + F = D^{'}(\Delta\theta)^2 + E^{'}(\Delta\theta) + F^{'} \quad (6.11)$$

However, a different pre-tension condition exists between samples elongated in the Instron machine and specimens subjected to elongation when integrated into leggings, and is confirmed by the different range of resistance values measured in the two cases (Figure 4.22 versus Figure 6.5). Although Equation 6.2 allowed straightforward transformations between linear and angular quantities, it can introduce inaccuracies when considering the knee's kinematic, which demands for more complex, non linear equations. Moreover, the knee's morphology generates during motion a varying strain on the samples which is not uniformly distributed along their widths (in contrast with the almost uniform strain applied by the clamps of the Instron machine) but mainly concentrated in proximity of the patella. As a result, the constants A$^{'}$ to F$^{'}$ in Equations 6.10 - 6.11 will differ from the corresponding constants shown in Table 4.3. This means that an attempt at predicting knee angle data based on the knowledge developed in Chapter 4 is not possible.

In addition, from the study of the fabric electrical resistance in terms of hysteresis, harmonics contents, and peak-to-peak span, it was proved that the electrical behaviour was strongly influenced by the mechanical status of the specimen (loosening). For instance, it was shown that the hysteresis cycle's position, shape and orientation change during extended use of the samples with the following consequences:

- The measured values for maximum and minimum resistances vary

with time with the final effect of reducing the resistance span and so the sensitivity;

- A phase delay between performed movement and measured resistance increases with time.

This is another reason why the immediate estimation of the knee angle from the measured resistance is not possible without improving first the samples design or creating a complex electro-mechanical model.

## 6.7 Conclusions

This Chapter described the analysis conducted on knitted conductive samples when integrated into supporting garments with different percentage of elastane and subjected to cyclic deformation. The effect of the supporting garment on the electrical properties (stability, sensitivity, linearity and hysteresis) exhibited by the SP27 and SP29 samples embedded into 15% and 18% elastane leggings was studied by using two methods: the *Visual Motion Tracking System* and the *HUMAC NORM System*.

Both methods assessed that the integration of conductive specimens in leggings accelerated the electrical stabilisation compared to the same knit patterns tested on the tensile machine. However, it was also proved that a quicker electrical stabilisation did not guarantee a good fabric sensing-wise performance. In fact, the study of sensitivity conducted with Methods One and Two showed that samples which stabilised more quickly (Figure 6.23) were the ones with the worst sensing properties (i.e. SP27 in the 15% elastane leggings and SP29 in 18% leggings), whereas the knit patterns requiring more cycles to reach stability were the specimens with the highest sensitivity (i.e. the SP29 in 15% elastane leggings and SP27 in 18% elastane). This confirmed that the electrical stabilisation and the time to reach stability were related to the loosening of the fabric under test, which was due to the slippage and/or permanent extension of the fibres depending on to their viscoelasticity.

In addition, fabrics' good sensing-wise performance was also related to the composition of the leggings they were integrated in. In fact, the sensing properties of the SP29 and SP27 were improved by the integration into the 15% and 18% elastane leggings respectively (Tables 6.2 and 6.4).

Conductive samples have still an elongation dependent behaviour even

when embedded into leggings, proving their non-linear behaviour under cyclic deformation. Lastly, from the microscope analysis it was possible to highlight the influence of the supporting garment with different percentage of elastane on the fabric parameters. In particular, it was discovered that the change of loop lengths was more evident for samples embedded into a more elastic support.

# Chapter 7

# Conclusions and future work

## 7.1 Introduction

The aim of this chapter is to summarise the findings of the work presented in this thesis as a whole, to highlight the significant conclusions and to make recommendations for future study in the field.

## 7.2 General summary and conclusions

The work presented in this thesis was aimed to characterise the electrical properties of knitted conductive textiles as fabric strain sensors and to discuss their integration into garments to act as wearable motion sensors. To do so, this manuscript described firstly the methodology and results of fabric testing on a tensile machine and, secondly, the techniques and outcomes of trials on two supporting garments worn by a participant.

### 7.2.1 Characterisation of knitted conductive textiles

The combination of stainless steel with polyester fibres adds a conductive behaviour to the yarn in which they are embedded. Fabrics knitted in such

a manner develop sensing properties that make the textiles suitable for smart/wearable applications. In particular, this thesis employed knitted conductive samples made of 20% stainless steel and 80% polyester fibres, whose strain sensitive behaviour was first investigated during a considerable number of stretch-recovery cycles performed by an Instron tensile machine. Influencing factors of the fabric resistance during tests were: length variation of the conductive yarn (contributing to the length-related resistance, $R_l$), structural deformations of the stitches causing variation of the contact forces (affecting the contact resistance, $R_c$), fabric mechanical and geometrical parameters (such as the number of contact points, loop length, cross-sectional area and loop geometry) and fibre-fibre slippage.

The fabric resistance variation with stretch-recovery cycles was therefore analysed with a dedicated measurement system based on a purposely designed electronic board to pass a constant current through the fabric rather than the traditional constant voltage method normally used. Moreover, the employment of a four wire measurement system and of suitably modified mechanical clamps enabled to minimise the errors due to wire and contact parasitic resistances.

To describe the mechanical and electrical status of the fabric under test electrical features of interest were individuated. In particular, the peak-to-peak span was the peak-to-peak amplitude of the fabric resistance variation during cyclic loading.

The main findings of the fabric electrical characterisation are summarised in the following:

- When knitted conductive textiles were tested for a considerable number of stretch-recovery cycles (i.e. 250), their electrical properties (i.e. peak-to-peak span) decreased over cycles with a tendency toward stabilisation after a number of cycle ($54 \pm 38, 106 \pm 55, 116 \pm 75$ and

$108 \pm 22$ for the Single Jersey, SP27, SP29 and SP31, respectively).

- Repeatability of the electrical features was maintained after a short rest period (i.e. 5 minutes), with the number of cycles to reach stability being considerably decreased ($9 \pm 6, 18 \pm 15, 17 \pm 6$ and $29 \pm 23$ for the Single Jersey, SP27, SP29 and SP31, respectively).

- The stabilised average resistance increased between tests as a result of both an increase of the contact resistance (due to the decreased contact pressure according to Equation 2.2) and an increase of the length-related resistance (due to the increased yarn length following the loosening of the fabric, according to Equation 2.1).

- Increasing sourced currents and elongation rates affected the resistance measurements by, respectively, decreasing the stabilised average resistance (proving the non linear behaviour of the metal-semiconductor contact between fibres) and reducing the number of cycles to reach the electrical stabilisation. The discovery of the non ohmic effect was possible by the constant current source method employed in the study and by the possibility of providing currents of different amplitude to the samples thanks to the purposely designed conditioning circuitry.

- The elongation to which the conductive samples were stretched influenced their electrical behaviour as the contribution of the contact and length-related resistances to the overall equivalent resistance varied with extension. The contact resistance dominated the overall equivalent resistance during the initial tensile process, whereas the length-related resistance determined the total resistance when further extensions were applied. The switchover from contact to length-related resistance and vice versa was found to be dependent on the fabric state of deformation during the trials.

Stretching and recovery phases during the first cycle were accurately modelled by quadratic curves for specimens elongated of 12 and 16 mm, whereas no low order polynomial described the electrical behaviour of the fabric elongated of 8 mm.

- The most critical condition affecting the samples electrical behaviour was the loosening of the fabric due to the fibre-fibre slippage. This phenomenon caused unpredictable fluctuations/noise of the electrical resistance in correspondence of the maximum resistance value/minimum elongation of the specimens and became significant cycle after cycle, especially during the repeatability test.

- The effect of the loosening of the fabric was evident in other performance indicators, such as the gauge factor and the signal-to-noise ratio. The gauge factor of all knit patterns decreased gradually with cycles during preconditioning test (up to 20 times smaller) and steeply during repeatability session (reducing to the minimum value from the 20th cycle onwards). In particular it was found that SP29 was the sample that generally maintained the highest sensitivity for the longest time interval but with the variation decreasing with cycles, whereas the SP27 guaranteed stable but lower sensitivity.
  The signal-to-noise ratio decreased with cycles as well during preconditioning and repeatability tests. The 5 minute rest was not sufficient for all specimens to fully recover from the effect of relaxation, resulting in no signal recovery from the noise in between tests.

- The highly non-linear effect of fibre loosening and slippage was also confirmed by the hysteresis and time-frequency analyses. In particular the hysteresis was large during the initial stretch-recovery cycles as a consequence of the progressive mechanical deformation of

the fabric and was considerably reduced once the sample reached its mechanical and electrical stabilisation. The time-frequency analysis confirmed the additional noise components introduced to the harmonics spectrum of the fabric resistance signal and that the fundamental component (at the same frequency of the stretch-recovery cycles) progressively decreased, causing a reduction of the signal-to-noise ratio.

### 7.2.2 Use of knitted conductive textiles as wearable motion sensors

From the electrical characterisation of knitted conductive textiles during cyclic deformation in the tensile machine, it was possible to select the best knit pattern candidates for integration in leggings to act as knee angle motion sensors. The textile-sensor performance was therefore studied with two measurement systems which captured the fabric electrical resistance variation during the cyclic deformation of the garment they were integrated in. The first method, called *Visual Motion Tracking System*, regarded the free motion of the participant's knee joint, which was tracked by using a camera, coloured markers and a purposely implemented algorithm. The second method, called *HUMAC NORM System*, was for repetitive constrained movements of the participant's knee joint in a isokinetic machine. The main outcomes of the use of knitted conductive samples as fabric transducer for motion capture are summarised in the following:

- The supporting garment accelerated the electrical stabilisation of the conductive fabric embedded in it. In fact, compared to the same knit patterns tested on the tensile machine, the number of cycles to reach stability for samples integrated in 15% and 18% elastane leggings is reduced, respectively, by 90% and 92% for the SP29 and by 93% and

86% for the SP27.

- The electrical stabilisation and the time to reach stability were related to the loosening of the fabric under test, which was due to the slippage and/or permanent extension of the fibres depending on their viscoelasticity.

- A quicker electrical stabilisation did not guarantee a good fabric sensing-wise performance. In fact, samples that stabilised more quickly were the ones with the worst sensing properties (i.e. SP27 in the 15% elastane leggings and SP29 in 18% leggings), whereas the knit patterns requiring more cycles to reach stability were the specimens with the highest sensitivity (i.e. the SP29 in 15% elastane leggings and SP27 in 18% elastane).

- The fabric electrical response to the knee movement performed was not linear during the extension and flexion phases but described by quadratic characteristic curves during the first cycle and by more complex polynomial during further cycles. In terms of application, these results mean that the immediate estimation of the knee angle from the measured resistance is not straightforward.

- An increased delay between the knee angle variation and the resulting resistance in the hysteresis graphs was the consequence of a loose fabric, which was not longer able to promptly and accurately follow the knee movement (especially during the recovery phase).

- The non-linear effect due to the contact resistance predominating over the length-related resistance was highlighted during free motion of the participant's knee joint (Method One) and not during constrained movement (Method Two). In particular, when the amplitude of the

knee movement changed even by a small amount, the strongly non linear effect of the contact resistance was evident, with the fabric resistance varying considerably.

- From the microscope analysis it was discovered that the change of loop lengths was more evident for samples embedded into a more elastic support. This confirmed that the supporting garment may contribute to the mechanical conditioning of the fabric under test.

### 7.2.3 Conclusions

The work presented in this thesis has shown strengths and weakness of the knitted conductive textiles under investigation. The fabric electrical response followed the movement/strain performed. However, all knit patterns lost their capability to accurately follow the movement performed after an extended use. For instance, samples tested for the first time in the tensile machine started being affected by the relaxation of the fabrics after hundreds of stretch-recovery cycles and after a few tens during the repeatability test. This phenomenon related to the slippage and/or permanent extension of the fibres (depending on their viscoelasticity) was irreversible in the short period and the limited rest period between tests was not sufficient to guarantee an adequate recovery. Similarly, for samples integrated into leggings, the textile-based performance worsened with cycles and, due to the presence of the supporting garment, this occurred in a smaller number of knee flexion-extension cycles. In both cases, the outcome was that additional noise components were introduced to the harmonics spectrum of the fabric resistance signal, with the noise overtaking the signal of interest over time and difficult extraction of useful features from the fabric resistance.

Moreover, the encountered non-linearities were due to the contact resistance affecting the overall fabric resistance during elongation in the course direction. The choice of evaluating the electrical properties of knitted textiles along the course direction stemmed from their limited resistance variation (kiloohms instead of megaohms measured along the wale direction) leading to the possibility in applying them in a portable application and avoiding resistance noise issues. On the contrary, an ideal working range is where the length-related resistance predominates over the contact resistance and thus the resistance variation mainly depends on the elongation of the conductive yarn during test.
Recommendations for improving the textile-based performance are reported in the following section.

## 7.3 Recommendations for future work

To increase knowledge and applicability of knitted conductive textiles as fabric strain transducer for wearable applications, the areas of research described in the following subsections require further investigation.

### 7.3.1 Improving the loose fabrics issue

The lower performance of the investigated samples as strain sensors after an extended use is due to the relaxation of the fabric during cyclic loading. An improvement of this problem requires further studies on both sensing fabrics and supporting garments, with particular attention to:

- The materials employed in terms of composition, treatment and use. By properly selecting suitable non-conductive fibres, by employing particular fibre superficial treatments or by embedding the fibres in a more elastic support it might be possible to control the fabric's

stretch-recovery behaviour, bringing down its irreversibility to acceptable values.

- The way the fabrics are integrated in the supporting garment. By testing different sewing strategy, by embedding the fabric inside the garment, or by choosing the optimum specimen length for the particular application it might be possible to considerably reduce the loosening effect.

### 7.3.2 Modelling the knitted conductive sample under cyclic deformation

Tests conducted so far have outlined the electrical behaviour of some knitted conductive samples. Many electrical properties have been highlighted and the knitting fabric parameters variation has been carried out through an analysis by microscope. What is desirable and challenging is modelling the behaviour of the textiles at rest and under strain. The outcome will be useful during the design and manufacturing process to optimise the final product. By determining the forces acting on a loop and the change of knitting fabric parameters during cyclic loading, a clearer understanding of the electro-mechanical behaviour of the knitted conductive samples is achievable. In particular through a model it will be possible to compare different stitch patterns, analyse the extent to which the contact and length-related resistances contribute to the overall resistance and investigate the causes of lack of accuracy after an extended use.

For instance, starting from the Peirce's loop model (Peirce 1937), the geometry of conductive loops can be depicted as head and sinker loops which are circular and the leg part of the loop which is a straight line (Figure 7.1).

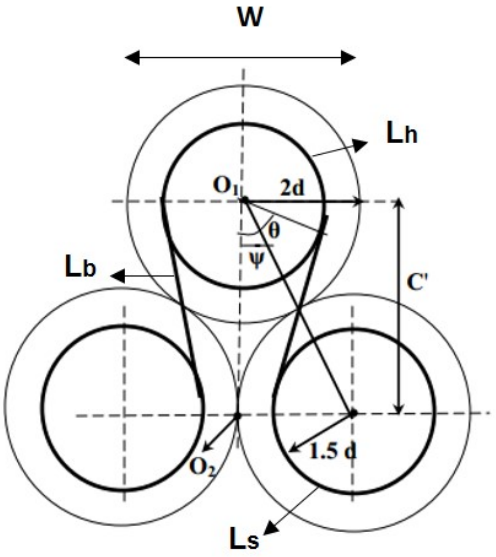


Figure 7.1: Loop geometry according to the Peirce's model (modified from Atalay O 2014)

From Figure 7.1, the course spacing is:

$$C = \sqrt{(4d)^2 - (2d)^2} = 3.46d \tag{7.1}$$

The wale spacing is:

$$W = 4d \tag{7.2}$$

The head and sinker loop lengths are:

$$L_{\mathrm{h}} = L_{\mathrm{s}} = 1.5d\pi \tag{7.3}$$

and the length of the leg part is:

$$L_{\mathrm{b}} = \sqrt{(C)^2 + (\frac{W}{2} - d)^2} = 3.60d, \tag{7.4}$$

with $d$ being the diameter of the yarn. Depending on the values of loop width and loop height, the knitted structure can be normal (for $W = 4d$ and $C = 3.46d$) or compact (for $W < 4d$ and $C < 3.46d$).

According to the Peirce's loop model, the compact knitted structure may be modelled as adjacent loops in contact with each other. For instance, by considering for simplicity one knitted course with all conductive loops being in contact by their head and their sinker loops (Figure 7.2), the electrical behaviour can be represented by a basic model based on an equivalent resistive circuit network (Figure 7.3).

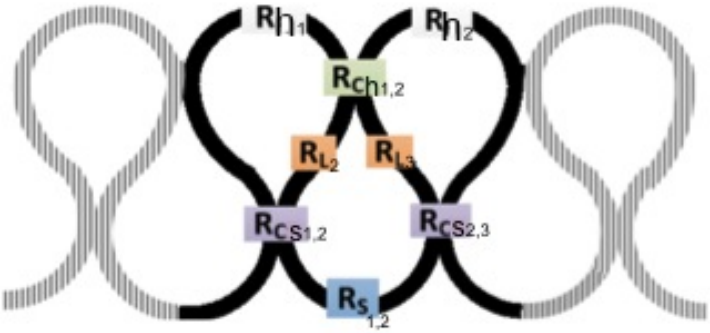


Figure 7.2: Simplified electrical diagram of one knitted conductive course (modified from Atalay O 2014)

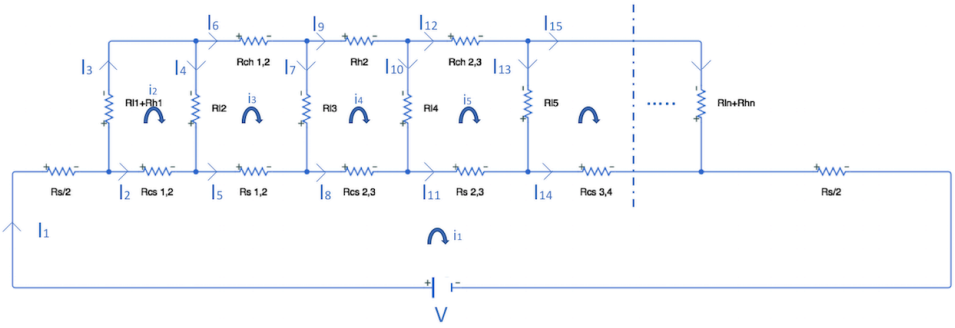


Figure 7.3: Equivalent resistive circuit network of one knitted conductive course

The electrical parameters of the conductive course in Figure 7.2 are:

- $R_h$, which is the resistance of the loop head;
- $R_l$, which is the resistance of the loop leg;

- $R_s$ is the resistance of the sinker loop.

Also, each conductive loop exhibits two contact resistances:

- $R_{ch}$, which is due to the touching of adjacent head loops between each other;
- $R_{cs}$, which is due to the pressing of sinker loops together.

When considering $n$ courses (or wales), the associated resistive network model of Figure 7.3 becomes more complex as consists of $n$ length-related and contact resistances.
The sensing mechanism of the knitted sensor shown in Figure 7.3 operates on the basis of changing the equivalent electrical resistance of the structure in response to applied tensile strain. The equivalent electrical resistance of the strain sensing fabric is calculated according to Ohm's law:

$$R_{\text{eq}} = \frac{V}{I_1} \tag{7.5}$$

Where:

- $V$ is the applied voltage across the fabric;
- $I_1$ is the current passing through the fabric and calculated by applying the Kirchhoff's current law (i.e. the algebraic sum of currents in a network of conductors meeting at a point is zero) and the voltage law (i.e. the directed sum of the electrical voltage around any closed network is zero).

When the sensing fabric undergoes tensile loading (i.e. under dynamic conditions), the equivalent electrical resistance changes in response to the applied tensile strain. In particular, so does the length of the loop segments and the contact resistance between touching points of adjacent loops and

sinker loops. Thus, changes of the loop geometry need to be taken into account, whereas the length of the conductive yarn within the elastic limits can be accepted as constant during the calculations. For instance, when the conductive loops are subjected, for simplicity, to unidirectional strain ($\epsilon$) along the course-wise direction, the length of the loop segments can be determined according to Peirce's loop model with the following equations:

$$L_{\mathrm{H}} = L_{\mathrm{S}} = L_0(1+\epsilon) \tag{7.6}$$

$$L_{\mathrm{B}} = \frac{l - 2L_{\mathrm{o}}(1+\epsilon)}{2} \tag{7.7}$$

Where:

- $L_H$ is the length of the head loop under tensile strain;
- $L_B$ is the length of the leg loop under tensile strain;
- $L_S$ is the length of the sinker loop under tensile strain;
- $l$ is the length of the conductive loop under tensile strain.

The electrical resistance values of head, sink and leg loops are respectively:

$$R_{\mathrm{LH}} = R_{\mathrm{LS}} = \rho L_0(1+\epsilon) \tag{7.8}$$

$$R_{\mathrm{LB}} = \rho\frac{l - 2L_{\mathrm{o}}(1+\epsilon)}{2} \tag{7.9}$$

with $\rho$ being the electrical resistance value of unit length of conductive yarn.

The contact resistances vary due the changes of the number of contact points and of the contact force acting on the two overlapped yarns during the deformation process (according to section 2.7.2). Hence, in place of Equation 2.2, a new modified equation can be predicted for $R_c$ at a given

strain:

$$R_{\mathrm{ct}} = \frac{\rho_{\mathrm{c}}}{2}\sqrt{\frac{\pi H}{n_{\mathrm{t}} P_{\mathrm{t}}}} \tag{7.10}$$

Where:

- $R_{ct}$ is the contact resistance at a given strain;
- $\rho_{\mathrm{c}}$ is the *contact* electrical resistivity described in section 2.7.2;
- $n_{\mathrm{t}} = n(\epsilon)$ is the ratio to the initial contact area (before extension) at a given strain;
- $P_{\mathrm{t}} = P(\epsilon)$ is the ratio to the initial contact pressure (before extension) at a given strain.

The relationship between the pressure and strain can be obtained experimentally from the load-strain curve of the proposed sensor whereas the contact areas depend on the sensor design.

Limitations of the application of the Peirce's loop model are the assumptions of circular cross-section, uniform structure along the longitudinal direction, perfect flexibility and incompressibility. Moreover, we have assumed an uniform strain in the whole sample and in any direction. These are all unrealistic hypotheses so further investigation for modelling the fabric under real conditions is needed.

The way of implementing a realistic model requires future work which may consist of:

- Develop a mechanical model which relates the past fabric motion or strain history to some mechanical parameters of particular interest such as number of contact points between yarns, pressure at the contact point, average yarn length.
- Develop a resistive-network-based electrical model expanding the model introduced in this work.

- Link mechanical and electrical models by expressing the dependence of the electrical parameters (length-related and contact related resistances) on mechanical parameters and environmental conditions.
- Implement the electro-mechanical model in a suitable modelling and simulation software.
- Compare the simulated results with the experimental results shown in this thesis or obtained from new tests made necessary by the particular model structure.
- Refine the model until a good agreement between simulated and experimental results is obtained.

### 7.3.3 Performing additional tests under new testing conditions and for different applications

The samples described in this thesis were all tested at specific tests conditions. For the tests performed on the tensile machine, the specimens were manufactured 250 mm x 50 mm (height x width) with a conductive area of 150 mm x 50 mm and tested with a distance of 10 cm between the clamps. For tests performed on a partecipant, samples of the same dimensions were sewn on leggings with two different percentages of elastane.
However, to provide additional information about the fabric sensing performances and show the importance of some design parameters, more experiments with different test parameters and conditions would be useful. Additional testing that could be carried out are:

- Test samples after washing cycles to establish whether stability, repeatability and the discussed sensing properties are maintained or

not. The outcome of this investigation is important to assess whether fabrics integrated into a garment are reliable over time.

- Manufacture samples with reduced dimensions to be integrated in the supporting garments in order to guarantee a more closely fit to the area of investigation and reduce the area subject to strain.

- Use several types of supporting garments with different compositions. This may involve more human partecipants to evaluate the effect of morphological differences (such as gender, height, weight, knee or joint dimensions) over the sensor performances. The outcome of this study may be useful for refining the designing or manufacturing process.

- Repeat the measurements for a different joint with one degree of freedom, e.g. the elbow. Similarly to the knee flexion-extension, the elbow can perform the same movements. Thus, the fabric resistance variation can be measured according to the stretching-recovery of the conductive knitted fabric. Specimens with ad-hoc dimensions can be manufactured to make the measurement accurate.

### 7.3.4 Making the applications of the sensing fabrics portable

The investigation of the electrical properties of knitted conductive samples under cyclic deformation was the first step for developing understanding about their feasibility as wearable motion sensors. Two acquisition systems were employed for measuring the knee flexion-extension and recording the corresponding fabric resistance variation:

1. A camera and RGB markers;

2. The HUMAC dynamometer for repetitive knee movements.

Both systems used:

- A power supply;
- A four-wire resistance measurement;
- A manufactured circuit working as a constant current generator;
- A Data Acquisition System (NI-USB 6003);
- Matlab codes to synchronise the knee angle measured with the two systems with the fabric resistance variation.

A new challenge is to use the conductive samples in a portable application to use, for instance, in healthcare. A portable solution can be achieved by using a Lilypad board embedded in the leggings (the power supply will be replaced by a battery) to collect any measurement of interest from the knitted conductive textile, i.e. fabric resistance and acceleration (by adding the Lilypad accelerometer ADXL335). Data could then be sent via Bluetooth to a pc with the built-in model that recognises the knee angle from the recorded fabric resistance.

# Bibliography


Allard, P., I.A.F. Stokes, and J.P. Blanchi (1995). *Three-dimensional Analysis of Human Movement*. Human Kinetics. ISBN: 9780873226233.

Aminian, K. et al. (2002). "Spatio-temporal parameters of gait measured by an ambulatory system using miniature gyroscopes." In: *Journal of Biomechanics* 35.5, pp. 689 –699. DOI: 10.1016/S0021-9290(02)00008-8.

Atalay, O (2014). "Development and investigation of weft knitted strain sensor." PhD thesis. The University of Manchester. URL: https://www.escholar.manchester.ac.uk/uk-ac-man-scw:231797.

Atalay, Ozgur et al. (2017). "Comparative study of the weft-knitted strain sensors." In: *Journal of Industrial Textiles* 46.5, pp. 1212–1240. DOI: 10.1177/1528083715619948.

Atalay O, Kennon WR (2014). "Knitted Strain Sensors: Impact of Design Parameters on Sensing Properties." In: *Sensors* 14.3, pp. 4712–4730. DOI: 10.3390/s140304712.

Atallah, Louis et al. (2010). "Sensor Placement for Activity Detection Using Wearable Accelerometers." In: *2010 International Conference on Body Sensor Networks*, pp. 24–29.

Bamberg, S et al (2008). "Gait analysis using a shoe-integrated wireless sensor system." In: *IEEE Transactions on Information Technology in*

*Biomedicine,July 2008*. Vol. 12. 4, pp. 413 –423. DOI: 10.1109/TITB.2007.899493.

Bourke, A.K., J.V. OBrien, and G.M. Lyons (2007). "Evaluation of a threshold-based tri-axial accelerometer fall detection algorithm." In: *Gait Posture* 26.2, pp. 194 –199. DOI: 10.1016/j.gaitpost.2006.09.012.

Bull, Anthony M.J and Alison H McGregor (2000). "Measuring spinal motion in rowers: the use of an electromagnetic device." In: *Clinical Biomechanics* 15.10, pp. 772 –776. DOI: 10.1016/S0268-0033(00)00043-7.

Cappozzo, Aurelio et al. (2005). "Human movement analysis using stereophotogrammetry: Part 1: theoretical background." In: *Gait Posture* 21.2, pp. 186 –196. DOI: 10.1016/j.gaitpost.2004.01.010.

Carnaby, GA and N Pan (1989). "Theory of the compression hysteresis of fibrous assemblies." In: *Textile Research Journal* 59.5, pp. 275–284.

Castano, Lina M and Alison B Flatau (2014). "Smart fabric sensors and e-textile technologies: a review." In: *Smart Materials and Structures* 23.5, p. 053001.

Chen, X. (2009). *Modelling and Predicting Textile Behaviour*. Woodhead Publishing Series in Textiles. Elsevier Science. ISBN: 9781845697211.

Chiari, Lorenzo et al. (2005). "Human movement analysis using stereophotogrammetry: Part 2: Instrumental errors." In: *Gait Posture* 21.2, pp. 197 –211. DOI: 10.1016/j.gaitpost.2004.04.004.

Cho, G. et al. (2011). "Performance Evaluation of Textile-Based Electrodes and Motion Sensors for Smart Clothing." In: *IEEE Sensors Journal* 11.12, pp. 3183–3193. DOI: 10.1109/JSEN.2011.2167508.

Cuden, A, A Hladnik, and F Sluga (2013). "Loop length of plain single weft knitted structure with elastane." In: *J. Eng. Fibers Fabr* 8.2, pp. 110–120.

De Focatiis, Davide S. A., D Hull, and A Sanchez-Valencia (2012). "Roles of prestrain and hysteresis on piezoresistance in conductive elastomers for strain sensor applications." In: *Plastics, Rubber and Composites* 41.7, pp. 301–309. DOI: 10.1179/1743289812Y.0000000022.

Ehrmann, A et al. (2014). "Suitability of knitted fabrics as elongation sensors subject to structure, stitch dimension and elongation direction." In: *Textile Research Journal* 84.18, pp. 2006–2012. DOI: 10.1177/0040517514548812.

Finley, Margaret A. and Raymond Y. Lee (2003). "Effect of sitting posture on 3-dimensional scapular kinematics measured by skin-mounted electromagnetic tracking sensors." In: *Archives of Physical Medicine and Rehabilitation* 84.4, pp. 563 –568. DOI: 10.1053/apmr.2003.50087.

Fraden, J (2010). *Handbook of Modern Sensors - Physics, Designs, and Applications*. Springer-Verlag New York. ISBN: 978-1-4419-6466-3. DOI: 10.1007/978-1-4419-6466-3.

Goel, Vishesh et al. (2017). "Specific Color Detection in Images using RGB Modelling in MATLAB." In: *International Journal of Computer Applications* 161.8, pp. 38–42. DOI: 10.5120/ijca2017913254.

Graham, D. et al. (2004). "Magnetoresistive-based biosensors and biochips." In: *Trends in Biotechnology* 22.9, pp. 455–462. DOI: 10.1016/j.tibtech.2004.06.006.

Greene, B et al (2010). "Adaptive estimation of temporal gait parameters using body-worn gyroscopes." In: *Annual International Conference of the IEEE Engineering in Medicine and Biology Society, EMBC 2010, 31 Aug-4 Sept 2010*. DOI: 10.1109/IEMBS.2010.5626400.

Grosberg, P and PA Smith (1966). "The strength of slivers of relatively low twist." In: *Journal Textile Institute* 57, pp. 15–23.

Guo, Li, Lena Berglin, and Heikki Mattila (2010). "Textile strain sensors characterization - Sensitivity, linearity, stability adn hysteresis." In: *The Nordic Textile Journal* 2, pp. 51–63.

Holm, R (1967). *Electric Contacts - Theory and Application*. 4th. Springer-Verlag. DOI: 10.1007/978-3-662-06688-1.

Isaia, Cristina, Donal McNally, and David T. Branson (2017). "Textile-based wearable sensors for human motion capture." In: *XXVI Congress of the International Society of Biomechanics, ISB 2017, Brisbane, Australia, July 23-27, 2017*.

Isaia, Cristina et al. (2018). "Effect of mechanical preconditioning on the electrical properties of knitted conductive textiles during cyclic loading." In: *Textile Research Journal* 0.0, p. 0040517517748496. DOI: 10.1177/0040517517748496.

Kaur, Gagan et al. (2015). "Electrically conductive polymers and composites for biomedical applications." In: *RSC Adv.* 5 (47), pp. 37553–37567. DOI: 10.1039/C5RA01851J.

Kavanagh, Justin J. and Hylton B. Menz (2008). "Accelerometry: A technique for quantifying movement patterns during walking." In: *Gait Posture* 28.1, pp. 1 –15. DOI: 10.1016/j.gaitpost.2007.10.010.

Kim, KJ et al. (2009). "A novel piezoelectric PVDF film-based physiological sensing belt for a complementary respiration and heartbeat monitoring system." In: *Integr. Ferroelectr.* 107, pp. 53–68.

Lee, K. C. (1999). "Dependence of contact resistance on current for ohmic contacts to quantized Hall resistors." In: *IEEE Transactions on Instrumentation and Measurement* 48.2, pp. 319–323. DOI: 10.1109/19.769592.

Leeder, J.D and R.L. Shishoo (1977). "Studies of wrinkling properties of wool fabrics. Part VI: Effect of variable recovery conditions." In: *Textile Research Journal* 47.8, pp. 542–545.

Legnani, Giovanni et al. (2000). "A model of an electro-goniometer and its calibration for biomechanical applications." In: *Medical Engineering Physics* 22.10, pp. 711 –722. DOI: 10.1016/S1350-4533(01)00009-1.

Li, Li et al. (2010). "A Resistive Network Model for Conductive Knitting Stitches." In: *Textile Research Journal* 80.10, pp. 935–947. DOI: 10.1177/0040517509349789.

Li, Li et al. (2012). "Electromechanical analysis of length-related resistance and contact resistance of conductive knitted fabrics." In: *Textile Research Journal* 82.20, pp. 2062–2070. DOI: 10.1177/0040517512447519.

Lu, Tung-Wu and Chu-Fen Chang (2012). "Biomechanics of human movement and its clinical applications." In: *The Kaohsiung Journal of Medical Sciences* 28.2, Supplement, S13 –S25. DOI: 10.1016/j.kjms.2011.08.004.

Luinge, H. J. and P. H. Veltink (2005). "Measuring orientation of human body segments using miniature gyroscopes and accelerometers." In: *Medical and Biological Engineering and Computing* 43.2, pp. 273–282. DOI: 10.1007/BF02345966.

Mahmoudi, M. R. and W. Oxenham (2002). "A new electro-mechanical method for measuring yarn thickness." In: *Autex Research Journal* Vol. 2, no. 1, pp. 28–37.

Mattmann, Corinne, Frank Clemens, and Gerhard Trster (2008). "Sensor for Measuring Strain in Textile." In: *Sensors* 8.6, pp. 3719–3732. DOI: 10.3390/s8063719.

Mayagoitia, Ruth E., Anand V. Nene, and Peter H. Veltink (2002). "Accelerometer and rate gyroscope measurement of kinematics: an inex-

pensive alternative to optical motion analysis systems." In: *Journal of Biomechanics* 35.4, pp. 537 –542. DOI: 10.1016/S0021-9290(01)00231-7.

Munro, Bridget J. et al. (2008). "The intelligent knee sleeve: A wearable biofeedback device." In: *Sensors and Actuators B: Chemical* 131.2, pp. 541 –547. DOI: 10.1016/j.snb.2007.12.041.

Paradiso, Rita et al. (2005). "WEALTHY, a Wearable Health-Care System: New Frontier on Etextile." In: *Journal of Telecommunications and Information Technology* 4, pp. 105–113.

Peirce, F (1937). "The geometry of cloth structure." In: *J Text Inst* 28, pp. 45–96.

Picard, Dominique (1985). "Testing and estimating change-points in time series." In: *Advances in Applied Probability* 17.4, pp. 841–867. DOI: 10.1017/S0001867800015433.

Sarker, E. (2016). "Basic weft Knitting Loops." In: URL: https://textilestudycenter.com/basic-weft-knitting-loops/.

Sawhney, Amit et al. (2006). "Piezoresistive Sensors on Textiles by Inkjet Printing and Electroless Plating." In: *MRS Proceedings* 920. DOI: 10.1557/PROC-0920-S05-04.

Scilingo, Enzo Pasquale et al. (2005). "Performance evaluation of sensing fabrics for monitoring physiological and biomechanical variables." In: *IEEE Transactions on Information Technology in Biomedicine* 9.3, pp. 345–352. DOI: 10.1109/TITB.2005.854506.

Seyedin, Shayan et al. (2015). "Knitted Strain Sensor Textiles of Highly Conductive All-Polymeric Fibers." In: *ACS Applied Materials & Interfaces* 7.38, pp. 21150–21158. DOI: 10.1021/acsami.5b04892.

Shedd, JC and MD Hershey (1913). "The history of Ohm's Law." In: *The Popular Science Monthly* Bonnier Corporation, pp. 599–614.

Sherburn, Martin (2007). *Geometric and Mechanical Modelling of Textiles*. PhD Thesis, University of Nottingham. URL: http://eprints.nottingham.ac.uk/10303/.

Shyr, Tien-Wei et al. (2014). "A Textile-Based Wearable Sensing Device Designed for Monitoring the Flexion Angle of Elbow and Knee Movements." In: *Sensors* 14.3, pp. 4050–4059. DOI: 10.3390/s140304050.

Sinclair, R. (2014). *Textiles and Fashion: Materials, Design and Technology*. Woodhead Publishing Series in Textiles. Elsevier Science, pp. 712–717. ISBN: 9780857095619.

Skorobogatiy, M and H Qu (2015). *Electronic Textiles: Smart Fabrics and Wearable Technology*. Woodhead Publishing Series in Textiles. Elsevier Science, pp. 21–53. ISBN: 9780081002230.

Stoppa, Matteo and Alessandro Chiolerio (2014). "Wearable Electronics and Smart Textiles: A Critical Review." In: *Sensors* 14.7, pp. 11957–11992. DOI: 10.3390/s140711957.

Sun, Yu Chai, Zhong Hao Cheng, and Yan Mei Zhang (2011). "Knitting Process Analysis of Stainless-Steel Yarn." In: *Advanced Textile Materials*. Vol. 332. Trans Tech Publications, pp. 1447–1450. DOI: 10.4028/www.scientific.net/AMR.332-334.1447.

Sutherland, David H (2001). "The evolution of clinical gait analysis part l: kinesiological EMG." In: *Gait Posture* 14.1, pp. 61 –70. ISSN: 0966-6362. DOI: 10.1016/S0966-6362(01)00100-X.

Takeda, Ryo et al. (2009a). "Gait analysis using gravitational acceleration measured by wearable sensors." In: *Journal of Biomechanics* 42.3, pp. 223 –233. DOI: 10.1016/j.jbiomech.2008.10.027.

Takeda, Ryo et al. (2009b). "Gait posture estimation using wearable acceleration and gyro sensors." In: *Journal of Biomechanics* 42.15, pp. 2486 –2494. DOI: 10.1016/j.jbiomech.2009.07.016.

Tao, S et al (2012). "Gait Analysis Using Wearable Sensors." In: *Sensors (Basel, Switzerland)* 12.2, pp. 2255–2283. DOI: 10.3390/s120202255.

Taya, M., W.J. Kim, and K. Ono (1998). "Piezoresistivity of a short fiber/elastomer matrix composite." In: *Mechanics of Materials* 28.1, pp. 53 –59. DOI: 10.1016/S0167-6636(97)00064-1.

Tunel, Orkun, Kerem Altun, and Billur Barshan (2009). "Classifying Human Leg Motions with Uniaxial Piezoelectric Gyroscopes." In: *Sensors* 9.11, pp. 8508–8546. DOI: 10.3390/s91108508.

Wijesiriwardana, R., T. Dias, and S. Mukhopadhyay (2003). "Resistive fibre-meshed transducers." In: *Seventh IEEE International Symposium on Wearable Computers, 2003. Proceedings.* Pp. 200–209. DOI: 10.1109/ISWC.2003.1241412.

Wong, Wai Yin, Man Sang Wong, and Kam Ho Lo (2007). "Clinical Applications of Sensors for Human Posture and Movement Analysis: A Review." In: *Prosthetics and Orthotics International* 31.1, pp. 62–75. DOI: 10.1080/03093640600983949.

Yamada, T et al. (2011). "A stretchable carbon nanotube strain sensor for human-motion detection." In: *Nat Nanotechnol* 6.5, pp. 296–301. DOI: 10.1038/nnano.2011.36.

Yang, Che-Chang et al. (2011). "Real-Time Gait Cycle Parameter Recognition Using a Wearable Accelerometry System." In: *Sensors* 11.8, pp. 7314–7326. DOI: 10.3390/s110807314.

Yang C-C, Hsu Y-L (2010). "A Review of Accelerometry-Based Wearable Motion Detectors for Physical Activity Monitoring." In: *Sensors (Basel, Switzerland)* 10.8, pp. 7772–7788. DOI: 10.3390/s100807772.

Yin, Jun, Ccile DHaese, and Bernard Nysten (2015). "Surface electrical properties of stainless steel fibres: An AFM-based study." In: *Applied*

*Surface Science* 330.Supplement C, pp. 65 –73. DOI: 10.1016/j.apsusc.2014.12.188.

Zhang, Hui et al. (2005). "Electro-Mechanical Properties of Knitted Fabric Made From Conductive Multi-Filament Yarn Under Unidirectional Extension." In: *Textile Research Journal* 75.8, pp. 598–606. DOI: 10.1177/0040517505056870.

Zheng, H., N. D. Black, and N. D. Harris (2005). "Position-sensing technologies for movement analysis in stroke rehabilitation." In: *Medical and Biological Engineering and Computing* 43.4, pp. 413–420. DOI: 10.1007/BF02344720.

# Appendix I: Test sessions

Table 7.1: Preconditioning and repeatability tests in the Instron tensile machine

| Test | Sample | Session | Current | Elongation | Elongation rate |
|---|---|---|---|---|---|
| 1 | Single Jersey | Preconditioning | 1 mA | 16 mm | 9.6 mm/s |
| 2 | Single Jersey | Repeatability | 1 mA | 16 mm | 9.6 mm/s |
| 3 | Single Jersey | Preconditioning | 3 mA | 16 mm | 9.6 mm/s |
| 4 | Single Jersey | Repeatability | 3 mA | 16 mm | 9.6 mm/s |
| 5 | Single Jersey | Preconditioning | 6 mA | 16 mm | 9.6 mm/s |
| 6 | Single Jersey | Repeatability | 6 mA | 16 mm | 9.6 mm/s |
| 7 | SP27 | Preconditioning | 1 mA | 16 mm | 9.6 mm/s |
| 8 | SP27 | Repeatability | 1 mA | 16 mm | 9.6 mm/s |
| 9 | SP27 | Preconditioning | 3 mA | 16 mm | 9.6 mm/s |
| 10 | SP27 | Repeatability | 3 mA | 16 mm | 9.6 mm/s |
| 11 | SP27 | Preconditioning | 6 mA | 16 mm | 9.6 mm/s |
| 12 | SP27 | Repeatability | 6 mA | 16 mm | 9.6 mm/s |
| 13 | SP29 | Preconditioning | 1 mA | 16 mm | 9.6 mm/s |
| 14 | SP29 | Repeatability | 1 mA | 16 mm | 9.6 mm/s |
| 15 | SP29 | Preconditioning | 3 mA | 16 mm | 9.6 mm/s |
| 16 | SP29 | Repeatability | 3 mA | 16 mm | 9.6 mm/s |
| 17 | SP29 | Preconditioning | 6 mA | 16 mm | 9.6 mm/s |

| | | | | | |
|---|---|---|---|---|---|
| 18 | SP29 | Repeatability | 6 mA | 16 mm | 9.6 mm/s |
| 19 | SP31 | Preconditioning | 1 mA | 16 mm | 9.6 mm/s |
| 20 | SP31 | Repeatability | 1 mA | 16 mm | 9.6 mm/s |
| 21 | SP31 | Preconditioning | 3 mA | 16 mm | 9.6 mm/s |
| 22 | SP31 | Repeatability | 3 mA | 16 mm | 9.6 mm/s |
| 23 | SP31 | Preconditioning | 6 mA | 16 mm | 9.6 mm/s |
| 24 | SP31 | Repeatability | 6 mA | 16 mm | 9.6 mm/s |
| 25 | Single Jersey | Preconditioning | 1 mA | 16 mm | 12 mm/s |
| 26 | Single Jersey | Repeatability | 1 mA | 16 mm | 12 mm/s |
| 27 | Single Jersey | Preconditioning | 3 mA | 16 mm | 12 mm/s |
| 28 | Single Jersey | Repeatability | 3 mA | 16 mm | 12 mm/s |
| 29 | Single Jersey | Preconditioning | 6 mA | 16 mm | 12 mm/s |
| 30 | Single Jersey | Repeatability | 6 mA | 16 mm | 12 mm/s |
| 31 | SP27 | Preconditioning | 1 mA | 16 mm | 12 mm/s |
| 32 | SP27 | Repeatability | 1 mA | 16 mm | 12 mm/s |
| 33 | SP27 | Preconditioning | 3 mA | 16 mm | 12 mm/s |
| 34 | SP27 | Repeatability | 3 mA | 16 mm | 12 mm/s |
| 35 | SP27 | Preconditioning | 6 mA | 16 mm | 12 mm/s |
| 36 | SP27 | Repeatability | 6 mA | 16 mm | 12 mm/s |
| 37 | SP29 | Preconditioning | 1 mA | 16 mm | 12 mm/s |
| 38 | SP29 | Repeatability | 1 mA | 16 mm | 12 mm/s |
| 39 | SP29 | Preconditioning | 3 mA | 16 mm | 12 mm/s |
| 40 | SP29 | Repeatability | 3 mA | 16 mm | 12 mm/s |
| 41 | SP29 | Preconditioning | 6 mA | 16 mm | 12 mm/s |
| 42 | SP29 | Repeatability | 6 mA | 16 mm | 12 mm/s |
| 43 | SP31 | Preconditioning | 1 mA | 16 mm | 12 mm/s |
| 44 | SP31 | Repeatability | 1 mA | 16 mm | 12 mm/s |
| 45 | SP31 | Preconditioning | 3 mA | 16 mm | 12 mm/s |

| | | | | | |
|---|---|---|---|---|---|
| 46 | SP31 | Repeatability | 3 mA | 16 mm | 12 mm/s |
| 47 | SP31 | Preconditioning | 6 mA | 16 mm | 12 mm/s |
| 48 | SP31 | Repeatability | 6 mA | 16 mm | 12 mm/s |

# Appendix II:

# Matlab code for fabric analysis

**FILTERING OF THE RAW DATA**

figure;

smoothR = sgolayfilt (R, 3, 151); Smooth the signal by applying a cubic Savitzky-Golay filter to data frames of length 151

plot (Time, R, Time, smoothR); Plot in the same graph the original and filtered signals

xlabel ('Time (s)');

ylabel ('Resistance (Ohm)');

legend ('Original signal', 'Filtered signal');

hold on

axes('position',[.65 .175 .25 .25]); Create a new pair of axes (bottom-right with width/height of 0.25) inside current figure

indexOfInterest=(Time < 100 ) & (Time > 0); Plot the interval of interest (the first 100 seconds) of the filtered resistance

plot(Time (indexOfInterest), smoothR (indexOfInterest));

**PEAK ANALYSIS - *Calculation of the local minima***

smoothR inverted = - smoothR; Find peaks on an inverted version of the filtered signal

[$MINValues, MINPos$] = findpeaks (smoothR inverted, 'MinPeakDistance', 3333); In every cycle there are one minimum and one maximum, whose minimum distance is the MinPeakDistance calculated as:
(1 / Test frequency) * Sampling frequency.
For example: (1 / 0.3) * 1000 = 3333
Minimi = MIN Values * (-1);
Time Min = Time (MIN Pos);

***Calculation of the maximum values***

[$MAXValues, MAXPos$] = findpeaks (smoothR, 'MinPeakDistance', 3333);
Time Max = Time (MAX Pos);

***Filtering maximum and minimum values***

MAX filt = sgolayfilt (MAX Values, 3, 21); Smooth the signal by applying a cubic Savitzky-Golay filter to data frames of length 21
MIN filt = sgolayfilt (Minimi, 3, 21);
plot (Time Max, MAX Values, 'y', Time Max, MAX filt, 'b', Time Min ,Minimi, 'g', Time Min, MIN filt, 'r');
xlabel ('Time (s)');
ylabel ('Resistance (Ohm)');
legend ('Maximum', 'Filtered maximum', 'Minimum', 'Filtered Minimum');

**INTERPOLATION OF THE FILTERED VALUES**

MAX filt interp = spline (Time Max, MAX filt, Time);
MIN filt interp = spline (Time Min, MIN filt, Time);
plot (Time Max, MAX Values, 'o', Time, MAX filt interp, Time Min, Minimi, 'o', Time, MIN filt interp);
xlabel ('Time(s)');

ylabel ('Resistance (Ohm)');

legend ('Maximum values', 'Interpolated filtered maximum', 'Minimum values', 'Interpolated filtered minimum');

**EXTRACTION OF FEATURES OF INTEREST - *Peak-to-peak span***

PEAK SPAN filt interp = MAX filt interp - MIN filt interp;

plot (Time, PEAK SPAN filt interp);

xlabel ('Time (s)');

ylabel ('Peak-to-peak span');

***Settling time***

B = PEAK SPAN filt interp;

findchangepts (B, 'Statistic', 'std') The findchangepts function finds where the standard deviation changes the most

xlabel ('Samples');

ylabel ('Span (Ohm)');

C = findchangepts (B, 'Statistic', 'std');

SETTLING TIME = Time(C); Time corresponding to the instant in which the standard deviation changes the most

***Stabilised average resistance and stabilised peak-to-peak span***

R SETTLING TIME = mean (smoothR (C: size (smoothR))); Average resistance calculated from the instant in which the standard deviation changes the most to the end

R Settling span = mean (PEAK SPAN filt interp (C: size (smoothR))); Average peak-to-peak span calculated from the instant in which the standard deviation changes the most to the end

***Number of cycles for electrical stabilisation***

START TIME = Time (findchangepts (R (1: 35000), 'Statistic', 'std'));

CYCLES = (SETTLING TIME - START TIME) / ( 3333 / 1000);

**STUDY OF SENSITIVITY**

$[b, a]$ = butter (2, 0.00005); Calculate the average resistance of the unfiltered fabric resistance with a Butterworth filter of order 2 and normalised cut-off frequency equal to $5 * 10^{-5}$

R avg = filter (b, a, R);

plot(Time, R, 'b', Time, R avg, 'r'); Draw a zoom of the average resistance of the original unfiltered resistance

xlabel ('Time (s)');

ylabel ('Resistance');

hold on

axes ('position', [.65 .175 .25 .25]);

box on

indexOfInterest = (Time < 120) & (Time > 70);

plot (Time (indexOfInterest), R (indexOfInterest), Time (indexOfInterest), R avg (indexOfInterest));

**GAUGE FACTOR**

The gauge factor is calculated as the ratio between the relative change in resistance (represented by the peak-to-peak span with respect to the average resistance, R avg) and the strain value (ratio between the absolute change in the specimen length ($\Delta L = 116 - 100 = 16mm$) and the original length of the specimen in the clamps (100 mm)

S = (PEAK SPAN filt interp ./ R avg) / 0.16;

plot (Time, S);

plot (CYCLES, S SJ, CYCLES, S SP27, CYCLES, S SP29, CYCLES, S SP31); Plot the gauge factor for all samples as a function of cycles

**FABRIC SPECTRAL ANALYSIS - *Spectrogram***

res = 0.01; Specify the resolution in Hz

max freq = 1.55; Maximum frequency in Hz to plot

Ts = Time (2) - Time (1); Calculate the sampling time

fs = 1 / Ts; Calculate the sampling frequency

NR = length (R); Calculate the number of samples

nsc = fs / res; To have 10 windows

nov = floor (nsc / 2); Overlap set to 50%

spectrogram (R, nsc, nov, 0 : res : max freq, fs); Return the spectrogram for R

figure

$[s, f, t]$ = spectrogram (R, nsc, nov, 0 : res: max freq, fs); Returns s, f, t of the spectrogram for R at the cyclical frequencies specified in f

spectrogram (R2, nsc, nov, 0 : res: max freq, fs); Return the spectrogram for R2

figure

$[s2, f2, t2]$= spectrogram (R2, nsc, nov, 0:res : max freq, fs); Return s, f, t of the spectrogram for R2

Fr 1=abs (s (31, : )); Create a matrix with the values of the power density for the 0.3Hz frequency. Such values are taken as the modulus of the values in the 31st position of the s complex matrix

Power Fundamental = Fr 1';

Fr 2 = abs (s (61, : )); Create a matrix with the values of the power density

for the 0.6Hz frequency (61st position)

Power 2nd harmonics = Fr 2';

Fr 3 = abs (s (91, : )); Create a matrix with the values of the power density for the 0.9 Hz frequency (91st position)

Power 3rd harmonics = Fr 3';

Fr 4 = abs (s (121, : )); Create a matrix with the values of the power density for the 1.2Hz frequency (121st position)

Power 4th harmonics = Fr 4';

Fr 5 = abs (s (151, : )); Create a matrix with the values of the power density for the 1.5Hz frequency (151st position)

Power 5th harmonics = Fr 5';

Fr 1 after = abs (s2 (31, : ));

Power Fundamental after = Fr 1 after';

Fr 2 after = abs (s2 (61, : ));

Power 2nd harmonics after = Fr 2 after';

Fr 3 after = abs (s2 (91, : ));

Power 3rd harmonics after = Fr 3 after';

Fr 4 after = abs (s2 (121, : ));

Power 4th harmonics after = Fr 4 after';

Fr 5 after = abs (s2 (151, : ));

Power 5th harmonics after = Fr 5 after';

samplesperperiod = 3333;

cycles = (t * 1000) / samplesperperiod; Define number of cycles

***SNR preconditioning***

Signal = Power Fundamental;

Noise = Power 2nd harmonics + Power 3rd harmonics + Power 4th harmonics + Power 5th harmonics;

SNR = Signal ./ Noise;

SNR dB = 10 * log (SNR);

if find (SNR dB $\leq$ 0) Find the first instant when the noise overtakes the signal during preconditioning

$[indCYCLE]$ = find (SNR dB $\leq$ 0);

CYCLE 0 = cycles (ind CYCLE (1))

else disp ('The noise power does not overtake the signal power during preconditioning test');

end

***SNR repeatability***

Signal after = Power Fundamental after;

Noise after = Power 2nd harmonics after + Power 3rd harmonics after + Power 4th harmonics after + Power 5th harmonics after;

SNR after = Signal after ./ Noise after;

SNR dB after = 10 * log (SNR after);

if find (SNR dB after $\leq$ 0) Find the first instant when the noise overtakes the signal during repeatability

$[indCYCLEafter]$ = find (SNR dB after $\leq$ 0);

CYCLE 0 after = cycles (ind CYCLE after(1))

else disp ('The noise power does not overtake the signal power during repeatability test');

end

plot (cycles, SNR dB, 'b', cycles, SNR dB after, 'r'); Express the SNR in terms of number of cycles

xlabel ('Number of cycles');

ylabel ('SNR (dB)');

legend ('SNR pre', 'SNR after');

figure

plot (t, SNR dB, 'b', t, SNR dB after, 'r'); Express the SNR as a function of time- Pre and after results

xlabel ('Time (s)');

ylabel ('SNR (dB)');

legend ('SNR pre', 'SNR after');

***Harmonics Amplitude***

The resistance variation is expressed in Ohm according to the formula:

A sin ( 2 $\pi * N * fo$) where: N is the harmonic, fo is 0.3 Hz and A is the amplitude expressed in Ohm.

To express the Amplitude A of the harmonic corresponding to a generic bin (whose frequency width is 0.01Hz) in Ohm the sqrt of the modulus of s is taken, multiplied by the bin amplitude (0.01Hz) and by 2 (the power of a sinusoidal signal is $V^2/2$).

Fr 0 = abs (s (1, : )); The values for s are expressed in $Ohm^2/Hz$

P 0 = Fr 0';

A 0 = sqrt (P 0 * 0.01 * 2);

Fr 1 = abs (s (31 , : ));

P 1 = Fr 1' ;

A 1 =sqrt (P 1* 0.01 * 2);

Fr 2 = abs (s (61 , : )); Create a matrix with the values of the power density for the 0.6 Hz frequency (61st position)

P 2 = Fr 2';

A 2 = sqrt (P 2 * 0.01 *2 ); Amplitude for the 0.6 Hz harmonic

Fr 3 = abs (s (91 , : )); Create a matrix with the values of the power density for the 0.9 Hz frequency (91st position)

P 3 = Fr 3';

A 3 = sqrt (P 3 *0.01 *2 ); Amplitude for the 0.9 Hz harmonic

Fr 4 = abs ( s (121 , : )); Create a matrix with the values of the power density for the 1.2 Hz frequency (121st position)

P 4 = Fr 4';

A 4 = sqrt (P 4 * 0.01 *2 ); Amplitude for the 1.2 Hz harmonic

Fr 5 = abs ( s (151, : )); Create a matrix with the values of the power density for the 1.5 Hz frequency (151st position)

P 5 = Fr 5';

A 5 = sqrt (P 5 * 0.01 *2 ); Amplitude for the 1.5 Hz harmonic

plot (t, A 1, 'b', t, A 2, 'o', t, A 3, 'g' , t, A 4, 'r' , t, A 5, 'm');

xlabel ('Time (s) ');

ylabel ('Harmonics Amplitude (Ohm)');

legend ('0.3 Hz', '0.6 Hz', '0.9 Hz' ,'1.2 Hz', '1.5 Hz');

yyaxis right

plot (t, A 0);

ylabel ('DC Amplitude (Ohm)');

figure;

***Harmonics Amplitude for repeatability test***

Fr 0 after = abs (s2 (1, : ));

P 0 after = Fr 0 after';

A 0 after = sqrt (P 0 after * 0.01 * 2);

Fr 1 after = abs ( s2 (31, : )); The values for s are expressed in $Ohm^2/Hz$

P 1 after = Fr 1 after';

A 1 after = sqrt (P 1 after * 0.01 * 2);

Fr 2 after = abs (s2 (61, : )); Create a matrix with the values of the power density for the 0.6Hz frequency (61st position)

P 2 after = Fr 2 after';

A 2 after = sqrt (P 2 after * 0.01 * 2); Amplitude for the 0.6 Hz harmonic

Fr 3 after = abs (s2 (91, : )); Create a matrix with the values of the power density for the 0.9 Hz frequency (91st position)

P 3 after = Fr 3 after';

A 3 after = sqrt (P 3 after * 0.01 * 2); Amplitude for the 0.9 Hz harmonic

Fr 4 after = abs (s2 (121, : )); Create a matrix with the values of the power density for the 1.2Hz frequency (121st position)

P 4 after = Fr 4 after';

A 4 after = sqrt (P 4 after * 0.01 * 2); Amplitude for the 1.2 Hz harmonic

Fr 5 after = abs (s2 (151, : )); Create a matrix with the values of the power density for the 1.5Hz frequency (151st position)

P 5 after = Fr 5 after';

A 5 after = sqrt (P 5 after * 0.01 * 2); Amplitude for the 1.5 Hz harmonic

plot (t, A 1 after, 'b', t, A 2 after, 'o' , t, A 3 after, 'g', t, A 4 after, 'r', t, A 5 after, 'm');

xlabel ('Time (s)');

ylabel ('Harmonics Amplitude (Ohm)');

legend ('0.3 Hz', '0.6 Hz' , '0.9 Hz', '1.2 Hz' , '1.5 Hz');

yyaxis right

plot (t, A 0 after);

ylabel ('DC Amplitude (Ohm)');

# Appendix III: Test results

Table 7.2: Results of preconditioning and repeatability tests described in Table 7.1 of Appendix I (7.3.4)

| Test | Settling time (s) | Cycles | $R_{\text{settling time}}$ ($\Omega$) | $R_{\text{settled span}}$ ($\Omega$) |
|---|---|---|---|---|
| 1 | 131.79 | 34 | 2701 | 834.47 |
| 2 | 60.09 | 14 | 3620 | 1160 |
| 3 | 66.08 | 17 | 1260 | 269 |
| 4 | 56.42 | 14 | 1350 | 262 |
| 5 | 292 | 83 | 557 | 100.14 |
| 6 | 68.02 | 15 | 650 | 105 |
| 7 | 135 | 37 | 1880 | 655 |
| 8 | 96 | 25 | 2160 | 793 |
| 9 | 90.80 | 18 | 1050 | 202 |
| 10 | 53.64 | 12 | 969 | 234 |
| 11 | 216 | 61 | 460 | 109 |
| 12 | 45.56 | 10 | 519 | 113 |
| 13 | 271.91 | 78 | 1100 | 864 |
| 14 | 115 | 30 | 1960 | 640 |
| 15 | 449.15 | 131 | 744 | 200 |
| 16 | 53.37 | 13 | 892 | 200 |
| 17 | 54.36 | 13 | 490 | 89.59 |

| | | | | |
|---|---|---|---|---|
| 18 | 37.81 | 8 | 544 | 107 |
| 19 | 405.14 | 118 | 1780 | 691 |
| 20 | 45.81 | 10 | 2060 | 650 |
| 21 | 289 | 83 | 737 | 183 |
| 22 | 54.6 | 12 | 913 | 230 |
| 23 | 561 | 164 | 401 | 105 |
| 24 | 48.19 | 11 | 497 | 124 |
| 25 | 173.42 | 63 | 2720 | 909 |
| 26 | 45.32 | 13 | 3010 | 1030 |
| 27 | 63.99 | 21 | 1150 | 221 |
| 28 | 42.44 | 12 | 1280 | 241 |
| 29 | 287 | 104 | 555 | 99.71 |
| 30 | 39.94 | 11 | 653 | 111 |
| 31 | 208 | 75 | 1060 | 1060 |
| 32 | 133.69 | 47 | 1765.92 | 592.23 |
| 33 | 485.91 | 179 | 730 | 192 |
| 34 | 41.934 | 13 | 832 | 185 |
| 35 | 726 | 267 | 365 | 115 |
| 36 | 43.75 | 13 | 423 | 100 |
| 37 | 140.56 | 49 | 1212.46 | 965.26 |
| 38 | 49.63 | 15 | 1864.54 | 617.82 |
| 39 | 740 | 273 | 709 | 190 |
| 40 | 78.21 | 26 | 816 | 186 |
| 41 | 410 | 150 | 384 | 77.52 |
| 42 | 48.74 | 13 | 468 | 75.04 |
| 43 | 207 | 74 | 1100 | 1140 |
| 44 | 263 | 95 | 1920 | 736 |
| 45 | 318 | 116 | 778 | 199 |

| | | | | |
|---|---|---|---|---|
| 46 | 155 | 55 | 920 | 228 |
| 47 | 53.77 | 17 | 485 | 106 |
| 48 | 38.09 | 10 | 537 | 118 |

Table 7.3: Signal-to-noise ratio for samples tested according to Table 7.1 of Appendix I (7.3.4)

| Test | Cycles when SNR $\leq 0$ (N) | SNR $_{max}$(dB) | SNR $_{min}$(dB) |
|---|---|---|---|
| 1 | $60 \leq N \leq 75$ | 7,61 | -12,44 |
| 2 | $30 \leq N \leq 45$ | 0,32 | -22,22 |
| 3 | $45 \leq N \leq 60$ | 10,12 | -6,01 |
| 4 | $30 \leq N \leq 45$ | 7,82 | -9,89 |
| 5 | never | 15,14 | 0,53 |
| 6 | $45 \leq N \leq 60$ | 9,51 | -4,6 |
| 7 | $45 \leq N \leq 60$ | 3,2 | -12,23 |
| 8 | $30 \leq N \leq 45$ | 3,86 | -6,74 |
| 9 | $75 \leq N \leq 90$ | 6,65 | -29,56 |
| 10 | $45 \leq N \leq 60$ | 4,98 | -4,89 |
| 11 | $135 \leq N \leq 150$ | 5,4 | -1,37 |
| 12 | $120 \leq N \leq 135$ | 4,7 | -0,76 |
| 13 | never | 16,26 | 1,84 |
| 14 | $75 \leq N \leq 90$ | 2,9 | -19,14 |
| 15 | $120 \leq N \leq 135$ | 16,15 | -5,23 |
| 16 | $30 \leq N \leq 45$ | 1,49 | -10,01 |
| 17 | $30 \leq N \leq 45$ | 3,68 | -7,38 |
| 18 | $15 \leq N \leq 30$ | 3,75 | -11,69 |
| 19 | $210 \leq N \leq 225$ | 11,7 | -1,96 |
| 20 | $60 \leq N \leq 75$ | 2,11 | -24,67 |
| 21 | $60 \leq N \leq 75$ | 11,92 | -8,95 |
| 22 | $15 \leq N \leq 30$ | -1,51 | -10,59 |
| 23 | $285 \leq N \leq 300$ | 20,98 | -0,19 |

| | | | |
|---|---|---|---|
| 24 | $15 \leq N \leq 30$ | 2,76 | -2,45 |
| 25 | 0 | -11,84 | -27,03 |
| 26 | 0 | -7,58 | -29,31 |
| 27 | 0 | -3,45 | -40,29 |
| 28 | 0 | -6,5 | -22,44 |
| 29 | 0 | -9,15 | -26,34 |
| 30 | 0 | -1,8 | -32,32 |
| 31 | 0 | -1,68 | -33,52 |
| 32 | 0 | -6,18 | -29,85 |
| 33 | 0 | -10,24 | -33,82 |
| 34 | 0 | -10,99 | -35,67 |
| 35 | 0 | -0,65 | -39,07 |
| 36 | 0 | -11,42 | -39,21 |
| 37 | 0 | -6,77 | -23,43 |
| 38 | 0 | -8,47 | -47,51 |
| 39 | 0 | -2,75 | -43,06 |
| 40 | 0 | -11,64 | -32,76 |
| 41 | 0 | -8,66 | -34,69 |
| 42 | 0 | -14,61 | -35,56 |
| 43 | 0 | -6,93 | -28,65 |
| 44 | 0 | -13,02 | -28,74 |
| 45 | 0 | -10,07 | -24,19 |
| 46 | 0 | -7,1 | -37,02 |
| 47 | 0 | -10 | -31,17 |
| 48 | 0 | -7,92 | -28,67 |

# Appendix IV: Fabric sensitivity

This section concludes the study of sensitivity (section 4.6) for the remaining cases. Figures 7.4 and 7.5 illustrate the gauge factor variation with cycles for Single Jersey, SP27, SP29 and SP31 at 1 mA and 6 mA during preconditioning (A) and repeatability tests (B). The comparison among GF for all samples at 3 mA has been illustrated in Figure 4.16.

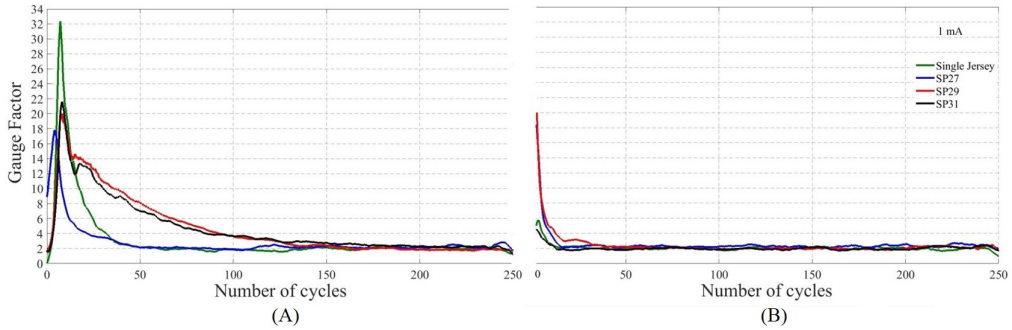


Figure 7.4: Sensitivity variation with cycle at 1 mA for Single Jersey, SP27, SP29 and SP31 during (A) preconditioning and (B) repeatability tests

Figure 7.6 compares the gauge factor for Single Jersey, SP27 and SP31 at 1 mA, 3 mA and 6 mA. The SP29 sample has been discussed in Figure 4.17.

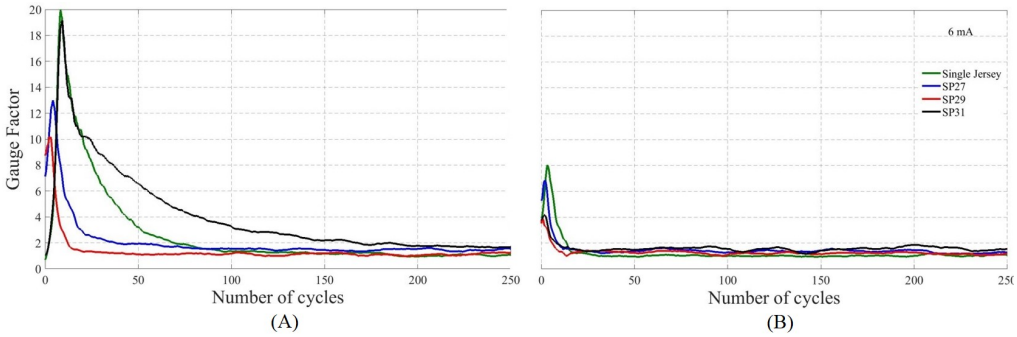


Figure 7.5: Sensitivity variation with cycle at 6 mA for Single Jersey, SP27, SP29 and SP31 during (A) preconditioning and (B) repeatability tests

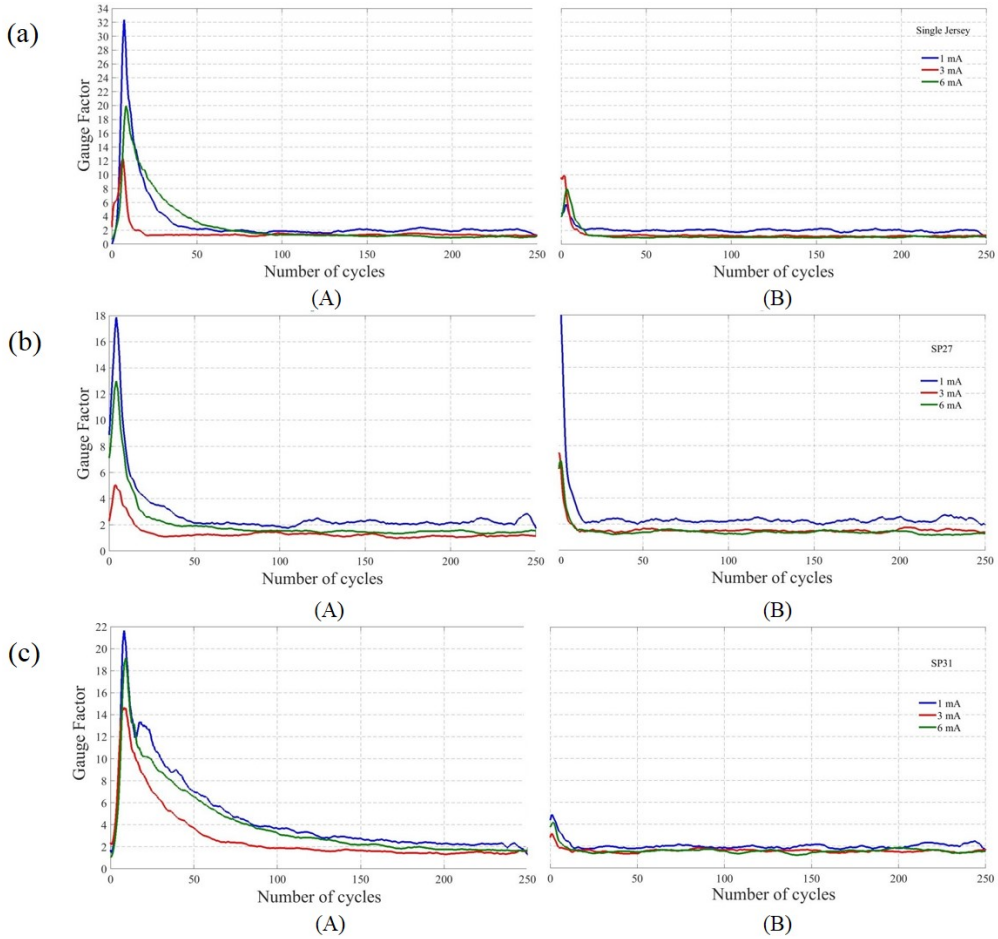


Figure 7.6: Sensitivity variation with cycle at 1 mA, 3 mA and 6 mA for (a) Single Jersey, (b) SP27 and (c) SP31 during (A) preconditioning and (B) repeatability tests

# Appendix V: Spectrograms and Harmonics Amplitude

Figure 7.7, Figure 7.8 and Figure 7.9 illustrate the results of the time-frequency analysis for Single Jersey, SP27 and SP31 under the same conditions (3 mA and 9.6 mm/s) described for SP29 in section 4.9.

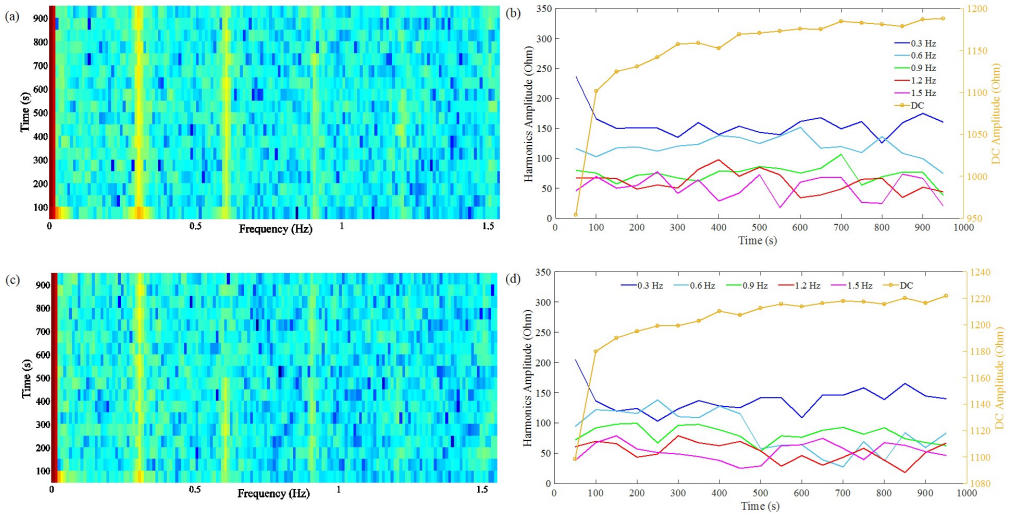


Figure 7.7: Spectrogram and amplitude variation of the most relevant components during preconditioning test ((a) and (b)) and during repeatability test ((c) and (d)) for the Single Jersey sample sourced with 3 mA and tested at 9.6 mm/s.

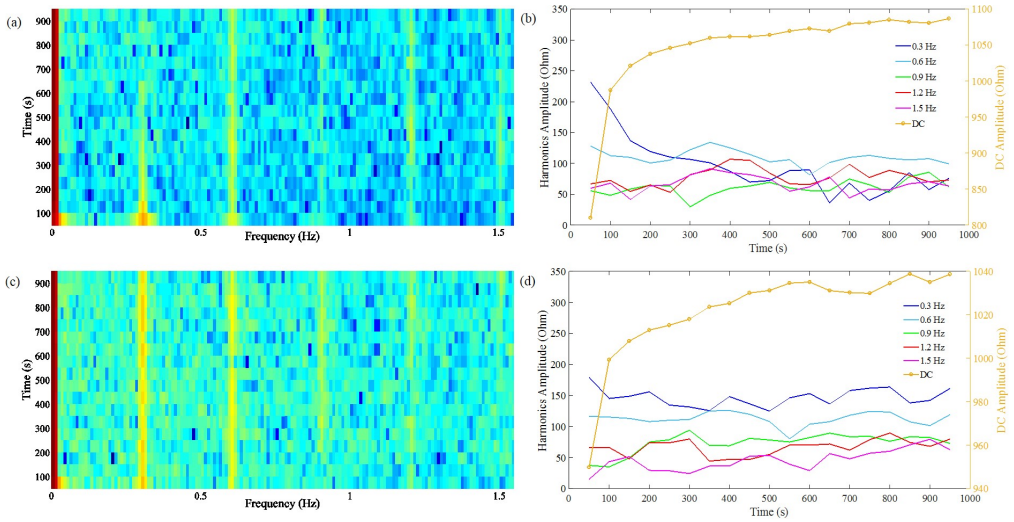


Figure 7.8: Spectrogram and amplitude variation of the most relevant components during preconditioning test ((a) and (b)) and during repeatability test ((c) and (d)) for the SP27 sample sourced with 3 mA and tested at 9.6 mm/s.

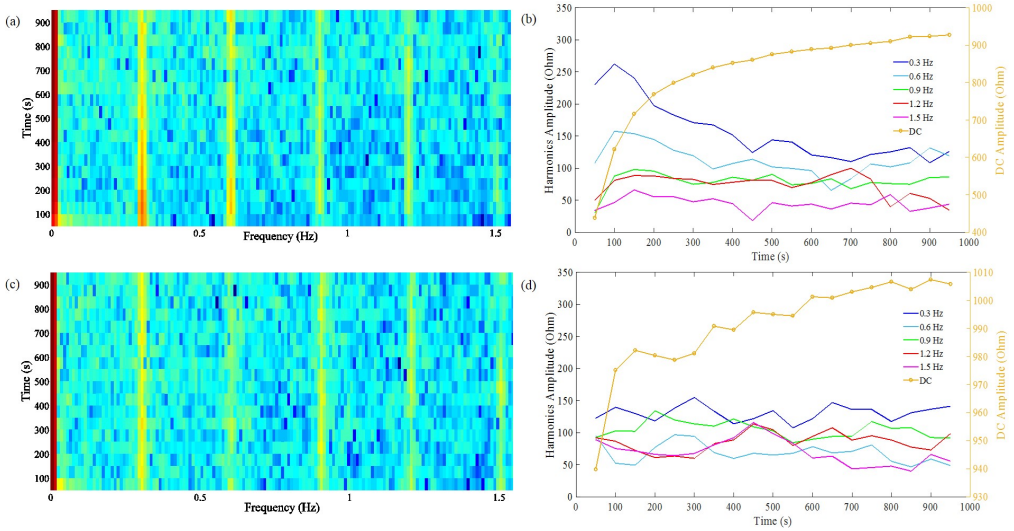


Figure 7.9: Spectrogram and amplitude variation of the most relevant components during preconditioning test ((a) and (b)) and during repeatability test ((c) and (d)) for the SP31 sample sourced with 3 mA and tested at 9.6 mm/s.

# Appendix VI:

# Matlab code for the *Visual Motion Tracking System*

IMAGE ACQUISITION FROM THE CAMERA

The following code calls the function 'getMarkerCoordinates', which is reported afterwards

vid=videoinput ('winvideo', 1); Capture the video frames using the videoinput function

set (vid, 'ReturnedColorspace', 'rgb'); Set the properties of the video object

vid.FrameGrabInterval = 10;

start (vid);

s = daq.createSession ('ni'); Create a new session with the National Instruments DAQ

ao0 = addAnalogOutputChannel (s, 'Dev1', 'ao0', 'Voltage'); Configure Analog Output 0

ao0.Name = 'KneeAngle';

hfig =figure;

while true

data = getsnapshot (vid);

imshow (data);

hold on;

$[x_{\text{thigh}}, y_{\text{thigh}}]$ = getMarkerCoordinates (data, 1); Extract coordinates for the red marker, the one placed on the thigh

$[x_{\text{knee}}, y_{\text{knee}}]$ = getMarkerCoordinates (data, 2); Extract coordinates for the green marker, the one placed on the knee

$[x_{\text{shank}}, y_{\text{shank}}]$ = getMarkerCoordinates (data, 3); Extract coordinates for the blue marker, the one placed on the shank

$R1 = [x_{\text{knee}}, y_{\text{knee}}] - [x_{\text{thigh}}, y_{\text{thigh}}]$; The knee angle between $r_{\text{thigh-knee}} and$ $r_{\text{knee-shank}}$ is calculated as the angle between their direction vectors

$R2 = [x_{\text{shank}}, y_{\text{shank}}] - [x_{\text{knee}}, y_{\text{knee}}]$; The direction vectors of two lines can be found by subtracting the position vectors of two points on the line

line([$x_{\text{thigh}}$, $x_{\text{knee}}$], [$y_{\text{thigh}}$, $y_{\text{knee}}$], 'Color', 'y', 'LineStyle', '–'); Draw the lines between the markers' centres

line([$x_{\text{knee}}$, $x_{\text{shank}}$], [$y_{\text{knee}}$, $y_{\text{shank}}$], 'Color', 'y', 'LineStyle', '–');

Kneeangle =mod (atan2 (det ([R1; R2]) , dot (R1, R2) ), 2*pi) ;

KneeangleInDegrees =Kneeangle *180 / pi ;

SupplementaryKneeAngle = 180−KneeangleInDegrees;

outputSingleScan (s, SupplementaryKneeAngle/9-10);

text($x_{\text{knee}}$-165,$y_{\text{knee}}$+55, strcat ('Knee angle:', num2str (SupplementaryKneeAngle)), 'FontName', 'Arial', 'FontWeight', 'bold', 'FontSize', 12, 'Color', 'yellow');

drawnow;

flushdata (vid); Keep the Frame Memory Used under the memory limit

p = get (gcf, 'CurrentCharacter');

if (p == 'q')

break;

end

```
end
stop (vid);
close (hfig);
release (s);
```

**GET MARKERS COORDINATES**

```
function [ x, y] = getMarkerCoordinates (data, markerColor)
diffFrame =imsubtract(data (:, :, markerColor), rgb2gray (data)); To track green objects in real time we have to subtract the green component from the grayscale image to extract the red components in the image
diffFrame = medfilt2 (diffFrame, [3 3]); Use a median filter to filter out noise
if (markerColor ==1)
thr = 0.18;
elseif (markerColor == 2)
thr = 0.05;
else
thr = 0.15;
end
diffFrame = im2bw (diffFrame, thr); Convert the resulting grayscale image into a binary image
diffFrame =bwareaopen (diffFrame, 300); Remove all those objects less than 300px
bw =bwlabel (diffFrame, 8);
stats =regionprops(bw, 'BoundingBox', 'Centroid'); We get a set of properties for each labeled region
numObjects = length (stats); Check if we have detected only one object
if (numObjects == 0)
```

x = NaN;

y = NaN;

else

bb = stats (1).BoundingBox;

bc = stats (1).Centroid;

rectangle ('Position', bb, 'EdgeColor', 'r', 'LineWidth', 2);

x = bc (1);

y = bc (2);

plot (x, y, '-m+');

text (x+15, y, strcat ('X: ', num2str(round(x)), ' Y: ', num2str(round(y))),

'FontName', 'Arial', 'FontWeight', 'bold', 'FontSize', 12, 'Color', 'yellow');

Write object's coordinates on the image

end

end

**ACQUISITION DATA FROM THE DAQ CHANNELS**

s = daq.createSession('ni'); Create a new session

ch 0 = addAnalogInputChannel (s, 'Dev1', 'ai0', 'Voltage'); Add three analog input channels from NI device to the session

ch 1 = addAnalogInputChannel (s, 'Dev1', 'ai1', 'Voltage');

ch 2 =addAnalogInputChannel (s, 'Dev1', 'ai2', 'Voltage');

ch 0.TerminalConfig = 'SingleEnded'; Change the configuration of the channels

ch 1.TerminalConfig = 'SingleEnded';

ch 2.TerminalConfig = 'SingleEnded';

s.IsContinuous = true; Specify that the session operation runs until you execute stop

basefilename = sprintf ('ChannelData %s', datestr (now,'_dd'_mmmm_yyyy

_HH_MM_SS')); Create the file .bin in which to write the acquired data in binary format. Save the file identifier in the variable file w

filename = strcat (basefilename, '.bin');

file_w = fopen (filename, 'w');

lh1 = addlistener (s, 'DataAvailable', @ (src, event) logData (src, event, file_w)); Add a listener for the DataAvailable event to record the data

s.startBackground; Acquire data in a non-blocking mode

figure;

while true

p = get (gcf, 'CurrentCharacter');

if (p == 'q')

break;

end

drawnow;

end

s.stop; To stop background operations

fclose (file_w); To close the file opened for writing

file_r = fopen (filename, 'r'); Read the log file and load the contents as a 3 columns matrix into data

$[data, count]$ = fread (file_r, [4,inf], 'double'); Read the values in the file_r into a 4-by-Inf array, called data. Return the number of characters that fread reads into data into count

title ('Channels Data'); Save the Channels data as a .JPEG image

xlabel ('Time (s)');

Time = data (1, :)';

V_0 = data (2, :)'; Ch_0 measures the voltage which is proportional to the knee angle

V_1 = data(3, :)'; Ch_1 measures the voltage across the fabric, i.e. V_1

V_2 = data (4, :)'; Ch_2 measures the voltage V_2 which is proportional to the current provided to the fabric

I = V_2/ 100; The current provided to the fabric is obtained as V_2 divided by 100 (i.e. the resistance value of the resistor in the manufactured circuit)

R =V_1. / I; The resistance measured along the fabric is R

KneeAngleinDegrees = (V_0 +10) * 9;

subplot (2, 1, 1); Plot the resistance vs time measured along the fabric

plot (Time, R);

title ('Resistance vs time');

xlabel ('Time (s)');

ylabel ('Resistance (Ohm)');

subplot (2, 1, 2);

plot (Time, KneeAngleinDegrees);

title ('Knee Angle vs time');

xlabel ('Time (s)');

ylabel ('Knee Angle (Degrees)');

filename = strcat (basefilename, '.jpeg');

saveas (gcf, filename);

figure;

Acq_Data = [Time, V_0, V_1, I, R, KneeAngleinDegrees]; Data acquired from the channels and calculated from them are saved in the array Acq_Data

fclose (filer); Close the log file

excelFileName = 'AcquiredData.xlsx'; Save the AcquiredData starting from the first Excel column

xlswrite (excelFileName, 'Time', 'V_0', 'V_1', 'I', 'R', 'Knee_Angle');

xlswrite (excelFileName, Acq_Data, 'Sheet1', 'A2');

delete (lh1); To delete the listeners

release (s);

## DATA POST-PROCESSING

START IDX R = findchangepts (R (1: 35000), 'Statistic', 'std'); Calculate index when R starts moving

START TIME R = Time (START IDX R);

START IDX ANGLE = START IDX R; Calculate index when Knee Angle starts moving (R and Knee Angle are synchronous)

START TIME ANGLE = Time (START IDX ANGLE);

Time R mov = Time (START IDX R: end); Define the beginning of movement for R and the corresponding signal

R mov = R (START IDX R: end);

Knee Angle mov = Knee Angle (START IDX ANGLE : end); Define the beginning of movement for Knee Angle and the corresponding signal

Time Knee Angle mov = Time (START IDX ANGLE : end);

### *Filtering the original signals*

smoothR = sgolayfilt (R, 3, 151);

To remove the staircase shape of the knee angle signal and the delay caused by the processing operations:

Time cut = Time (3000 : length (Knee Angle) - 3000); Remove first and last three seconds from the signals of interest

Knee Angle cut = Knee Angle (3000 : length (Knee Angle) - 3000);

Knee Angle changes = [diff (Knee Angle cut); 0]; Calculate difference between adjacent samples

Knee angle steps start = (abs (Knee Angle changes)> 0.05); Mark with ones the array's elements where a step change occurs

Pos Knee Angle changes = find(Knee angle steps start); Find the indexes where the step changes occur

Knee Angle step lengths = Pos Knee Angle changes - [3000; Pos Knee Angle changes (1: (length (Pos Knee Angle changes) -1))]; Calculate the lengths of the found step changes

camera proc time = mean(Knee Angle step lengths(2 : length(Knee Angle step lengths))); Assuming the mean of the step's lengths as the time required by the camera for processing each frame

Knee Angle delay = round (camera proc time); Approximate the camera processing time (expressed as number of samples) to the nearest integer

smoothKnee Angle delay = round (camera proc time * 1.5); The Savitzky-Golay filter introduces a delay equal to half the step's width since it uses the least squares algorithm inside windows of a given length. Thus, the filtered waveform will pass through the center of each step if the filter delay is not compensated. The overall delay is 1.5 times the step's width.

Knee Angle compensated = [Knee Angle((Knee Angle delay + 1): end); zeros (Knee Angle delay, 1)]; Shift left the knee angle signal in order to compensate the overall effect of camera processing delay

smoothKneeAngle= sgolayfilt (Knee Angle, 1, 151);

smoothKneeAngle compensated = [smoothKneeAngle ((smoothKnee Angle delay+1): end); zeros (smoothKnee Angle delay, 1)]; Shift left the knee angle signal in order to compensate the overall effect of camera and filter processing delays

plot (Time, Knee Angle, Time, Knee Angle compensated, Time, smoothKneeAngle compensated);

***Peak analysis for R and Knee Angle***

The function findpeaks returns the peaks, the locations, the widths (as the vector w) and the prominences of the peaks (as the vector p) for Knee Angle and R

$[Anglepks, Anglelocs, Anglew, Anglep]$ = findpeaks (smoothKneeAngle (START IDX ANGLE : end - 8000));

$[Rpks, Rlocs, Rw, Rp]$ = findpeaks (smoothR (START IDX R : end - 8000));

p2p R = peak2peak (smoothR (START IDX R : end - 8000));

p2p Angle = peak2peak (smoothKneeAngle (START IDX ANGLE : end - 8000));

findpeaks (smoothR,Time, 'MinPeakProminence', p2p R ./5, 'Annotate', 'extents'); Determine the peaks for R

$[RMAXValues, RMAXPos]$ = findpeaks (smoothR, 'MinPeakProminence', p2p R ./5, 'MinPeakDistance', mean ($Rw$));

Time Max R = Time (R MAX Pos);

smoothR inverted = - smoothR; Find peaks on an inverted version of the filtered signal to determine the minimum values

$[RMINValues, RMINPos]$ = findpeaks (smoothR inverted, 'MinPeakProminence', p2p R ./5, 'Annotate', 'extents', 'MinPeakDistance', mean($Rw$));

Minimi R = R MIN Values * (- 1);

Time Min R = Time (R MIN Pos);

findpeaks (smoothKneeAngle, Time, 'MinPeakProminence', p2p Angle ./2, 'Annotate', 'extents'); Determine the peaks for KneeAngle

$[AngleMAXValues, AngleMAXPos]$ = findpeaks (smoothKneeAngle, 'MinPeakProminence', p2p Angle ./2, 'MinPeakDistance', mean ($Anglew$));

Time Max Angle = Time (Angle MAX Pos);

$[AngleMINValues, AngleMINPos]$ = findpeaks (-smoothKneeAngle, 'MinPeakProminence', p2p Angle ./2, 'MinPeakDistance', mean($Anglew$));

Minimi Angle = Angle MIN Values * (-1);

Time Min Angle = Time (Angle MIN Pos);

plot (Time, smoothR, 'b', Time Max R, R MAX Values, '*', Time Min R, Minimi R, 'o'); Plot the peaks for R

xlabel ( 'Time(s)');

ylabel( 'Resistance (Ohm)');

legend ('Filtered signal', 'Max Values', 'Min Values');

plot (Time, smoothKneeAngle, Time Max Angle, Angle MAX Values, '*', Time Min Angle, Minimi Angle, 'o'); Plot the peaks for KneeAngle

xlabel ('Time(s)');

ylabel ('KneeAngle (Degrees)');

legend ('Filtered signal', 'Max Values', 'Min Values');

***Interpolation of the filtered values***

MAX interp R = spline (Time Max R, R MAX Values, Time);

MIN interp R = spline (Time Min R, Minimi R, Time);

Add a fictitious max/min point at the beginning and at the end of the found min/max values. This is necessary for later interpolation since we need a common time/pos interval for both curves.

if (R MIN Pos (1)< R MAX Pos (1))

If the position of the first minimum point is lower than the one of the first maximum point, we add a fictitious maximum point in the same position of the first minimum point and with value equal to the value of the first maximum point. The final result is that the first two maximum points have same value but different positions, but the first maximum is perfectly aligned with the first minimum.

MAX Mod Pos = [R MIN Pos (1); R MAX Pos];

MAX Mod Values = [R MAX Values (1); R MAX Values];

MIN Mod Pos = R MIN Pos;

MIN Mod Values = Minimi R;

elseif (R MAX Pos (1) < R MIN Pos (1))

MIN Mod Pos = [R MAX Pos (1); R MIN Pos];

MIN Mod Values = [Minimi R (1); Minimi R];

MAX Mod Pos = R MAX Pos;

MAX Mod Values = R MAX Values;

else

MIN Mod Pos = R MIN Pos;

MIN Mod Values = Minimi R;

MAX Mod Pos = R MAX Pos;

MAX Mod Values = R MAX Values;

end

if (R MIN Pos (end) > R MAX Pos (end))

If the position of the last minimum point is greater than the position of the last maximum point, we add a fictitious maximum point in the same position of the last minimum point and with value equal to the value of the last maximum point. The final result is that the last two maximum points have the same value but different positions, but the last maximum is perfectly aligned with the last minimum.

MAX Mod Pos = [MAX Mod Pos; R MIN Pos (end)];

MAX Mod Values = [MAX Mod Values; R MAX Values (end)];

elseif (R MIN Pos (end) < R MAX Pos (end))

MIN Mod Pos = [MIN Mod Pos; R MAX Pos (end)];

MIN Mod Values = [MIN Mod Values; Minimi R (end)];

end

MAX Mod Time = Time (MAX Mod Pos);

MIN Mod Time = Time (MIN Mod Pos);

MAX MIN interp Time is the time vector used for interpolating the curves of maximum and minimum points. Since now the positions of the first min-

imum and maximum points are the same, as well the positions of the last minimum and maximum points, we use as interpolation time the interval between the first and last minimum/maximum points.

MAX MIN interp Time = Time (MIN Mod Pos(1): MIN Mod Pos (end));

MAX interp R= spline (MAX Mod Time, MAX Mod Values, MAX MIN interp Time);

MIN interp R=spline (MIN Mod Time, MIN Mod Values, MAX MIN interp Time);

plot (Time Max R, R MAX Values,'*', Time Min R, Minimi R, 'o',

MAX MIN interp Time, MAX interp R, MAX MIN interp Time, MIN interp R);

xlabel ('Time (s)');

ylabel ( 'Resistance (Ohm)');

legend ('Max Values', 'Interpolated max', 'Min Values', 'Interpolated min');

The same procedure is applied to Knee Angle. The outcome is:

MAX Mod Time Angle = Time (MAX Mod Pos Angle);

MIN Mod Time Angle = Time (MIN Mod Pos Angle);

MAX MIN interp Time Angle is the time vector used for interpolating the curves of maximum and minimum points. Similarly to the procedure for R, the positions of the first minimum and maximum points of Knee Angle are now the same, as well the positions of the last minimum and maximum points. Thus, we use as interpolation time for Knee Angle the interval between the first and last minimum/maximum points.

MAX MIN interp Time Angle = Time (MIN Mod Pos Angle (1): MIN Mod Pos Angle (end));

MAX interp Angle = spline (MAX Mod Time Angle, MAX Mod Values

Angle, MAX MIN interp Time Angle);

MIN interp Angle = spline (MIN Mod Time Angle, MIN Mod Values Angle, MAX MIN interp Time Angle);

plot (Time Max Angle, Angle MAX Values, '*', Time Min Angle, Minimi Angle, 'o', MAX MIN interp Time Angle, MAX interp Angle, MAX MIN interp Time Angle, MIN interp Angle);

xlabel ('Time (s)');

ylabel ('Knee Angle (Degrees)');

legend ('Max Values', 'Interpolated max', 'Min Values', 'Interpolated min')

***Peak-to-peak span for R and Knee Angle***

PEAK SPAN interp R = MAX interp R - MIN interp R;

plot (MAX MIN interp Time, PEAK SPAN interp R);

xlabel ('Time (s)');

ylabel ('Peak-to-peak span (Ohm)');

SPAN Angle interp = MAX interp Angle - MIN interp Angle;

plot (MAX MIN interp Time Angle, SPAN Angle interp);

xlabel ('Time (s)');

ylabel ('Peak-to-peak span (Degrees)');

MAX MIN interp Time and MAX MIN interp Time Angle can differ since obtained from maximum and minimum points extracted from different source signals. To calculate the ratio between PEAK SPAN interp R and SPAN Angle interp, it is necessary to consider those spans in a time interval where both exist, that is in the intersection time interval.

[SPAN interp Time, SPAN smoothKneeAngle interp Pos, SPAN smoothR interp Pos] = intersect (MAX MIN interp Time Angle, MAX MIN interp Time);

Calculate the average time interval between minimum points for R

MIN InterTime = Time Min R - [0; Time Min R (1: end - 1)];

PERIOD = mean (MIN InterTime ( 1: end - 1));

Calculate the average number of samples between minimum points for R

MIN InterSamples = R MIN Pos - [0; R MIN Pos ( 1: end -1)];

SAMPLES PER PERIOD = mean (MIN InterSamples ( 1: end - 1));

CYCLES = (SPAN interp Time . / SAMPLES PER PERIOD) * 1000;

***Settling time, number of cycles to reach stability and stabilised average resistance (the change point analysis applied again to the span)***

B = PEAK SPAN interp R (START IDX R : end);

C = findchangepts (B, 'Statistic', 'std');

SETTLING TIME = MAX MIN interp Time(C);

CYCLES settling = (SETTLING TIME - START TIME R) / (SAMPLES PER PERIOD/1000);

R SETTLING TIME = mean (smoothR ( find ( Time == SETTLING TIME) : end)); Average resistance calculated from the instant in which the standard deviation changes the most to the end

R Settling span = mean (PEAK SPAN interp R (C : end));

***Gauge Factor and Sensitivity***

Calculate the average resistance of the unfiltered fabric resistance with a Butterworth filter of order 2 and normalised cut-off frequency equal to 5 * $10^{-5}$

[ b, a ] = butter ( 2, 0.00005);

R first cycles = R (START IDX R : uint32 (START IDX R + SAMPLES PER PERIOD * 5));

Calculate the average angle value over the first cycles only. It does it multiple times using the final conditions of the previously done filtering as initial condition for the next filtering in order to reduce the initial transient/convergence delay.

[R avg zf ]= filter (b, a, R first cycles);

[R avg zf ]= filter (b, a, R first cycles, zf);

[R avg zf ]= filter (b, a, R first cycles, zf);

[R avg zf ]= filter (b, a, R first cycles, zf);

[R avg zf ]= filter (b, a, R first cycles, zf);

R avg = filter (b, a, R mov, zf);

plot (Time R mov, R mov, 'b', Time R mov, R avg, 'r');

xlabel ( 'Time (s)' );

ylabel ( 'Resistance (Ohm) ');

The same filtering procedure is applied to the Knee Angle

Knee Angle avg = filter (d, c, Knee Angle mov, zf);

plot (Time Knee Angle mov, Knee Angle mov, 'b', Time Knee Angle mov, Knee Angle avg, 'r');

xlabel ( 'Time (s)' );

ylabel ( 'Knee Angle (Degrees)' );

To convert an angle in a length variation we use the formula that associates an angle (express in degrees) to its arc length: L = 2* pi* r* (Angle ./360)

r = 60;

r is the distance (in mm) between the condyle and the centre of the knee

SPAN L = 2 * pi * r * SPAN Angle interp . / 360;

Length variation with respect to the extended full extension (180 degrees)

L avg = 2 * pi * r * (180 - Knee Angle avg ) . / 360;

Temp R = find (Time R mov == SPAN interp Time (1) );

Temp R end = find (Time R mov == SPAN interp Time (end));

```
Temp Knee Angle = find (Time Knee Angle mov == SPAN interp Time
(1));
Temp Knee Angle end = find (Time Knee Angle mov == SPAN interp
Time (end));
GF = (PEAK SPAN interp R (SPAN smoothR interp Pos) ./R avg (Temp
R : Temp R end)) ./ (SPAN L (SPAN smoothKneeAngle interp Pos) ./L
avg (Temp Knee Angle : Temp Knee Angle end));
plot (SPAN interp Time, GF);
xlabel ( 'Time (s)' );
ylabel( 'Gauge Factor' );
plot (CYCLES, GF);
xlabel ( 'Cycles' );
ylabel ( 'Gauge Factor' );
Sensitivity = PEAK SPAN interp R (SPAN smoothR interp Pos) ./SPAN
Angle interp (SPAN smoothKneeAngle interp Pos);
plot( CYCLES, Sensitivity);
xlabel( 'Cycles' );
ylabel ( 'Sensitivity (Ohm/Degrees)' );
```

# Appendix VII:

# Matlab code for the *HUMAC NORM* System

ACQUISITION WITH HUMAC MACHINE

s = daq.createSession('ni'); Create a new session

Add four analog input channels from NI device to the session

ch 1 = addAnalogInputChannel (s, 'Dev1', 'ai1', 'Voltage'); Ch 1 measures the voltage across the fabric, i.e. V 1

ch 2 = addAnalogInputChannel (s, 'Dev1', 'ai2', 'Voltage'); Ch 2 measures the voltage V 2 which is proportional to the current provided to the fabric

ch 3 =addAnalogInputChannel (s, 'Dev1', 'ai3', 'Voltage'); Add the channel for the position signal

ch 4 =addAnalogInputChannel (s, 'Dev1', 'ai7', 'Voltage'); Add the channel for the velocity signal

Change the configuration of the channels

ch 1.TerminalConfig = 'SingleEnded';

ch 2.TerminalConfig = 'SingleEnded';

ch 3.TerminalConfig = 'SingleEnded';

ch 4.TerminalConfig = 'SingleEnded';

s.IsContinuous = true; Specify that the session operation runs until you

execute stop

basefilename = sprintf ('ChannelData %s', datestr (now,'_dd'_mmmm_yyyy _HH_MM_SS')); Create the file .bin in which to write the acquired data in binary format. Save the file identifier in the variable file_w

filename = strcat (basefilename, '.bin');

file_w = fopen (filename, 'w');

lh1 = addlistener (s, 'DataAvailable', @ (src, event) logData (src, event, file_w)); Add a listener for the DataAvailable event to record the data

s.startBackground; Acquire data in a non-blocking mode

figure;

while true

p = get (gcf, 'CurrentCharacter');

if (p == 'q')

break;

end

drawnow;

end

s.stop; To stop background operations

fclose (file_w); To close the file opened for writing

file_r = fopen (filename, 'r'); Read the log file and load the contents as a 3 columns matrix into data

Read the values in the file_r into a 5-by-Inf array, called data. Return the number of characters that fread reads into data into count

$[data, count]$ = fread (file_r [5, inf], 'double');

title ( 'Channels Data' ); Save the Channels data

xlabel ( 'Time (s)' );

Time = data (1, : )' ;

V 1 = data ( 2, : )' ;

```
V 2 = data ( 3, : )' ;
V 3 = data ( 4, : )' ;
V 4 = data ( 5, : )' ;
I = V 2 / 100; The current provided to the fabric is obtained as V 2 divided
by 100 (i.e. the resistance value of the resistor in the manufactured circuit)
R = V 1 ./ I; The resistance measured along the fabric is R
Gain and offset must be equal to the one set in the HUMAC software
GAIN P = 1024;
OFFSET P = 0;
GAIN V = 1024;
OFFSET V = 0;
The position and velocity outputs are:
POSITION = (V 3. * 32768 * 1024 / (GAIN P * 10) - OFFSET P) / 16;
VELOCITY = (V 4. * 32768 * 1024 / (GAIN V * 10) - OFFSET V) / 16;
Subplot the Resistance vs Time, the Knee Angle vs Time and Velocity vs
Time
subplot (3, 1, 1);
plot (Time, R);
title ( 'Resistance vs time' );
xlabel ( 'Time (s)' );
ylabel ( 'Resistance (Ohm)' );
subplot (3, 1, 2);
plot (Time, POSITION);
title ( 'Knee Angle vs time' );
xlabel ( 'Time (s)' );
ylabel ( 'Knee Angle (Degrees) ');
subplot (3, 1, 3);
plot (Time, VELOCITY);
```

title ( 'Velocity vs time' );

xlabel ( 'Time (s)' );

ylabel ( 'Velocity (Degrees/s)' );

filename = strcat (basefilename, '.jpeg');

Save the Channels data as a .JPEG image

saveas (gcf, filename);

figure;

Data acquired from the channels and calculated from them are saved in the array Acq Data

Acq Data = $[Time, V0, V1, I, R, POSITION, VELOCITY]$;

Close the log file

fclose (file_r);

Save the AcquiredData starting from the first Excel column

excelFileName = 'AcquiredData.xlsx';

xlswrite (excelFileName, 'Time', 'V 0', 'V 1', 'I', 'R', 'Position', 'Velocity');

xlswrite (excelFileName, Acq Data, 'Sheet1', 'A2');

Delete the listener

delete ( lh1 );

release ( s );

## DATA POST-PROCESSING

The data processing is the same of the one used in Appendix VI (7.3.4). The only difference is the window length of the Savitzky-Golay filter:

smoothR = sgolayfilt (R, 3, 651);

# Appendix VIII:

# Data post processing results with the HUMAC NORM System

Figures 7.10, 7.11 and 7.12 are the outcome of the post processing described in section 6.4.1 for the SP29 in 18% elastane, SP27 in 15% elastane and SP27 in 18% elastane, respectively.

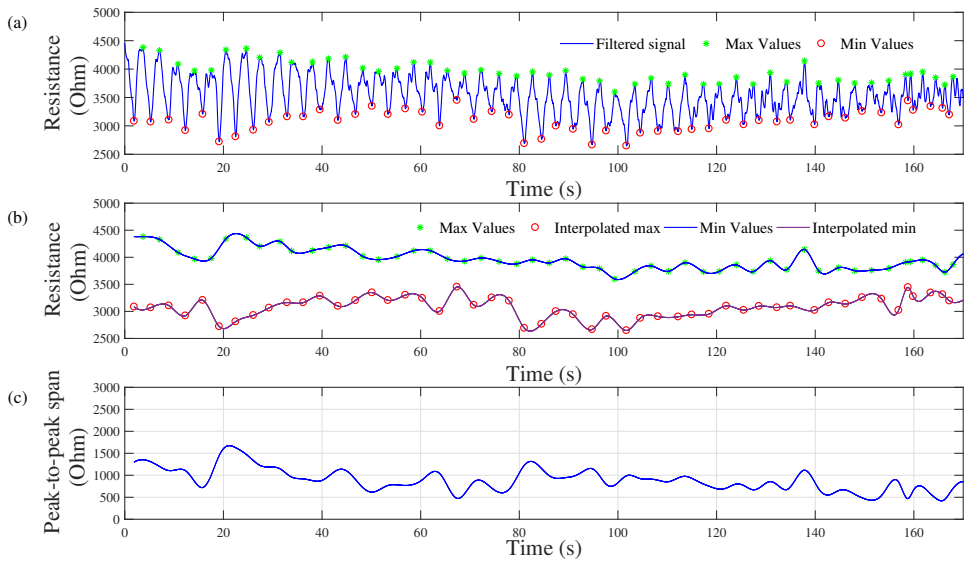


Figure 7.10: (a) Filtered fabric resistance (N=3, f=651), (b) Peaks detection and interpolation curves and (c) Peak-to-peak span for the SP29 embedded into a pair of leggings with 18% elastane

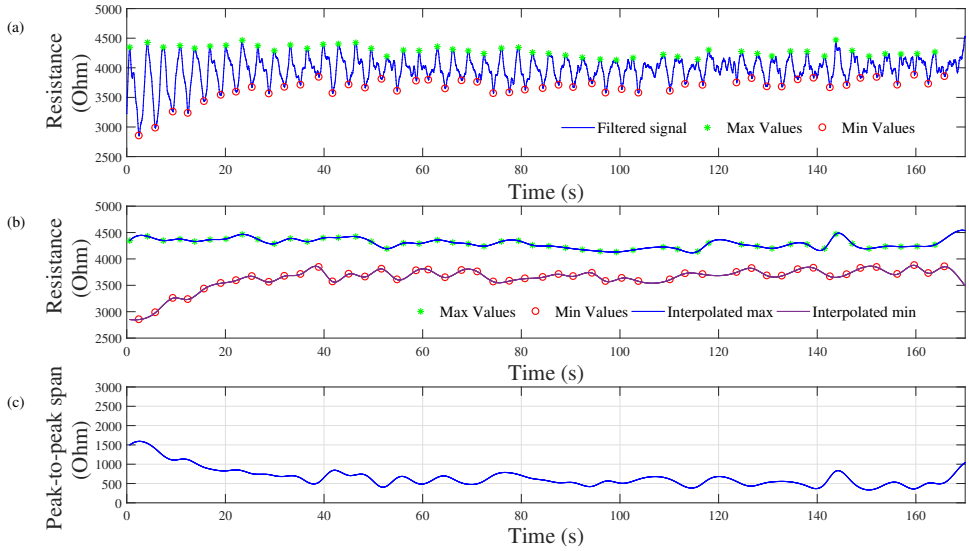


Figure 7.11: (a) Filtered fabric resistance (N=3, f=651), (b) Peaks detection and interpolation curves and (c) Peak-to-peak span for the SP27 embedded into a pair of leggings with 15% elastane

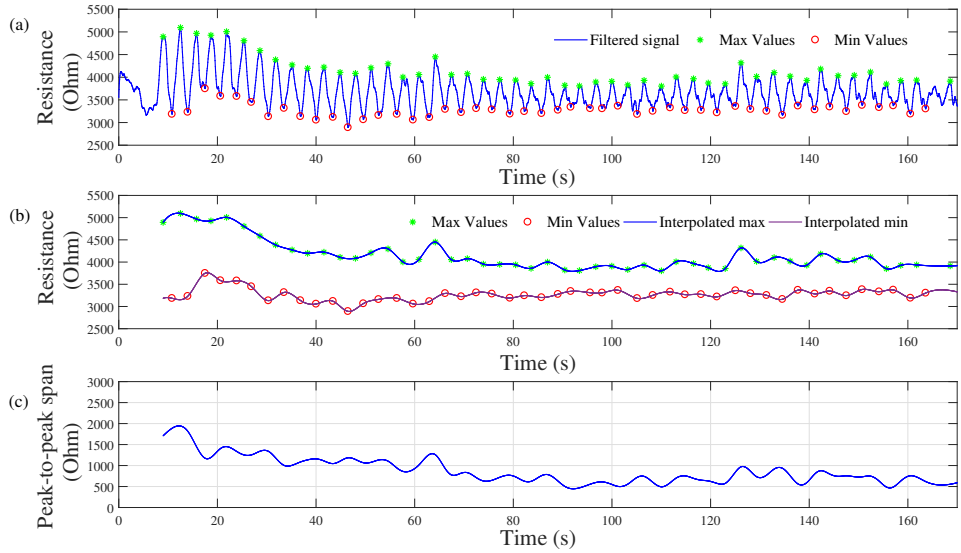


Figure 7.12: (a) Filtered fabric resistance (N=3, f=651), (b) Peaks detection and interpolation curves and (c) Peak-to-peak span for the SP27 embedded into a pair of leggings with 18% elastane

# Appendix IX: Statistical formula

### ARITHMETIC MEAN

$$\overline{x} = \frac{1}{n}\sum_{i=1}^{n} x_{\mathrm{i}} \tag{7.11}$$

with n the number of observations and $x_{\mathrm{i}}$ the observations.

### STANDARD DEVIATION

$$\sigma = \sqrt{\frac{\sum_{i=1}^{n}(x_{\mathrm{i}} - \overline{x})^2}{n}} \tag{7.12}$$

with n the number of observations, $x_{\mathrm{i}}$ the observations and $\overline{x}$ the arithmetic mean.

### WEIGHTED ARITHMETIC MEAN

$$\overline{x} = \frac{\sum_{i=1}^{n} x_{\mathrm{i}} w_{\mathrm{i}}}{\sum_{i=1}^{n} w_{\mathrm{i}}} \tag{7.13}$$

with n the number of observations, $x_{\mathrm{i}}$ the observations and $w_{\mathrm{i}}$ the weights.

## WEIGHTED STANDARD DEVIATION

$$\sigma = \sqrt{\frac{\sum_{i=1}^{n}(x_\mathrm{i} - \overline{x})^2 w_\mathrm{i}}{\sum_{i=1}^{n} w_\mathrm{i}}} \tag{7.14}$$

with n the number of observations, $x_\mathrm{i}$ the observations, $\overline{x}$ the weighted mean and $w_\mathrm{i}$ the weights.

# Appendix X: Participant Information Sheet

- The study will be conducting by Cristina Isaia, a PhD student in Mechanical Engineering.
- The study will be sponsored by the University of Nottingham, who will own data to use in a research project about motion analysis with a wearable sensor system.
- The nature of the survey is quantitative with the purpose of obtaining repeated measures of motion with a wearable sensor system attached to the participant's body. The duration of the study involving the participant is estimated to be approximately one month.
- The procedure consists of gathering direct measurements of motion parameters by using a wearable sensor system.
  The participant will be asked to execute two different types of trials:
  1. Knee flexion-extension in an upright position;
  2. Knee flexion-extension in a seated position.
- The hazards associated with the study are obstacles (e.g. objects and/or wires) that obstruct the trials.

- The risk associated with the study is the injury of the participant. The risk is low considering the following action plan:

    1. Making the working area clear of obstacles;
    2. Making sure that the wires closely attached to the participant's body.

- The procedure to follow in case of injury is calling for professional help (8888 from a University internal phone or 0115951888 from a mobile phone). First aid equipment is provided by the University and is available in the lab.

- No benefits are attached to the study.

- The procedure to follow in order to maintain confidentiality and anonymity consists of:

    1. Avoiding any personal details in any report;
    2. Using identification code numbers to correspond to research data in the computer files;
    3. Keeping data in locked files, stored in the applicant's desktop computer protected by password;
    4. No photos with identifying features of the participants will be taken, or said features will be blurred out for use in dissemination materials.

  Data collected by the applicant will be used to obtain an accurate resistance-strain characteristic to use for the sensing fabric sample's classification. Research data will be stored in their original form

(complying with the Data Protection Act 1998) in locked files in the password-protected applicant's desktop computer at University. At the first opportunity, all data files will be saved onto the password protected University of Nottingham central server.

Data will be disseminated in journal article as the written representation of the project findings.

Data gathered from the participant may be used for further analysis based on motion parameters (i.e. knee joint angle, acceleration).

- The photographs will be used for illustration purposes and printed in public domain documents to describe the experimental set up.
- The video records will be displayed to sponsors to identify the equipment required and the results obtained.
- If any questions or problems arise, the participant can contact:

    1. The student researcher conducting the study: Cristina Isaia (eaxci@nottingham.ac.uk).
    2. The Supervisors: David Branson (David.Branson@nottingham.ac.uk) and Donal McNally (Donal.McNally@nottingham.ac.uk)

- The participant's involvement in the study is voluntary. The participant is free to withdraw at any time and request that the information provided is not used in the project.
- The participant's information will be confidential and his/her identity will not be disclosed in any use of the information he/she has supplied during the survey.

Dear Participant,

Thank you for agreeing to participate in this survey in connection with my PhD research at the University of Nottingham. The project is a study of quantitative measures of motion obtained with a wearable sensor system attached to the participant's body.

Your participation in the survey is voluntary. You are able to withdraw from the survey at any time and to request that the information you have provided is not used in the project. Any information provided will be confidential. Your identity will not be disclosed in any use of the information you have supplied during the survey.

The research project has been reviewed according to the ethical review processes in place in the University of Nottingham. These processes are governed by the University's Code of Research Conduct and Research Ethics. Should you have any question now or in the future, please contact me or my supervisor. Should you have concerns related to my conduct of the survey or research ethics, please contact my supervisors or the University's Ethics Committee.

Yours truly,
Cristina Isaia

**Contact details**:

*Student Researcher*: Cristina Isaia (eaxci@nottingham.ac.uk)

*Supervisors*: David Branson (David.Branson@nottingham.ac.uk), Donal McNally (Donal.McNally@nottingham.ac.uk)

*University Research Ethics Committee Coordinator*: Ms Joanna Huang (Joanna.Huang@nottingham.edu.cn)

# Appendix XI: Participant Consent Form

**Project title:** A novel wearable sensor system for motion analysis

**Researcher's name:** Cristina Isaia

**Supervisors' names:** David Branson, Donal McNally

- I have read the Participant Information Sheet and the nature and purpose of the research project has been explained to me. I understand and agree to take part.
- I understand the purpose of the research project and my involvement in it.
- I understand that I may withdraw from the research project at any stage and that this will not affect my status now or in the future.
- I understand that while information gained during the study may be published, I will not be identified and my personal results will remain confidential.
- I understand that the data collection will be recorded.
- I understand that data will be stored in accordance with data protection laws.

- I understand that I may contact the researcher or supervisors if I require more information about the research, and that I may contact the Research Ethics Sub-Committee of the University of Nottingham if I wish to make a complaint related to my involvement in the research.

**Signed** ..... (participant)

**Print name** ..... **Date** .....

**Contact details**:

*Student Researcher*: Cristina Isaia (eaxci@nottingham.ac.uk)

*Supervisors*: David Branson (David.Branson@nottingham.ac.uk), Donal McNally (Donal.McNally@nottingham.ac.uk)

*UNNC Research Ethics Sub-Committee Coordinator*: Ms Joanna Huang (Joanna.Huang@nottingham.edu.cn)

# Appendix XII: Publications

1. C. Isaia, D. McNally, S.A. McMaster and D.T. Branson (2016), "Investigation of Changes in the Electrical Properties of Novel Knitted Conductive Textiles during Cyclic Loading". In: *38th Annual International Conference of the IEEE Engineering in Medicine and Biology Society, EMBC 2016, Orlando, FL, USA, August 16-20, 2016*. IEEE, pp. 6058-6061.
   isbn: 978-1-4577-0220-4. doi: 10.1109/EMBC.2016.7592110.

2. Cristina Isaia, Donal McNally and David T. Branson (2017), "Textile-based wearable sensors for human motion capture ". In: *Proceedings of the XXVI Congress of the International Society of Biomechanics, ISB 2017, 23-27 July 2017, Brisbane, Australia*.

3. Cristina Isaia, Donal McNally, Simon McMaster and David T. Branson (2018), "Effect of mechanical preconditioning on the electrical properties of knitted conductive textiles during cyclic loading ". In: *Textile Research Journal*, SAGE, doi:10.1177/0040517517748496.